UNIVERSIDADE DA CORUÑA
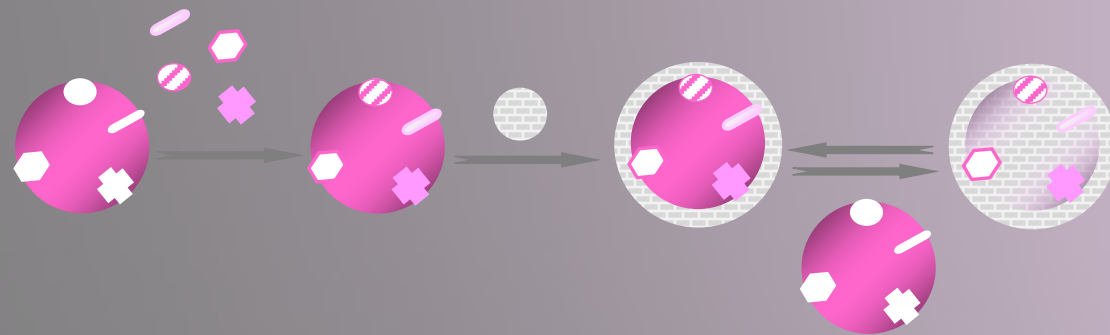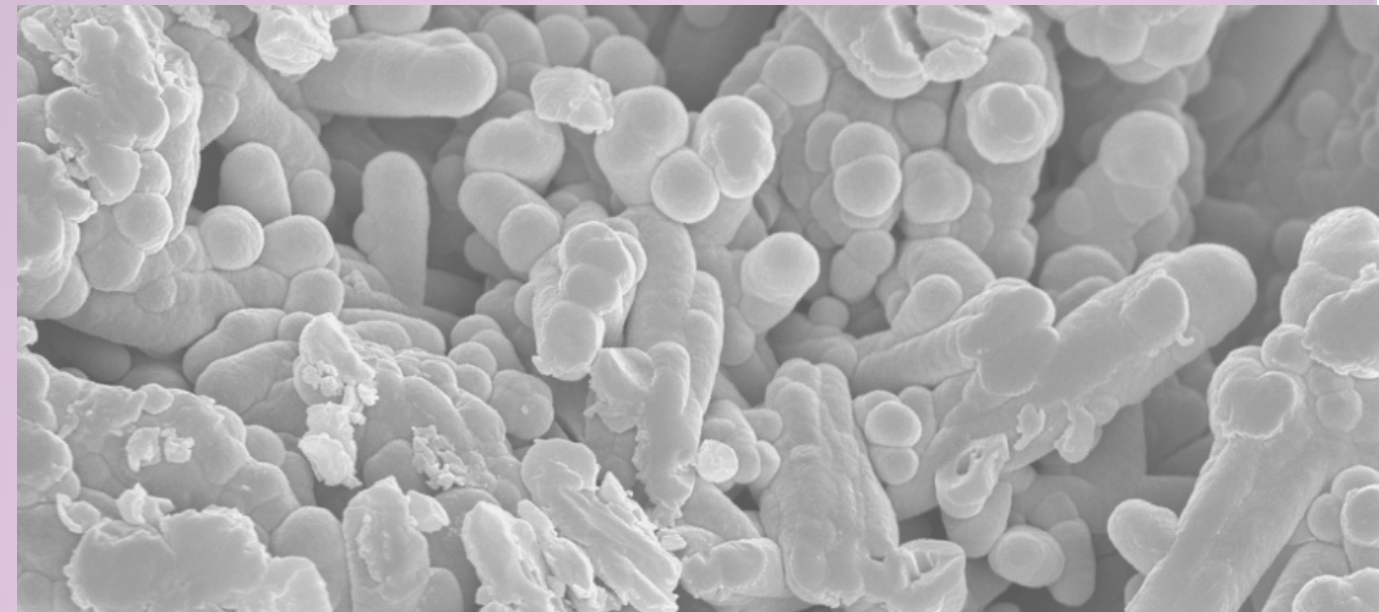
Síntesis y Caracterización de Polímeros de Impresión Molecular para Aplicaciones Analíticas

M.C. Cela Pérez

M.C. Cela Pérez

Septiembre 2015

UDC

2015

SÍNTESIS Y CARACTERIZACIÓN DE POLÍMEROS DE IMPRESIÓN MOLECULAR PARA APLICACIONES ANALÍTICAS

TESIS DOCTORAL
Departamento de Física

M.C. Cela Pérez
Septiembre 2015

Síntesis y caracterización de polímeros de impresión molecular para aplicaciones analíticas

M.C. Cela Pérez

Tesis doctoral UDC/2015

Directores:

Dra. M. Victoria González Rodríguez, Dr. José Manuel López Vilariño

Tutor:

Dr. Luis F. Barral Losada

Física Aplicada

UNIVERSIDADE DA CORUÑA

LABORATORIO DE QUÍMICA

Centro de Investigacións Tecnolóxicas

Campus de Esteiro, s/n,

15403 Ferrol

Tel: 981 33 74 00 – Ext. 3416

Fax: 981 33 74 16

e-mail: iquimica@udc.es

M. VICTORIA GONZÁLEZ RODRÍGUEZ, Catedrática de Escuela Universitaria del Departamento de Química Analítica de la Universidad de A Coruña, **JOSÉ MANUEL LÓPEZ VILARIÑO**, doctor, **AUTORIZAN** a M. Concepción Cela Pérez a presentar la memoria titulada: 'Síntesis y caracterización de polímeros de impresión molecular para aplicaciones analíticas' que ha sido realizada bajo su dirección en el Laboratorio de Química del Centro de Investigacións Tecnolóxicas para optar al grado de Doctora por la Universidad de A Coruña.

Y para que así conste a los efectos oportunos firman la presente en Ferrol, a 7 de Septiembre de 2015.

Fdo. **M.V. González Rodríguez**   **J.M.L. Vilariño**

DEPARTAMENTO DE FÍSICA
Campus da Zapateira, s/n
15071 A Coruña
España - Spain
Teléfono 981 16 70 00
Fax 981 16 70 65

LUIS F. BARRAL LOSADA, Catedrático del Departamento de Física de la Universidad de A Coruña, **RATIFICA** la autorización que la Dra. Mª Victoria González Rodríguez y el Dr. José Manuel López Vilariño realizan a M. Concepción Cela Pérez, a presentar el trabajo titulado 'Síntesis y caracterización de polímeros de impresión molecular para aplicaciones analíticas', en base al nivel científico y originalidad del mismo, para optar al Grado de Doctor.

Ferrol, 7 de Septiembre de 2015

Fdo. **Luis F. Barral Losada**

A tod@s mis amig@s, por estar siempre ahí y por los buenos ratos que pasamos que hacen que todo sea más fácil.

Y por supuesto a mi familia, a Fran, a mis padres, abuelos, hermanas, Jorge y mi sobrino Guille, lo sois todo para mí, siempre.

¡¡¡¡Muchísimas gracias a tod@s!!!

1. INTRODUCCIÓN

3. RESULTADOS

3.1. CAPÍTULO 1: DISEÑO, EVALUACIÓN Y CARACTERIZACIÓN DE POLÍMEROS IMPRESOS

Artículo 1: 'A study of competitive molecular interaction effects on imprinting of molecularly imprinted polymers'

Fig. 1. Chemical structures of the template molecule (ATM), functional monomers (MAA and 4-Vpy) and crosslinkers (EGDMA and TRIM) used in the polymerization...91

Fig. 2. ATR spectra of (a) solid Atmer, (b) MIP 6', (c) NIP 6', (d) MIP 7' and (e) NIP 7'.The arrows at 2850 cm^{-1} correspond to stretching of Atmer 129 methylene groups (υ- CH$_2$-). The arrows at 1725, 1245 and 1140 cm^{-1} indicate υ-C=O, asymmetric and symmetric υ-C-O-C of poly (EGDMA),

Artículo 2: 'Insight into BPA-4-vinylpyridine interactions in molecularly imprinted polymers using complementary spectroscopy techniques'

Fig. 2. IR titration study of BPA with 4-Vpy in CCl$_4$ in the spectral region between 1650-1500 cm^{-1}: BPA (4.0×10^{-3} M) (solid line); titration of BPA

3.2. CAPÍTULO 2: APLICACIÓN DE MIPS EN EL TRATAMIENTO DE MUESTRA PREVIO AL ANÁLISIS

Fig.1. HPLC-UV chromatogram and absorption spectrum of Irganox 1076 (50 mg L^{-1}).

Fig. 2. Selection of the monomer, porogen and polymerization method. Experimental conditions according to Table 1.

Fig. 3. UV absorption spectra of Irganox 1076 in the presence of various concentrations of MAA. [Irganox 1076] = 50 mg L^{-1}, molar ratio Irganox 1076:MAA 1:1, 1:4, 1:8. Corresponding MAA solution without Irganox 1076 as blanks.

Fig. 4. Schematic illustration of the possible interaction between Irganox 1076 and methacrylic acid.

Fig. 5. Selection of the initiator. Experimental conditions according to Table 1.

Fig. 6. Selection of the crosslinker. Experimental conditions according to Table 1.

Artículo 7: 'Selective removal of ATP degradation products from food matrices II: rapid screening of Hypoxanthine and Inosine by molecularly imprinted matrix solid-phase dispersion for evaluation of fish freshness'

Fig. 1. Schematic procedure of MIP–MSPD: (A) sample-MIP sorbent blending, (B) transfer blend to cartridge, (C) washing and elution under vacuum, (D) washing eluate (hexane) to be evaporated, (E) redisolution of

1. INTRODUCCIÓN

3. RESULTADOS

3.1. CAPÍTULO 1: DISEÑO, EVALUACIÓN Y CARACTERIZACIÓN DE POLÍMEROS IMPRESOS

Artículo 1: 'A study of competitive molecular interaction effects on imprinting of molecularly imprinted polymers'

Artículo 2: 'Insight into BPA-4-vinylpyridine interactions in molecularly imprinted polymers using complementary spectroscopy techniques'

Artículo 3: 'Selective removal of ATP degradation products from food matrices I: design and characterization of a dummy molecularly imprinted specific sorbent for hypoxanthine'

3.2. CAPÍTULO 2: APLICACIÓN DE MIPS EN EL TRATAMIENTO DE MUESTRA PREVIO AL ANÁLISIS

Artículo 6: 'An approach to imprint Irganox 1076: Potential application to the specific migration test in olive oil'

Artículo 7: 'Selective removal of ATP degradation products from food matrices II: rapid screening of Hypoxanthine and Inosine by molecularly imprinted matrix solid-phase dispersion for evaluation of fish freshness'

4-Vpy	4-vinilpiridina
a	parámetro indicativo de la capacidad y afinidad del polímero impreso en la ecuación de Freundlich
ACN	acetonitrilo
AIBN	2,2-azobisisobutironitrilo
AM	acrilamida
ATP	adenosín trifosfato
ATR-IR	espectroscopía de infrarrojo de reflexión total atenuada
B	concentración de analito enlazada en el polímero
BET	método de Brunauer-Emmett-Teller
BPA	bisfenol-A
BPF	bisfenol-F
C	agente entrecruzante y concentración de analito libre
C_i	constante de velocidad del modelo de difusión intraparticular
C_p	concentración de analito libre en el cálculo del coeficiente de reparto
C_s	concentración de analito enlazado en el polímero en el cálculo del coeficiente de reparto
CAF	cafeína
CBD	cannabidiol
CBN	cannabinol

CCl$_4$	tetracloruro de carbono
CHCl$_3$	cloroformo
DA	distribución de afinidad en el polímero
DAEM	N,N-dietil-2-aminoetilmetacrilato
DC	grado de conversión de monómero
DCM	diclorometano
DIGLYME	bis (2-metoxietil) éter
DMF	dimetilformamida
DMPA	2,2-dimetoxi-2-fenilacetofenona
D-R	ecuación de Dubinin-Radushkevich
DSC	calorimetría diferencial de barrido
DVB	divinilbenceno
E	energía de enlace
EC	electroforesis capilar
EGDMA	dimetacrilato de etilenglicol
ε	potencial de Polanyi
F	concentración de analito libre
FTIR	espectroscopía infrarroja con transformada de Fourier
HAc	ácido acético
HEMA	2-hidroxietil-metacrilato
HPLC-PDA	cromatografía líquida de alta resolución con detector de diodos
HYP	hipoxantina
IA	ácido itacónico

IF   factor de impresión

$\overline{IF}$ factor de impresión promedio

INO   inosina

K   constante de afinidad o de asociación

$\overline{K}_{K1\text{-}K2}$ constante de afinidad promedio de Freundlich

K_0 constante de afinidad promedio de Langmuir-Freundlich

k_1 constante de velocidad de pseudo orden uno

k_2 constante de velocidad de pseudo orden dos

K_{DR} constante de Dubinin-Radushkevich

k_i pendiente del modelo de difusión intraparticular

k_{MIP} coeficiente de reparto del analito en el polímero impreso

k_{NIP} coeficiente de reparto del analito en el polímero no impreso

LC-MS/MS   cromatografía de líquidos con espectrómetro de masas

LOQ   límite de cuantificación

m   índice de heterogeneidad de Freundlich

M   monómero funcional

MAA   ácido metacrílico

MeOH   metanol

MIP   polímero de impresión molecular o polímero impreso

MISPE   extracción en fase sólida con polímeros impresos

MSPD   dispersion en fase sólida

N   número de sitios de unión

N$_{K1-K2}$	número de sitios de unión promedio de Freundlich
N$_t$	número total de sitios de unión según Langmuir-Freundlich
NIP	polímero no impreso
PAR	paracetamol
pK$_a$	logaritmo negativo de la constante de acidez de un ácido débil
PVAc	polivinilacetato
P$_{vap}$	presión de vapor del disolvente porógeno
q$_e$	cantidad de analito enlazado en el equilibrio
q$_m$	capacidad de adsorción máxima del MIP
q$_t$	cantidad de analito enlazado a un tiempo determinado
R	constante de los gases ideales
RMN	resonancia magnética nuclear
RSD	desviación estándar relativa
SEM	microscopía electrónica de barrido
SF	factor de selectividad
SPE	extracción en fase sólida
T	molécula plantilla y temperatura absoluta
t	tiempo
t^{0,5}	tiempo requerido para la adsorción de al menos la mitad de analito adsorbido en el equilibrio
TGA	análisis termogavimétrivo
THC	tetrahidrocannabinol
THC-COOH	carboxitetrahidrocannabinol

THF   tetrahidrofurano

TMPTA   triacrilato de trimetilpropano

TPH   teofilina

TRIGLYME 1,2-bis (2-metoxietoxi) etano

TRIM   trimetacrilato de trimetilolpropano

UPLC-PDA cromatografía líquida de ultra-alta resolución

US   ultrasonidos

UV-Vis   espectroscopía ultravioleta-visible

RESUMEN

Los polímeros de impresión molecular (MIPs) se caracterizan por ser materiales sintéticos con propiedades de reconocimiento molecular altamente específicas y selectivas, característica que los ha convertido en herramientas analíticas indispensables en numerosas aplicaciones.

Esta tesis doctoral comprende el desarrollo de distintas estrategias de diseño de polímeros impresos para simplificar y optimizar su obtención, además de las metodologías involucradas en la evaluación de sus propiedades de enlace, el estudio de la naturaleza de la interacción analito-MIP y el mecanismo mediante el cual se produce dicha unión, la caracterización morfológica del polímero impreso y su aplicación como material adsorbente en la extracción de diversos analitos (drogas de abuso y sus metabolitos, aditivos migrantes de envases plásticos alimentarios, sustancias indicadoras de la calidad en alimentos) en muestras reales (fluidos biológicos humanos, aceite de oliva, carne de pescado). Al mismo tiempo, describe la preparación de una nueva configuración de MIPs en forma de pastilla, que en su empleo como material adsorbente en extracción en fase sólida, genera una novedosa metodología MISPE que permite trabajar en matrices complejas con volúmenes muy bajos de muestra.

RESUMO

Os polímeros de impresión molecular (MIPs) caracterízanse por ser materiais sintéticos con propiedades de recoñecemento molecular altamente específicas e selectivas, característica que os converteu en ferramentas analíticas indispensables en numerosas aplicacións.

Esta tese doctoral comprende o desenvolvemento de distintas estratexias de deseño de polímeros impresos para simplificar e optimizar a súa obtención, ademáis das metodoloxías involucradas na avaliación das súas propiedades de enlace, o estudo da natureza da interacción analito-MIP e o mecanismo mediante o cal prodúcese dita unión, a caracterización morfolóxica do polímero impreso e a súa aplicación como material adsorbente na extracción de diversos analitos (drogas de abuso e os seus metabolitos, aditivos migrantes de envases plásticos alimentarios, sustancias indicadoras da calidade en alimentos) en mostras reais (fluídos biolóxicos humanos, aceite de oliva, carne de peixe). Ao mesmo tempo, describe a preparación dunha nova configuración de MIPs en forma de pastilla, que no seu emprego como material adsorbente en extracción en fase sólida, xera unha novedosa metodoloxía MISPE que permite traballar en matrices complexas con volumes moi baixos de mostra.

ABSTRACT

Molecularly imprinted polymers (MIPs) are synthetic materials with highly specific and selective molecular recognition properties, making them indispensable analytical tools for a large number of applications.

This dissertation includes the development of several design strategies to simplify and optimize the synthesis of molecularly imprinted polymers, in addition to the methodologies involved in the evaluation of their binding properties, the study of analyte-MIP interaction and the adsorption mechanism, the morphological characterization of the imprinted polymers and the application of MIPs as adsorbent materials for the extraction of diferent analytes (drugs of abuse and their metabolites, additives of food packaging, food quality indicators) from real samples (human biological fluids, olive oil, fish meat). At the same time, this work describes the preparation of a new configuration of imprinted polymers (pills) which, used as adsorbent materials in solid phase extraction, generate a new MISPE methodology to work in complex matrices with very low sample volumes.

INTRODUCCIÓN

1. INTRODUCCIÓN

La eficacia de la preparación de la muestra dentro del procedimiento analítico es crítica en el análisis de muestras en las que los analitos se encuentran en niveles traza y/o en matrices complejas, siendo imprescindible aislarlos para su concentración y/o purificación.

En este sentido, una de las técnicas más utilizadas es la extracción en fase sólida (SPE). Esta técnica se basa en la diferente afinidad que presenta el analito (o la matriz) por una fase sólida o por la propia muestra líquida (o el extracto obtenido). En un principio, las propiedades exigidas a los materiales adsorbentes para usarlos como fase sólida fueron una estructura tridimensional rígida al tiempo que porosa y con una elevada área superficial, siendo la sílice y las resinas poliméricas los materiales que mejor se ajustaron a estas características. Con el tiempo, fue cobrando importancia la selectividad del adsorbente y los materiales convencionales se fueron mejorando con la introducción de grupos funcionales, mejorando la eficacia, la robustez y los límites de detección del procedimiento analítico.

En este ámbito surge la Tecnología de Impresión Molecular, que consiste en la síntesis de polímeros estables altamente entrecruzados con propiedades de reconocimiento molecular selectivo hacia los analitos de interés. Dicho reconocimiento se basa en la generación durante la polimerización de '*cavidades que son complementarias en tamaño, forma y*

funcionalidad química al analito' (Haupt, 2001), pudiendo llegar a tener constantes de afinidad y selectividad comparables a las del reconocimiento de los pares antígeno-anticuerpo.

Los polímeros impresos (MIPs) se preparan poniendo en contacto el analito (molécula plantilla) o un 'mimic template' (compuesto de estructura similar al analito) con un monómero funcional que presente grupos funcionales complementarios en un disolvente apropiado, para que se forme un complejo de prepolimerización estable. A continuación tiene lugar la polimerización en presencia de un agente entrecruzante. Una vez obtenido el polímero, la molécula plantilla se elimina lavando el MIP, normalmente, con un disolvente de elevada constante dieléctrica (alta polaridad). El uso de disolventes de polaridad superior a la del porogen favorece la eliminación de la molécula plantilla dejando así *'cavidades complementarias'* disponibles en la matriz polimérica capaces reconocer y enlazar el analito selectivamente (Figura 1). Es esta capacidad la que convierte a los polímeros impresos en materiales ideales para su empleo como adsorbentes en procesos que requieran extracción en fase sólida (MISPE) para la limpieza selectiva de muestras y/o preconcentración de analitos. La tecnología MIP también puede utilizarse en otras técnicas preparativas para mejorar su eficacia, como es el caso de la dispersión en fase sólida (MSPD) para el tratamiento de muestras sólidas.
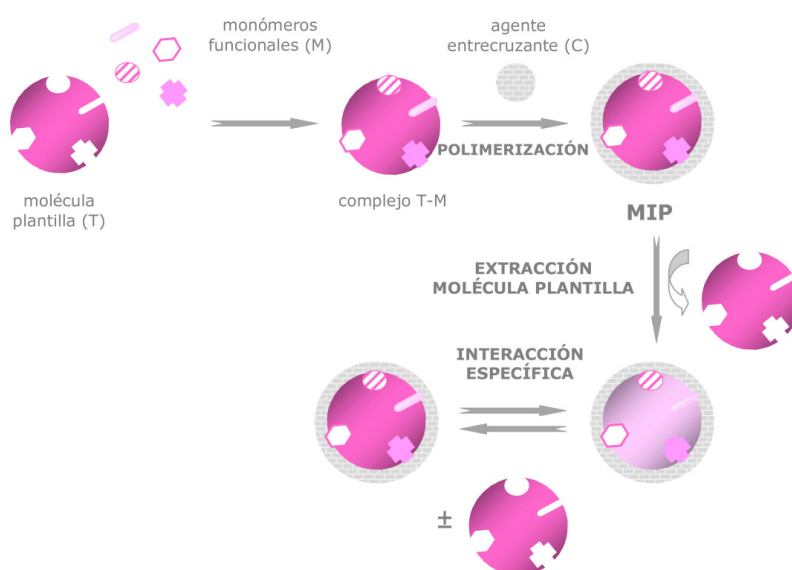
Figura 1. Esquema del procedimiento de preparación de un polímero impreso

Antes de su uso, los MIPs sintetizados se validan para cada aplicación mediante la evaluación de la cinética de unión y de las propiedades de enlace (reconocimiento molecular, selectividad…) así como a través de su caracterización física y química ('swelling' o nivel de hinchamiento, grado de polimerización, morfología…).

En la parte experimental de este trabajo se han sintetizado MIPs para su aplicación en las distintas técnicas preparativas mencionadas, SPE y MSPD, en función del tipo de matriz de la muestra. En todos los casos, los datos obtenidos en las etapas de diseño, evaluación y caracterización han permitido seleccionar el MIP más adecuado según la aplicación, incorporando la extracción con MIPs a un método analítico previo o desarrollando un método analítico completo y su validación.

1.1. PRINCIPIOS DE LA TECNOLOGÍA DE MIPs

1.1.1. Fundamentos del reconocimiento molecular

El complejo entre molécula plantilla y monómero funcional puede formarse a través de enlaces covalentes reversibles, interacciones no covalentes o por una combinación de ambos tipos de interacciones. Existen tres estrategias para llevar a cabo la polimerización en función del tipo de interacción involucrada en el proceso de impresión o reconocimiento molecular.

En la impresión molecular **covalente** las interacciones entre los grupos funcionales de la molécula plantilla y el monómero funcional son uniones covalentes que dan lugar a sitios de unión homogéneos y definidos. Además, debido a la adición estequiométrica de los monómeros funcionales, el porcentaje de unión no específica derivado es muy pequeño. Las interacciones responsables del enlace selectivo posterior del analito son también covalentes, lo que implica alta afinidad y selectividad hacia el analito, pero bajas cinéticas de enlace. Ésta es la mayor limitación de la síntesis covalente, junto con el número limitado de reactivos potencialmente utilizables y la complejidad tanto de la ruta de síntesis como de la eliminación final de la molécula plantilla (normalmente hidrólisis catalizada). Dichos factores limitan el campo de aplicación de estos MIPs, por ejemplo en el análisis cromatográfico, donde son preferibles interacciones de cinética rápida que conduzcan a tiempos de análisis cortos [1-4].

14

En la polimerización **semicovalente**, aunque la interacción molécula plantilla-monómero funcional es covalente, la interacción implicada en el reconocimiento posterior de los analitos es de naturaleza no covalente. Es una técnica más versátil que la anterior que puede adaptarse a diferentes condiciones de polimerización, aunque de nuevo, la complejidad de la ruta de síntesis y de la química implicada en la eliminación de la molécula plantilla, la convierten en una opción poco utilizada [4-6].

En la impresión **no covalente**, los monómeros funcionales interaccionan con la molécula plantilla en la mezcla de prepolimerización (molécula plantilla + porogen + monómero funcional), originándose un reordenamiento molecular en el que se maximiza la interacción, que puede ocurrir en uno o más puntos de las moléculas y suelen involucrar enlaces de hidrógeno, interacciones π-π, dipolo-dipolo, iónicas y/o hidrofóbicas. Posteriormente, en presencia de un agente entrecruzante y un iniciador de la polimerización, se sintetiza el MIP. Esta polimerización generalmente sigue un mecanismo de propagación radicalario y puede estar inducida térmica o fotoquímicamente. Es una técnica simple y versátil, con la generación durante la síntesis de una amplia variedad de uniones, que aunque son de carácter débil y no específico, el conjunto de los múltiples puntos de unión posibilita esta opción de reconocimiento altamente selectivo. Las cinéticas de unión son más favorables que en la polimerización covalente ya que en el reconocimiento de la molécula están involucradas interacciones débiles.

Esta ruta de síntesis ofrece más alternativas que las vías covalentes en relación a la selección de reactivos y por lo tanto es más fácil de llevar a cabo. El principal inconveniente de esta técnica es que los polímeros preparados de esta forma presentan una distribución heterogénea de los sitios de unión, debido al alto número de asociaciones que pueden formarse entre la molécula plantilla y los precursores durante la etapa de preorganización. La consecuencia es que parte de ellos pueden interaccionar favorablemente con la molécula plantilla mientras que otros pueden hacerlo de forma menos favorable o incluso pueden unirse a otras especies químicas.

Debido a la amplia disponibilidad comercial de monómeros funcionales y analitos capaces de dar lugar a una interacción estable de este tipo, junto a la mayor simplicidad práctica, los polímeros impresos no covalentes son los más empleados en la actualidad. La correcta elección de los reactivos de síntesis es de máxima importancia ya que de ella depende que el procedimiento de reconocimiento molecular sea específico y selectivo [7-9].

Molécula plantilla

La molécula plantilla puede ser el propio analito que interesa extraer y cuantificar o bien puede ser otra molécula similar estructuralmente ('dumy template' o 'mimic template'). La selección de una u otra dependerá principalmente del nivel de concentración que se espera encontrar en la muestra. Si se trata de analitos en concentraciones traza, la mejor opción

es emplear como molécula plantilla un 'mimic' para evitar interferencias en la determinación derivadas del 'sangrado' del analito durante la aplicación del polímero si no se logró su completa eliminación en la etapa de lavado [10-12].
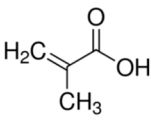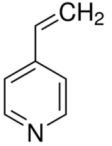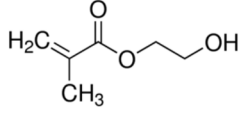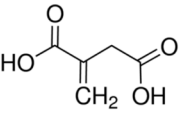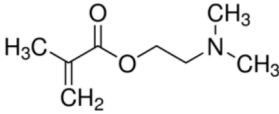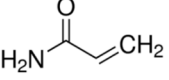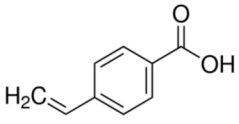
La elección de un 'mimic' como molécula plantilla es también inevitable cuando el analito no es soluble en el porogen a la concentración requerida y/o no es estable bajo las condiciones de polimerización aplicadas [13-14].

Monómero funcional

En general, el monómero funcional (Tabla 1) se selecciona de acuerdo a las características de la molécula plantilla. Si ésta tiene grupos funcionales de carácter básico en su estructura, monómeros ácidos como el ácido metacrílico (MAA), el ácido itacónico (IA) o el ácido 4-vinilbenzoico son los adecuados para que entre ambos se generen interacciones electrostáticas o por puente de hidrógeno. Si por el contrario, la molécula plantilla tiene grupos ácidos, el monómero funcional apropiado debe presentar carácter básico como la 4-vinilpiridina (4-Vpy) o el N,N-dietil-2-aminoetilmetacrilato (DAEM) [4, 15-16]. A veces, son las propiedades de la matriz de la aplicación en la que se va a utilizar el MIP las que determinan la selección del monómero funcional; así, monómeros funcionales neutros como el 2-hidroxietil metacrilato (HEMA) o la acrilamida (AM) aparecen con frecuencia en formulaciones preparadas para trabajar en medios acuosos [13, 17].

Normalmente, los equilibrios de formación del complejo estable obtenido a partir del monómero funcional y la molécula plantilla están regulados por constantes con valores muy bajos, por esta razón se emplea un exceso de los mismos con el fin de desplazar el equilibrio hacia la formación del complejo.

Tabla 1. Estructuras de los principales monómeros funcionales empleados en la impresión no covalente.

ÁCIDOS	BÁSICOS	NEUTROS
Ácido metacrílico (MAA)	*4-vinilpiridina (4-Vpy)*	*2-hidroxietil metacrilato (HEMA)*
Ácido itacónico (IA)	*N,N-dietil-2-aminoetilmetacrilato (DAEM)*	*Acrilamida (AM)*
Ácido 4-vinilbenzoico		

La impresión con un único tipo de monómero funcional es el caso más sencillo y también el más habitual, aunque pueden combinarse distintos monómeros funcionales para incrementar el número de puntos de interacción y mejorar la complementariedad con la molécula plantilla proporcionando así mayor selectividad al polímero [4].

Agente entrecruzante

La principal labor del agente entrecruzante es la formación de la red polimérica, cuyas características están directamente relacionadas con el proceso de impresión. La red polimérica ejerce influencia sobre el grado de hidrofobicidad y morfología del polímero impreso, afectando al diámetro y al volumen del poro al tiempo que estabiliza los sitios de unión selectivos formados y confiere estabilidad mecánica al material sintetizado. La cantidad de agente entrecruzante es determinante de la rigidez del polímero, al tiempo que afecta a la cinética de difusión del analito hacia los sitios de unión, además, debe existir un compromiso en la proporción entre el agente entrecruzante y el resto de componentes de la mezcla de prepolimerización, puesto que un defecto del mismo conduciría a un polímero con una baja capacidad de reconocimiento y baja selectividad, mientras que un exceso importante generaría un polímero muy rígido, carente de flexibilidad que podría impedir la accesibilidad de la molécula a las cavidades. Como norma general, el agente entrecruzante (C) se introduce en la ruta de síntesis de MIPs en exceso respecto a la molécula plantilla (T) y al monómero funcional (M), siendo habitual la relación T:M:C 1:4:20 para asegurar un grado de entrecruzamiento mayor del 80% y lograr una buena impresión molecular [18-20].
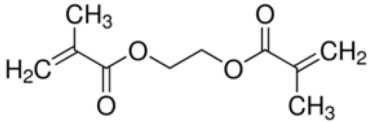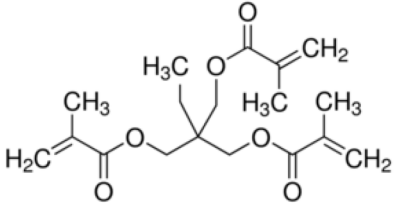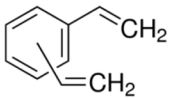
Algunos de los agentes entrecruzantes más utilizados son el dimetacrilato de etilenglicol (EGDMA), trimetacrilato de trimetilolpropano (TRIM) o el divinilbenceno (DVB) [4, 21] (Tabla 2). En la mayoría de formulaciones

publicadas predominan los agentes entrecruzantes bifuncionales como el EGDMA (tiene dos grupos metacrilato) aunque los trifuncionales como el TRIM (con tres grupos metacrilato) y multifuncionales en general, demostraron en algunos casos generar sitios de reconocimiento mejor definidos y robustos, trasladando al MIP mejores valores de afinidad y capacidad [13, 22-24].

Tabla 2. Principales agentes entrecruzantes empleados en impresión no covalente.

Dimetacrilato de etilenglicol (EGDMA)

Trimetacrilato de trimetilolpropano (TRIM)

Divinilbenceno (DVB)

Iniciador radicalario

Los más empleados son los de tipo azo, en concreto el 2,2-azobisisobutironitrilo (AIBN), con el que se logra una velocidad de descomposición apropiada con un calentamiento de la mezcla de reacción entre 50 y 60 ºC [25]. Aunque si la molécula plantilla es térmicamente

inestable, es posible generar radicales libres a baja temperatura (<4 ºC) mediante radiación UV empleando un fotoiniciador radicalario como la 2,2-dimetoxi-2-fenilacetofenona (DMPA) [26].

Disolvente porógeno

El disolvente en la impresión no covalente es determinante en la interacción molécula plantilla-monómero funcional, tanto su naturaleza como el volumen empleado afectan al proceso de reconocimiento molecular. De manera general, si las uniones predominantes molécula plantilla-monómero funcional se establecen mediante enlaces de hidrógeno, el uso de disolventes apróticos de polaridad moderada como el cloroformo ($CHCl_3$) o el acetonitrilo (ACN), o con bajas constantes dieléctricas como el tolueno o el diclorometano (DCM), facilita la formación del complejo; mientras que no es recomendable el empleo de disolventes polares próticos como el agua o el metanol (MeOH), puesto que compiten con los monómeros funcionales por los puntos de interacción con la molécula plantilla y el reconocimiento molecular resultante es menor [13].

El disolvente condiciona también la morfología del polímero, controlando el área superficial y el tamaño y distribución de poros, determinantes en el proceso de reconocimiento, puesto que a menor tamaño de poro, mayor dificultad de difusión de los analitos a las cavidades. Por este motivo, el disolvente de polimerización suele denominarse porógeno o porogen [18].

1.1.2. Configuración de MIPs obtenidos por impresión no covalente

Los MIPs pueden obtenerse en diferentes configuraciones (Figura 2), siendo habitual su preparación en forma de partículas amorfas, partículas esféricas o 'films'. En función de la aplicación a la que se destine el MIP, éste se preparará con un formato u otro [27-28].
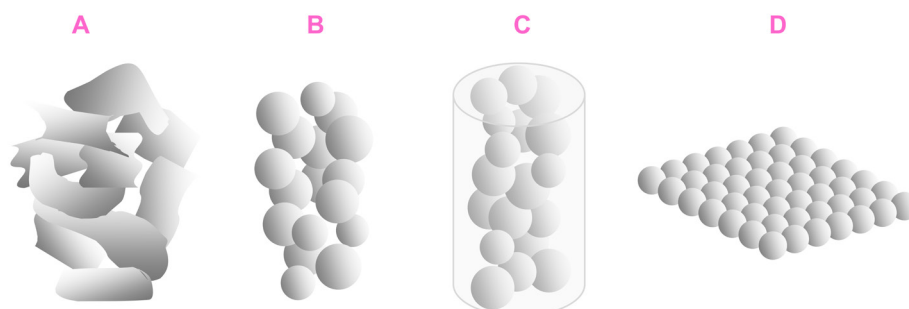
Figura 2. Distintas configuraciones en que pueden preparase los polímeros impresos no covalentes: A) partículas amorfas, B) partículas esféricas, C) pastillas, D) films.

Partículas amorfas

Los sistemas que emplean pequeños volúmenes de porógeno conducen a mezclas de prepolimerización muy concentradas, de forma que el polímero obtenido es un monolito insoluble ('bulk'), el cual hay que moler y tamizar para obtener partículas amorfas de tamaño deseado [29-30]. La distribución de los sitios de enlace es muy heterogénea al coexistir la formación de la cadena polimérica y la evaporación del porógeno, ya que suelen emplearse disolventes orgánicos con presiones de vapor (P_{vap})

elevadas, muy volátiles. Además, una parte de los sitios de enlace se destruyen en el proceso de trituración lo que conlleva una pérdida importante de la capacidad de carga del polímero. Por otro lado, aunque la metodología es sencilla y barata, lleva asociada una pérdida importante de reactivos al aprovecharse sólo una parte del polímero obtenido [31-32].

Partículas esféricas

Los sistemas que emplean un exceso de disolvente, de forma que la mezcla de reactivos se encuentra muy diluida en el porógeno, conducen a la formación de partículas esféricas, que presentan menor heterogeneidad de los puntos de unión analito-MIP en comparación con las amorfas. Se trata de dispersiones de micropartículas independientes en el seno de la disolución con una distribución de tamaño reducida [33-35]. Como ventajas de esta técnica cabe destacar la mayor capacidad y mejor distribución de los sitios de unión, así como un gran rendimiento de la polimerización. Además, es una síntesis sencilla y directa, al no precisar operaciones de molienda y tamizado. Todas estas características han favorecido que su uso sea generalizado.

Films

Los polímeros de impresión molecular pueden prepararse también en forma de finas láminas por inmersión del elemento soporte en la disolución de prepolimerización (cobertura por inmersión) o mediante el empleo de un 'spin-coating' (cobertura por rotación). De nuevo, las cavidades

obtenidas tienen forma y tamaño bien definidos e inalterables, al no haber molienda o trituración posteriores a la polimerización. Además, esta configuración facilita la accesibilidad del analito a prácticamente la totalidad de los sitios de unión [40-41].

Estas características convierten a los MIPs en formato 'film' en recubrimientos ideales de sensores químicos, debido a sus rápidos tiempos de respuesta y sencillez de uso [41-44].

Pastillas

El principal logro de este trabajo es la obtención de MIPs en un formato totalmente novedoso que mejora de forma sencilla y eficaz el tratamiento de muestras complejas, minimizando el volumen de muestra necesario y eliminando la mayor parte de los problemas surgidos en la preparación habitual de las mismas mediante SPE, al tiempo que reduce el tiempo total de análisis.

Los polímeros impresos se obtienen en forma de 'minimonolitos' o 'pastillas' que se emplean directamente sin necesidad de moler y/o tamizar. Para proporcionarle a la pastilla la forma y el tamaño necesarios según la aplicación final, se han diseñado distintos dispositivos en el laboratorio en los cuales se deposita la mezcla de prepolimerización y se procede a la obtención de las pastillas bajo condiciones térmicas [36-37].

Estos sistemas requieren mínimo volumen y baja volatilidad de la mezcla de prepolimerización. Los monómeros funcionales y agentes

entrecruzantes habituales tienen presiones de vapor bajas por lo que son poco volátiles, pero los disolventes orgánicos comúnmente empleados como porógenos suelen tener P_{vap} elevadas, son muy volátiles, por lo que en estos sistemas es necesario sustituirlos por otros de menor volatilidad como DIGLYME (bis (2-metoxietil) éter) o TRIGLYME (1,2-bis (2-metoxietoxi) etano), disolventes que además presentan constantes dieléctricas bajas que facilitan la formación del complejo molécula plantilla-monómero funcional. Por otro lado, la adición a la mezcla de prepolimerización de un polímero lineal e inerte demostró favorecer una polimerización ordenada, aumentando la porosidad y facilitando así el acceso del analito a los sitios de enlace, lo que implica a su vez una mejora de la capacidad de enlace. El MIP así obtenido presenta cavidades con forma y tamaño bien definidos e inalterables al no ser necesarios tratamientos de molienda o trituración posteriores [38-39].

1.1.3. Diseño de MIPs

Como ya se ha indicado en el apartado 1.1.1. de esta memoria, la obtención de un MIP óptimo, específico y selectivo hacia un determinado analito, con unas buenas propiedades de enlace, depende de las variables del proceso de síntesis. Teniendo en cuenta que por cada molécula plantilla seleccionada el número de monómeros funcionales y agentes entrecruzantes disponibles para llevar a cabo una polimerización no covalente es elevado, las composiciones posibles son muy numerosas,

siendo necesario realizar un cribado en el número de formulaciones, para lo que existen varias metodologías.

1.1.3.1. *Estudios de prepolimerización*

Consisten en el estudio detallado de las interacciones a nivel molecular en la mezcla de prepolimerización, dónde tiene lugar la formación del complejo entre la molécula plantilla y el monómero funcional. El complejo se forma principalmente a través de fuerzas intermoleculares e interacciones de tipo iónico que dependen del tipo y la naturaleza del monómero funcional, el disolvente porógeno y la relación molécula plantilla-monómero funcional (estequiometría). La influencia de los dos primeros ya se ha descrito con anterioridad. Con respecto a la estequiometría del complejo, a mayor número de interacciones molécula plantilla-monómero funcional en la mezcla de prepolimerización, mayor número de sitios de unión en el MIP, lo que favorecerá una mayor capacidad de adsorción, además de una mayor especificidad y selectividad.

Estudios previos han relacionado directamente la estabilidad del complejo con las propiedades mencionadas en el MIP mediante el análisis de las interacciones descritas a través de la modelización molecular y técnicas espectroscópicas como el Ultravioleta-visible (UV-Vis), el Infrarrojo por Transformada de Fourier (FTIR) y la Resonancia Magnética Nuclear (RMN) [45-53].

Espectroscopía UV-Vis

La espesctroscopía UV-Vis ofrece un procedimiento rápido para la determinación de la estequiometría del complejo mediante el método de variación continua (Job Plot), basado en la variación de absorbancia (ΔA) de la molécula plantilla, en presencia y ausencia del monómero funcional [45, 54, 59].

Experimentalmente, suelen prepararse una serie de disoluciones con diferentes relaciones molares T:M, manteniendo constante la concentración total (T+M). El gráfico se construye representando el producto de la variación de absorbancia por la fracción molar de molécula plantilla frente a la fracción molar de monómero funcional. De este modo el máximo de la curva se corresponderá con la estequiometría del complejo. Si el máximo corresponde con una fracción molar de monómero funcional 0,5, se debe a que el complejo presenta una estequiometría 1:1, mientras que si el máximo llega a 0,6, se puede asociar a una estequiometría 1:2. La Figura 3 muestra los espectros obtenidos en UV-Vis y el 'Job plot' derivado para el sistema formado por teofilina (TPH) y MAA en $CHCl_3$. El máximo de la curva obtenida es 0,5, lo que indica una estequiometria 1:1 [55].
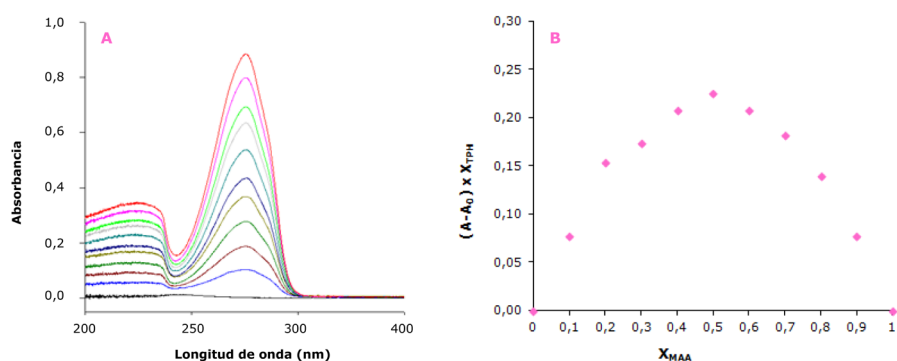
Figura 3. A) Espectros de absorción de TPH en ausencia y presencia de MAA a diferentes relaciones molares en $CHCl_3$, B) 'Job plot' para el sistema TPH-MAA.

Como complemento al método de la variación continua, mediante la aplicación de las ecuaciones de Benesi-Hildebrand, que varían según la estequiometría del complejo, se puede obtener el valor de la constante de estabilidad aparente del complejo molécula plantilla-monómero funcional [52, 59].

Pero la espectroscopía UV-Vis presenta limitaciones en su aplicación, ya que no todos los complejos formados exhiben variaciones de absorbancia en función de la concentración de monómero funcional, además de limitaciones en la información obtenida, ya que no es posible conocer ni el número, ni la posición exacta de los enlaces de hidrógeno que intervienen. Debido a estas limitaciones, distintos autores recurren al FTIR y al RMN, que permiten un estudio más detallado de los grupos funcionales involucrados.

Espectroscopía FTIR

Se emplea sobre todo en la identificación del grupo o grupos funcionales dadores y aceptores del enlace o enlaces de hidrógeno implicados en la interacción entre molécula plantilla y monómero funcional, en la que intervienen como mínimo un grupo funcional dador y otro grupo funcional aceptor.

El estudio se lleva a cabo a través de los desplazamientos observados en las frecuencias debidas a los grupos implicados en el enlace. De la misma forma se puede detectar si tiene lugar la autoasociación entre moléculas de monómero funcional o entre moléculas plantilla.

Esta técnica también permite estimar la estequiometria y la constante de estabilidad aparente del complejo aplicando metodologías similares a las descritas en UV-Vis [53, 56-60].

El principal inconveniente de la espectroscopía FTIR en los estudios de prepolimerización de MIPs son las interferencias producidas por la señal del disolvente.

La Figura 4 muestra los espectros de una disolución mezcla de MAA:TPH (A) y de disoluciones individuales de TPH (B) y de MAA (C) en la región del espectro entre 1775 y 1600 cm^{-1}, correspondiente a la zona de vibración de tensión de los grupos carbonilo. El espectro azul (C) representa las bandas correspondientes a los grupos carbonilo del MAA en forma de monómero y de dímero (1730 y 1697 cm^{-1} respectivamente), mientras que

en rojo (B) se muestra la banda de vibración de tensión del carbonilo de la TPH en posición 2 (a 1705 cm^{-1}). En el espectro diferencia (verde) (D), resultado de restar al espectro de la mezcla cada uno de los espectros individuales de los componentes, aparecen dos nuevas bandas, una a 1680 cm^{-1} atribuida al C=O del MAA enlazado al grupo –NH de la TPH, y otra a 1643 cm^{-1} correspondiente al carbonilo de la TPH unido al grupo –OH del ácido. De este modo, a través de un doble enlace de hidrógeno entre MAA y los grupos carbonilo en posición 6 y amino en posición 7 de la TPH [55], se confirma la estequiometría 1:1 observada en el estudio de esta misma interacción por UV-Vis (Figura 3).
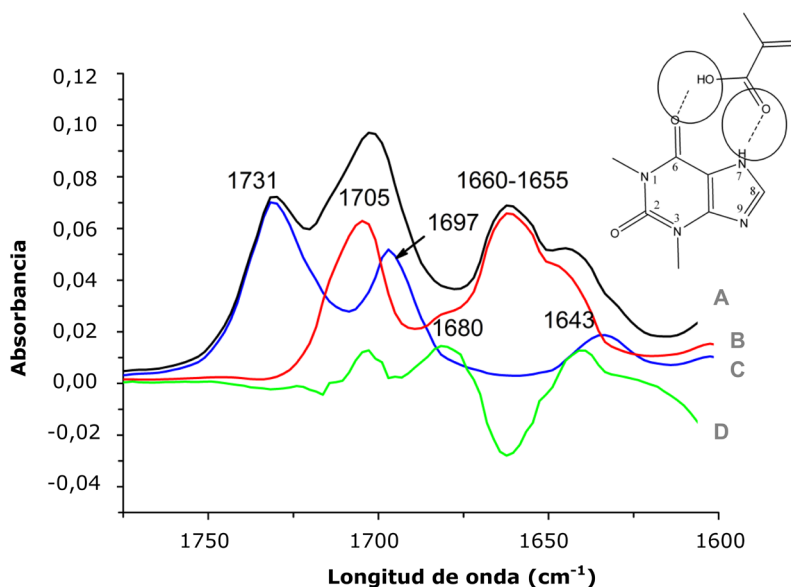
Figura 4. Valoración FTIR de MAA con TPH en CHCl$_3$ en la región entre 1750-1600 cm^{-1} A) MAA:TPH 1:1, B) TPH (5,0 x 10^{-3} M), C) MAA (5,0 x 10^{-3} M), D) espectro diferencia.

Espectroscopía RMN

La espectroscopía RMN normalmente se emplea como complemento a los estudios FTIR mencionados anteriormente, aportando información sobre la naturaleza de la interacción molécula plantilla-monómero funcional a nivel atómico. El espectro monodimensional de ^{1}H informa acerca del número y tipo de hidrógenos diferentes que hay en la mezcla de prepolimerización. Estos espectros consisten en un registro en forma de picos de las señales de resonancia correspondientes a los distintos hidrógenos presentes; cuya posición, anchura, área y subestructura permiten su identificación. La posición en el espectro (desplazamiento químico) está asociada a la identidad de los grupos vecinos a los protones, proporcionando información sobre los grupos funcionales a los que pertenecen o de los que están cerca [46, 61-62].

De nuevo, la estequiometria y las constantes de acoplamiento molécula plantilla-monómero funcional en prepolimerización se determinan mediante una metodología similar a la descrita en espectroscopía UV-Vis [9, 63-65].

1.1.3.2. *Modelización molecular*

La modelización molecular permite evaluar un número elevado de posibles polímeros impresos sin tener que realizar ningún tipo de ensayo en el laboratorio. Esta técnica se basa en el estudio de la fuerza de los enlaces que se formarían entre la molécula plantilla y los monómeros funcionales simulando las condiciones existentes durante la polimerización. De todas

las opciones posibles, se lleva a cabo únicamente la síntesis de aquellas para las que el diseño computacional predice un enlace adecuado, que garantice de algún modo la estabilidad y eficacia de la impresión [66-70].

Al tratarse de una estimación 'virtual', puede ocurrir que las combinaciones óptimas no sean viables en el laboratorio por diversos motivos, como que la molécula plantilla no sea soluble en el disolvente porógeno a las concentraciones requeridas para una impresión satisfactoria, que al pH de la mezcla de polimerización alguno de los componentes esté presente en su forma protonada o desprotonada y no neutra, no estableciéndose entonces las interacciones deseadas molécula plantilla-monómero funcional, o que experimentalmente el agente entecruzante modifique la polaridad de la mezcla y sea imposible alcanzar la polimerización por precipitación, entre otros obstáculos.

La Figura 5 muestra la simulación de la interacción a través de enlaces de H entre TPH y AM (SYBYL 7.0^{TM}); donde se puede observar como hasta 5 moléculas de AM se unen a cada molécula de TPH mediante un total de 8 enlaces de hidrógeno.
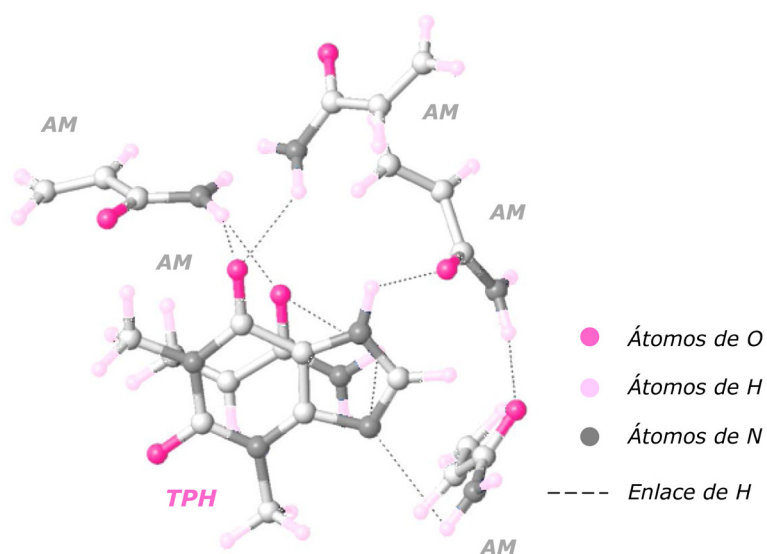
Figura 5. Simulación de la interacción TPH-AM (SYBYL 7.0™).

1.1.3.3. Estudios de enlace postpolimerización en miniMIPs

La obtención a pequeña escala de un determinado número de polímeros impresos derivados de las múltiples formulaciones teóricas posibles y viables mediante la polimerización en formato miniMIPs, constituye otra alternativa para el cribado de composiciones. El estudio incluye una etapa de lavado de los miniMIPs con el disolvente porógeno para hacer una primera aproximación al grado de impresión, seguido de otra etapa en la que se llevan a cabo ensayos de unión analito-miniMIP en el disolvente apropiado. El balance de las dos etapas se utiliza en la discriminación de miniMIPs en la búsqueda de la composición ideal [71-77].

1.1.3.4. Estudios de enlace postpolimerización en NIPs ('NIP library')

Estudios recientes han demostrado la conexión existente entre las propiedades de enlace de los MIPs y sus correspondientes polímeros no-impresos o NIPs, preparados de la misma forma que los MIPs pero en ausencia de molécula plantilla. En líneas generales, si un NIP no presenta propiedades de enlace mínimamente satisfactorias hacia un analito, su correspondiente MIP presentará un reconocimiento molecular pobre. Mientras que el caso contrario, un NIP con propiedades de enlace significativas hacia un analito, tendrá un MIP con un importante factor de impresión [78-82].

Para llevar a cabo este estudio, después de seleccionar los monómeros funcionales susceptibles de interaccionar con la molécula plantilla, se procede a la síntesis de los correspondientes NIPs, de la 'NIP library', mediante la reacción de cada monómero funcional con el agente entrecruzador disueltos ambos en el porogen y en presencia del iniciador. Posteriormente, ensayos de unión molécula plantilla-MIP en disolventes de distinta polaridad, conducirán al cribado de formulaciones mediante el cálculo de los coeficientes de reparto.

1.1.4. Evaluación de MIPs

Las propiedades de enlace reales de los MIPs se estiman en términos de factor de impresión, constantes de afinidad y capacidad de adsorción, para

el analito diana y para otros analitos de estructura similar. Los valores de estos indicadores se obtienen de ensayos de unión analito-MIP de forma sencilla y eficaz.

En estos ensayos se equilibran, en un tiempo establecido, una cantidad constante de polímero con una concentración de analito fija y conocida. El disolvente empleado suele ser el mismo que se usará en la aplicación final del MIP o si se trata de muestras reales, un simulante apropiado. La concentración de analito libre en la disolución después del tiempo de contacto puede medirse mediante espectroscopia UV, fluorescencia, HPLC con distintos tipos de detección etc. o en general cualquier técnica analítica con suficiente sensibilidad. La concentración de analito enlazado (B) se calcula como la diferencia entre la concentración de analito disponible al inicio y la concentración libre (F). Paralelamente, los ensayos de enlace se llevan a cabo en el NIP, que actúa como polímero de referencia.

1.1.4.1. Evaluación de la eficacia de la impresión

A partir de los datos obtenidos en los ensayos de enlace analito-MIP, en condiciones fijas de tiempo, concentración de analito y cantidad de polímero impreso, se puede estimar la eficacia del proceso de impresión calculando el factor de impresión IF, que se define como el cociente de los coeficientes de reparto k (del analito entre el polímero y la disolución) de MIP y NIP. Las ecuaciones correspondientes se muestran a continuación:

$$k = C_p/C_s$$

donde C_p (g mol^{-1}) es la concentración de analito en el polímero y C_s (mol mL^{-1}) es la concentración de analito libre en la disolución.

$$IF = k_{MIP}/k_{NIP}$$

donde k_{MIP} es el coeficiente de partición del analito en el polímero impreso y k_{NIP} es el coeficiente de partición del analito en el polímero no impreso.

Valores de IF < 1 indican que no se ha producido impresión molecular durante la polimerización del MIP, que el MIP no tiene capacidad de reconocimiento molecular; mientras que valores de IF > 1 garantizan la impresión molecular, al tiempo que cuanto mayor sea IF, mayor será la afinidad hacia el analito [83-84].

Este método de normalización elimina el enlace debido a las interacciones no específicas.

1.1.4.2. Isotermas de adsorción

Los datos de equilibrio obtenidos de la realización de una serie de ensayos de enlace analito-MIP en un intervalo de concentraciones establecido (normalmente entre 8 y 12 puntos) a temperatura constante, representan una isoterma de adsorción que habitualmente enfrenta la concentración de analito enlazado al polímero (B) y la concentración de analito libre en la disolución sobrenadante (F).

La capacidad de enlace relativa de dos polímeros puede determinarse de forma cualitativa superponiendo sus respectivas isotermas, aunque también es posible realizar su cuantificación comparando algunos parámetros de enlace, como son el número de sitios de unión (N) y la constante de afinidad o de asociación (K), que pueden calcularse a partir de las isotermas. Este cálculo requiere la aplicación de un modelo de enlace específico, cada uno de los cuales determina una relación matemática entre B y F, asumiendo determinadas hipótesis al considerar la distribución de sitios de unión.

Estos modelos de enlace pueden agruparse en dos clases: modelos de distribución discretos y continuos.

Las isotermas de Langmuir y bi-Langmuir, son ejemplos de modelos de enlace discretos. Estos modelos reducen la distribución a un número finito de clases diferentes de sitios, cada clase con distinta afinidad. El modelo de Langmuir considera que hay un sólo tipo de clase de sitios, y el modelo bi-Langmuir asume la existencia de dos tipos.

Las isotermas de Freundlich y Langmuir-Freundlich son ejemplos de modelos de distribución continuos en los que una función continua contiene un número infinito de tipos diferentes de sitios de unión. La distribución de sitios de unión o distribución de afinidad (DA), representa el número de sitios de unión que tienen una determinada constante de afinidad.

Modelos de enlace discretos: Langmuir y bi-Langmuir

Los modelos de Langmuir y bi-Langmuir son los más sencillos de tratar matemáticamente y permiten obtener de forma inmediata los parámetros de enlace K y N a partir de la denominada curva de Scatchard.

En la representación de Scatchard, la isoterma de enlace experimental se ajusta al formato q/C vs q, siendo q y C las concentraciones de analito enlazado y libre respectivamente. En sistemas homogéneos que contienen sólo un tipo de sitios de unión (Langmuir), del ajuste anterior se obtiene una línea recta con pendiente igual a la constante de afinidad promedio en negativo (-K) y una ordenada en el origen relacionada con el número total de sitios de unión (N):

$$q/C = KN - Kq$$

Esta representación para la mayoría de los MIPs no es lineal, sino curva, hecho que pone en evidencia la heterogeneidad de los sitios de unión. Sin embargo, en este caso también es posible obtener las constantes de afinidad y número de sitios de unión para dos clases de sitios (K_1, N_1 y K_2, N_2) ajustando la curva a dos líneas rectas (modelo bi-Langmuir) [85-87].

La Figura 6 muestra dos gráficos Scatchard. El de la izquierda es la isoterma de bi-Langmuir correspondiente a la adsorción en medio acuoso de bisfenol (BPA) en un MIP preparado usando el propio BPA como molécula plantilla y 4-Vpy como monómero funcional. La curvatura observada

muestra la heterogeneidad típica de los MIPs sintetizados por via no covalente. La linea de mayor pendiente corresponde a los sitios de enlace de mayor afinidad hacia el BPA, mientras que la linea inferior representa el comportamiento de los sitios de menor afinidad. La constante de afinidad en el primer caso es del orden de $1,19 \times 10^4$ M^{-1}, siendo varios órdenes de magnitud menor para los sitios de baja especificidad ($1,08 \times 10^1$ M^{-1}). En base a este modelo se calcula en este ejemplo una capacidad de adsorción específica de $26,9 \, \mu$mol g^{-1}. El gráfico Scatchard de la derecha correponde al polímero no impreso de referencia. En este caso se aplica el modelo de Langmuir para el cálculo de los parámetros de enlace pues la ausencia de curvatura indica la existencia de un único tipo de sitios de unión (K_{NIP} = $9,81 \times 10^2$ M^{-1}) [38].
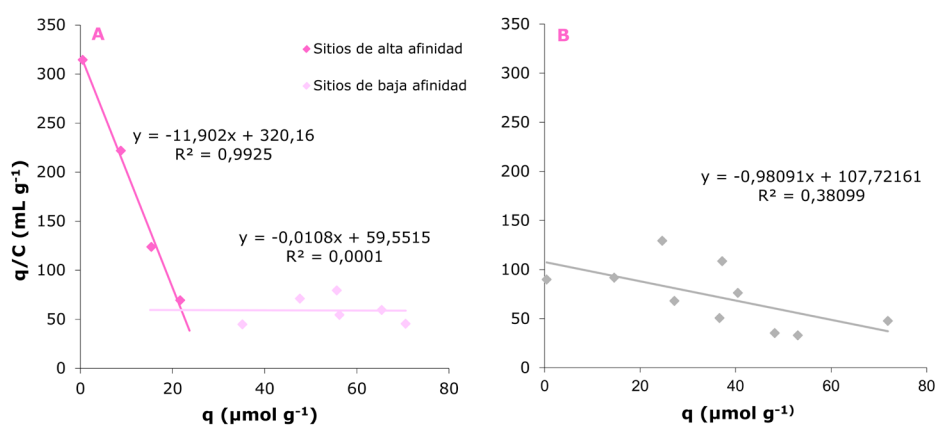
Figura 6. A) 'Scatchard plot' para la adsorción de BPA en BPA-4-Vpy-MIP y para B) la adsorción de BPA en su correspondiente NIP.

Los modelos de Langmuir y bi-Langmuir se basan en la hipótesis de que los MIPs son relativamente homogéneos y contienen sólo uno o dos tipos de sitios de unión. Constituyen un modelo simplificado que puede tener cierto grado de validez dependiendo del caso. Sin embargo, en general, la medida de las distribuciones de sitios de unión para los MIPs revela un amplio intervalo de constantes de afinidad.

Modelos de enlace continuos: Freundlich y Langmuir-Freundlich

Los modelos de enlace continuos consideran al MIP como un sistema heterogéneo, con sitios de unión de afinidad y selectividad variable. Estos modelos se aproximan más a la realidad y permiten explicar hechos experimentales, observados en la aplicación de los MIPs, relacionados con la heterogeneidad, como el amplio rango de constantes de afinidad calculadas para un mismo MIP, la anchura de picos cromatográficos cuando el MIP se usa como fase estacionaria o la baja selectividad observada en algunos MIPs.

El modelo más simple de distribución continua es la isoterma de Freundlich (IF) basado en la ecuación: $q = aC^m$, donde q y C vuelven a ser las concentraciones de analito enlazado y libre respectivamente, y a y m son dos parámetros de ajuste que tienen significado físico. El factor preexponencial a, es una medida del número de sitios de unión (N) y la constante promedio de afinidad (K). El segundo parámetro de ajuste, m, se conoce como índice de heterogeneidad y su valor varía de 0 a 1, siendo el

sistema más homogéneo a medida que se aproxima a 1. La isoterma de Freundlich se aplica fácilmente mediante el ajuste de los datos experimentales al formato logarítmico.

$$\log q = m \log C + \log a$$

Las isotermas que cumplen la isoterma de Freundlich se ajustan a una línea recta: con pendiente m y ordenada en el origen log a. Una ventaja del ajuste lineal es que para definirse requiere menos datos experimentales que una función curvilínea [85, 88-90].

En el caso de los modelos homogéneos, los parámetros de enlace se extraen de forma directa de la isoterma; sin embargo, los modelos heterogéneos requieren la solución de la integral de Langmuir que no tiene solución analítica, por lo que se han desarrollado métodos aproximados para su resolución. Uno de estos métodos aproximados es el método de Hunston [91] que calcula la distribución de afinidad (DA) de las isotermas de adsorción usando una diferencia finita de segundo orden para resolver la integral.

$$N(K) = 2{,}303 \, am(1 - m^2) e^{-2{,}303 m \log K}$$

La DA calculada a través de esta ecuación es válida en un rango de afinidades (K_{min} y K_{max}) que están determinadas por los límites de concentración libre (C_{max} y C_{min}) definidas por las siguientes ecuaciones:

$$K_{max} = 1/C_{min}$$

$$K_{min} = 1/C_{max}$$

El número de sitios de unión promedio N_{k1-k2} y la constante de afinidad promedio K_{k1-k2} se calculan a partir de:

$$N_{K1-K2} = a(1-m^2)(K_1^{-m} - K_2^{-m})$$

$$\overline{K}_{K1-K2} = \frac{m}{m-1} \frac{K_1^{1-m} - K_2^{1-m}}{K_1^{-m} - K_2^{-m}}$$

Los valores para estos parámetros se determinan para cualquier rango de constantes de afinidad K_1-K_2 dentro de los límites K_{min}-K_{max}.

La Figura 7 muestra la isotermas de Freundlich en formato log K - log N correspondiente a la adsorción en medio acuoso de hipoxantina (HYP) en un MIP preparado usando teofilina como molécula plantilla y AM como monómero funcional (linea superior) y la equivalente en el NIP (linea inferior). La más alta posición alcanzada en el caso del MIP se traduce en una mayor capacidad de adsorción respecto al NIP. A partir de las ecuaciones descritas en los párrafos anteriores, el número de sitios de enlace disponibles para HYP en el MIP en el rango de concentraciones estudiado es de 2,706 µmol g^{-1}, mientras que en el NIP el valor de N no supera los 0,028 µmol g^{-1} [92].
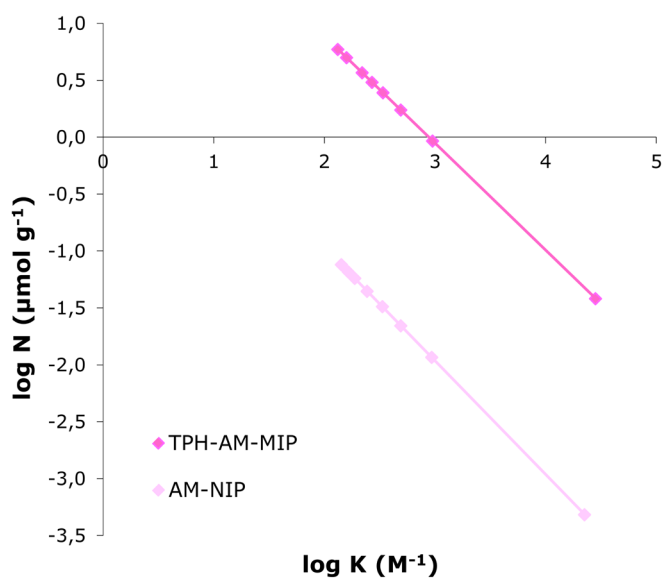
Figura 7. Isotermas de Freundlich en formato log K - log N para la adsorción de HYP en medio acuoso en TPH-AM-MIP y AM-NIP.

De forma general, los MIPs parecen contener una distribución unimodal de sitios de unión con dos regiones características: un pico unimodal de baja afinidad y una región asintótica decreciente de alta afinidad. El pico unimodal corresponde a la zona de la isoterma en la que el polímero alcanza la saturación. Una importante limitación de la isoterma de Freundlich es que sólo es exacta para la región intermedia de la isoterma completa. Se observan discrepancias del modelo tanto a concentraciones muy elevadas (región de saturación) como a concentraciones muy bajas. Sin embargo, en la mayor parte de aplicaciones analíticas se trabaja en la zona de subsaturación correspondiente a la región exponencial decreciente y que se corresponde con la porción lineal de la isoterma de Freundlich en

formato log B vs. log F. La región de saturación no es observable para la mayoría de los MIPs debido a la heterogeneidad de los mismos y a las extremadamente altas concentraciones necesarias para alcanzarla (superiores al rango miliMolar) y de igual forma, el extremo de concentraciones inferior (< nanoMolar) es difícil de medir si se ha usado el analito diana como molécula plantilla, debido al posible sangrado.

La incapacidad de la isoterma de Freundlich para modelizar la región de saturación limita los tipos de parámetros de enlace que pueden calcularse a partir de ella. Así, a partir de la isoterma de Freundlich no puede determinarse el número total de sitios de unión (N_t) o la constante de afinidad promedio (K_0). Para calcular estos parámetros es necesario desarrollar modelos híbridos que puedan modelizar las regiones de saturación y subsaturación al mismo tiempo en la misma isoterma como son los modelos de Jovanovic-Freundlich o Langmuir-Freundlich [93]. Por este motivo, la isoterma de Langmuir-Freundlich tiene una aplicabilidad más general en la caracterización de los MIPs, aunque como se explicó anteriormente, no suele ser necesaria debido a que las isotermas para la mayor parte de los MIPs se miden en la región de subsaturación donde es suficiente con aplicar la isoterma de Freundlich.

Modelo de Dubinin-Radushkevich

Existen además otros modelos de isotermas como el modelo de Dubinin-Radushkevich (D-R), que permite analizar la naturaleza de la interacción

entre el adsorbato y el adsorbente, es decir, entre el analito y el MIP, a través de las siguiente ecuación [86-87, 94]:

$$\ln q = \ln q_m - K_{DR}\varepsilon^2$$

donde q_m es la capacidad de adsorción máxima del MIP en µmol g^{-1}, K_{DR} (kJ^2 mol^{-2}) es la constante de Dubinin-Radushkevich y ε es el potencial de Polanyi dado por la ecuación:

$$\varepsilon = RT\ln\left(1+\frac{1}{C}\right)$$

K_{DR} está relacionada con la energía de adsorción libre por molécula (E, kJ mol^{-1}) de analito transferido desde la disolución a la superficie del MIP. Se estima que cuando este valor es inferior a 8 kJ mol^{-1}, la intensidad de la interacción analito-MIP es comparable a una interacción de tipo físico, mientras que cuando el valor de la energía libre asociada supera esta cifra, la intensidad de la interacción analito-MIP es similar a la fortaleza de un enlace químico [95]. El valor de E puede calcularse através de ela siguiente ecuación:

$$E = (2K_{DR})^{-1/2}$$

1.1.4.3. Evaluación de la selectividad

Los ensayos de unión analito-MIP no sólo sirven para evaluar las propiedades de enlace de los MIPs sino también para evaluar su

selectividad frente a sustancias interferentes. Las posibles interferencias se seleccionan bien por su similitud estructural al analito o pertenencia a la misma familia de compuestos, bien porque suelen aparecer junto con él en las muestras en las que se va a aplicar el MIP.

Experimentalmente, el procedimiento es idéntico al descrito en apartados anteriores, excepto que en este caso, la disolución no contiene únicamente el analito diana sino una mezcla de éste con las posibles interferencias. El tratamiento de los datos derivados para el cálculo de constantes de selectividad y capacidades de enlace se lleva a cabo a través de su ajuste a los modelos de isotermas mencionados en el apartado anterior.

En este caso puede calcularse el factor de selectividad (SF) como el cociente entre factores de impresión, como se indica a continuación:

$$SF = IF_{analito}/IF_{interferencia\_i}$$

donde $IF_{interfrencia\_i}$ es el factor de impresión para cada compuesto interferente considerado. SF sirve para evaluar globalmente la selectividad del MIP hacia el analito. De la misma manera que ocurría con IF, valores de SF>1 indican la mayor selectividad del polímero impreso hacia el analito respecto otras sustancias [83-84].

1.1.4.4. Estudios cinéticos de adsorción

El tiempo de incubación o contacto necesario en los ensayos de unión analito-MIP para que se alcance el equilibrio se determina a través de la

construcción del perfil de adsorción mediante ensayos de enlace analito-MIP a una misma concentración pero a distintos tiempos de incubación.

En los procesos de difusión es necesario identificar el mecanismo o paso dominante en la adsorción, tales como la transferencia de masa, la reacción química, etc. Existen variedad de modelos cinéticos para interpretar los resultados experimentales, siendo los modelos de pseudo primer orden, pseudo segundo orden y difusión intraparticular los más empleados. La elección del modelo cinético que define mejor los datos experimentales se realiza de acuerdo con los valores del coeficiente de correlación obtenido en cada caso.

Modelo de pseudo primer orden

En el modelo de pseudo primer orden de Lagergren, la ecuación cinética toma la siguiente forma:

$$log\ (q_e - q_t) = log\ q_e - \frac{k_1}{2,303}t$$

donde q_t y q_e son la capacidad de adsorción en mg g^{-1} a tiempo t y en el equilibrio respectivamente, y k_1 (min^{-1}) es la constante de velocidad de pseudo orden uno.

En este modelo, la variación en la tasa de adsorción debería ser proporcional a la primera potencia de la concentración para una adsorción estrictamente superficial. A partir de la pendiente y la ordenada en el origen se pueden deducir los valores de k_1 y contrastar los valores de q_e

experimentales y teóricos; si hay discrepancia entre ellos, la cinética de primer orden no describe este sistema [96].

Modelo de pseudo segundo orden

El modelo cinético de pseudo segundo orden representa la quimisorción debida a la formación de enlaces químicos entre adsorbente y adsorbato y está basado en la capacidad de adsorción del sólido. El modelo lineal es el siguiente:

$$\frac{t}{q_t} = \frac{1}{k_2 q_e^2} + \frac{t}{q_e}$$

Para obtener las constantes de la cinética de segundo orden es necesario realizar una grafica de t/q_t vs t. A partir de la pendiente y la ordenada de la recta obtenida se deducen la concentración de equilibrio teórica y la constante de la ecuación respectivamente (k_2, en g mg^{-1} min^{-1}); el valor de q_e teórico es comparado con el experimental; si los valores son cercanos, la cinética obedece al modelo de pseudo segundo orden [96-98].

Modelo de difusión intrapartícula

El modelo de difusión intrapartícula, basado en la teoría propuesta por Weber y Morris [99], identifica el mecanismo de difusión del analito en el MIP a través de la siguiente ecuación:

$$q_t = k_i t^{0,5} + C_i$$

Si la representación de $t^{0,5}$ frente a la cantidad de analito adsorbida en mg g^{-1} (q_t) es lineal, entonces está teniendo lugar el proceso de difusión intrapartícula; k_i es la pendiente y C_i la constante de velocidad, en mg g^{-1} min^{-1}. Si además esta línea pasa por el origen, esta etapa será la limitante en el proceso de adsorción [100].

Cuando en la representación gráfica se pueden establecer diferentes segmentos definidos por varias lineas rectas consecutivas, entonces se puede intuir que el proceso de adsorción consta de al menos una etapa más. La primera línea recta se debe a la adsorción en la superficie externa del MIP. En la segunda etapa, ocurre una adsorción gradual donde la difusión intrapartícula es la limitante de la velocidad, es decir, el analito viaja dentro de los poros del adsorbente. En algunos casos existe una tercera línea recta que representa el equilibrio final donde la difusión intrapartícula comienza a disminuir debido a la baja concentración de analito disponible; la adsorción ocurre en el interior del MIP [96, 98, 100]. En estos casos, el modelo de Boyd suele ser útil para determinar cuál de ellas es la etapa limitante [101].

La Figura 8 muestra el mecanismo de adsorción en medio acuoso, en reposo y en tres etapas de BPA en BPA-4-Vpy-MIP. La primera etapa representa la transferencia de BPA desde la disolución a la superficie del MIP; se trata de la etapa más rápida que trascurre a una velocidad de 0,1621 mg g^{-1} $min^{0,5}$. La segunda etapa corresponde a la difusión de BPA a través de los poros del polímero; de pendiente menos pronunciada, este

tramo es más lento que el inicial (0,05113 mg g^{-1} min^{0,5}). La tercera etapa, con mínima pendiente, es indicadora del equilibrio alcanzado por el sistema [38].
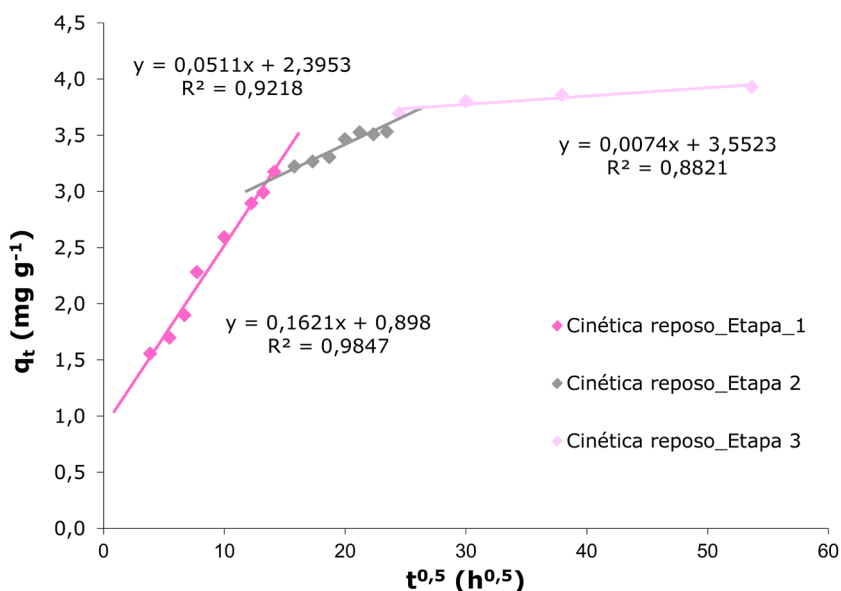
Figura 8. Difusión intrapartícula de BPA en medio acuoso en BPA-4-Vpy-MIP

1.1.5. Caracterización de MIPs

Los MIPs, como sólidos no solubles, únicamente se pueden caracterizar por un número limitado de técnicas como la espectroscopía IR, el grado de 'swelling' o técnicas de caracterización morfológica como la microscopía electrónica de barrido o la medida del área superficial y la porosidad por adsorción de gases [52, 83, 102].

1.1.5.1. Ensayos de 'Swelling'

La técnica conocida como 'swelling' consiste en determinar el grado de hinchamiento que sufre una determinada cantidad de polímero en contacto con un volumen concreto de disolvente. El cambio de volumen que sufre un MIP al ponerse en contacto con el disolvente empleado en los ensayos de unión respecto al que experimentó durante la síntesis en el porogen, ayuda a comprender el comportamiento de enlace derivado de los ensayos de unión analito-MIP, ya que la forma de la cavidad y la separación original entre grupos funcionales pueden alterarse y modificar el reconocimiento molecular [102-106].

1.1.5.2. Caracterización de la red polimérica

La espectroscopía de infrarrojo mediante reflectancia total atenuada (ATR-IR) permite medir la reactividad y el grado de polimerización de cada tipo de grupo polimerizable [83, 107]. El poder seleccionar bandas de vibración específicas permite, por ejemplo, medir el porcentaje de enlaces C=C sin reaccionar a través de la relación entre el área de la banda a 1638 cm^{-1} y el área de la banda correspondiente al grupo C=O del EGDMA a 1720 cm^{-1}, antes y después de la polimerización, eliminando cualquier dependencia de la cantidad de polímero utilizada. La ecuación descrita a continuación calcula el 'grado de conversión de monómero' (DC) para el ejemplo mencionado [55, 108-110].

$$DC(\%) = 100 - \frac{[(abs(C=C)_{1638}/abs(C=O)_{1720})_{polímero}]}{[(abs(C=C)_{1638}/abs(C=O)_{1720})_{EGDMA}]} \times 100$$

Por otro lado, a través de ATR-IR también se puede comprobar si la estequiometria determinada para el complejo molécula plantilla-monómero funcional en la mezcla de prepolimerización se mantiene en el MIP, así como la probabilidad de formación de enlaces de hidrógeno intramoleculares en la molécula plantilla durante la polimerización y/o la relevancia de las uniones no específicas molécula plantilla-agente entrecruzante; interacciones que condicionan la impresión [55, 110].

1.1.5.3. Caracterización morfológica

El tamaño de partícula es determinante en el éxito de algunas aplicaciones de los MIP. Como se explicará más adelante, hay técnicas separativas que necesitan un tamaño de particulado del orden de micras, por ejemplo, para asegurar su eficacia.

Entre las técnicas más utilizadas en el estudio del tamaño de partícula de los MIPs se encuentran la microscopía electrónica de barrido o la adsorción de gases.

Microscopia electrónica de barrido

Cuando un haz de electrones incide sobre la superficie de un sólido, se producen interacciones entre los electrones del mismo haz y los átomos del sólido pudiendo producirse reemisión de una parte de la radiación

incidente, emisión de luz, etc. Por otro lado, la energía que pierden los electrones al 'chocar' contra el sólido puede hacer que otros electrones salgan despedidos (electrones secundarios) y producir rayos X, electrones Auger, etc. Todas estas señales se pueden utilizar para obtener información acerca de la naturaleza del polímero empleando el detector adecuado en cada caso. El más común es el detector de electrones secundarios, con el que se obtienen la mayoría de las imágenes de microscopios de barrido electrónico (SEM) [39].

El análisis de MIPs mediante esta técnica aporta información macroscópica de la morfología del MIP, pero obviamente no permite la caracterización estructural de los sitios de enlace (Figura 9).
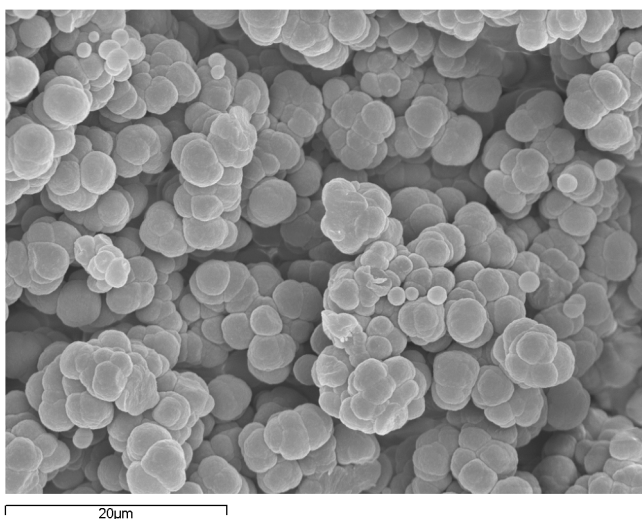
Figura 9. Imagen SEM de un MIP impreso con paracetamol y la mezcla de monómeros funcionales 4-Vpy y MAA.

Adsorción física de gases

La superficie específica y la distribución de tamaño de poro son parámetros fundamentales para la caracterización de polímeros. Propiedades como porosidad, fuerza, dureza, permeabilidad, corrosión, selectividad en la separación, etc. pueden estar directamente relacionadas con la estructura porosa del MIP. La técnica de adsorción de gases o fisisorción es una de las técnicas más utilizadas para determinar estos parámetros y estudiar propiedades de textura del material.

El procedimiento consiste en procesos de adsorción-desorción de N_2 en el polímero a incrementos de presión controlados. La evaluación de las ramas de adsorción y desorción de las isotermas generadas, junto con la histéresis observada, revelan información sobre el tamaño, área y forma del poro.

Todos estos datos adquiridos son procesados y evaluados aplicando distintos métodos. La teoría del método BET (Brunauer, Emmet, y Teller), por ejemplo, es el modelo más popular para determinar la superficie específica [52, 102, 111].

1.2. APLICACIONES ANALÍTICAS DE LOS MIPs

Debido a la gran especificidad y selectividad alcanzada por los polímeros impresos, su campo de aplicación es muy amplio, pudiendo utilizarse como fase estacionaria en cromatografía [112-114] y electroforesis [115-118] o

como material de reconocimiento en la fabricación de distintos tipos de sensores [119-123] aunque sin duda, es su empleo como adsorbente selectivo en procesos de extracción en fase sólida su principal aplicación [9, 124-128].

1.2.1. Cromatografía líquida y electroforesis capilar

La cromatografía líquida (HPLC) y la electroforesis capilar (EC) fueron las primeras técnicas analíticas que incorporaron los MIPs como fase estacionaria, lo que permitió la separación eficaz y selectiva de los analitos además de una notable reducción del tiempo total de análisis de muestra [129-133].

Para poder pasar un flujo de fase móvil a través de la columna de MIP, es necesario que el material de relleno sea poroso y que el número de sitios de enlace disponibles sea lo más alto posible. Ambos factores pueden controlarse cuidando tanto la formulación como la metodología de preparación del MIP.

Lo más habitual es preparar columnas monolíticas, es decir, los MIPs se preparan 'in situ' en la columna; después de eliminar la molécula plantilla, la fase estacionaria estaría lista para ser usada. Aunque esta aplicación sólo es útil para la separación de partículas de pequeño tamaño, si la molécula plantilla es demasiado grande, su eliminación no es completa y el material de relleno puede ser un obstáculo al paso de los analitos a lo largo de la columna. Una alternativa es preparar el MIP fuera de la columna,

lavar la plantilla, molerlo y tamizarlo al tamaño de partícula deseado y rellenar luego la columna. Pero como ya se comentó en secciones anteriores, esta metodología genera partículas con gran variabilidad de tamaños y muy heterogéneas en cuanto a la distribución de los sitios de unión, ambas características originan picos cromatográficos anchos y baja reproducibilidad.

El empleo de MIPs preparados por polimerización por precipitación, con tamaños de partícula uniformes y una mayor homogeneidad de puntos de enlace, corrige los problemas anteriores aunque se siguen necesitando tiempos elevados para forzar el paso de la fase móvil a través de la columna.

También pueden prepararse columnas recubiertas de MIP sólo en su superficie, por polimerización 'in situ' previa inmovilización del iniciador en la superficie de la columna. La regeneración de la columna es sencilla ya que no suelen producirse atascos como ocurre con frecuencia en el empleo de los otros formatos, pero presentan el inconveniente que la capacidad de la columna es muy limitada debido a la escasa cantidad de MIP en su interior, lo que en muchas ocasiones limita el análisis de muestra, haciendo necesaria una preconcentración previa [134].

1.2.2. Sensores

En los últimos años se han desarrollado diversos tipos de sensores químicos basados en el empleo de MIPs para la detección selectiva de los

analitos en muestras complejas y condiciones extremas (altas temperaturas o medios químicos agresivos). La elevada especificidad y selectividad de los MIPs junto con su robustez y estabilidad, los convierten en una excelente alternativa al empleo de biomoléculas, generalmente utilizadas como medio de reconocimiento selectivo en la fabricación de sensores.

Se pueden encontrar MIPs acoplados a sensores ópticos, electroquímicos (potenciométricos, amperométricos…), de masa (microbalanzas de cristal de cuarzo…) etc. [26, 135-145].

1.2.3. Extracción en fase sólida

Sin duda, la aplicación más importante y desarrollada de los MIPs es su empleo como adsorbente en procesos de extracción en fase sólida (MISPE) para la limpieza y preconcentración de muestra previos al análisis [21, 124, 128, 146-148]. Al ser materiales altamente selectivos, la eficacia del proceso MISPE aumenta notablemente respecto al uso de materiales adsorbentes tradicionales como por ejemplo la sílice modificada (C_{18}) o las resinas de intercambio iónico [149]. Además, permitirá desarrollar métodos analíticos más robustos y obtener límites de detección más bajos.

Subrayar una vez más que para aplicaciones analíticas con MISPE conviene no usar el analito de interés como molécula molde, ya que la eliminación total de la molécula plantilla del MIP siempre es difícil y pueden verse afectadas la exactitud y la precisión de la medida analítica. La solución es

usar como molécula plantilla un análogo estructural del analito para realizar la impresión, un mimic, tal y como se explicó al inicio de esta memoria.

La opción más habitual y sencilla es la SPE 'off-line', para la cual, una vez obtenido el polímero y extraída la molécula molde para liberar las cavidades formadas (normalmente por extracción Soxhlet), se trasvasa una pequeña cantidad (200 mg por ejemplo) a un cartucho típico SPE para realizar las extracciones en discontinuo y se llevan a cabo las etapas características de un proceso de la extracción en fase sólida [127, 150-152].

La elección del disolvente apropiado para cada etapa debe basarse en la capacidad de solubilizar los analitos y en el tipo de interacción implicada en la unión analito-MIP. De este modo, el disolvente más adecuado para efectuar la carga de la muestra será el que favorezca la interacción entre el analito y el polímero, siendo el porogen la primera opción a considerar. Por el contrario, el disolvente empleado en la elución se seleccionará en función de su facilidad para destruir la interacción específica entre el analito y el MIP.

Antes de cargar la muestra es obligatoria una etapa de acondicionamiento del cartucho MISPE. Aunque los posibles procedimientos son tan numerosos como las aplicaciones posibles, normalmente suele emplearse metanol seguido del disolvente que se va a emplear en la etapa de elución y por último el disolvente de carga de muestra seleccionado. El metanol se

utiliza para eliminar la humedad que pueda haber en el empaquetado, que en el caso de carga de muestra en disolvente orgánico, disminuiría la eficacia de la extracción. El lavado del cartucho con el disolvente de elución tiene como objetivo arrastrar cualquier tipo de interferencia que pueda coeluir con los analitos en la última etapa. El acondicionamiento final empleando el mismo disolvente que se usará para cargar la muestra facilitará la transferencia de materia. Es habitual la inclusión de una etapa intermedia entre la carga de la muestra y la elución de los analitos, empleando un disolvente que mantenga retenidos los compuestos de interés al tiempo que elimine la posibles interferencias de la matriz [125, 127, 150, 153-154].

La Figura 10 muestra el mecanismo genérico de adsorción-desorción implicado en las extracciones tipo MISPE. Tras cargar la muestra, se produce la adsorción específica y selectiva del analito en el polímero impreso, eluyendo el resto de compuestos al final de la columna. Posteriormente, la aplicación de un disolvente capaz de romper las uniones analito-MIP en un volumen apropiado, provoca la extracción del compuesto purificado y concentrado.

Con la aplicación MISPE, al igual que con la SPE tradicional, no sólo se pueden realizar extracciones y concentraciones de muestra de la manera que se ha explicado, sino también limpiezas de extractos. En este caso, los analitos pasan a través de la columna con ayuda de un disolvente con alta

afinidad hacia ellos y esta vez son las interferencias las que quedan retenidas en el MIP.
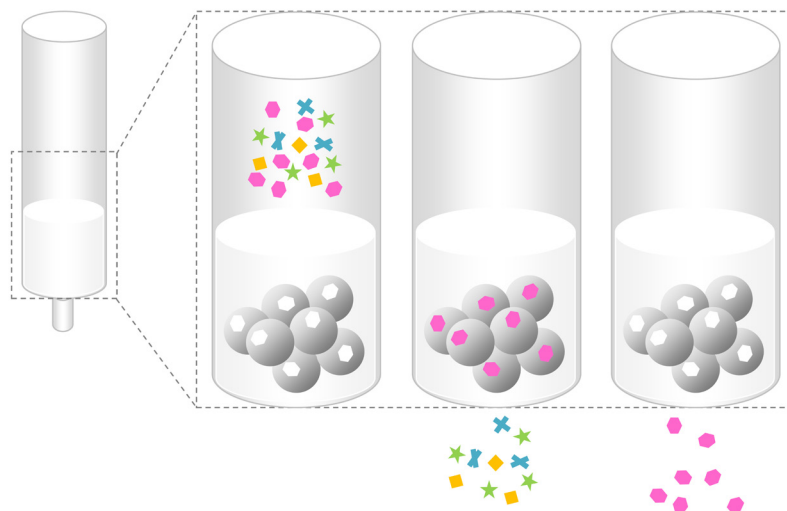
Figura 10. Esquema general del procedimiento MISPE: A) carga de muestra, B) retención del analito en el MIP y eliminación de interferencias de la columna C) elución del analito retenido.

Como en todo proceso de tratamiento de muestra, son varios los factores que intervienen en la eficacia de la SPE, desde la naturaleza de la muestra a la proporción MIP:muestra o las condiciones de trabajo. Por ejemplo, si la muestra líquida es poco compleja, es habitual el tratamiento de grandes volúmenes, pero si es heterogénea o viscosa, es necesario diluir para rebajar la presión en el sistema. Por otro lado, hay que tener en cuenta que cuando se emplean grandes cantidades de muestra o ésta es muy concentrada, a partir de cierto punto se interrumpe la retención en el MIP; es lo que se conoce como 'volumen de ruptura' y ocurre porque se ha

alcanzado la capacidad máxima de adsorción del MIP empaquetado. En cuanto a las condiciones experimentales, el pH es el factor más influyente en el proceso MISPE, tanto en la etapa de adsorción en el MIP como en la de elución, ya que a pHs superiores al valor de pK_a del analito, éste se encontrará en forma iónica y su adsorción se verá disminuida de la misma manera que pHs que garanticen la neutralidad del analito no servirán para eluirlo, es necesario ionizarlo para liberarlo de su unión al MIP.

1.2.4. Dispersión en fase sólida

La dispersión en fase sólida con MIPs (MIP-MSPD) puede considerarse una variación de la MISPE. La diferencia entre ambas se fundamenta en que la MISPE es una técnica de preparación de muestra para muestras líquidas o extractos orgánicos de muestras sólidas, mientras que la MSPD se aplica exclusivamente a muestras sólidas y semisólidas, directamente.

Al igual que en la MSPD tradicional, en la MIP-MSPD, la disrupción de la estructura de la matriz tiene lugar mediante fricción hasta homogenización sobre el soporte sólido, en este caso el MIP, con la ayuda de un mortero y un pistillo. La mezcla muestra-MIP se transfiere a continuación a un cartucho de tipo SPE con ayuda de un disolvente de arrastre para un mayor aprovechamiento de la mezcla, al tiempo que servirá como etapa de acondicionamiento del cartucho. El disolvente de arrastre debe por tanto garantizar que los analitos quedan retenidos en el MIP y eliminan en lo posible las interferencias de la matriz [155-158]. A continuación se

procede a la elución de los analitos retenidos en el MIP, seleccionando el eluyente conforme a los criterios explicados para esta etapa en MISPE.

En MIP-MSPD, uno de los parámetros determinantes de la eficacia del procedimiento es el tamaño de partícula del MIP. En general, se requieren tamaños del orden de varias decenas de μm de diámetro, para lograr un flujo adecuado de los distintos disolventes a través del cartucho, ya que si el particulado es muy pequeño, la compactación del relleno puede provocar un flujo demasiado bajo o incluso inexistente. En la aplicación de esta técnica también es importante la relación muestra:MIP, siendo ratios habituales los comprendidos entre 1:1 y 1:4. Esta relación se optimiza experimentalmente en cada aplicación. Las condiciones de pH condicionan la eficacia del proceso de la misma forma que en SPE.

1.3. REFERENCIAS

[1] G. Wulff, A.A. Sarchan, Angew. Chem., Int. Ed. Engl. 11 (1972) 341

[2] G. Wulff, W. Vesper, J. Chromatogr. 167 (1978) 171

[3] G. Wulff, M. Minarik, J. Liq. Chromatogr. 13 (1990) 2987

[4] A.G. Mayes, M.J. Whitcombe, Adv. Drug Deliver. Rev. 57 (2005) 1742

[5] B. Sellergren, L.I. Andersson, J. Org. Chem. 55 (1990) 3381

[6] M.J. Whitcombe, M.E. Rodriguez, P. Villar, E. Vulfson, J. Am. Chem. Soc. 117 (1995) 7105

[7] R. Arshady, K. Mosbach, Makromol. Chem. 182 (1981) 687

[8] O. Norrlöw, M. Glad, K. Mosbach, J. Chromatogr. 299 (1984) 29

[9] C. Alexander, H.S. Andersson, L.I. Andersson, R.J. Ansell, N. Kirsch, I.A. Nicholls, J. O'Mahony, M.J. Whitcombe, J. Mol. Recognit. 19 (2006) 106

[10] R.F. Venn, R.J. Goody, en: E. Reid, H.M. Hill, I.D. Wilson (Eds.), Methodological Surveys in Bioanalysis of Drugs, Royal Society of Chemistry 25 (1998)13

[11] P. Martin, I.D. Wilson, G.R. Jones, K. Jones, en: E. Reid, H.M. Hill, I.D. Wilson (Eds.), Methodological Surveys in Bioanalysis of Drugs, Royal Society of Chemistry, 25 (1998) 21

[12] L.I. Andersson, Analyst 125 (2000) 1515

[13] V. Pichon, F. Chapuis-Hugon, Anal. Chim. Acta 622 (2008) 48–61

[14] Y. Watabe, T. Kubo, T. Nishikawa, T. Fujita, K. Kaya, K. Hosoya, J. Chromatogr. A 1120 (2006) 252

[15] M. Kempe, L. Fischer, K. Mosbach, J. Mol. Recog. 6 (1993) 25

[16] 0. Ramstrom, L.I. Andersson, K. Mosbach, J. Org. Chem. 58 (1993) 7562

[17] H. Zhang, Polymer 55 (2014) 699

[18] P.A.G. Cormack, A.Z. Elorza, J. Chromatogr. B 804 (2004) 173

[19] B. Sellergren, Molecularly Imprinted Polymers: Man-made mimics of antibodies and their applications in anaytical chemistry, Elsevier, Amsterdam (Holanda), 2001

[20] E. Benito-Peña, Tesis Doctoral, Universidad Complutense de Madrid, 2006

[21] M. Kempe, Anal. Chem. 68 (1996) 1948

[22] V. Pichon, K. Haupt, J. Liq. Chromatogr. Related Technol. 29 (2006) 989

[23] G. Wulff, J. Vietmeier, H.G. Poll, Makromol. Chem. 188 (1987) 731

[24] M. Sibrian-Vazquez, D.A. Spivak, J. Polym. Sci. A: Polym. Chem. 42 (2004) 3668

[25] B. Sellergren, Macromol. Chem. 190 (1989) 2703

[26] M. Ávila, M. Zougagh, A. Escarpa, Á. Ríos, Trend. Anal. Chem. 27 (2008) 54

[27] J. Haginaka, J. Chromatogr. B 866 (2008) 3

[28] M.E. Díaz-garcía, A. Fernández-González, Molecularly imprinted polymers, Encyclopedia of Analytical sciences, 2ª Ed., Elsevier Ltd., 2005, 172

[29] K. Mosbach, O. Ramstron, BioTechnology 14 (1996) 163

[30] G. Wulff, Angew. Chem. Int. Ed. Engl. 34 (1995) 1812

[31] N. Pérez-Moral, A.G. Mayes, Anal. Chim. Acta 504 (2004) 15

[32] O. Bruggemann, K. Haupt, L. Ye, E. Yilmaz, K. Mosbach, J. Chromatogr. A 889 (2000) 15

[33] L. Ye, P.A.G. Cormack, K. Mosbach, Anal. Commun. 36 (1999) 35

[34] R. Carabias-Martínez, E. Rodríguez-Gonzalo, E. Herrero-Hernández, M.E. Díaz-García, J. Sep. Sci. 28 (2005) 453

[35] E. Turiel, J.L. Tadeo, P.A.G. Cormack, A. Martin-Esteban, Analyst 130 (2005) 1601

[36] E. Lendoiro, A. de Castro, H. Fernández-Vega, M.C. Cela-pérez, J.M. López-Vilariño, M.V. González-Rodriguez, A. Cruz, M. López-Rivadulla, Anal. Bioanal. Chem. 406 (2014) 3589

[37] M.C. Cela-Pérez, THC nuevo

[38] R.H. Schmidt, A.S. Belmont, K. Haupt, Anal. Chim. Acta 542 (2005) 118

[39] M.C. Cela-Pérez, M.M. Castro-López, A. Lasagabáster-Latorre, J.M. López-Vilariño, M.V. González-Rodríguez, L.F. Barral Losada; Anal. Chim. Acta 706 (2011) 275

[40] R.H. Schmidt, K. Mosbach, K. Haupt, Adv. Mater. 16 (2004) 719

[41] R.H. Schmidt, K. Haupt, Chem. Mater. 17 (2005) 1007

[42] R.H. Schmidt, T. Zhao, J.B. green, D.J. Dyer, Langmuir 18 (2002) 1281

[43] K. Haupt, K. Noworyta, K. Mosbach, Anal. Commun. 36 (1999) 391

[44] Cela-Pérez, M.C., López-Vilariño, J.M., González-Rodríguez, M.V, Proc. IEEE Sensors, (2011) 1740

[45] H.S. Andersson, I.A. Nicholls, Bioorg. Chem. 25 (1997) 203

[46] B. Sellergren, M. Lepistö, K. Mosbach, J. Am. Chem. Soc. 110 (1988) 5853

[47] M.J. Whitcombe, L. Martin, E.N. Vulfson, Chromatographia 47 (1998) 457

[48] L. Idziak, A. Benrebouh, F. Deschamps, Anal. Chim. Acta 435 (2001) 137

[49] J.G. Karlsson, B. Karlsson, L.I. Andersson, I.A. Nicholls, Analyst 129 (2004) 456

[50] S.A. Piletsky, K. Karim, E.V. Piletska, C.J. Day, K.W. Freebairn, C. Legge, A.P.F. Turner, Analyst 126 (2001) 1826

[51] K. Farrington, E. Magner, F. Regan, Anal. Chim. Acta 566 (2006) 60

[52] J. O'Mahony, K. Nolan, M.R. Smyth, B. Mizaikoff, Anal. Chim. Acta 534 (2005) 31

[53] A. Mollinelli, J. O'Mahony, K. Nolan, M.R. Smyth, M. Jakusch, B. Mizaikoff, Anal. Chem. 77 (2005) 5196

[54] W.M. Mullett, M.F. Dirie, E.P.C. Lai, H. Guo, X. He, Anal. Chim. Acta, 414 (2000) 123

[55] A. Lasagabáster-Latorre, M.C. Cela-Pérez, S. Fernández-Fernández, J.M. López-Vilariño, M.V. González-Rodríguez, React. Funct. Polym. 91-92 (2015) 51

[56] J.Y. Wang, F. Liu, Z.I. Xu, K. Li, Chem. Eng. Sci. 65 (2010) 3322

[57] D.J. Duffy, K. Das, S.L. Hsu, J. Penelle, V.M. Rotello, H.D. Stidham, J. Am. Chem. Soc. 124 (2002) 8290-8296

[58]C.Y. Huang, Method. Enzymol. 87 (1982) 509-525

[59] J.M. Bosque-Sendra, E. Almansa-López, A.M. García-Campaña, L. Cuadros-Rodríguez, Anal. Sci. 19 (2003) 1431

[60] H.A. Benesi, J.H. Hildebrand, J. Am. Chem. Soc., 71 (1949) 2703

[61] G. Lancelot, J. Am. Chem. Soc. 99 (1977) 7037

[62] I. Idziak, A. Benrebouh, F. Deschamps, Anal. Chim. Acta 435 (2001) 137

[63] M. Quaglia, K. Chenon, A.J. Hall, E. De Lorenzi, B. Sellergren, J. Am. Chem. Soc. 123 (2001) 2146

[64] G. Wulff, Chem. Rev. 102 (2002) 1

[65] Connors, K.A., Binding Constants: The Measurement of Molecular Complex Stability, 1987

[66] I. Chianella, S.A. Piletsky, I.E. Tothill, B. Chen, A.P.F. Turner, Biosens. Bioelectron. 18 (2003) 119

[67] S. Subrahmanyam, S.A. Piletsky, E.V. Piletska, B.N. Chen, K. Karim, A.P.F. Turner, Biosens. Bioelectron. 16 (2001) 631

[68] S.A. Piletsky, K. Karim, E.V. Piletska, C.J. Day, K.W. Freebairn, C. Legge, A.P.F. Turner, Analyst 126 (2001) 1826

[69] I. Chianella, M. Lotierzo, S.A. Piletsky, I.E. Tothill, B.N. Chen, K. Karim, A.P.F. Turner, Anal. Chem. 74 (2002) 1288

[70] A. Guerreiro, A. Soares, E. Piletska, B. Mattiasson, S. Piletsky, Anal. Chim. Acta 612 (2008) 99

[71] T. Takeuchi, D. Fukuma, J. Matsui, Anal. Chem. 71 (1999) 285

[72] F. Lanza, B. Sellergren, Anal. Chem. 71 (1999) 2092

[73] T. Takeuchi, A. Seko, J. Matsui, T. Mukawa, Sci. Technolog. 29 (2001) 1

[74] B. Dirion, F. Lanza, B. Sellergren, C. Chassaing, R. Venn, C. Berggren, Chromatographia 56 (2002) 237

[75] T. Takeuchi, D. Fukuma, J. Matsui, T. Mukawa, Chem. Lett. 30 (2001) 530

[76] J. Cederfur, Y.X. Pei, Z.H. Meng, M. Kempe, J. Com. Chem. 5 (2003) 67

[77] B. Dirion, Z. Cobb, E. Schillinger, L.I. Andersson, B. Sellergren, J. Am. Chem. Soc. 125 (2003) 15101

[78] T. Muhammad, L. Cui, W. Jide, E.V. Piletska, A.R. Guerreiro, S.A. Piletsky, Anal. Chim. Acta 709 (2012) 98

[79] C. Baggiani, C. Giovannoli, L. Anfossi, C. Passini, P. Baravalle, G. Giraudi, J. Am. Chem. Soc. 134 (2012) 1513

[80] E.V. Piletska, A.R. Guerreiro, M. Romero-Guerra, I. Chianella, A.P.F. Turner, S.A. Piletsky, Anal Chim. Acta 607 (2008) 54

[81] I. Bakas, N.B. Oujii, G. Istamboulié, S. Piletsky, E. Piletska, E. Ait-Addi, I. Ait-Ichou, T. Noquer, R. Rouillon, Talanta 125 (2014) 313

[82] L. Chen, W. Ji, W. Duan, X. Wang, Q. Gao, Y. Geng, L. Huang; J. Chromatogr. B 965 (2014) 1

[83] D.A. Spivak, Adv. Drug Deliver. Rev. 57 (2005) 1779

[84] S.H. Cheong, S. McNiven, A. Rachkov, R. Levi, K. Yano, I. Karube, Macromolecules 30 (1997) 1317

[85] R.J. Umpleby, R.C. Baxter, A.M. Rampey, G.T. Rushton, Y. Chen, K.D. Shimizu; J. Chromatogr. B 804 (2004) 141

[86] T.Y. Guo, Y.Q. Xia, G.J. Hao, M.D. Song, B.H. Zhang; Biomaterials 25 (2004) 5905

[87] J. Pan, X. Zou, X. Wang, W. Guan, Y. Yan, J. Han; Chem. Eng. J. 162 (2010) 910

[88] A.M. Rampey, R.J. Umpleby, G.T. Rushton, J.C. Iseman, R.N. Shah, K.D. Shimizu; Anal. Chem. 76 (2004) 1123

[89] R.J. Umpleby II, S.C. Baxter, M. Bode, J.K. Berch, R.N. Shah, K.D. Shimizu, Anal. Chim. Acta 435 (2001) 35

[90] R.J. Umpleby II, M. Bode, K.D. Shimizu, Analyst 125 (2000) 1261

[91] D.L. Hunston; Anal. Biochem. 63 (1975) 99

[92] M.C. Cela-Pérez, L. Barbosa-Pereira, X. Vecino, M. Pérez-Ameneiro, A. Lasagabaster-Latorre, J.M. López-Vilariño, M.V. González-Rodríguez, A.B. Moldes, J.M. Cruz, Talanta 135 (2015) 58

[93] J.A. García-Calzón, M.E. Díaz-García; Sens. Actuators B 123 (2007) 1180

[94] I.A.W. Tan, A.L. Ahmad, B.H. Hameed; J. Hazard. Mater. 164 (2009) 473

[95] C.Y. Chen, C.H. Wang, A.H. Chen; Talanta 84 (2011) 1038

[96] B. Subramanyam, D. Ashutosh, Desalination 249 (2009) 914

[97] Z.J. Wu, H. Joo, K. Leel, Chem. Eng. J. 112 (2005) 227

[98] Q.S. Liu, T. Zheng, P. Wang, J.P. Jiang, N. Li, Chem. Eng. J. 157 (2010) 348

[99] W.J. Weber, J.C. Morris, J. Sanitary Eng. Division ASCE 89 (1963) 31

[100] I.A.W. Tan, A.L. Ahmad, B.H. Hameed, J. Hazard. Mater. 164 (2009) 473

[101] W. Liu, J. Zhang, C. Zhang, Y. Wang, Y. Li, Chem. Eng. J. 162 (2010) 677

[102] B. Sellergren, K.J. Shea, J. Chromatogr. 635 (1993) 31

[103] V.K. Sarin, S.B.H. Kent, R.B, J. Am. Chem. Soc. 102 (1980) 5463

[104] N.W. Turner, E.V. Piletska, K. Karim, M. Whitcombe, M. Malecha, N. Magan, C. Baggiani, S.A. Piletsky, Biosens. Bioelectron. 20 (2004) 1060

[105] B. Sellergren, K. J. Shea, J. Chromatogr. 635 (1993) 31

[106] N. Holland, J. Frisby, E. Owens, H. Hughes, P. Duggan, P. McLoughlin, Polymer 51 (2010) 1578

[107] H. Kim, D.A. Spivak, J. Am. Chem. Soc. 125 (2003) 11269

[108] K.J. Shea, D.Y. Sasaki, J. Am. Chem. Soc. 113 (1991) 4109

[109] L.C. Mendes, A.D. Tedesco, M.S. Miranda, Polym. Test. 24 (2005) 418

[110] M.C. Cela-Pérez, A. Lasagabáster-Latorre, M.J. Abad-López, J.M. López-Vilariño, M.V. Gónzalez-Rodríguez, Vib. Spectrosc. 65 (2013) 74

[111] O. Brüggemann, Biomol. Eng. 18 (2001) 1

[112] M. Kempe, K. Mosbach, J. Chromatogr. A 694 (1995) 3

[113] F.G. Tamayo, M.M. Titirici, A. Martin-Esteban., B. Sellergren, Anal. Chim. Acta 542 (2005) 38

[114] J. Haginaka, C. Kagawa, J. Chromatogr. A 948 (2002) 77

[115] T. Takeuchi, J.Haginaka, J. Chromatogr. B 728 (1999) 1

[116] L. Schwitz, P. Spegel, S. Nilsson, Electrophoresis 22 (2001) 4053

[117] E. Turiel, A. Martin-Esteban, Anal. Bioanal. Chem. 378 (2004) 1876

[118] Y. Xu, Z. Liu, H. Wang, C. Yan, R. Gao, Electrophoresis 26 (2005) 804

[119]] M. Ávila, M. Zougagh, A. Rios, A. Escarpa, Trends Anal. Chem. 27 (2008) 54

[120] M.C. Blanco-López, M.J. Lobo-Castanon, A.J. Miranda-Ordieres, P. Tuñón-Blanco, Trends Anal. Chem. 23 (2004) 36

[121] K. Haupt, K. Mosbach, Chem. Rev. 100 (2000) 2495

[122] F.L. Dickert, O. Hayden, Trends Anal. Chem. 18 (1999) 192

[123] D. Kriz, O. Ramstrom, K. Mosbach, Anal. Chem. 69 (1997) 345

[124] F.G. Tamayo, E. Turiel, A. Martin-Esteban, J. Chromatogr. A 1152 (2007) 32

[125] T. Pap, V. Horváth, A. Tolokán, G. Horvay, B. Sellergren, J. Chromatogr. A 973 (2002) 1

[126] E. Caro, N. Masqué, R.M. Marcé, F. Borrull, P.A.G. Cormack, D.C. Sherringon, J. Chromatogr. B 963 (2002) 169

[127] F. Chapuis, V. Pichon, F. Lanza, B. Sellergren, M.C. Hennion, J. Chromatogr. A 999 (2003) 23

[128] E. Caro, R.M. Marcé, F. Borrull, P.A.G. Cormack, D.C. Sherrington, Trends Anal. Chem. 25 (2006) 143

[129] B. Sellergren in Chiral Separation Techniques: A Practical Approach, G. Subramanina (Ed.), Wiley-VCH, Winheim (2001) 151

[130] H.F. Zou, X.D. Huang, M.L. Ye, Q.Z. Luo, J. Chromatogr. A, 954 (2002) 5

[131] E. Turiel, A. Martin-Esteban, J. Sep. Sci., 28 (2005) 719

[132] Z.S. Liu, C. Zheng, C. Yan, R.Y. Ga, Electrophoresis 28 (2007) 127

[133] C.Y. Liu, C.C. Lin, Electrophoresis 25 (2004) 3997

[134] P. Qu, J. Lei, R. Ouyang, H. Ju, Anal. Chem. 2009, 81, 9651–9656

[135] F. Dickert, M. Tortschanoff, W.E. Bulst, G. Fisherauer, Anal. Chem. 71 (1999) 4559

[136] J.L. Suárez-Rodríguez, M.E. Díaz-García, Anal. Chim. Acta, 405 (2000) 67

[137] S.A. Piletsky, E.V. Piletskaya, K. Yano, A. Kugimiya, A.V. Elgersma, R. Levi, V. Kahlow, T. Takeuchi, I. Karube, T.Y. Panesyuk, A.V. El'skaya, Anal. Lett. 29 (1996) 157

[138] Y. C. Chen, J. Brazier, M. Yan, P.R. Bargo, S.A. Prahl, Sensors and Actuators B 102 (2004) 107

[139] S.A. Piletsky, A.P.F. Turner, Electroanalysis 14 (2002) 317

[140] S. Huan, G. Shen, R. Yu, Electroanalysis 16 (2004) 1019

[141] U. Lange, N. V. Roznyatovskaya, V.M. Mirky, Anal. Chim. Acta 614 (2008) 1

[142] F.L. Dickert, O. Hayden, K.P. Halikias, Analyst 126 (2001) 766

[143] T. Kobayashi, Y. Murawaki, P.S. Reddy, M. Abe, N. Fujii, Anal. Chim. Acta 435 (2001) 141

[144] H. Liao, Z. Zhang, H. Li, L. Nie, S. Yao, Sensor. Actuat. B-CHEM 105 (2005) 176

[145] C.J. Percival, S. Stanley, M. Galle, A. Braithwaite, M.I. Newton, G. McHale, W. Hayes, Anal. Chem. 73 (2001) 4225

[146] J. Haginaka, J. Sep. Sci. 32 (2009) 1548

[147] M. Lasáková, P. Jandera, J. Sep. Sci. 32 (2009) 799

[148] B. Sellergren, A. Martin-Esteban, in: J. Pawliszyn, H.L. Lord (Editors), Handbook of Sample Preparation, John Wiley & Sons, Hoboken, New Jersey, USA, 2010, p. 445

[149] D. Stevenson, Trends Anal. Chem. 18 (1999) 154

[150] E. Caro, R.M. Marcé, P.A.G. Cormack, D.C. Sherrington, F. Borrull, J. Chromatogr., A 1047 (2004) 175

[151] I. Ferrer, F. Lanza, A. Tolokan, V. Horvath, B. Sellergren, G. Horvai, D. Barcelo, Anal. Chem. 72 (2000) 3934.

[152] Yuling Hu, Jialiang Pan, Kaige Zhang, Haixian Lian, Gongke Li, Trends Anal. Chem. 43 (2013) 37

[153] E. Caro, R.M. Marcé, P.A.G. Cormack, D.C. Sherrington, F. Borrull, J. Chromatogr., A 995 (2003) 233

[154] F. Chapius, V. Pichon, F. Lanza, B. Sellergren, M.C. Hennion, J. Chromatogr., B 804 (2004) 93

[155] S.A. Barker, J. Biochem. Biophys. Methods 70 (2007) 151

[156] E.M. Kristenson, L.Ramos, U.A.Th. Brinkman, Trends Anal. Chem. 25 (2006) 96

[157]] F. Qiao, H. Yan, J. Chromatogr. B 879 (2011) 3551

[158] H. Yan, H. Wang, J. Qiao, G. Yang, J. Chromatogr. A 1218 (2011) 2182

OBJETIVOS

2. OBJETIVOS

El objetivo de esta tesis doctoral es el **desarrollo de nuevas formulaciones de polímeros impresos de naturaleza no covalente y el estudio de sus posibilidades como material adsorbente en técnicas de preparación de muestra** para el análisis de diversas familias de compuestos en diferentes matrices.

Debido al gran número de factores que entran en juego en la polimerización y el diseño de MIPs, es necesario investigar en profundidad las formulaciones poliméricas posibles para garantizar la idoneidad del MIP en la aplicación posterior. Con esta finalidad, los objetivos parciales planteados han sido:

1. Desarrollo de metodologías de diseño de polímeros impresos en prepolimerización y/o postpolimerización para el cribado de las distintas formulaciones posibles y viables.

2. Desarrollo de metodologías de evaluación y caracterización postpolimerización que permitan predecir el comportamiento de los MIPs sintetizados en muestras reales a través de la determinación de las propiedades de enlace del MIP, el mecanismo de adsorción analito-MIP o determinadas características estructurales y morfológicas del material polimérico.

3. Desarrollo de una nueva estrategia de polimerización no covalente para la obtención de MIPs capaces de trabajar con matricres complejas y volúmenes de muestra mínimos en su aplicación como adsorbente en SPE, superando así las limitaciones propias de la técnica MISPE tradicional.

4. Síntesis de MIPs para la purificación y/o concentración de contaminantes emergentes, drogas de abuso e indicadores de calidad alimentaria en medios acuosos, y para diversos aditivos plásticos en medios orgánicos.

5. Desarrollo y optimización de metodologías MISPE y MIP-MSPD que prueben la aplicabilidad de los MIPs en el tratamiento de muestra previo al análisis.

RESULTADOS

3. RESULTADOS

El conjunto de publicaciones derivadas del trabajo realizado para alcanzar los objetivos planteados se presenta en dos bloques o capítulos diferenciados.

El primer capítulo agrupa las publicaciones en las que se describen y desarrollan las etapas de diseño, evaluación y caracterización de polímeros impresos. Los tres primeros trabajos explican la utilización y el aprovechamiento de distintas técnicas espectroscópicas tanto en prepolimerización como en postpolimerización, mientras que los dos que cierran el capítulo profundizan en la evaluación del reconocimiento molecular y la caracterización de MIPs en postpolimerización.

El segundo capítulo está integrado por tres publicaciones en las cuales los MIPs se incorporan como materiales adsorbentes en técnicas separativas convencionales para el tratamiento de matrices de distinta naturaleza. Dentro de este bloque destaca la preparación de una nueva configuración de MIPs y el desarrollo y validación de la metodología MISPE derivada, para la extracción y concentración de cannbinoides en fluidos biológicos.

CAPÍTULO 1: DISEÑO, EVALUACIÓN Y CARACTERIZACIÓN DE POLÍMEROS IMPRESOS

'A study of competitive molecular interaction effects on imprinting of molecularly imprinted polymers'

'Insight into BPA-4-vinylpyridine interactions in molecularly imprinted polymers using complementary spectroscopy techniques'

'Selective removal of ATP degradation products from food matrices I: Design and characterization of a dummy molecularly imprinted specific sorbent for Hypoxanthine'

'Synthesis and characterization of bisphenol-A imprinted polymer as a selective recognition receptor'

'Impact of functional cross-linker on recognition properties of a Bisphenol-A imprinted polymer film for coating a Quartz Crystal Microbalance'

3.1. CAPÍTULO 1: DISEÑO, EVALUACIÓN Y CARACTERIZACIÓN DE POLÍMEROS IMPRESOS

Artículo 1: 'A study of competitive molecular interaction effects on imprinting of molecularly imprinted polymers'

Artículo 2: 'Insight into BPA-4-vinylpyridine interactions in molecularly imprinted polymers using complementary spectroscopy techniques'

Artículo 3: 'Selective removal of ATP degradation products from food matrices I: Design and characterization of a dummy molecularly imprinted specific sorbent for Hypoxanthine'

Artículo 4: 'Synthesis and characterization of bisphenol-A imprinted polymer as a selective recognition receptor'[*]

Artículo 5: 'Impact of functional cross-linker on recognition properties of a Bisphenol-A imprinted polymer film for coating a Quartz Crystal Microbalance'[**]

---

[*] Trabajo desarrollado durante la realización del Máster que permite el acceso a los estudios de Doctorado (2011)

[**] 'Trabajo publicado en el libro de 'Proceedings' en 10th IEEE SENSORS Conference 2011, SENSORS 2011, Limerick-Ireland, durante la realización del Máster que permite el acceso a los estudios de Doctorado (2011)

A STUDY OF COMPETITIVE MOLECULAR INTERACTION EFFECTS ON IMPRINTING OF MOLECULARLY IMPRINTED POLYMERS

M.C. Cela-Pérez[1], A. Lasagabáster-Latorre[1,2],
M.J. Abad-López[1], J.M. López-Vilariño[1],
M.V. González-Rodríguez[1]

[1] Grupo de Polímeros, Centro de Investigacións Tecnolóxicas, Universidade da Coruña, Campus de Esteiro s/n, Ferrol 15403, Spain, Tel.: +34 981 337 400 3051/3485; fax: +34 981 337 416, email: victoria.gonzalez.rodriguez@udc.es, iquimica@udc.es

[2] Dpto Química Orgánica I, Escuela de Óptica, Universidad Complutense de Madrid, Arcos de Jalón, n° 118, Madrid 28037, Spain, email: aurora@ucm.es

85

ABSTRACT

The work herein reports on an approach to obtain molecularly imprinted polymers (MIPs) for Atmer 129, an antistatic added to polyolefins and a previously non imprinted template with intra molecular H-bonding capability. The template-monomer interactions occurring in pre and postpolymerization media were analyzed by FTIR and ATR-FTIR, respectively. After the prepolymerization study, the synthesis conditions were discussed and suitable porogens and potential template:monomer stoichiometries were suggested. The imprinting efficiency and selectivity of MIPs were evaluated in batch assays by HPLC or UPLC and compared with thermal behavior and morphological characteristics checked by Thermogravimetric Analysis (TGA), Differential Scanning Calorimetry (DSC) and Scanning Electron Microscopy (SEM). The best results were obtained for MIPs synthesized at 60 ◦C. A relation between imprinting effect and template shape recognition was suggested by selectivity studies. The major conclusion, which has been drawn from FTIR and DSC studies, is that independently of the H-bonding strength between Atmer 129 and monomer, the template started to crystallize out during the polymerization reaction, thus reducing the imprinting effect.

Keywords: *Molecularly imprinted polymers, H-bond, Intra- and self-intermolecular interactions, Prepolymerization and polymerization complex, Imprinting effect.*

1. INTRODUCTION

MIPs have been a focus of research as a consequence of their molecular recognition properties and are now receiving considerable attention for applications that require binding and release of specific molecular species [1-3]. The relative ease with which these polymers may be prepared, the wide range of chemical compounds which could be imprinted and the apparent mechanical and chemical stability of these polymers have made them extremely attractive in numerous areas ranging from chromatography, assays, sensor technology, catalysis to controlled delivery systems [4-10].

MIP polymerizations follow a general procedure. In a solution of appropriate functional monomers, a template molecule (or the molecule to be recognized) is added, and the solution is mixed. This mixing allows for "self-assembly" of the template with the complementary monomers to form a pre-polymerization complex. The functional monomer contains specific chemical structures designed to interact with the template either by covalent chemistry, non covalent chemistry or both. The polymerization occurs by free radical initiation in the presence of a crosslinking monomer and an appropriate solvent. The template can then be extracted from the formed polymer usually via diffusion, and the structure formed is a porous matrix with specific recognition elements for the template molecule. Thus, MIP creates stereo-specific threedimensional binding cavities based on the template molecule of interest [6, 7, 11-18].

88

Initially, any chemical compound could be made a corresponding MIP. However, the efficiency of the imprinting process is reported only for a limited number of compounds. Different factors play an important role, such as the forming of a stable complex during MIP preparation, the disruption of monomer–template complexes by the cross-linker or porogen and competitive molecular interactions if the template or the functional monomer forms intra-or/and self-intermolecular interactions. The latter can affect the proportion of the template–monomer complex because the use of high template concentrations in the prepolymerization solution is recommended to achieve high imprinting values [1].

Thus, it is essential to investigate the interactions between the template, functional monomers and cross-linker both in the pre-polymerization and polymerization stages. In this way, FT-IR spectroscopy has demonstrated to be a valuable tool for deeper investigation of the binding mechanism in molecularly imprinted polymers with samples in solution and in the solid state [19].

The goal of the present work is to evaluate and characterize several non-covalent MIPs with specific recognition for an antistatic additive, Atmer 129 (glycerol monostearate; CAS [31566-31-1]). Actually, Atmer 129 migrates fast to the polyolefin surface. The antistatic effect is noticed very quickly, but only for a short period of time. In view of that, this study is focused on the first stage in the development of a potential system to release Atmer 129 to plastic surfaces in the long term. As a non-ionic surfactant, Atmer

129, possesses a polar (hydrophilic) and a non-polar (hydrophobic) region. The polar region of Atmer 129 is provided by glycerol and it is able to form intra- or/and self-intermolecular interactions.

A systematic study of the factors influencing the polymerization yields and recognition capabilities was conducted. The template–monomer interactions occurring in pre- and post-polymerization media were studied by FTIR and UV/Vis Spectroscopy and ATR-FTIR, respectively. Chromatographic evaluation was used to analyze the imprinting efficiency and the selectivity of MIPs in comparison with three structurally related compounds. The thermal behavior and morphology of the MIPs providing the best performance were further evaluated by TGA, DSC and SEM.

2. MATERIALS AND METHODS

2.1. MATERIALS

MAA, EGDMA and the initiator, AIBN, were purchased from Fluka (Buchs, Switzerland). Atmer 129 was from Ciba (Basel, Switzerland). TRIM, 4-Vpy, acetone, acetic acid, α-tocoferol, linoleic acid and oleic acid were supplied by Sigma–Aldrich (Steinheim, Germany) and 2-propanol and THF of HPLC grade for instrumental analysis and ACN and dichloromethane for the synthesis of polymers, rebinding, elution and selectivity assays were from Merck (Darmstadt, Germany). The chemical structures of the template molecule (Atmer 129), functional monomers (MAA and 4-Vpy) and crosslinkers (EGDMA and TRIM) are shown in Fig. 1. Visiprep™-DL Solid

Phase Extraction Vacuum Manifolds, equipped with integral flow control valves and disposable Teflon® flow control valve liners, were from SUPELCO (Bellefonte, PA, USA). The solid phase extraction tubes were 6 mL pre-fritted polypropylene tubes and the frits employed to pack the columns were 6 Ml polyethylene frits (20 µm porosity).
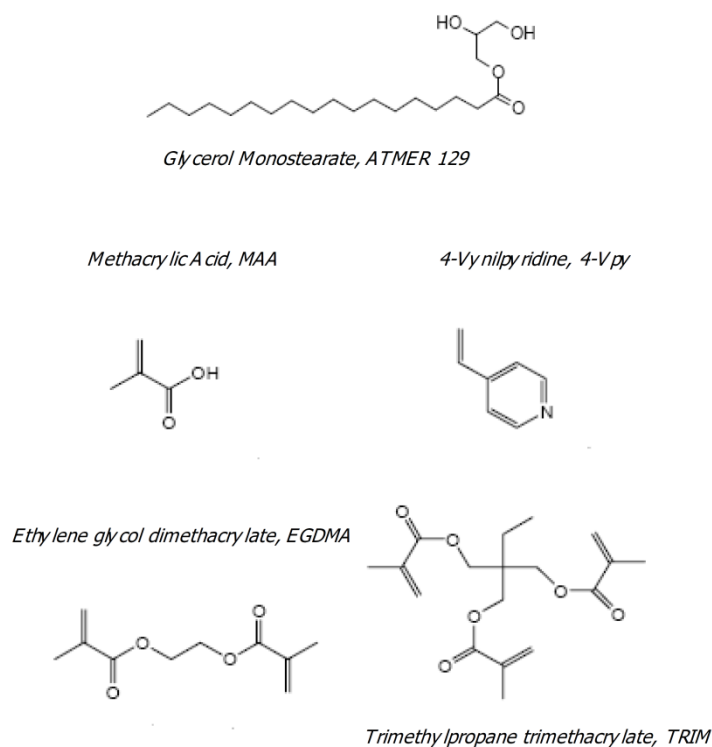
Glycerol Monostearate, ATMER 129

Methacrylic Acid, MAA   *4-Vynilpyridine, 4-Vpy*

Ethylene glycol dimethacrylate, EGDMA

Trimethylpropane trimethacrylate, TRIM

Fig. 1. Chemical structures of the template molecule (ATM), functional monomers (MAA and 4-Vpy) and crosslinkers (EGDMA and TRIM) used in the polymerization.

2.2. INSTRUMENTS

2.2.1. Liquid chromatography

HPLC analyses were performed in a Waters Alliance 2695 system equipped with a quaternary pump, autosampler and a DAD detector (Waters, Milford, MA, USA). Chromatographic separation was performed on a 150 x 3.0 mm HPLC stainless steel column (3.5 μm SunFireTM C_{18}) kept at 50 ∘C. The gradient elution program consisted of a binary mobile phase at a flow rate of 0.3 mL min^{-1} made up of 2-propanol:water (60:40) (Solvent A) and 2-propanol (Solvent B). The gradient elution was programmed as follows: 0-2 min, 100 to 0% A, 2-15, 100% B, 15-17 min return to the initial condition, 17–20 min equilibrium of the column. The amount injected was 20 μL and chromatograms were recorded at 220 nm. Fig. 1. Chemical structures of the template molecule (ATM), functional monomers (MAA and 4-Vpy) and crosslinkers (EGDMA and TRIM) used in the polymerization. UPLC analyses were carried out using an Acquity system from

Waters equipped with a gradient pump and an automatic injector. A 50 x 2.1 mm Acquity UPLC stainless steel column (1.7 μm BEH C_{18}) operating at 35 ∘C was used (Waters). Needle-over-fill injection mode was selected. The gradient binary mobile phase consisted of solvent A: water (100%) and solvent B: THF (100%) and it was programmed as follows: initial = 50% A + 50% B; 0-3.00 min linear gradient to 0% A + 100% B; 3-3.5 min return to initial condition; 3.5-4 min equilibrium of the column. The flow rate was 0.4 mL min^{-1} and the injection volume was 3 μL. An ELSD was used; the pressure of nebulizer gas was maintained at 40 psi, and the evaporation temperature was set at 50 ∘C. The signal acquired from both detectors was

recorded by personal computers running Empower 2 software (Waters). All solvents were passed by 0.2 µL filters.

The chromatographic methods were adapted from procedures previously developed in the laboratory [20].

2.2.2. ATR-FTIR spectroscopy

The IR data were recorded on a Bruker IR PS 15 spectrometer. The transmission/absorption measurements of the pre-polymerization mixtures were performed in a thin-film liquid cell at room temperature with a 1 mm Teflon spacer and CaF_2 windows (Spepac) in the spectral range of 4000-900 cm^{-1}. The spectra were the results of 100 coadded interferograms at a spectral resolution of 2 cm^{-1}.

The FTIR analysis of solid samples was performed in ATR mode by using the above mentioned spectrometer equipped with a thermostated MK II Golden GateTM Diamond 45◦ ATR accessory. The samples were pulverized into fine powder and compressed onto the ATR crystal with the Sapphire Anvil (10531). The spectra were the results of 100 coadded interferograms at 2 cm^{-1} resolution between 4000 and 400 cm^{-1}. Owing to the hygroscopic character of these copolymers, the study was carried out after heating at 55 ◦C during 15 min to avoid interferences with water bands and H-bonding due to water vapor sorption.

2.2.3. UV–Vis spectroscopy

93

UV–Vis absorption spectra were recorded on a Cary 100 Conc double-beam UV-Vis Spectrophotometer (Varian, USA) at 0.2 cm^{-1} resolution between 200 and 400 nm.

2.2.4. Thermal study

The DSC traces and the TGA were obtained to survey the glass transition temperature and thermal stability of the polymers.

TGA was performed with a Perkin Elmer TGA-7 microbalance coupled with a 1022 Perkin Elmer microprocessor. The microbalance was calibrated making use of the Curie points of perkalloy and nickel. Dynamic experiments were conducted under Argon atmosphere. The heating rate was 10 ◦C min^{-1}. The temperature range of the experiments was from room temperature to 600 ◦C. The T_{deg} was measured in the onset point of the loss mass curve.

The DSC measures were performed using 5-10 mg of the samples under an atmosphere of nitrogen gas. The samples were first heated to 100 ◦C and held at that temperature for 5 min to remove the thermal history. Then the samples were cooled to -50 ◦C at the rate of 20 ◦C min^{-1}, held for 5 min, and again heated from -50 to 250 ◦C at 20 ◦C min^{-1} (second scan). Glass transition values (T_g) were taken as the midpoint of transition in the second scan of DSC thermograms.

2.2.5. Morphology observation

The surface morphology of the particles was characterized by SEM, JEOL JSM-6400. The microscope has an accelerating voltage from 0.2 to 30 kV and provides a theoretical resolution of 3.5 nm at 8 mm working distance with a magnification range of 20-300000X. Samples were sputter-coated with gold before SEM analysis to make them conductive.

3. THEORY/CALCULATION

3.1. PREPOLYMERIZATION STUDIES

In this work, the mechanism of interaction between Atmer 129 and functional monomers 4-Vpy or MAA was explored by transmission FTIR and UV-spectroscopy. CH_2Cl_2 and CCl_4:CH_2Cl_2 (9:1) were the solvents of choice for FTIR studies in order to facilitate the observation of H-bonding [21] while the UV spectroscopy study was conducted in the porogen solvents, CH_2Cl_2 and acetone:CAN (3:1) mixture.

Firstly, in order to investigate how the spectral behavior of the template varies with concentration and type of solvent, several solutions of increasing Atmer 129 concentration (0.002-0.009 M and 0.018 M) were prepared in a mixture of CCl_4:CH_2Cl_2 (9:1) and in CH_2Cl_2. Secondly, the fundamental interactions of Atmer 129 with the monomers, MAA or 4-Vpy, in the prepolymerization stage were studied in CH_2Cl_2. The concentration chosen to evaluate the Atmer 129:4-Vpy system was identical to the prepolymerization mixture (Atmer 129 (0.018 M):4-Vpy (0.072 M), 1:4). To study the interactions of Atmer 129 and MAA lower concentrations had

to be used in order to avoid signal saturation. Five solutions with a constant template concentration of 0.004 M were prepared while increasing the concentration of the monomer from 0 to 4 molar equivalents. An analogous set of solutions of MAA alone was recorded for subtraction spectral purposes.

UV/Vis Jobs plots were used to confirm the stoichiometry of the Atmer 129:monomer complexes. 5 x 10^{-3}M stock solutions of template and monomer were prepared in CH_2Cl_2 and acetone:ACN (3:1); then a set of 10 mL solutions was prepared by mixing different portions of the template and the monomer. The mole fraction was varied from 0 to 1 and the total concentrations of Atmer 129 and monomer were kept constant at 1 x 10^{-4} M. The spectra of the above solutions were recorded by using the corresponding pure solvents as blank references, and used to construct the plot.

3.2. PREPARATION AND CHARACTERIZATION OF MIPS

Eighteen Atmer 129 imprinted polymers were synthesized by precipitation polymerization with 0.734 mmol of Atmer. Three T:M:C molar ratios were studied (1:1:5, 1:4:20 and 1:6:30). In all cases, the prepolymerization mixture was dissolved in the porogen solvent (acetone, CH_2Cl_2 or a mixture of acetone and ACN) (Table 1). Then, the crosslinker (EGDMA or TRIM) and the initiator (AIBN, 0.341 mmol) were added. The solutions were purged with N_2 for 5 min in order to remove oxygen. Afterwards, glasswares with solutions were placed in the UV photoreactor at 4, 28 ∘C or immersed in a

thermostatic water bath at 60 ∘C and left during 24 h for the polymerization to proceed. After polymerization, MIPs were dried and weighted. Precipitates with relatively uniform particle size were obtained, which avoided crushing, grinding and sieving steps.

In order to remove the template, the remaining un-reacted monomers and soluble oligomers, the collected polymers were extracted with 6 mL of the porogen solvent, followed by several volumes of acidic porogen solvent until no Atmer 129 could be detected by HPLC-PDA in the eluting solution.

As a control, NIPs were prepared by the above procedure except that the template was not added.

3.2.1. ATR polymer characterization

3.2.1.1.Major bands

Fig. 2 show representative ATR spectra of the imprinted and control copolymers prepared with EGDMA-co-MAA and EGDMA-co-4Vpy, together with an Atmer 129 powdered sample. The main characteristics of the template are briefly discussed first (Fig. 2a): the broad absorption between 3660 and 3050 cm^{-1} is attributed to the stretching vibrations of intra- and intermolecular H-bonded OH groups (v_{OH}); the sharp absorption bands at 2916 and 2850 cm^{-1}, correspond to the stretching vibrations of methyl and methylene groups, respectively, and a single band is observed at the carbonyl stretching region ($v_{C=O}$) at 1729 cm^{-1}. The broad absorption at

the hydroxyl stretching region is barely detected in the polymerization mixture; therefore, the band at 2850 cm^{-1} which does not overlap any bands in the polymer provides an unambiguous means of identifying the presence of Atmer 129 in the MIPs (Fig. 2b and **d**).

Concerning the polymers (Fig. 2b-e), the presence of three significant bands at 1725 cm^{-1} ($\upsilon_{C=O}$), 1245 and 1140 cm^{-1} (asymmetric and symmetric (υ_{C-O-C}) support the existence of poly (EGDMA). MIPs and NIPs synthesized with TRIM exhibit basically the same pattern. A small band at 1638 cm^{-1} is allotted to the stretching vibration of C=C unreacted methacrylate groups ($\upsilon_{C=C}$).

In addition, the characteristic bands due to the σC=N of the pyridine ring, at 1597 and 1558 cm^{-1}, are observed in the polymers with 4-Vpy monomer (Fig. 2d and e). The Atmer band at 2850 cm^{-1} is detected in original MIPs except in the polymers synthesized at 60 ∘C. The band vanished after washing and drying, implying that all template molecules have leached out.

Table 1. Composition of the produced polymers and methods of preparation.

Polymer	Template (T) (0.2620 g)	Functional monomer (M)	Cross-linker (C)	Ratio T:M:C	Porogen (40 mL)	Initiation method (5.599E-02 g AIBN)
MIP 1	ATMER 129				Acetone	
NIP 1	—					
MIP 2	ATMER 129	4-Vpy				
NIP 2	—	(0.0772 g)				
MIP 3	ATMER 129		EGDMA	1:1:5		
NIP 3	—		(0.7361 g)		CH$_2$Cl$_2$	
MIP 4	ATMER 129					60 ºC, 24 h
NIP 4	—	MAA (0.0629 g)				
MIP 5	ATMER 129					
NIP 5	—					
MIP 6	ATMER 129	MAA (0.2527 g)				
NIP 6	—					
MIP 7	ATMER 129	4-Vpy				
NIP 7	—	(0.3090 g)				
MIP 6′	ATMER 129	MAA (0.2527 g)				UV, 28 ºC, 24 h
NIP 6′	—		EGDMA	1:4:20	Acetone:ACN (3:1)	
MIP 7′	ATMER 129	4-Vpy	(2.914 g)			
NIP 7′	—	(0.3090 g)				
MIP 6″	ATMER 129	MAA (0.2527 g)				UV, 4 ºC, 24 h
NIP 6″	—					
MIP 7″	ATMER 129	4-Vpy				
NIP 7″	—	(0.3090 g)				
MIP 8	ATMER 129	MAA (0.2527 g)	EGDMA		Acetone:ACN (3:1)	
NIP 8	—		(2.914 g)	1:4:20	200 mL	
MIP 9	ATMER 129	4-Vpy				
NIP 9	—	(0.3090 g)				
MIP 10	ATMER 129	MAA (0.3786 g)				
NIP 10	—		EGDMA	1:6:30		
MIP 11	ATMER 129	4-Vpy	(4.665 g)			
NIP 11	—	(0.4635 g)				
MIP 12	ATMER 129	MAA (0.2527 g)	TRIM		Acetone:ACN (3:1)	
NIP 12	—		(4.968 g)	1:4:20		
MIP 13	ATMER 129	4-Vpy				60 ºC, 24 h
NIP 13	—	(0.3090 g)				
MIP 14	ATMER 129	MAA (0.3786 g)	TRIM			
NIP 14	—		(7.452 g)	1:6:30		
MIP 15	ATMER 129	4-Vpy				
NIP 15	—	(0.4635 g)				
MIP 16	ATMER 129		TRIM			
NIP 16	—	MAA (0.2527 g)	(4.968 g)	1:4:20		
MIP 17	ATMER 129		EGDMA		CH$_2$Cl$_2$	
NIP 17	—		(2.914 g)			
MIP 18	ATMER 129	MAA (0.3786 g)	EGDMA	1:6:30		
NIP 18	—		(4.665 g)			
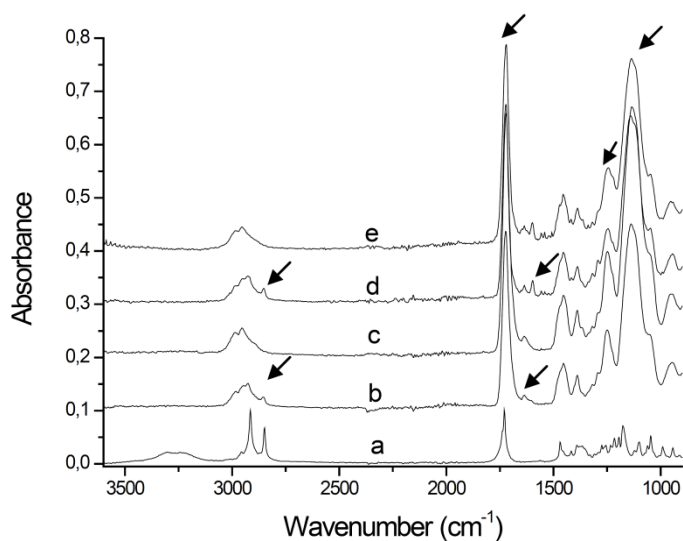
Fig. 2. ATR spectra of (a) solid Atmer, (b) MIP 6', (c) NIP 6', (d) MIP 7' and (e) NIP 7'.The arrows at 2850 cm^{-1} correspond to stretching of Atmer 129 methylene groups (υ_{CH_2-}). The arrows at 1725, 1245 and 1140 cm^{-1} indicate $\upsilon_{C=O}$, asymmetric and symmetric υ_{C-O-C} of poly (EGDMA), respectively. The arrow at 1638 cm^{-1} indicates the $\upsilon_{C=C}$ of unreacted methacrylate groups of EGDMA. In MIP 7' and NIP 7' the arrow at 1597 cm^{-1} is assigned to the $\upsilon_{C=N}$ bands of the pyridine ring.

3.2.1.2. Degree of monomeric conversion

The extent of unreacted carbon–carbon double bonds was determined from the ratio of absorbance areas of the band at 1638 cm^{-1} against an internal standard (the asymmetric C H deformation band (δ_{C-H}) at 1460 cm^{-1} of the cross linker, EGDMA or TRIM) before and after polymerization. After that, the degree of monomeric conversion (DC%) was calculated using the following equation [22]:

$$DC(\%) = 100 - \frac{[(abs(C=C)_{1638})/(abs(C-H)_{1460})_{polymerized}]}{[(abs(C=C)_{1638})/(abs(C-H)_{1460})_{monomer}]}$$

100

3.2.1.3. Estimation of incorporation of functional monomer in MIPs

Another concern was the possibility for leaching of the functional monomer by the presence of the template. Thus, the incorporation of 4-Vpy in polymers with different template concentrations or/and polymerization conditions was estimated using the ratio of the area under the pyridine ring band at 1597 cm^{-1}, relative to the area of the internal standard band at 1460 cm^{-1}; the higher this ratio, the greater the content of pyridine versus the cross-linker [23].

Conversely, the incorporation of MAA in the copolymers cannot be estimated. As the amount of the monomer is low in comparison to the cross-linker, the characteristic MMA band in the range of 3300-3500 cm^{-1}, which corresponds to the carboxylate OH stretching (υ_{OH}), is below the signal to noise ratio in dried samples; on the other hand, the band due to the carbonyl stretching ($\upsilon_{C=O}$) lies in the same region than the EGDMA ester linkage, and hence cannot be distinguished [24].

3.3. BATCH REBINDING EXPERIMENTS

Batch adsorption experiments were carried out to evaluate binding and compare MIPs formulations. These experiments were conducted in a Visiprep™-DL Solid Phase Extraction Vacuum Manifolds.

The experiments were carried out in the same solvent used for imprinting [25]. Thus, solutions of Atmer 129 in acetone:ACN (3:1) 2 mL, 1000 mg

L^{-1} (2.791 x 10^{-3} M) were loaded above the packed columns (200 mg of the MIPs selected were packed in 6 mL polypropylene tubes). The concentration of the free template in the extraction solution was determined by HPLC-PDA. The amount of template bound to the polymers was calculated by subtracting the concentration of free Atmer 129 from the initial Atmer 129 loading.

Batch rebinding assays were also performed for selectivity tests to compare the affinity of the polymers for different compounds. The concentration of template and related compounds were quantified using HPLC (Atmer 129, α-tocopherol) and UPLC (oleic and linoleic acid) systems.

3.3.1. Evaluation and characterization parameters

3.3.1.1.Imprinting factor

It is measured from batch rebinding experiments. The affinity of the template for the polymer is measured by the partition coefficient (K$_p$), which is defined as the ratio of the amount of compound bound to the MIP (S$_b$) relative to the concentration of free compound (C$_f$).

The effect of the imprinting process is measured by the imprinting factor (I) (modified partition coefficient) that is defined as

$$I = \frac{K_{pMip}}{K_{pNip}}$$

where K_{pMip} is the partition coefficient of a compound on an imprinted polymer and K_{pNip} is the partition coefficient of the same compound on a non-imprinted polymer with the same monomer formulation. This normalization method removes binding due to non-specific interactions [26].

3.3.1.2. Selectivity

The binding selectivity of MIPs was evaluated by measuring their rebinding capacities toward the template (Atmer 129) and three structural related compounds, α-tocopherol (antioxidant compound), oleic acid and linoleic acid (fatty acids). Solutions of Atmer 129 or its related compounds (2 mL, 1000 mg L^{-1}) were loaded above the packed columns (200 mg). Acetone:ACN (3:1) was the solvent of choice for Atmer 129. Acetone:ACN (3:1), THF and EtOH were used as solvents for α-tocopherol and fatty acids, respectively. The same acidified solvents (solvent:acetic acid, 9:1) were used for elution assays.

The specific selectivity factor (S) was calculated by the ratio of imprinting factors:

$$S = \frac{I_{ATMER\ 129}}{I_X}$$

Being I_X the imprinting factor for X compound. "S" is a measure of how well the inherent selectivity of the polymer improves upon imprinting. The

specific selectivity factor does not take into account partitioning effects between two molecules due to non-imprinted effects [26, 27].

4. RESULTS AND DISCUSSION

4.1. STUDIES OF THE MIP PRE-POLYMERIZATION COMPLEX BY FTIR AND UV/VIS

In the pre polymerization solutions several kinds of competitive molecular interactions can take place. Besides monomer-template complexation, the template or the functional monomer can form intra-or/and self-intermolecular interactions.

4.1.1. Template intra- and self-intermolecular interactions

Atmer 129, as other long chain esters of glycerol, is capable of intra- and self-intermolecular interactions. The same groups that form intermolecular H-bonds may form intramolecular H-bonds if the spatial configuration is favorable [21, 28]. It has been found that the molecular recognition ability of a MIP based on H-bonding decreased with templates capable of forming intramolecular H-bonds [18, 29]. Thus, in order to discriminate between intra- and intermolecular interactions, the spectral behavior upon increasing the template concentration in $CCl_4:CH_2Cl_2$ (9:1) was investigated. Two bands are observed in the carbonyl region of the IR spectra at 1742 and 1717 cm^{-1} (Fig. 3(I)). The former is allotted to free C=O groups while the latter arises from the formation of H-bonds between

OH and C=O groups. These H-bonds can be either intra or intermolecular although the effects of concentration on each kind of interaction are significantly different. Since the intramolecular interaction is an internal effect, it persists even at the lowest concentrations in contrast with the bands resulting from intermolecular interactions. Therefore, the spectra in Fig. 3(I) strongly indicate that the band profile originates from intramolecular interactions. Notwithstanding, at the concentration used in the prepolymerization mixture, 0.018 M, the lower frequency band appears as a shoulder. The maximum of this band is located at 1722 cm^{-1} as revealed by the second derivative spectrum; this shift is due to the increasing contribution of intermolecular H-bonding.

Fig. 3(II) displays the spectral range for the σOH vibrations. The band values of the most dominant spectral features are found at 3620, 3600 and 3513 cm^{-1}. Studies of monoglycerid lipids and diols provide information about these bands [21]. The 3620 and 3600 cm^{-1} bands may be assigned to free OH groups and to OH groups that form weak H-bonds with the carbonyl group of another molecule with free OH groups, respectively. The band at 3513 cm^{-1} has a shoulder around 3485 cm^{-1}. Both bands have been ascribed to intramolecular H-bonding since they remain at low concentration. At 0.018 M the relative intensity and width of the 3513 cm^{-1} band increases but no downward shift is observed by effect of intermolecular H-bonding, contrary to Holmgren et al. [21].
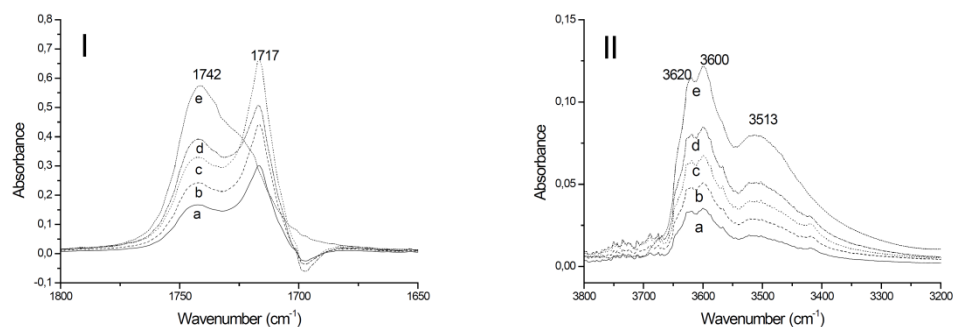
Fig. 3. Infrared spectra of (I) the $v_{C=O}$ and (II) the v_{O-H} mode regions of Atmer 129 in $CCl_4:CH_2Cl_2$, 9:1. The concentrations were (a) 0.002, (b) 0.004, (c) 0.006, (d) 0.009 and (e) 0.018 M.

4.1.2. Template-porogen interactions

Another way to gain information about intramolecular interactions is to replace CCl_4 by solvents able to "loosen" H-bonds as CH_2Cl_2. By this choice of solvent the intramolecularly H-bonded carbonyl groups would be solvated by CH_2Cl_2 and give rise to a single band. On the other hand, ACN is capable of forming H-bonds with the OH groups, thereby reducing the effect of H-bonding to the carboxyl moiety. As expected, only one absorption band is observed at the $v_{C=O}$ region for both solvents at 0.018 M (Fig. 4) and the spectral profile do not change with concentration. In short, due to the absence of intra molecular H-bonding in CH_2Cl_2 and ACN, these solvents have been chosen as porogens.

4.1.3. Atmer 129–4 Vpy interactions

In a second step, the study was focused on the template–monomer interactions in CH_2Cl_2. The Atmer 129 band at 2850 cm^{-1} and the 4-Vpy band at 1549 cm^{-1}, which are insensitive to H-bonding, are taken as internal standard for spectral subtraction. The complex difference spectrum (Fig. 5d) is obtained by subtracting the normalized Atmer 129 spectrum (Fig. 5b) and the normalized 4-Vpy spectrum (Fig. 5c) from the binary system (Fig. 5a).

Focusing on the υ_{OH} region (Fig. 5(I)), the template–monomer complex is easily detectable, since the intensity of the Atmer 129 bands at 3687 and 3601 cm^{-1} bands decrease and a broad band centered at 3197 cm^{-1}

appears. The latter confirms the formation of H-bonds between the Atmer 129 OH groups (H donors) and the heterocyclic N (H acceptor) of 4-Vpy. The frequency difference between the free and H-bonded OH bands has been used to investigate the average strength of the interaction [30]. Thus, the template-pyridine inter association ($\Delta v = 490$ cm^{-1}) is more favorable than Atmer 129 self-association ($\Delta v \cong 87$ and 207 cm^{-1}). Additionally, H-bonding causes significant spectral changes on the ring stretching modes of pyridine; particularly, the band at 1597 cm^{-1}, due to the $v_{C=N}$ mode, and the ring breathing mode at 992 cm^{-1}. Fig. 5(II) and (III) illustrate the FTIR spectra of binary mixtures in the corresponding spectral regions. Two bands at 1603 and 1001 cm^{-1}, which were absent in both the neat 4-Vpy and Atmer 129 spectra, appeared at the expense of the 1597 and 992 cm^{-1} bands, respectively. These new features have been assigned to the ring breathing modes of the H-bonded 4-Vpy [31].

From another point of view, the Atmer 129:4-Vpy complex stoichiometry was determined by UV spectrophotometry using the continuous variation method (Job's plot analysis) [32, 33]. The changes in absorbance were measured at 244 nm and 205 nm in CH$_2$Cl$_2$ and acetone:ACN (3:1), respectively. The plots of (ΔAbsorbance *Atmer 129 mole fraction) against the mole fraction of 4-Vpy gave maxima at about 0.6-0.7 in both solvents, indicating the formation of Atmer 129:4-Vpy, 1:2 complexes (Fig. 6(I)).

4.1.4. Atmer 129–MAA interactions

In connection with Atmer 129-MAA interactions in CH_2Cl_2, the template concentration was kept constant (0.004 M) while the molar ratio Atmer 129:MAA was increased from 1:0 to 1:4. The study is focused in the carbonyl C=O stretching region and the MAA out of plane C=O deformation vibration at 950 cm^{-1}. Even at low concentrations, MAA is found in equilibrium between the monomeric and dimeric forms. The $\upsilon_{C=O}$ of the MAA monomer and dimer are evident at 1735 and 1698 cm^{-1}, respectively, and the relative intensity 1698/1735 increases with MAA concentration. Due to the overlapping of the monomer and template bands a double spectral subtraction has been carried out. Each binary mixture spectrum is subtracted either the pure Atmer 129 spectrum, normalized at the 2850 cm^{-1} band (υ_{CH2}), or the spectrum of pure MAA of the same concentration, normalized at the 1603 cm^{-1} band ($\upsilon_{C=C}$). No evidence of H-bonding between Atmer 129 and MAA could be proved in CH_2Cl_2, no shifting, band broadening or changes in intensity were observed for the H-bonding sensitive bands.
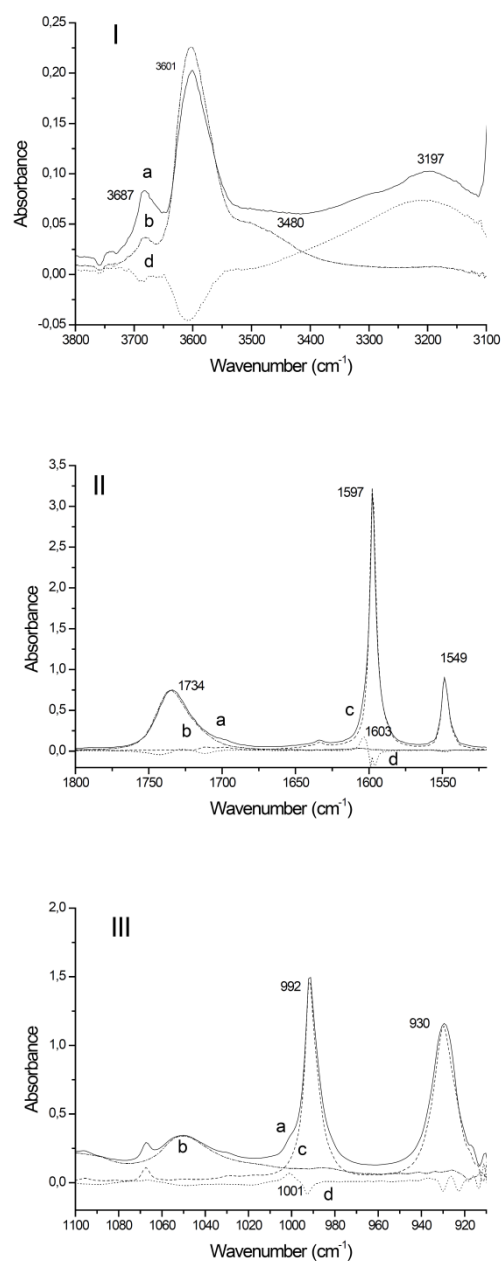
Fig. 5. Infrared spectra of (a) Atmer 129:4-Vpy, 1:4; (b) Atmer 129; (c) 4-Vpy and (d) difference spectrum in CH_2Cl_2 corresponding to (I) the σO-H mode region, (II) the $\upsilon_{C=O}$ and $\upsilon_{C=N}$ region and (III) the region between 1100 and 900 cm^{-1}.

Finally, the Atmer 129:MAA complex stoichiometry was determined by the continuous variation method (Job's plot analysis) using UV spectrophotometry. The changes in absorbance were measured at 227 nm and 206 nm in CH_2Cl_2 and acetone:ACN (3:1), respectively. The plot of (ΔAbsorbance*Atmer 129 mole fraction) against the mole fraction of the monomer gave a maximum at 0.5 in acetone:ACN (3:1), indicating the formation of 1:1 complex (Fig. 6 (II)). As expected, no maximum was observed in CH_2Cl_2.
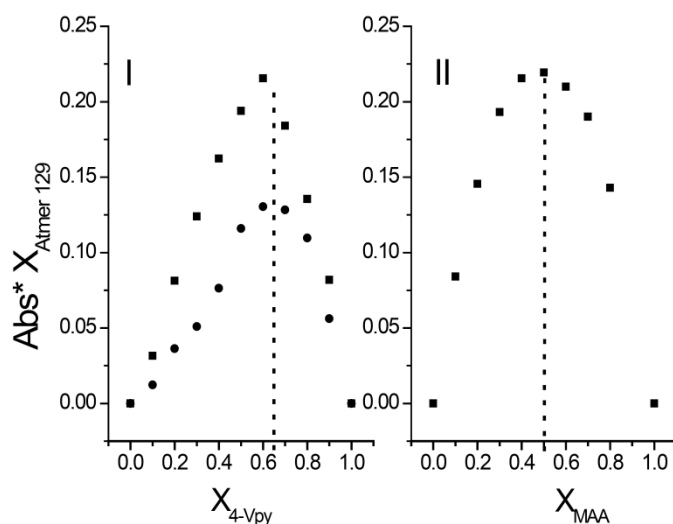
Fig. 6. Jobs plot analysis of (I) Atmer 129:4-Vpy, 1:4 complex in dichloromethane at 245 nm (squares) and in acetone:ACN (3:1) at 204 nm (dots) and (II) Atmer 129:MAA complex in acetone:ACN (3:1) at 206 nm.

It is apparent that the dimerization of MAA molecules diminishes the template–monomer complex. Dimerization is not only related to the acid concentration but also to the interaction with the porogen. Previous H NMR results showed that MAA has a stronger tendency to form dimers in $CDCl_3$

than in acetone-d$_6$ as a result of the stronger interaction with the latter [34]. Similarly, our analysis suggested a weaker dimerization in acetone:ACN (3:1) in contrast with CH$_2$Cl$_2$. The low dielectric constant value of CH$_2$Cl$_2$ (9.08 at 20 ◦C) in comparison with those of ACN (37.5) and acetone (21), may help to explain this behavior [31]. Hence, to control the extent of dimerization, it is essential to consider the porogen properties besides the monomer concentration.

4.2. Studies of the MIP post-polymerization complex

4.2.1. MIPs synthesis

The synthesized polymers (Table 1) were characterized to determine the type of functional monomer and crosslinker, template concentration and polymerization conditions which lead to better recognition capabilities.

First of all, three T:M:C molar ratios were studied (1:1:5, 1:4:20 and 1:6:30). Either inhibition of the polymerization reaction or difficulties for polymer treatment were encountered when assays were carried out using the molar composition 1:1:5 (MIPs 1-5). Consequently, these polymers were discarded at the first stage increasing volumes of different porogens. A high detection limit was shown when CH$_2$Cl$_2$ is used as porogen (MIPs 16, 17, 18) and difficulties for polymer treatment were observed if high volumes of porogen (200 mL) (MIPs 8, 9) were added. In contrast, the best results were achieved for 40 mL of acetone:ACN (3:1).

On the other hand, MIPs synthesized with TRIM (MIPs 12-15) led to poor yields and EGDMA was selected as the preferred crosslinker for final polymerization conditions. Further analyses were conducted with MIPs 6, 6′, 6″, 7, 7′, 7″, 10 and 11 which were obtained in good yields (∼ 100%). Notwithstanding, MIPs with T:M:C (1:6:30) (MIPs 10, 11) were eliminated at the next stage due to their poor I values (Table 2).

Table 2. Values of imprinting factor (I), selectivity (S), glass transition point (T_g), degradation temperature (T_{deg}) and degree of conversion (DC%) for the tested polymers.

Polymer	I	S			T_g (ºC)	T_{deg} (ºC)	DC(%)	A_{1597}/A_{1460}
		(1)	(2)	(3)				
MIP 6	2.46	2.24	2.88	0.77	45.03	277.6	93±2	—
MIP 7	1.62	1.78	1.26	0.43	39.71	309.7	95±1	0.16±0.01
MIP 6′	1.03	1.28	1.35	1.19	48.17	283.7	93±1	—
MIP 7′	1.21	1.52	1.22	0.72	42.40	305.1	90±1	0.15±0.02
MIP 6″	0.96	—	—	—	—	297.5	66±2	—
MIP 7″	1.36	—	—	—	—	291.4	86±3	0.18±0.02
MIP 10	0.82	—	—	—	42.00	288.3	—	—
MIP 11	0.41	—	—	—	33.36	309.7	—	0.12±0.01

(1) Linoleic acid; (2) oleic acid; (3) α-tocopherol

Finally, in order to evaluate selectivity of the imprinted membranes against Atmer 129 the same binding experiments using oleic, linoleic acids and α-tocopherol were performed. The differences in the chemical structure between the analytes might result in different interactions with the polymeric matrices. The chemical structure of the fatty acids differ from Atmer 129 in both the nature of the polar groups (carboxylic acid versus 2,3- dihydroxylester) and the higher esteric effect of the hydrophopic alkyl chains due to the presence of unsaturations. As can be inferred from Table

2, MIP 6 displayed the best selectivity for Atmer 129 in relation to oleic and linoleic acid. The amount of fatty acids bound to the polymers was considerably lower than that of the original template. Considering that the carboxyl hydrogen atom of the acids is sufficiently active to compete with the bonding tendencies of the hydroxyl groups of the alcohols [35], the results strongly suggested that the template recognition by polymer originates from the shape complementarity of binding sites. Furthermore, the amounts of α-tocopherol bound to imprinted membranes were in most cases higher with respect to Atmer 129. This result clearly showed the non-specific nature of these interactions.

4.2.2. MIPs characterization

To account for these results the thermal behavior, the degree of monomeric conversion (DC%), the incorporation of the functional monomer and the morphology of the best performing MIPs and NIPs were evaluated by a combination of analytical techniques: TGA, DSC, ATR and SEM.

As a starting point, all the polymers exhibited in Table 2 showed high thermostability by TGA analysis with no mass loss under 275 ∘C; although, the polymers synthesized with 4-Vpy were the most stable, up to 325 ∘C, leaving residue of ≈ 5% mass at 600 ∘C. Besides, the average degree of monomeric conversion (DC%) together with the ratio A_{1597}/A_{1460} for selected MIPs and NIPs were estimated by ATR according to Sections 3.2.1.2 and 3.2.1.3. Only the results for the MIPs are shown in Table 2 as

the corresponding NIPs led to similar values for both parameters, within experimental error. Regarding the extent of polymerization, the DC% values were also similar to that of pure poly (EGDMA) synthesized (DC% = 94 ± 1). Nonetheless, the degree of cross-linking depended on the polymerization conditions, specifically the energy source and temperature. Conversion was lower when UV radiation is used instead of heat, except for MIP-6', and deeply decreased on lowering the reaction temperature (4 ◦C compared with 28 ◦C, 24 h). DSC analysis confirmed incomplete polymerization for photochemical synthesized MIPs. The greater DC% of MIPs 6 and 7 might have been favored by high temperature [25]. Furthermore, the incorporation of the monomer 4-Vpy in the copolymers was not modified either by the polymerization conditions or the presence of the template.

From another point of view, the best I values were achieved for thermal synthesis conducted at 60 ◦C. As the polymerizations of these MIPs were carried out at a temperature superior than the glass transition point (T_g) of the blends, the enhanced molecular mobility might have allowed the formation of a new equilibrium between free functional groups. [37]. Thus, to some extent, enhanced performance of MIPs obtained at 60 ◦C can be attributed to improved mass-transfer kinetics [38, 39].

In addition, the morphology of MIPs 6 and 6' was compared by Scanning Electron Microscopy (Fig. 7). Both MIPs had similar feed compositions but they were synthesized under different conditions: MIP 6 was immersed in a

water bath at 60 ◦C and MIP 6' was polymerized under a UV source at 28 ◦C. The images show appreciable differences in their morphology. The former (Fig. 7(I)) has uniform morphology, whereas MIP 6' (Fig. 7(II)) has rough morphology. The difference in polymer morphology together with the enhanced molecular mobility previously discussed, may account for the greater efficiency found for the thermal polymer, as they both have the same DC%.

These reasons may explain the best behavior of thermal MIPs in spite of the fact that low polymerization temperatures stabilize non-covalent interactions, theoretically increasing the number and quality of binding sites [36].

(I)   (II)
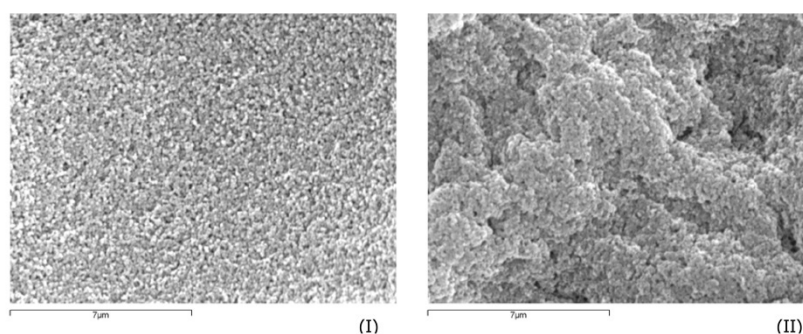
Fig. 7. SEM micrographs of MIP-6 (I) and MIP-6' (II), polymers with the same compositions but synthesized by thermal and photochemical conditions respectively.

4.2.3. Rebinding step

MIP and NIP rebinding with template molecule Atmer 129 were studied by ATR-FTIR spectra. The spectra were recorded before and after adsorption of Atmer 129 for the selected polymers: MIP and NIPs 6, 6', 7 and 7'.

The characteristic Atmer band at 2850 cm^{-1} was not observed either in MIPs or NIPs. This result was ascribed to the high detection limit of the technique. Thus, the presence of Atmer 129 in the ATR spectra of unwashed MIPs 6' and 7' (Fig. 2b and d) was investigated and was attributed to Atmer 129 crystals rather than to Atmer 129 molecules bound to the monomer in accordance with the subsequent DSC results.

One broad band corresponding to long range disorder copolymer crystals is observed in the DSC curve of NIP 6 (Fig. 8). However, at 60 ∘C two bands can be detected in the DSC curve of MIP 6: a broad band analogous to the one observed in NIPs, made up of copolymer crystals of several sizes, and an intense and narrow band, corresponding to crystals of similar size distribution. The latter is formed of Atmer 129 micelles as has been proved by independent DSC analysis of pure Atmer 129 crystals (not shown). This result is directly related to the crystallization of Atmer 129 during the polymerization reaction. It is well known that the strength of self-H-bonding intermolecular H-bonding is related to the concentration of components [18]. For that reason, in surfactant solutions and above a critical concentration range micelles can be formed with a narrow size distribution, resulting in the formation of large aggregates of finite size [40]. In fact, the distribution of species consisting of "free" monomers,

self- and inter-H-bonded dimers and multimers is affected by changes in the temperature and concentration taking place during the polymer synthesis [41] and Atmer 129 may start to crystallize out as the polymerization reaction proceeds; consequently, reducing imprinting.
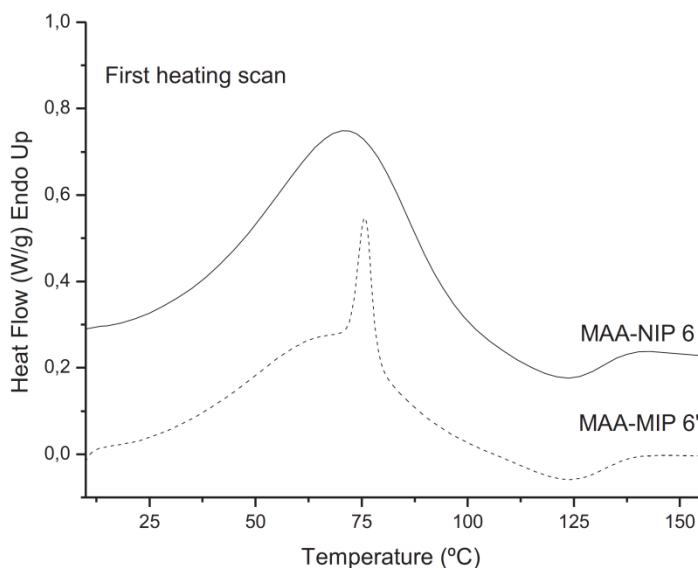
Fig. 8. DSC curves of thermal MAA-NIP 6 non-imprinted polymer and thermal MAA-MIP 6 imprinted polymer.

Furthermore, specific (only in MAA copolymers) plus non specific (both in MAA and 4-Vpy copolymers) interactions between the network and the template can be investigated by analyzing the carbonyl stretching region ranging from 1760 to 1660 cm^{-1}. It is informative to perform a second derivative analysis. This method relies on the fact that the second derivative of a spectral band is normally much narrower that the original band. Thus, overlapping bands can be separated by double differentiation.

As can be appreciated in Fig. 9, at 55 ∘C in water vapor and solvent free spectra, the carbonyl ester linkage from EGDMA is located at 1727 cm^{-1} and has a half band width of 35 cm^{-1} in MIP 6. The second derivative spectrum exhibits three negative bands: two main bands at 1722 and 1730 cm^{-1} and a very small band at 1700 cm^{-1}. Some authors have attributed the bands at 1722 and 1730 cm^{-1} to crystalline and amorphous states of free C=O of EGDMA [42, 43]. The presence of a crystalline phase has already been confirmed by the appearance of the aforementioned broad band in the DSC curves. The band at 1700 cm^{-1}, absent in 4-Vpy copolymers, has been assigned to MAA. When the spectrum is recorded after equilibrium sorption of the template, the carbonyl band shifts downward to 1723 cm^{-1} and broadens ($w_{1/2}$ = 37 cm^{-1}), indicating the presence of H-bonding. Correspondingly, the second derivative spectrum exhibits a more complex feature with extra negative bands around 1717 and 1710 cm^{-1}, which have been ascribed to H-bonded carbonyl ester groups of EGDMA and H-bonded carboxylate groups of MAA [42, 43]. A similar downward shift and broadening are not seen either in the control polymer, which does not contain the imprint cavities, or the rest of the selected MIPs (with the exception of a slight downshift with no broadening in MIP 7 from 1724 cm^{-1} to 1722 cm^{-1}) due to unspecific interactions with the cross linker.

From another point of view, H-bonding between Atmer 129 and the pyridine ring can be investigated by comparing the IR spectra of MIPs and NIPs 7 and 7′ in the region 1600–1590 cm^{-1}. After exposure to the Atmer

119

129 solutions, the 4-Vpy H-bonding sensitive band at 1597 cm^{-1} does not shift or change half band width within experimental error ($w_{1/2}$ = 13 cm^{-1}), either in MIPs or the reference polymer [44]. Hence, no specific H-bonding interactions between 4-Vpy and Atmer 129 were observed upon rebinding at the concentration used.
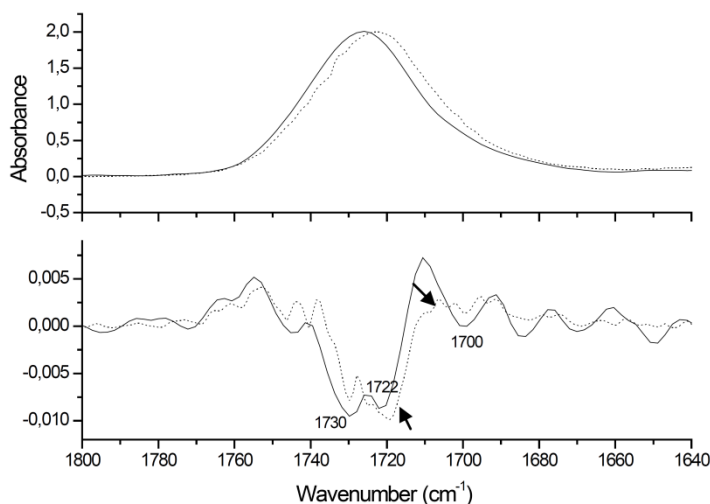
Fig. 9. ATR spectra of the $\upsilon_{C=O}$ mode region of MIP 6 (solid line) and MIP 6 after rebinding with a 2.791 × 10^{-3} M Atmer 129 solution in acetone:ACN (3:1) (dotted line) and their corresponding second derivative spectra. The arrows indicate the extra negative bands around 1717 and 1710 cm^{-1}, ascribed to H-bonded carbonyl ester groups of EGDMA and carboxylate groups of MAA.

The ATR rebinding results are surprising since the prepolymerization studies suggested the formation of a strong 1:2, Atmer 129:4-Vpy complex and a weak 1:1, Atmer 129:MAA complex and according to previous authors at least two points of interaction are required to induce molecular specificity [45]. On the other hand, they are consistent with the imprinting

factor results: keeping the rest of polymerization factors constant, the best behavior corresponds to MIP 6 (2.46), followed by MIP 7 (1.62); the former has been synthesized with acid MMA monomer and the latter with the basic 4-Vpy. Besides the low signal to noise ratio of the technique, another possible explanation could be the aforementioned crystallization of Atmer 129 during the polymerization reaction, leading to a reduction in the number of specific binding cavities, but this fact affected both MIPs. From another point of view, it has been proved in the pre-polymerization analysis that the strong MAA dimerization prevented the formation of a strong complex with the template in solution. But H-bonds are dynamic, continually breaking and reforming under the influence of thermal motion, monomer concentration, and interaction between monomer building blocks and the porogenic solvent, and there exists at any instant of time a distribution of "free" monomers, H-bonded dimers and multimers [41]. Thus, the equilibrium may shift to free MAA formation as the polymerization proceeds and the acid concentration decreases in the polymerization media; accordingly, the concentration of free MAA molecules that can form complexes with the template increases. These phenomena can explain why the number of intermolecular H-bonds in the imprinted polymer does not necessarily correspond to those in the prepolymerization mixture [38].

5. CONCLUSIONS

After analyzing the molecular interactions between template and functional monomers in solution by FTIR and UV-Vis spectroscopy, a wide range of Atmer 129 imprinted polymers had been synthesized and the influence of the T:M:C molar ratio, nature of the cross linker, monomer and porogen as well as the porogen volume and polymerization conditions (temperature, energy source), was evaluated.

1. Based on the prepolymerization analysis, ACN and CH_2Cl_2 were chosen as suitable porogens for the polymerization step. The absence of intra-molecular H-bonding in Atmer 129 solutions of the selected porogens and the increase of self inter-molecular H-bonding with concentration were observed. Additionally, FTIR spectra showed the formation of a strong H-bonded Atmer 129:4-Vpy complex, being the hydroxyl-pyridine inter-association in CH_2Cl_2 more favorable than self-association of pure Atmer 129. UV-Vis spectroscopy suggested 1:2 stoichiometry for the Atmer 129:4-Vpy complex both in acetone:ACN (3:1) and CH_2Cl_2 and 1:1 stoichiometry for the Atmer 129:MAA complex in acetone:ACN (3:1).

2. The best imprinting factor was found for a MIP copolymer consisting of Atmer 129:MAA:EGDMA (1:4:20) synthesized at 60 ◦C (MIP 6, 2.46), followed by the corresponding Atmer 129:4Vpy:EGDMA (1:4:20) copolymer obtained under the same polymerization conditions (MIP 7, 1.62). MIP 6 displayed the best selectivity for Atmer 129 in relation to oleic

and linoleic acid. Selectivity studies suggested that the imprinting effect could be mainly ascribed to shape recognition of template.

3. The best performance of thermal polymers was due to a higher degree of monomer conversion and sufficient compromise between rigidity of the polymer network, preserving the imprinted cavity shape, and flexibility to facilitate substrate access and rebinding. This behavior might be related to the enhanced molecular mobility at the reaction temperature above the glass transition point (T_g) of the blend. From another point of view, the ATR spectra of unwashed MIPs proved that the presence of Atmer 129 crystals was greater in the polymers synthesized with UV radiation, suggesting a lower degree of Atmer 129 crystallization at 60 ∘C, which is another factor contributing to the best performance of thermal polymers.

4. Specific interactions between the MIP 6 network (MAA) and the template were shown by the carbonyl band shifts in the rebinding spectra, recorded after equilibrium sorption of the template.

5. Finally, the results obtained upon rebinding were not completely correlated with the prepolymerization analysis. In spite of the fact that inter-H-bonding between the 4-Vpy and Atmer 129 was stronger than the self-H-bonding in Atmer 129, the template started to crystallize out during the polymerization as shown by DSC. The pre-polymerization study does not fully account for effects such as disruption of monomer–template complexes by the cross-linker, self-association of the template and/or monomer molecules as they increasingly incorporate into the growing

polymer network, or the actual polymerization conditions including high temperature or UV radiation.

References

[1] A.M. Rampey, R.J. Umpleby, G.T. Rushton, J.C. Iseman, R.N. Shah, K.D. Shimizu, Anal. Chem. 76 (2004) 1123

[2] L.E. Gómez-Pineda, G.E. Pina-Luis, Á. Cuán, J.A. García-Calzón, M.E. Díaz-García, React. Funct. Polym. 71 (2011) 402

[3] D.A. Kirby, C. Alexander, Adv. Drug Deliv. Rev. 57 (2005) 1836–1853

[4] B. Sellergren, TRAC – Trends Anal. Chem. 18 (1999) 164

[5] K. Haupt, Anal. Chem. 75 (2003) 376 A

[6] R.H. Schmidt, A.S. Belmont, K. Haupt, Anal. Chim. Acta 542 (2005) 118

[7] B. Sellergren, C.J. Allender, Adv. Drug Deliv. Rev. 57 (2005) 1733

[8] S.A. Piletsky, N.W. Turner, P. Laitenberger, Med. Eng. Phys. 28 (2006) 971

[9] Y.H. Yun, H.K. Shon, S.D. Yoon, J. Mater. Sci. 44 (2009) 6206

[10] M.E. Byrne, K. Park, N.A. Peppas, Adv. Drug Deliv. Rev. 54 (2002) 149

[11] N.M. Bergmann, N.A. Peppas, Prog. Polym. Sci. 33 (2008) 271

[12] M.C. Cela-Pérez, M.M. Castro-López, A. Lasagabáster-Latorre, J.M. López-Vilariño, M.V. González-Rodríguez, L. Barral-Losada, Anal. Chim. Acta 706 (2011) 275

[13] B.S. Ebarvia, A.Ch. Binag, Anal. Bioanal. Chem. 378 (2004) 1331

[14] E. Oral, N.A. Peppas, Polymer 45 (2004) 6163

[15] C. Alexander, H.S. Andersson, L.I. Andersson, R.J. Ansell, N. Kirsch, I.A. Nicholls, J. O'Mahony, M.J. Whitcombe, J. Mol. Recognit. 19 (2006) 106

[16] R. Simon, M.E. Collins, D.A. Spivak, Anal. Chim. Acta 591 (2007) 7

[17] L.Y.Z. Lin, W. Geng, T. Tan, Chromatographia 66 (2007) 339

[18] T. Zhang, F. Liu, W. Chen, J. Wang, K. Li, Anal. Chim. Acta 450 (2001) 53

References

[19] M. Jakusch, M. Janotta, B. Mizaikoff, K. Mosbach, K. Haupt, Anal. Chem. 71 (1999) 4786

[20] M.V. González-Rodríguez, M.S. Dopico-García, R. Noguerol-Cal, T. Carballeira-Amarelo, J.M. Lopez-Vilariño, G. Fernández-Martínez, J. Sep. Sci. 33 (2010) 3595

[21] A. Holmgren, G. Lindblom, L.B.A. Johansson, J. Phys. Chem. 92 (1988) 5639

[22] L.C. Mendes, A.D. Tedesco, M.S. Miranda, Polym. Test. 24 (2005) 418

[23] H. Kim, D.A. Spivak, J. Am. Chem. Soc. 125 (2003) 11269

[24] V.P. Joshi, R.N. Karmalkar, M.G. Kulkarni, R.A. Mashelkar, Ind. Eng. Chem. Res 38 (1999) 4417

[25] J.F. He, Q.H. Zhu, Q.Y. Deng, Spectrochim. Acta A 67 (2007) 1297

[26] D.A. Spivak, Adv. Drug Deliv. Rev. 57 (2005) 1779

[27] S.H. Cheong, S. McNiven, A. Rachkov, R. Levi, K. Yano, I. Karube, Macromolecules 30 (1997) 1317

[28] W.J. Baumann, H.W. Uslhofer, Chem. Phys. Lipids 2 (1968) 114

[29] W. Cummins, P. Duggan, P. McLoughlin, Anal. Chim. Acta 22 (2006) 372

[30] J.Y. Lee, P.C. Painter, M.M. Coleman, Macromolecules 21 (4) (1988) 954

[31] F.S.F. Jacinto, L.J.A. Siqueira, W.A. Alver, J. Raman Spectrosc. 40 (2009) 1585

[32] P. Job, Ann. Chim. Appl. 9 (1928) 113

[33] Y.Ch. Huang, Methods Enzymol. 87 (1982) 509

[34] S. Wei, M. Jakush, B. Mizaikoff, Anal. Bioanal. Chem. 389 (2007) 423

[35] C.W. Hoerr, H.J. Harwood, J. Phys. Chem. 56 (9) (1952) 1068

[36] E.V. Piletska, A.R. Guerreiro, M.J. Whitcombe, S.A. Piletsly, Macromolecules 42 (2009) 4921

[37] B. Fei, Ch. Chen, S. Pens, X. Zhao, X. Wang, L. Dong, Polym. Int. 53 (2004) 2092

[38] J. O'Mahony, K. Nolan, M.R. Smyth, B. Mizaikoff, Anal. Chim. Acta 534 (2005) 31

[39] A.A. Silva Jr., J.R. Matos, T.P. Formariz, G. Rossanezi, M.V. Scarpa, E.S. Egito, A.G Oliveira, Int. J. Pharm. 368 (2009) 45

[40] T. Gilanyi, Colloids Surf. A 104 (1995) 111

[41] H.K. Can, Z.M.O. Rzaev, A.C. Guner, J. Mol. Liq. 111 (2004) 77

[42] N. Hameed, Q. Guo, Polymer 49 (2008) 922

[43] L.C. Cesteros, J.R. Isasi, I. Katime, Macromolecules 26 (1993) 7256

[44] V. Villar, L. Irusta, M.J. Fernandez-Berridi, J.J. Iruin, M. Iriarte, L. Gargallo, D. Radi Thermochim. Acta 402 (2003) 209

[45] G. Wulff, Angew. Chem. Int. Ed. Engl. 34 (1995) 1812

INSIGHT INTO BPA-4-VINYLPYRIDINE INTERACTIONS IN MOLECULARLY IMPRINTED POLYMERS USING COMPLEMENTARY SPECTROSCOPY TECHNIQUES

A. Lasagabáster-Latorre[1], M.C. Cela-Pérez[2],

S. Fernández-Fernández[2], J.M. López-Vilariño[2],

M.V. González-Rodríguez[2], M.J. Abad, L.F. Barral-Losada[2]

[1] Dpto Química Orgánica I, Escuela de Óptica, Universidad Complutense de Madrid, Arcos de Jalón, n∘ 118, Madrid 28037, Spain, email: aurora@ucm.es

[2] Grupo de Polímeros, Centro de Investigacións Tecnolóxicas, Universidade da Coruña, Campus de Esteiro s/n, Ferrol 15403, Spain, Tel.: +34 981 337 400 3051/3485; fax: +34 981 337 416, email: victoria.gonzalez.rodriguez@udc.es

ABSTRACT

The influence of solvent polarity on the nature and extent of non-covalent interactions responsible for BPA:4-Vinlypyridine complex formation has been investigated in the pre polymerization mixture and correlated with polymer-ligand recognition. The combination of FTIR, ^{1}H NMR and UV-Vis spectroscopy has made possible the development of a more comprehensive understanding of pre-polymerization events at a molecular level, and how they govern the properties of subsequent polymerized MIPs. The MIP ATR characterization provides direct insight into the bonding within matrix-template system, confirming that monomer:template H-bonded complexes survived the polymerization process and the presence of two functional monomers in the binding sites. The polymer has shown an excellent affinity for BPA in aqueous solutions with poor recognition in organic solvents. Loss of affinity in organic solvents together with selectivity studies suggested that the binding mechanism depended critically on the conformation of the polymeric binding pockets, which when combined with H-bonding and weak electrostatic interactions allowed for selective recognition.

Highlights: *MIP ATR analysis confirmed BPA:4Vpy H-bonded complexes survived polymerization*; *MIP ATR analysis confirmed two functional groups in MIP binding sites*; *Reversible conformational changes explained the poor results in nonpolar solvents; Detailed description of rebinding mechanism in water based on MIPATR spectroscopy; Selectivity depended on analyte:monomer interactions, shape, solubility*

Keywords: *Polymers, Shape memory effects, Nuclear magnetic resonance (NMR), Fourier transform infrared spectroscopy (FTIR), Visible and ultraviolet spectrometers.*

1. INTRODUCTION

Molecularly imprinted polymers (MIPs) synthesized via noncovalent self-assembly processes are biomimetic recognition materials selectively binding a target analyte in analogy to biological receptor-substrate interactions. Since non-covalent MIPs rely on complex formation between the target analyte and functional monomers in porogenic solution prior to radical copolymerization, the achievable selectivity is governed by the nature and stability of these complexes. Prior studies correlating polymer recognition properties with characteristics of the pre-polymerization mixture system can be found in the literature and include simulation via molecular modeling, UV spectroscopy, solution state NMR and FTIR [1, 2]. These studies support the inherent correlation between the formation of pre-polymerization complexes and polymer affinity for specific substrates. Therefore, molecular-level investigations of the interactions governing complex formation and stability are crucial to fundamental rational understanding of designed biomimetic recognition materials.

The main non-covalent interactions responsible for molecular recognition in biomimetic systems are hydrogen bonding (H-bonding) and ion pairing. Furthermore, a number of weak interactions such as Coulombic attraction, charge transfer, and molecular stacking contribute to complex formation, especially in protic solvents partly compensating for the loss of polar interactions [1]. The analytical challenge is identifying methods for tracing complex formation in the pre-polymerization solution and to accurately

evaluate how variable parameters influencing complex formation govern the properties of the subsequently formed imprinted polymers [2].

When applicable, UV-Vis spectroscopy will provide a simple and valuable tool for the rapid investigation of new monomer-target interactions. However, in order to use optical absorbance there must be either a shift in the wavelength of maximum absorbance or a change in A_{max} as a function of ligand concentration [3-6]. Solution NMR is probably the most widely used of the spectroscopic techniques as it affords high specificity and can yield structure information on the nature of the monomer:template complex: H-bonding [1, 7, 8] ionic, π-π stacking interactions [9] and self-association [10, 11]. Changes in the chemical shift values in NMR titration experiments have been used to establish the stoichiometry of complexes or the association constants between monomer: and template [12]. Concerning FTIR spectroscopy, despite being a powerful method for studying H-bonding, its application to analyze MIP pre-polymerization complexes is scarce in current literature [13-15]. With a few exceptions, the combination of spectroscopic methods for a more comprehensive understanding of pre-polymerization events has not been explored in detail [1, 16-18].

Regarding polymer physical characterization, FTIR has already been demonstrated to be a valuable tool in the characterization of post-polymerization binding properties in MIPs both in the transmission [13, 19-21] or the ATR-mode [22-24]. An additional advantage of this technique is

133

the higher information content of the spectra that in some cases allows not only detecting but also to quantify the analyte [25] and study the mechanism of interaction of the template with the MIP matrix [26]. The utility of the method depends ultimately on a careful choice of template and MIP to avoid overlapping FTIR bands, thereby improving the sensitivity in detecting templates [27].

Another aspect to consider in relation with MIP-template interactions is that optimum binding occurs when the polymer is exposed to the same conditions used for polymerization. The reason for this lies in the postulated mechanism of template recognition by a MIP, which originates from two factors: shape of the imprinted cavity and the spatial positioning of the functional groups coordinated by the template and integrated into the polymer network during polymerization. The solvent polarity may affect the sorption capacity and selectivity in two ways. In the first place, the solvent competes with the template for both specific and non-specific sites [28]. Secondly, a solvent induced swelling/shrinking process can affect the shape of the cavity and the distance between functional groups and due to this MIP can lose its specificity when exposed to the "wrong conditions" [29].

By combining solution-state NMR, FTIR and UV-Vis spectroscopy and solid ATR-FTIR spectroscopy a more complete picture of the nature of the imprinted sites and of the interactions with an analyte may be obtained. We have made use of these tools for the characterization of a polymer

imprinted with Bisphenol A (BPA). The potential toxicity (estrogen mimic) and abundance of BPA in environmental media and foodstuff have boosted the research for sensitive and selective methods for its determination in water samples. Therefore, numerous papers have been published dealing with the successful synthesis of BPA-imprinted polymers employing both covalent [28, 30, 31] and non-covalent imprinting techniques. Among the latter, most MIPs were prepared by non-aqueous bulk free radical polymerization and it has been proved that 4-vinylpyridine (4-Vpy) was the optimal functional polymer whereas ethylene glycol dimethacrylate (EGDMA) or trimethylolpropane trimethacrylate (TRIM) performed better than other crosslinkers [11, 32-35]. Most of these MIPs have high selectivity but exhibit serious templates leakage and poor site accessibility. To avoid the leakage structural analogs of BPA were used as templates whereas surface imprinted materials improved transport properties [36-44].

Despite all this background information, apart the NMR titration data of Nguyen and Ansell [11] no detailed analysis either of the BPA-monomer-solvent interactions in the pre-polymerization solution or the mechanisms of recognition of the template with the polymer matrix have been undertaken. Hence such a study is presented here. Previous work within our research group involved a systematic chromatographic characterization of the adsorptive performance of a non-covalent BPA-4-Vpy-EGDMA MIP developed in the presence of a low volatile solvent, triethylenglycol dimethyl ether (TRIGLYME), in combination with a non reactive linear

polymer, poly (vinyl acetate) (PVAc), as porogen. The results proved the large sorption capacity, high recognition ability and fast binding kinetics for BPA in water samples. The MIP selectivity demonstrated higher affinity for target BPA and BPA-analogs over other common water pollutants. Bisphenol F was chosen as a structural related molecule while paracetamol (phenolic compound) and caffeine (not phenolic compound) were selected between several contaminants usually found in natural waters [45].

This study further investigates the behavior of the pre-polymerization mixture of the selected template, BPA, its analog BPF and the aforementioned competitive compounds with 4-Vpy in organic solvents with a view to the potential use of spectroscopic techniques for understanding the process of binding site formation and selection of the most suitable rebinding conditions. First of all, the mechanism of analyte:monomer interaction was determined by comparing the shifts and/or broadening of the monomer and analyte infrared bands. After Job plot analysis of spectroscopic data (using IR, UV-Vis or ^{1}H NMR spectroscopy) provided information on the complex stoichiometry, FTIR titrations were carried out to calculate the apparent binding constants. In order to confirm the mechanism and compare the spectroscopic techniques, ^{1}H NMR titrations were also performed.

Additionally, ATR-FTIR studies enabled the detection and quantification of BPA, both in the pre-polymerization porogen solution and the polymer matrix. The template-monomer, template-template and template-

crosslinker interactions and their effects on the polymerization reaction were further discussed. Accordingly, we examined whether the conversion profiles and copolymer composition could be altered significantly in the presence of an interacting template-monomer pair and if the solution complexes were translated into the polymer through the templating process. The ultimate goal of our research was to apply this direct detection technique to characterize the post-polymerization binding mechanism.

2. EXPERIMENTAL SECTION

2.1. MATERIALS

Bisphenol A (BPA), Poly (vinyl acetate) (PVAc) (Mw = 100 g mol^{-1}), 4-vinylpyridine (4-Vpy), Triethylenglycol dimethyl ether (TRIGLYME) and Acetaminophen (Paracetamol) were purchased from Sigma Aldrich (Steinheim, Germany). Bisphenol F (BPF), Caffeine, 2, 2-azobis (2-methylpropionitrile) (AIBN) and Ethylene glycol dimethacrylate (EGDMA) were obtained from Fluka (Buchs, Switzerland). All solvents used for rebinding, extraction and IR studies, supplied form Merck (Darmstadt, Germany), were of HPLC grade and used without further purification. Acetic acid (HAc) was supplied from Scharlab (Barcelona, Spain). Water used in the experiments was purified using a Milli Q Ultrapurewater-purification system (Millipore, Bedford, MA, USA). Solvents and reagents

used for NMR analysis were CDCl$_3$ (99.8%), CD$_3$CN (99.8%) d$_6$-acetone, D$_2$O and d$_5$-pyridine, purchased from Merck and used as supplied.

2.2. INSTRUMENTS

2.2.1. FTIR spectroscopy

The IR data were recorded on a Bruker OPUS/IR PS 15 spectrometer. The transmission/absorption measurements of the prepolymerization mixtures were performed in a thin-film liquid cell at room temperature with a 1 mm Teflon spacer and CaF$_2$ windows (Spepac) in the spectral range of 4000-900 cm^{-1}. The spectra were the results of 64 coadded interferograms at a spectral resolution of 2 cm^{-1}.

The FTIR analysis of the pre-polymerization mixture in porogen and solid samples were performed in the attenuated reflection mode (ATR) by using the already described OPUS/IR PS 15 spectrometer (Bruker) equipped with a thermostated MK II Golden Gate^{TM} Diamond 45 ºATR accessory. The non-polymerized sample solution or the analyte or monomers solved in porogen were flushed into the stainless steel micro reaction flow cell anvil (10568) clamped on the ATR crystal. For the polymerized samples, the disks were compressed onto the ATR crystal with the Sapphire Anvil (10531). Owing to the hygroscopic character of these copolymers, the study was carried out after heating at 55 ºC during 15 min to avoid interferences with water bands and H-bonding due to water vapor sorption. Both the spectra of

138

liquid and solid samples were the results of 100 coadded interferograms at 2 cm^{-1} resolution between 400 and 4000 cm^{-1}.

2.2.2. H NMR spectroscopy

^{1}H NMR measurements were performed on an AV500 (N/I 59369) spectrometer operating at 500 mHz at room temperature. For the purpose of spectral clarity 4-Vpy was replaced with d$_5$-pyridine, limiting the observations of changes in chemical shifts of protons only to those of the template species. Spectra were calibrated with respect to the solvent reference signal and chemical shift changes of the template protons were analyzed.

2.2.3. UV-Vis spectroscopy

UV-Vis absorption spectra were recorded on a Cary 100 Conc double-beam UV-Vis spectrophotometer (Varian, USA) at 0.2 cm^{-1} resolution between 200 and 400 nm.

2.3. PRE-POLYMERIZATION STUDIES

The role of electrostatic interactions on MIP-template recognition has been examined through the influence of solvent polarity on the relative strength of template:monomer non-covalent interactions in solution [46].

2.3.1. FTIR analysis

The stoichiometry of the BPA:4-Vpy complex in CCl_4 was calculated by the method of continuous variation (Job's plot) [47] and confirmed by the molar ratio plot (Yoe and Jone's method) [48]. To construct a Job plot, 2.0 x 10^{-2} M stock solutions of 4-Vpy, BPA were prepared. Then a set of 2 mL solutions were prepared by mixing different portions of the template and the monomer. The mole fraction was varied from 0 to 1 and the total concentrations of template and 4-Vpy were kept constant at 6.0 x10^{-3} M. The spectra of the above solutions were recorded and used to construct the plot. To obtain the molar ratio plot, samples of increasing 4-Vpy concentration (1.0 x 10^{-3}-14.0 x 10^{-3} M) were prepared while keeping the concentration of BPA constant (6.0 x 10^{-3} M).

Similar titration experiments using a different concentration range were performed to determine the complex stability constants in CCl_4 (carbon tetrachloride), $CHCl_3$ (chloroform), CH_2Cl_2 (dichloromethane) and ACN (acetonitrile). Solutions of raising 4-Vpy content (1.0 x 10^{-2}-5.0 x 10^{-2} M) were prepared in the mentioned solvents while keeping the concentration of BPA constant (4.0 x 10^{-3} M). The results were the average of three replicate analyses. In order to explain selectivity results, analog titration studies were performed for BPF in $CHCl_3$ and CCl_4 and for paracetamol and caffeine in $CHCl_3$. Owing to the low solubility of BPA and BPF in CCl_4, 300 and 1000 mL of ACN were added to their 2.0 x 10^{-2} M stock solutions, respectively. These stock solutions were then diluted to the proper concentration (4.0 x 10^{-3} M) with pure CCl_4.

Modified Benesie-Hildebrand (BeH) [49,50] equations for 1:1 and 1:2 complexes were used to analyze the data. For the latter, Eq. (1), was applied.

$$\frac{[4-Vpy]_0^2[BPA]_0}{A_c} = \frac{[4-Vpy]_0^2}{2l\varepsilon_c} + \frac{1}{K_H 2l\varepsilon_c} \qquad (1)$$

where $[4\text{-}Vpy]_0$ and $[BPA]_0$ are molar initial concentrations of acceptor and donor monomers, respectively, A_c is the peak area or peak height intensity of the H-bonded pyridine, ε_c means the molar extinction coefficient of the H-bonded pyridine, l is the optical path length (l = 0.1 cm) and K_H is the overall apparent binding constant of complex-formation. In CCl_4 it had also been possible to use the σOH band area of the H-bonded template (donor). In this case Eq. (1) was not be divided by a factor of 2. The values of ε_c and K_H are determined from the slope and the intercept obtained from a linear regression analysis of the double reciprocal linear plot of $[4-Vpy]_0^2[BPA]_0/A_c$ vs $[4-Vpy]_0^2$.

Whereas for complexes with 1:1 (donor-acceptor) stoichiometry Eq. (2) was used,

$$\frac{[BPA]_0}{A_c} = \frac{1}{lK_H\varepsilon_c[4-Vpy]_0} + \frac{1}{l\varepsilon_c} \qquad (2)$$

K_H is determined from the slope and the intercept obtained from a linear regression analysis for the "double reciprocal linear plot" of $[BPA]_0/A_c$ vs. $1/[4\text{-}Vpy]_0$. Eq. (1) and (2) are valid under the condition $[4\text{-}Vpy]_0 \gg [BPA]_0$.

141

2.3.2. ^{1}H NMR analysis

The stoichiometry of the BPA:4-Vpy complex in D_2O:Acetone-d_6 % 50:50 was investigated by H NMR. A mixture of D_2O:d_6-acetone (50:50) was used due to the poor solubility of BPA in D_2O. A Job plot was constructed by mixing varying amounts of equimolar solutions (6.9×10^{-2} M) of template and monomer to constant final volume of 0.750 mL, so that the resulting mixtures ranged from 90% to 10% BPA. The concentration of the complex was calculated as follows:

$$[complex] = [template]_{tot}(\delta_{obs} - \delta_{template}/\delta_{complex} - \delta_{template}) \quad (3)$$

where $[template]_{tot}$ is the total template concentration, δ_{obs} is the observed chemical shift, $\delta_{template}$ is the shift of the free template molecule and $\delta_{complex}$ is the chemical shift of the complex provided by the titration curve [9].

In order to calculate the association constants ^{1}H NMR titration studies were performed by maintaining a constant amount of BPA (4.0×10^{-3} M in $CDCl_3$, 2.0×10^{-2} M in CD_3CN and 2.0×10^{-2} M in CD_3CN and 2.0×10^{-2} M in D_2O:Acetone-d_6 % 50:50) at increasing amounts of d_5-pyridine (from 1 up to 50 or 100 equiv.) with a constant sample volume of 0.750 mL. For selectivity studies, solutions of caffeine (4.0×10^{-3} M) in $CDCl_3$ and paracetamol (3.0×10^{-3} M) in CD_3CN were titrated with pyridine solutions ranging from 1 up to 50 or 100 equiv. of monomer. In all cases, the shifts were used to calculate apparent association constants for the observed

interactions applying a non-linear regression method using the software package Mathcad 11.

For 1:1 stoichiometry the binding constant and limiting chemical shift for the complexes at 25 ºC were estimated by using the following equations and iterative-two parameter fit:

$$\Delta\delta_{obs} = \frac{\Delta\delta_{11}^0 K_{11}[L]}{1+K_{11}[L]} \qquad (4)$$

$$[L] = [L]_t - [T]_t\left(\frac{\Delta\delta_{obs}}{\Delta\delta_{11}^0}\right) \qquad (5)$$

Defining $\Delta\delta_{obs} = \delta - \delta_0$ and $\Delta\delta_{11} = \delta - \delta_{complex}$, where d is the observed chemical shift, δ_0 is the chemical shift without addition of monomer, $\delta_{complex}$ is a limiting chemical shift of the complex, K_{11} is the binding constant of the complex, $[L]_t$ and $[T]_t$ are the total concentration of monomer and template (known to the experimenter), respectively, and [L] are the free equilibrium monomer concentrations [51]. Regarding 1:2 complexes the experimental NMR data have been fit to Eq. (6):

$$\Delta\delta_{obs} = \frac{K_{11}\Delta\delta_{11}^0 + 2K_{11}K_{12}[L]\Delta\delta_{12}^0}{\frac{1}{[T]}+K_{11}+2K_{11}K_{12}[L]} \qquad (6)$$

where $\Delta\delta_{obs}$ difference between the chemical shifts of the template proton in the absence and in the presence of the monomer, $\Delta\delta_{11}^0$ and $\Delta\delta_{12}^0$ are the differences between the chemical shifts of the free and 1:1 and 1:2 complexed species, respectively, K_{11} and K_{12} are the stepwise binding constants, and [T] and [L] are the concentrations of free BPA and 4-Vpy,

respectively. In this equation [T], the (approximate) free template concentration is substituted as a function of [L], $[L]_t$ and the equilibrium constants [52]:

$$[T] = \frac{[L]_t - [L]}{K_{11}[T] + 2K_{11}K_{12}[L]^2} \qquad (7)$$

The (approximate) free monomer concentration is a function of the total concentrations of template and monomer ($[T]_t$ and $[L]_t$, respectively), K_{11} and K_{12} for all points in the experimental curve according to Eq. (8):

$$[L] = \frac{[L]_t + 2K_{11}K_{12}[T]_t[L]_t^2}{1 + K_{11}[T]_t + 4K_{11}K_{12}[T]_t[A]_t} \qquad (8)$$

while $\Delta\delta_{obs}$ and $[T]_t$ are experimentally measured values, $\Delta\delta_{11}^0$, $\Delta\delta_{12}^0$, K_{11} and K_{12} are variables to be estimated from the curve fit to Eq. (6) and [L] is an intermediate variable whose value must be iteratively calculated (Eq. (8)) for all points of the experimental curve. The equation requires fitting with four variables, and thus many combinations may satisfy the model.

2.3.3. UV-Vis spectroscopy

UV-Vis spectroscopy was employed for the rapid determination of the complex stoichiometry whenever the application of alternative techniques was impeded due to low sensitivity, solubility problems or strong solvent absorption. Job's plots were constructed by mixing varying volumes of equimolar solutions (5.0×10^{-3} M) of 4-Vpy and analyte to a constant final volume (10 mL), so that the mole fractions of the resulting mixtures

ranged 0 to 1 and the total concentrations of analyte and monomer were kept constant at 1.0×10^{-4} M. The systems assayed were: BPA:4-Vpy in ACN and water; caffeine:4-Vpy in $CHCl_3$ and paracetamol: 4-Vpy in ACN.

2.3.4. ATR-IR study of template-monomer interactions in triglyme:PVAc porogen

In order to know the relative contribution of the "free" and "associated" pyridine groups with increasing template content, the spectral region between 1615 and 1575 cm^{-1} was deconvoluted using a least-squares curve fitting method. The number of parameters to be determined by the least-squares optimization procedure was minimized to improve the results.

(1) A flat baseline was set between 1800 and 1560 cm^{-1}.

(2) The number of components was defined as two on the basis of the second-derivative spectrum: free pyridine band and H-bonded pyridine.

(3) The peak shape best fits a purely Lorentzian profile. The curve fitting program was allowed to calculate peak position, peak width at half height.

The fraction of H-bonded pyridine groups can be calculated using Eq. (9):

$$f_b = \frac{A_b}{\frac{a_f}{a_b}A_b + A_f} \qquad (9)$$

A_f and A_b are the peak areas of the free and associated pyridine groups. The conversion constant a_f/a_b is the specific absorption ratio of the above two bands. Its value has been estimated by comparing the spectra of a sample (pre-polymerization mixture identical to MIP 5, Table 1) recorded at 60 ºC to that of the same sample recorded at 30 ºC. This is possible because a fraction of free pyridines transform to associated pyridines upon reducing the temperature. In mathematical terms

$$\frac{a_f}{a_b} = (A_b^* - A_b)/(A_f - A_f^*) \qquad (10)$$

where a_b and a_f are the absorptivities of the associated and free pyridine, respectively, A_b^* and A_b are the respective areas of the associated pyridine at 30 and 60 ºC. The areas of the free bands are similarly defined as A_f^* and A_f^*. Three replicate were examined and the average value of the absorptivity ratio was found to be approximately 2.0 ± 0.4 [53].

2.4. PREPARATION OF MIPS

A series of polymers were synthesized using increasing amounts of template. The conditions for each polymer are listed in Table 1. The cross-linker:monomer (EGDMA:4-Vpy) ratio was 1:1 whereas the template:monomer (BPA:4-Vpy) ratio in the mixtures varied from 5.0 x 10^{-2}:1 to 5.1 x 10^{-1}:1. TRIGLYME was used as porogenic solvent for its low vapor pressure to minimize evaporation and PVAc was added as a coporogen to accelerate pore formation. Thin polymer disks were obtained casting the pre-polymerization solution directly onto an appropriate silicon

device. The latter was placed in a suitable airtight container to keep nitrogen atmosphere after purging with nitrogen gas for 5 min to completely evacuate the air. Finally, the polymerization was carried out at 60 ºC for 24 h. Control non-imprinted polymers (NIPs) were similarly prepared [45]. The template was extracted by ten incubations in 5 mL of MeOH:HAc 4:1 during 10 min in an ultrasound bath, followed by five incubations in methanol. The disks were then dried in a vacuum drying oven (40 ºC) and stored at ambient temperature until used.

Table 1. Polymer compositions and polymer ATR characterization.

Polymer entry	0	MIP 1	MIP 2	MIP 3	MIP 4	MIP 5
BPA (mmol)	0	7.5E-03				
4-Vpy (mmol)	1.50E-01	1.50E-01	1.50E-01	1.50E-01	1.50E-01	1.50E-01
EGDMA (mmol)	1.50E-01	1.50E-01	1.50E-01	1.50E-01	1.50E-01	1.50E-01
TRIGLYME-PVAc (µL)	85	85	85	85	85	85
BPA:4-Vpy	0	5E-02:1	9E-02:1	1.7E-1:1	3.4E-01:1	5.1E-01:1
X_{BPA}	0	9.5E-03	1.75E-02	3.16E-02	6.13E-02	8.93E-02
DC (%)	8.8E01± 2E-01	8.31E01± 3E-01	7.99E01± 6E-01	8.54E01± 1E-01	8.73E01± 2.9	8.51E01± 6.1
A1597/1720	1.1E-01± 2E-02	1.2E-0.1± 1E-02	1.4E-01± 1E-02	1.0E-01± 1E-02	1.1E-0.1± 1E-02	9.9E-02± 2E-03
A1513/1720	—	1.0E-0.2± 2E-03	2.4E-0.2± 3E-03	4.7E-0.2± 2E-03	7.3E-0.2± 3E-03	8.4E-0.2± 4E-03
A1513/1720	—	6.5E-0.2± 4E-03	4.3E-0.2± 2E-03	6.1E-0.2± 1E-03	4.9E-0.2± 3E-03	4.6E-0.2± 3E-03

*Changes in BPA content upon rebinding with a 2.6 mM BPA water solution.

2.5. ATR-IR BATCH REBINDING EXPERIMENTS

Several replicates of MIP 3 composition were further synthesized and used for batch adsorption experiments to evaluate binding. As a starting point,

the equilibrium experiments were carried out in solvents of increasing polarity to assess the role played by the solvent in binding capacity. 1.79 x 10^{-3} M BPA solutions in $CHCl_3$, ACN and water were prepared. The polymer disks were incubated in 2.0 mL BPA solutions during 20 min in ultrasound bath in a 5 mL vessel at room temperature. As reported elsewhere, the adsorption equilibrium was achieved during this period [45]. The samples were thoroughly rinsed with the rebinding solvent to remove any physisorbed molecules and dried in vacuum oven at 40 ºC. The amount of analyte bound to the polymer was directly estimated by ATR-FTIR. Between rebinding tests, the polymers were washed twice with MeOH:HAc 4:1 followed by washing twice with MeOH to ensure the extraction of bound BPA. For comparison, several NIPs were subjected to the assays described above.

Secondly, we were interested in recording binding isotherms in water. Therefore, MIPs and NIPs disks were incubated with 2 mL BPA water solutions of concentrations ranging from 2.2 x 10^{-4} to 2.64 x 10^{-3} M. Finally, to evaluate selectivity MIPs and NIPs were incubated with water solutions of BPF, caffeine and paracetamol (1.79 x 10^3 M). The procedure used in both type of studies was the same to that described in the previous paragraph. In all cases, the results were the average of triplicate analysis.

2.6. ATR-IR STUDY OF TEMPLATE-POLYMER INTERACTIONS

A quantitative study of the fraction of associated pyridine groups upon increasing the template content has been performed in the MIPs before

extraction and after rebinding. The methodology employed was similar to the one carried out in Section 2.3.4, except that the number of components was defined as three on the basis of the second-derivative spectra and the peak shape best fits a purely Gaussian profile. The fraction of pyridine bonded groups was calculated using Eq. (9) although the value of the specific absorption ratio of the two pyridine bands in the polymer, a, is 1, according to literature [54, 55].

2.7. PARTICLE SIZE ANALYSIS

The MIP type 3 discs were ground by hand and suspended in water, ACN and $CHCl_3$ for more than 48 h. A light transmission microscope (Leica DM2500 microscope) combined with a DFC295 camera was used for particle analysis. Images of the particles were taken with 20X and 100X objectives and 10X optic magnifications. The images were then analyzed using the program ImageJ to obtain particles size distribution. On average ~ 100 particles were measured for each analysis of the polymer suspension.

3. RESULTS AND DISCUSSION

3.1. STUDIES OF THE MIP PRE-POLYMERIZATION COMPLEX

3.1.1. IR transmission spectroscopy of template-monomer interactions

To confirm the nature of the BPA:4-Vpy interactions in a nondissociating solvent such as CCl_4 a titration was performed keeping the BPA concentration constant. The reaction of a phenol (H-bond donor) and a pyridine (H-bond acceptor) may lead to the formation of an H-bonded complex. FTIR spectroscopy enabled identifying the free and hydrogen-bonded species since both the spectral features of the alcohol and 4-Vpy can be traced following the complexation event [1].

The main characteristics of the BPA spectrum in CCl_4 are described first: two bands in the hydroxyl stretching frequency (σOH) region, a sharp peak 3612 cm^{-1} and a broad band at 3462 cm^{-1}; the para-substituted aromatic system produces well defined peaks at 1611, 1595, 1513, 1175 cm^{-1} [56]. In the FTIR spectra, the most sensitive region for H-bond interaction is the absorption of σOH. In the absence of 4-Vpy, self-association was observed between the BPA molecules (Fig. 1). The sharp band at 3612 cm^{-1} ($w_{1/2}$ = 16 cm^{-1}), the only one detected at low BPA concentrations ($<1.0 \times 10^{-3}$ M), was assigned to free OH groups. At higher concentrations a broad band centered at approximately 3462 cm^{-1} ($w_{1/2}$ = 78 cm^{-1}) became increasingly important and was attributed to the wide distribution of H-bonded dimmers and multimmers [57] (Fig. 1, solid line). When titrated with solutions of various 4-Vpy concentrations, the spectral features revealed distinct changes which were highlighted through spectral subtraction. The vibrational mode at 1513 cm^{-1} had been employed for the digital subtraction of the BPA spectrum from the binary mixtures. The difference spectra were characterized by the progressive decrease of the bands at

3612 and 3462 cm^{-1} and a gradual increase of a very broad band centered at 3135 cm^{-1} (w$_{1/2}$ = 300 cm^{-1}) (Fig. 1, discontinuous lines). The latter suggested the presence of intermolecular H-bonding between BPA and the monomer. Furthermore, the shifting of the H-bonded hydroxyl band to a lower wavenumber revealed that the inter-molecular OH-pyridine interaction is stronger than the self-association. The frequency difference between the H-bonded and the free OH absorption has been used to investigate the average strength of intermolecular interaction [58]. From this point of view, the OH-pyridine inter association (ΔσOH = 477 cm^{-1}) is more favorable than the OH self-association of pure BPA (ΔσOH = 150 cm^{-1}) in accordance with previous findings [17, 59].
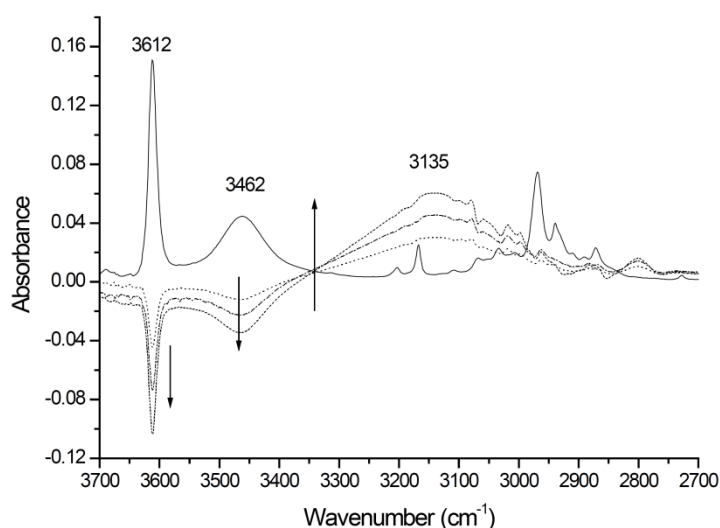
Figure 1. IR titration study of BPA with 4-Vpy in CCl$_4$ in the υ$_{OH}$ spectral region: BPA (4.0 x 10^{-3} M) (solid line); difference spectra obtained after subtraction of a normalized BPA spectrum to solutions of BPA and increasing concentrations of 4-Vpy (1.0 x 10^{-2} to 5.0 x 10^{-2} M) (discontinuous lines).

From another point of view, the most intense bands corresponding to pyridine ring modes are those located at 1596 and 1549 cm^{-1} in CCl$_4$ (Fig. 2). These bands showed different behavior. The latter peak was not affected by H-bonding. Conversely, the pyridine ring mode at 1596 cm^{-1} ($\upsilon_{C=N}$) became broad and shifted toward higher wavenumber. As a result of H-bonding, a new band appeared at 1604 cm-1 ($\Delta\upsilon$ = 8 cm^{-1}). Unfortunately, this band is overlapped to the 1596 cm^{-1} pyridine peak. In addition, BPA absorbs in the region 1650-1575 cm^{-1} with two bands at 1611 and 1595 cm^{-1} (Fig. 2); therefore, to account for the evolution of the pyridine modes without interferences a double spectral subtraction was carried out. Firstly, the BPA contribution was removed as described in the preceding paragraph. Afterward, a spectrum of pure pyridine of similar concentration was subtracted normalizing to the 1549 cm^{-1} peak. In the double difference spectra, the augment of the 1604 cm^{-1} band upon titration was clearly observed (Fig. 2 inset). This effect is attributed to an increase of the stiffness in the pyridine ring due to changes in electronic distribution upon formation of H-bonds [55] and has been found to be dependent on the nature of the H-donor [60]. From another point of view, no new band around 1630-40 cm^{-1}, assigned to a ringstretching vibration of the pyridinium cation, has been observed, discarding ionization [61].
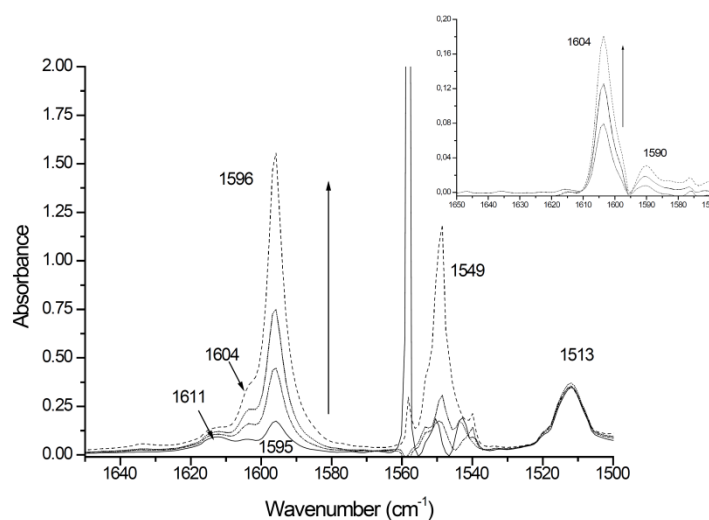
Figure 2. IR titration study of BPA with 4-Vpy in CCl_4 in the spectral region between 1650-1500 cm^{-1}: BPA (4.0×10^{-3} M) (solid line); titration of BPA with 4-Vpy (1.0×10^{-2} to 5.0×10^{-2} M) (discontinuous lines); Inset: double difference spectra.

Another pyridine ring band affected by H-bonding is the ring breathing mode at 991 cm^{-1}. This band, which is overlapped to another one insensitive to H-bonding at 988 cm^{-1}, shifted toward higher wavenumbers in a larger magnitude than the previously described pyridine ring mode and resulted in a new peak at 1002 cm^{-1} ($\Delta\upsilon = 11\ cm^{-1}$) (Fig. 3). The increasing profile of this peak with the monomer content showed a similar trend than the 1604 cm^{-1} band, supporting the existence of a BPA:4-Vpy H-bonded complex (Fig. 3 inset) [55, 60].
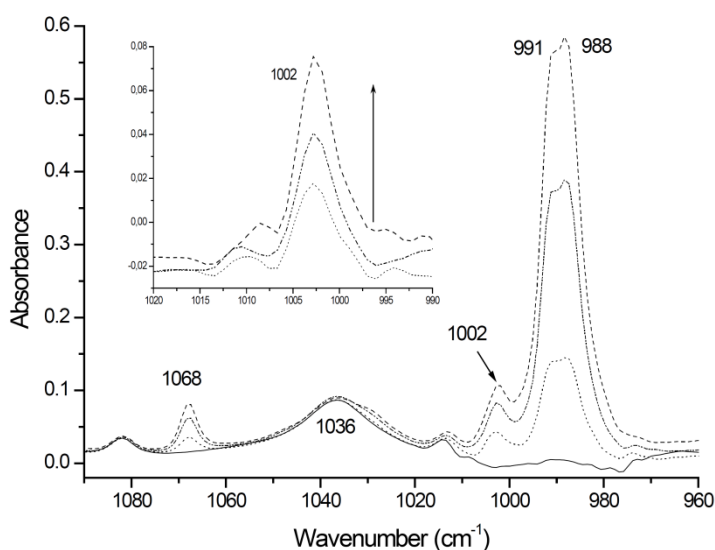
Figure 3. IR titration study of BPA with 4-Vpy in CCl_4 in the spectral region between 1080-960 cm^{-1}: BPA (4.0 x 10^{-3} M) (solid line); titration of BPA with 4-Vpy (1.0 x 10^{-2} to 5.0 x 10^{-2} M) (discontinuous lines); Inset: double difference spectra.

To perform a quantitative analysis of the described interactions the double difference spectra of the BPA:4-Vpy mixtures were evaluated. The area or peak height of the BPA band at 3135 cm^{-1} and pyridine peaks at 1604 and 1002 cm^{-1} were proportional to the complex concentration. The complex stoichiometry was determined by both continuous variation (Job's plot) and mole ratio methods. A plot of the (area of the peak at 1604 cm^{-1}...X_{4-Vpy}) against X_{BPA} gave a maximum at about 0.3-0.4 indicating the formation of a BPA:4-Vpy 1:2 complex (Fig. 4(I), left axis). When the areas of the 4-Vpy at 1604 cm^{-1} were plotted against the mole ratio [4-Vpy]/[BPA], the plot leveled off at around 2, confirming the 1:2 complex (Fig. 4(II)). A similar result was obtained plotting the peak height of the H-bonded pyridine band at 1002 cm^{-1} (not shown).

154
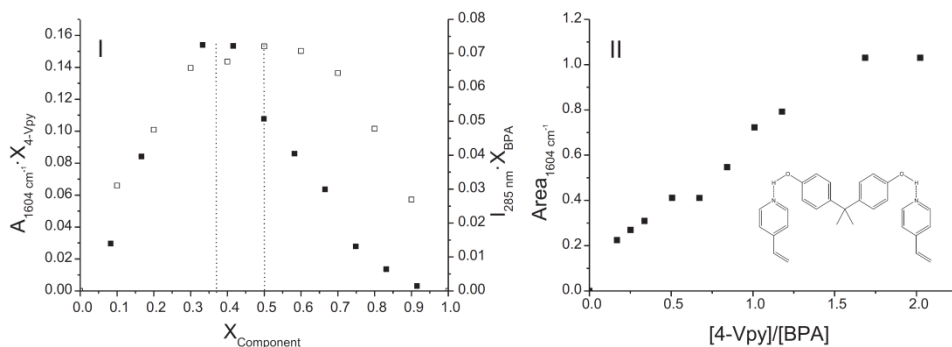
Figure 4. BPA: 4-Vpy complex stoichiometry : (I) Job´s plot: (left axis, filled squares) FTIR analysis in CCl_4 against X_{BPA} ; (right axis, blank squares) UV-Vis analysis in ACN against X_{4-Vpy} and (II) FTIR mole ratio plot in CCl_4.

To determine the complex binding constants, independent titration experiments were performed in CCl_4, $HCCl_3$, CH_2Cl_2, and ACN. In the three chlorinated solvents, experimental data showed good correlation when Eq. (1) was tried, supporting the formation of a 1:2 complex. On the contrary, data showed wide scatter and bad correlation with Eq. (1) in ACN, but a better linear plot according to Eq. (2). The 1:1 stoichiometry of the complex BPA:4-Vpy in ACN was further confirmed by UV-Vis spectroscopy. A plot of (Absorbance at 285 nm x X_{4-Vpy}) against X_{BPA} gave a maximum at 0.5 (Fig. 4(I), right axis). These results contradicted the 1:2 complexation model that best fitted Nguyen and Ansell NMR titration data for the same system and solvent, though using a higher concentration [11].

The analysis was performed at different wavelengths for which the complex showed absorption. In all the solvents assayed, the area and peak height of the H-bonded pyridine at 1604 cm^{-1} plus the area at 1002 cm^{-1} were

considered. In addition, it had been possible to use the σOH band area of the H-bonded template in CCl_4. Table 2 lists the values of the apparent binding equilibrium constants (K_H) and ε_c for the H-bonded complexes at 25 ºC as a function of solvent polarity [62, 63]. For comparison, the molar absorption coefficients of the free monomer, εfree 4-Vpy, were calculated from standard 4-Vpy solutions of increasing concentration on the basis of the Lambert-Beer Law. In principle, the K_H values for each acceptor: donor pair in the same solvent should be alike independently of the wavelength considered. The variations observed are ascribed to experimental error, especially when the small 1005 cm^{-1} band areas are considered.

More to the point, except for ACN, the binding constant values (2.15×10^3-4.95×10^3 M^{-1}) suggested a good stability for these complexes. They are in the range expected for strong H-bonded complexes, though not as strong as 1:2 complexes formed by two or more-point cooperative hydrogen-bonding [5, 6]. As the polarity of the solvent increased the binding constant was expected to decrease [13]. This assessment did not apparently apply for CCl_4, owing to the small volumes of ACN added in order to solve solubility problems which altered the solvent polarity. ACN is capable of forming H-bonds with the hydroxyl groups, thereby reducing the effect of H-bonding to 4-Vpy.

Table 2. Apparent equilibrium constants (KH) and molar extinction coefficients (ε_c) for the H-bond formation of BPA:4-Vpy and BPF:4Vpy systems at 25 ºC as a function of solvent polarity.

Template	Solvent (log P)*	Parameters	$Area_{3140}$	$Area_{1605}$ $Area_{1598}$**	$Intensity_{1605}$ $Intensity_{1598}$**	$Area_{1005}$
BPA	CCl$_4$ (2.83)	K_H (M^{-1})	4.35E03±5.10E02	3.40E03±6.40E02	3.02E03±2.67E02	4.46E03±9.92E02
		ε_C (M^{-1} cm^{-1})	3.33E04±1.36E03	1.52E03±2.52E02	2.27E02±3.4E01	4.70E02±1.1E01
		ε_F (M^{-1} cm^{-1})	-	2.94E03±9.0E01**	2.95E02±2.1E01**	-
	CHCl$_3$ (2.0)	K (M^{-1})	-	4.48E03±2.80E02	4.87E03±1.00E02	4.95E03±5.00E02
		ε_C (M^{-1} cm^{-1})	-	2.50E03±1.25E02	3.43E02±7	1.02E03±2.1E01
		ε_F (M^{-1} cm^{-1})	-	3.24E03±6.4E01**	4.05E02±1.3E01**	-
	CH$_2$Cl$_2$ (0.60,1.25)	K (M^{-1})	-	2.15E03±1.50E02	2.97E03±2.8E01	4.91E03±2.22E02
		ε_C (M^{-1} cm^{-1})	-	3.11E03±6.60E02	3.40E02±5.0E01	7.18E02±1.8E01
		ε_F (M^{-1} cm^{-1})	-	2.64E03±7.00E02**	3.90E02±1.0E01**	-
	CAN (-0.34)	K (M^{-1})	-	1.20E01±6	7.0±2E-01	-
		ε_C (M^{-1} cm^{-1})	-	-	3.90E02±8.0E01	-
		ε_F (M^{-1} cm^{-1})	-	2.94E03±9.0E01**	4.58E02±1.6E01**	-
BPF	CCl$_4$ (2.83)	K (M^{-1})	4.00E03±1.00E02	2.75E03±2.12E02	2.49E03±1.0E01	3.47E03±3.30E02
		ε_C (M^{-1} cm^{-1})	2.33E04±2.89E03	1.83E03±1.40E2	2.50E02±2.0E01	4.81E02±5
		ε_F (M^{-1} cm^{-1})	-	2.94E03±9.0E01**	2.95E02±2.1E01**	-
	CHCl$_3$ (2.0)	K (M^{-1})	-	5.83E03±6.50E02	5.63E03±6.82E02	8.23E03±7.42E02
		ε_C (M^{-1} cm^{-1})	-	1.24E03±2.98E02	1.58E02±0.25E01	3.05E02±2.7E01
		ε_F (M^{-1} cm^{-1})	-	3.24E03±6.4E01**	4.05E02±1.3E01**	-

* log P is the logarithm of a given compound in the octanol-water two- phase system [62, 63].

**$\varepsilon_{free\ 4\text{-}Vpy}$ calculated from standard 4-Vpy solutions.

3.1.2. ^{1}H NMR spectroscopy of template-monomer interactions

To validate the results obtained in the IR studies and to assess the molecular interactions in aqueous solutions, ^{1}H NMR titrations studies of

the BPA:d_5-py system were performed in CDCl$_3$, CD$_3$CN and D$_2$O:d_6-acetone (50:50). These studies confirmed that the primary interaction mechanism in organic solvents was based on H-bonding. The signal of the phenyl hydroxyl protons of BPA strongly migrated downfield as the titration progressed up to $\cong$ $\Delta\delta$ = 5 ppm in CDCl$_3$ (Fig. 5). The hydrogen interaction could also be observed by monitoring the chemical shift of the neighboring protons although to a lesser extent than the OH shift change. Generally speaking, the extent was proportional to their proximity to the H-donor group: changes were more notable in H3 than in H2 and negligible for H1. The corresponding binding isotherms from a BPA:d_5-py titration in CD$_3$CN showed the same trends although the magnitudes of the changes in chemical shifts were smaller (results not shown).

On the contrary, the hydroxyl protons in polar media were difficult to observe in D$_2$O:d_6-acetone (50:50), owing to rapid exchange between the labile protons of BPA and the solvent deuterium atoms. However, the hydrogen interaction could still be followed by monitoring the chemical shift of the neighboring protons [64]. The signal of the H3 protons migrated downfield in the presence of increasing amounts of d_5-pyridine. Notwithstanding, the different nature of the interaction between BPA and d_5-py in the presence of D$_2$O might explain for the opposite direction of the changes it caused to the chemical shifts of the H2 and H1 protons (Fig. 6(I)). O'Mahony et al. concluded that the ionic pair complex formed between 2,4-diclorophenoxyacetic acid and d_5- pyridine in aqueous solution was further stabilized by secondary aggregation of aromatic components

induced by the hydrophobic phenomenon [9]. Likewise, the opposite trend of BPA H2 and H1 protons could be provoked by a π-π stacking effect along with H-bonding due to hydrophobic effects.
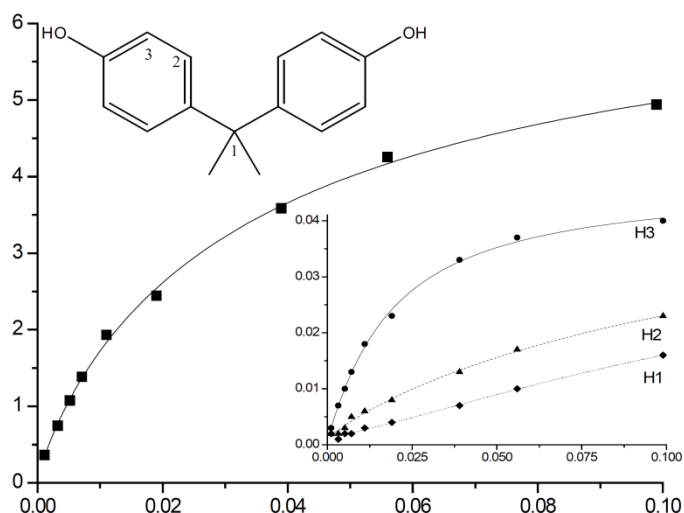
Figure 5. ^{1}H NMR titration of BPA with d_5-pyridine in CDCl$_3$ ([BPA] = 4 x 10^{-3} M). The symbols correspond to the experimental data points; the solid curves are the best fit based on Eqs. (6) and (8).

To clarify this point, the stoichiometry of complexation was further investigated using a Job's plot. The analysis indicated a 1:1 template-monomer stoichiometry (Fig. 6(II)). Another Job's plot was performed in pure water by UV-Vis spectroscopy, confirming a 1:1 template-monomer complex in the absence of acetone (results not shown). Hence, albeit no pep stacking of additional molecules were present in our system, the ^{1}H NMR shifts suggested that the 1:1 complex conformation in aqueous environment may be different to the one formed in CD$_3$CN. The

hydrophobic contribution due to the strong solvent-solvent interactions is the main driving force for complexation in water. If the cavity model point of view is adopted, it is found that the hydrophobic contribution to the free energy of binding is proportional to the decrease in cavity surface area on complex formation [51]; thus, in order to reduce the total surface area of hydrocarbon exposed to aqueous media the system could alter the conformation so that the overlapping area between the template and monomer rings in the 1:1 complex might be greater in water than in CD_3CN.
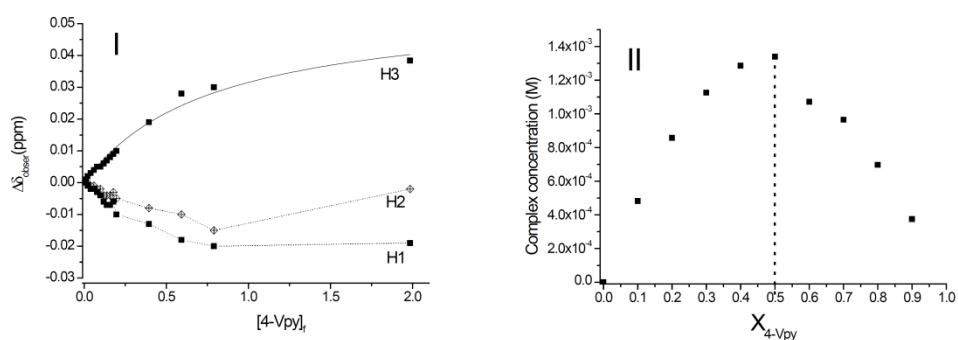
Figure 6. (I) ^{1}H NMR titration of BPA with d_5-pyridine in d_6-acetone: D_2O (50:50). ([BPA] = 2.0 x·10^{-2} M). The symbols correspond to the experimental data points; the solid curve for H3 is the best fit based on Eqs. (4) and (5); (II) ^{1}H NMR Job´s plot for the complexation between BPA and d_5-py in d_6-acetone:D_2O (50:50).

Our results are in accordance with the observations of Zhu et al. [65] based on FTIR analysis and molecular dynamic calculations. They proved that the interaction between BPA and aromatic molecules in waste water samples occurred primarily by H-bonding and not aromatic interactions. On the contrary, other authors concluded from Molecular dynamic simulations and indirect rebinding studies that 4-Vpy based MIPs recognized phenol

mainly trough hydrophobic interactions (Van der Waals and π-π stacking) when the rebinding medium was water [17]. In any event, though Van der Waals interactions could not be discarded, π-π stacking of additional pyridine molecules had not been demonstrated in water.

Although the extent of template-monomer complexation is influenced by self-association of monomer and template [11], this has been neglected in this primarily quantitative study. Hence, assuming that the chemical shift changes reflected basically 1:1 complexation between BPA and d_5-Py in CD_3CN and D_2O:d_6-acetone (50:50) and 1:2 complex in $CDCl_3$, their binding constants and limiting chemical shifts were estimated as described in Section 2.3.3.

The parameter values obtained from the curve fitting analysis are displayed in Table 3. They should be regarded as indicating trends rather than strict numbers due to the non-straightforward calculations from the NMR data that rule out an exact solution, specially for 2:1 complexes [51, 52], but are in general agreement with the FTIR results. Moreover, although the magnitudes of the changes in chemical shift of the various protons considered differed in relation to proximity to the site of interaction, the calculated apparent constants were similar within experimental error. The strongest H-bonded complex between BPA and pyridine was formed in $CDCl_3$, followed by D_2O:d_6-acetone (50:50) mixture and CD_3CN. It has been demonstrated than when polar solvents were used for MIP synthesis, they were liable for rupturing the H-bonds of the pre-

polymerization complex. BPA is solvated in CD_3CN and d_6-acetone:D_2O to a greater extent, which hinders the access of d_5-pyridine.

Table 3. Parameter values obtained by fitting titration ^1H NMR curves for BPA: d_5-Py complex formation in different solvents.

Solvent	Proton	K_{11} (M^{-1})	$\Delta\delta_{11}$ (ppm)	K_{12} (M^{-1})	$\Delta\delta_{12}$ (ppm)
$CDCl_3$	OH	5.15E03±6.5E01	9.97E-03±2E-05	9.28E01±6E-01	6.08±1.8E-01
	H3	5.59E03±6.5E01	-	1.18E02±1E-01	5.77E-02±6E-04
	H2	5.41E03±4.46E02	8.95E-04±6E-06	1.09E02±6	2.45E-02±6E-04
CD_3CN	OH	9.47E-01±3.2E-02	4.61±4E-02	-	-
	H3	3.34E-01±2.8E-02	2.04E-01±1.7E-02	-	-
d_6-acetone:D_2O	H3	1.16±1.2E-01	5.57E-02±3.0E-03	-	-

*Each regression is based on 11-16 data points and is presented with the standard error. The goodness of fit (R^2) was 0.98 or better in all cases

3.1.3. ATR-FTIR studies of the MIP pre-polymerization complex in Triglyme-PVAc
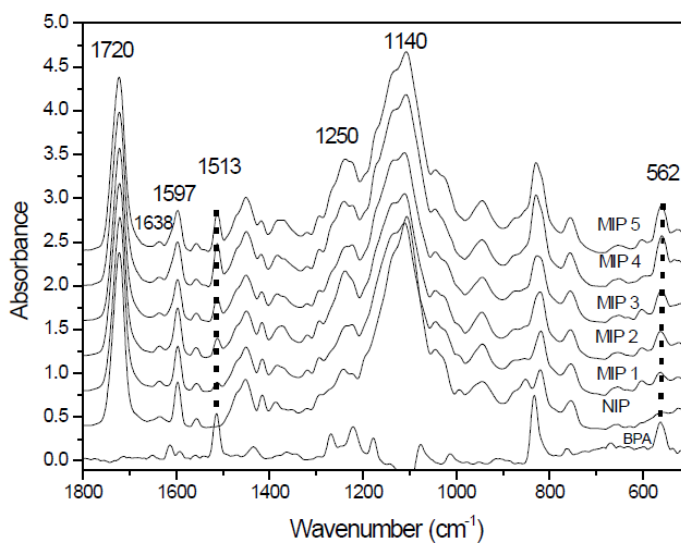
Figure 7. ATR spectra of BPA in porogen solution, non-imprinted polymer (NIP) and BPA-MIPs of increasing template: monomer ratio. The spectra were normalized according to the EGDMA peak at 1720 cm^{-1}.

Initially the ATR spectra of the MIP components in porogen were monitored to obtain characteristic "fingerprints" for their identification. The BPA bands at 1513 cm^{-1} and at 562 cm^{-1} did not overlap any bands of the monomers and therefore have been used to identify the presence of the template both in the prepolymerization mixture and in the MIP (Fig. 7).

The spectra of the pre-polymerization mixtures described in Table 1 were recorded before the polymerization reaction. In spite of the high noise to signal ratio and only in the more concentrated mixtures (pre-MIP 4 and 5), two broad absorption bands were observed in the σOH region. The first one around 3366 cm^{-1} was allotted to self-bonded OH groups of BPA as is the only one observed in the BPA spectrum in porogen. The second one about 3090 cm^{-1} was ascribed to BPA OH groups H-bonded to 4-Vpy monomer. The H-bonding complex formation between BPA and 4-Vpy in the porogen mixture was further confirmed by analyzing the monomer bands sensitive to H-bonding at 1596 and 991 cm^{-1}. Upon increasing the template content two new bands attributed to pyridine-hydroxyl H-bonding appeared at 1604 and 1002 cm^{-1}. The fraction of associated pyridine groups upon increasing the template:monomer ratio was evaluated as described in Section 2.3.4 and shown in Fig. 8(II). The extent of H-bonded pyridines increased almost linearly with the template:monomer ratio. TRIGLYME is an aprotic ethylene oxide based solvent of high viscosity and strong IR absorption. Due to its physical properties neither the complex stoichiometry nor the binding constant could be calculated; nonetheless, the results suggested weak complexation explained by its polar nature (log

P = -1.9 in the octanol-water two-phase system) [63] and its capacity to form H-bonds with the template OH groups.
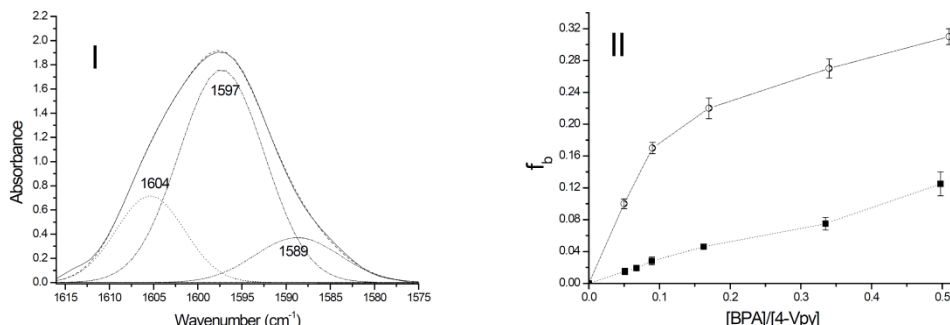
Figure 8. (I) Curve-fitting analysis of the 4-Vpy $\upsilon_{C=N}$ absorptions for MIP 5 ATR–spectrum after subtraction of BPA contributions; (II) Fraction of H-bonded pyridine (f_b) *versus* BPA:4-Vpy molar ratio in porogen pre-polymerization solution (filled squares) and in MIPs minus an average 0.15 bonded fraction to water vapor (half filled circles).

The interaction of the crosslinker with the template and the functional monomer 4-Vpy was investigated, resulting in no significant changes of the monitored spectral features (neither band shift nor broadening of the EGDMA ($\upsilon_{C=O}$ band at 1720 cm^{-1}). Hence, it is concluded that, in the selected concentration range, the crosslinker did not have a measurable impact on the BPA:4-Vpy complex formation in the pre-polymerization mixture.

3.2. STUDIES OF THE MIP POST-POLYMERIZATION COMPLEX

3.2.1. ATR spectra of MIPs

The ATR spectra of the MIPs together with the non-imprinted polymer (NIP) and BPA spectrum in porogen solution are displayed in Fig. 7. The BPA peaks at 1513 and 562 cm^{-1} were present in the MIPs, thus providing an unambiguous means of identifying the analyte. Their intensities clearly increased upon raising the template: monomer ratio. Conversely, the broad asymmetric absorption at 3366 cm^{-1}, attributed to self-bonded OH groups of BPA, was only vaguely detected in the spectra corresponding to the MIPs of the highest template:monomer ratios, MIPs 4 and 5 (region not shown).

Regarding the polymer, the presence of three significant peaks around 1720 cm^{-1} (carbonyl ester stretching mode, $\upsilon_{C=O}$), 1250 and 1140 cm^{-1} (ant symmetric and symmetric C-O-C stretching mode, υ_{C-O-C}) supported the existence of poly (EGDMA) in the obtained MIPs and NIPs. The characteristic peaks at 1597 and 1558 cm^{-1} corresponding to the $\upsilon_{C=N}$ in the pyridine ring could also be observed. Besides, the existence of a small peak around 1638 cm^{-1}, allotted to the $\upsilon_{C=C}$ mode, demonstrated that less than 100% of the bonded EGDMA molecules were cross-linked in the polymers [66].
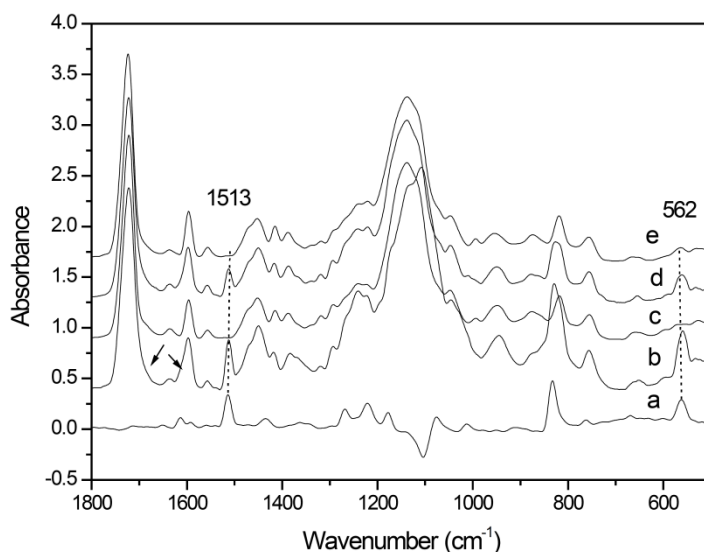
Figure 9. Effect of washing and rebinding: BPA in porogen solution (a), MIP 4 (b), extracted MIP 4 (c), MIP 4 rebound with a water BPA solution of 2.6 x 10^{-3} M (d) and washed non-imprinted polymer (e).

The effect of washing and rebinding was also examined. The removal of BPA from its MIP is shown upon comparing **Fig. 9b** and **c**. The BPA peaks at 1513 and 562 cm^{-1}, disappeared in the extracted polymer and the reduction of the EGDMA and 4-VPy bands widths was evident at 1720 and 1598 cm^{-1}; there was also a decrease in absorbance in the region between 3600 and 3200 cm^{-1}. In summary, the extracted spectrum was identical to that of the washed NIP (Fig. 9e). Concerning the rebinding, after the MIP immersion in BPA-water solutions the characteristics bands at 1512 and 562 cm^{-1} reappeared in the spectrum (Fig. 9d) and an increase in absorbance around 3400 cm^{-1} could also be spotted for high BPA concentrations. These observations present spectroscopic evidence that

both molecular transport and binding occurred in the synthesized polymers.

3.2.2. ATR-polymer characterization

The polymers were characterized to determine if there were any differences between their chemical composition and degree of crosslinking [67, 68]. The percentage of unreacted carbon-carbon double bonds was determined from the ratio of absorbance areas of the peak at 1638 cm^{-1} against an internal standard (the $v_{C=O}$ EGDMA band at 1720 cm^{-1}) before and after polymerization. The degree of monomer conversion (DC%) was calculated using Eq. (11) [69]:

$$DC(\%) = 100 - \frac{[(abs(C=C)_{1638})/(abs(C=O)_{1720})_{polymerized}]}{[(abs(C=C)_{1638})/(abs(C=O)_{1720})_{monomer}]} x100 \qquad (11)$$

Another concern was the possibility for leaching of the monomer by the presence of the template. This would be more severe as the amount of template increased. Thus, the incorporation of 4-Vpy in MIPs was estimated using the ratio of the area under the pyridine ring at 1597 cm^{-1} over that found for the band at 1720 cm^{-1}. The higher the ratio, the greater would be the content of pyridine versus the cross-linker. Extracted MIPs spectra were used for both calculations. The averaged values corresponding to triplicate analysis together with the standard deviations are displayed in Table 1.

All MIPs had roughly the same degree of crosslinking and identical relative amounts of 4-Vpy to EGDMA. Furthermore, the mean DC% values of 8 MIPs of 0.17:1 template:monomer ratio (MIP 3) and 8 NIPs synthesized in identical conditions, 86.5 ± 4.3 and 87.7 ± 2.2, respectively, were not statistical significant (Student test, P > 0.05). Likewise, their respective mean ratios 4- Vpy:EGDMA, $1.0 \times 10^{-1} \pm 1 \times 10^{-2}$ and $1.2 \times 10^{-1} \pm 1 \times 10^{-2}$, were also equivalent (Student test, P > 0.05). The above results revealed that the crosslinking densities were high enough for stabilizing the shapes of the imprinted cavities [66]. Furthermore, even though increasing the amount of template changes the distribution of monomers in the MIPs, the polymer composition and degree of cross-linking were unaffected.

The ratio of the template and polymer band areas (A_{1513}/A_{1720}) offers the potential to use such an approach for quantitative assessment of the template level. When the whole concentration range was considered (MIP 1 to MIP 5, Table 1), the ratio variation with BPA concentration in the pre-polymerization mixture is nonlinear (polynomic grade 2, r = 0. 998). Such a behavior was directly related to an augment in the self-association of BPA upon increasing its molar fraction [56]. Yet, the ratio variation with concentration is linear up to a BPA:4-Vpy molar ratio of 0.17:1 (MIP 3) (r = 0.996).

One undesirable effect of adding an excess of template is the loss of site integrity due to coalescence of the binding sites, which is related to the extent of template aggregation [70]. Besides, no improvement in loading

capacity upon increasing the BPA content in the pre-polymerization solution is observed after rebinding with a 2.6 x 10^{-3} M BPA water solution (Table 1). As a result, the MIP 3 was selected as the optimized composition for further rebinding and selectivity studies. More to the point, the ratio A_{1513}/A_{1720} provides an effective means for the measurement calibration provided that the analyte:monomer molar ratio is within the linear behavior [27].

3.2.3. Template-polymer interactions

ATR-FTIR analysis confirmed the presence of specific H-bonding interactions between the template and the monomer in the polymers under study. As it has been pointed out in the preceding sections, the most sensitive region for H-bond interaction is the absorption of v_{OH} but the noise to signal ratio is high in the ATR mode. Accordingly, the wide bands at 3366 cm^{-1} and 3100 cm^{-1}, attributed to self-H-bonds and BPA:4-Vpy H-bonds, respectively, were scarcely detected in the spectra of MIPs with the highest template:monomer ratios (MIP 4 and MIP 5); as a result, a further discussion in this region was not possible.

Hence, in the following analysis we were mainly concerned with the region from 1620 to 1540 cm^{-1}, where the pyridine ring modes are located at 1597 and 1558 cm^{-1}. After subtraction of the BPA spectrum normalized to band 1513 cm^{-1}, it was clearly seen that upon increasing the template content the 1597 cm^{-1} band shifted toward high wavenumber and

broadened. The second-derivative analysis revealed the peaks at 1597 and 1604 cm^{-1}, ascribed to free and H-bonded pyridine rings, respectively, plus a smaller one at 1589 cm^{-1}. The latter could arise from a conformational rearrangement of the BPA aromatic groups as a result of H-bonding complexation, as the in-plane aromatic group stretching vibrations around 1600 cm^{-1} are conformationally sensitive [71]. These three peaks could be observed independently using the curve-fitting methods described in Section 2.6 (Fig. 8(I)).

The fraction of H-bonded pyridine groups (f_b) in the MIPs was evaluated as a function of the template:monomer molar ratio. As expected, the f_b raised with the template content. Notwithstanding, NIPs and extracted MIPs had between 15 and 20% of their pyridine sites H-bonded, owing to the hygroscopic character of the amorphous polymers and insufficient water evaporation after heating 15 min at 55 ºC. Therefore, the MIPs f_b, values were subtracted an average figure of 0.15 to deduct the pyridine fraction bonded to water vapor. The final data were plotted versus the template:monomer composition and compared with the f_b in the corresponding porogen pre-polymerization solutions (Fig. 8(II)). As a starting point, the f_b in polymers increased linearly up to a BPA:4-Vpy molar ratio of approximately 0.1; from then onwards the rising slowed down. For MIP 1 and MIP 2 the fb was almost twice the BPA:4-Vpy molar ratio, suggesting that nearly all the BPA hydroxyl groups participated in inter-H bonds with 4-Vpy forming 1:2 complexes and providing direct physical evidence that non-covalent monomer-template interactions

survived the polymerization process [10]. However, beyond MIP 3 the f_b was evidently lower than the BPA:4-Vpy molar ratio, partly due to the aforementioned increase in the template aggregation.

A noteworthy point is that the f_b in the pre-polymerization mixture does not correlate with the number of H-bonded monomers found in the corresponding polymer. Similarly, Kim and Spivak [67] found that the behavior of the polymer binding sites cannot always be explained by the complex concentration in solution. Therefore, the number of binding sites is not determined directly by the solution phase pre-polymerization complex; rather, it is determined during polymerization. They hypothesized that phase separation phenomena that take place during polymerization could allow for the aggregation of polar functional groups in binding site "pockets", resulting in binding sites with multiple functionalities.

Correspondingly, the other pyridine ring band affected by H-bonding, the spectral mode at 993 cm^{-1}, shifted toward high wavenumbers and resulted in a new peak at 1003 cm^{-1} [55]. Unfortunately, the latter peak overlapped with the intense σC-O band of the crosslinker and a quantitative analysis was complicated, but a qualitative discussion was possible. The band ratio 993/1003 cm^{-1} declined upon increasing the template:monomer molar ratio and the decreasing profile showed an inverse trend than the pyridine bonded fraction calculated from the 1597 cm^{-1} band.

Concerning the template:crosslinker interactions, no shift of the EGDMA carbonyl peak at 1720 cm^{-1} was observed but a broadening of this band

was detected in MIPs with high template:monomer ratio ($w_{1/2}$ = 29, 30 and 31 cm^{-1} for MIP 3, MIP 4 and MIP 5, respectively) in comparison with NIPs ($w_{1/2}$ = 27.5 cm^{-1}). Strikingly, no such broadening had been observed in the pre-polymerization solution. Upon extraction, the carbonyl band width reverted to $w_{1/2}$ = 27 ± 0.5 cm^{-1} in all MIPs. This fact suggested the presence of an overlapped small peak around 1715 cm^{-1}, further confirmed by the second derivative spectrum, which is assigned to C=O groups H-bonded with template OH groups. This observation was somewhat surprising as the hydroxyl-4-Vpy intermolecular association and the hydroxyl-hydroxyl BPA associations are known to prevail over the hydroxyl-carbonyl association ratio [55, 59]. Even so, the large excess of carbonyl groups and their accessibility account for these unspecific binding.

3.2.4. ATR evaluation of the MIP recognition process

3.2.4.1. Rebinding

Experiments under equilibrium conditions give an idea as to the absolute imprinting efficiency of the polymers wherein the hydrodynamic and diffusional effects are nullified. At the outset, the effect of solvent on rebinding was analyzed because the solvent plays an important role in the sorption process due to competing affinity to the template and to the specific and nonspecific absorption sites [28, 70, 72]. In the present MIPs, the specific sorption sites are the "cavities" containing 2 molecules of 4-Vpy created by imprinting whereas the non-specific absorption sites are

the randomly located 4-Vpy, the ester linkages from EGDMA, plus different degrees of self associated BPA molecules trapped in polymer meso- and macropores.

The effect of the imprinting was estimated by an ATR-imprinting factor defined as

$$I = [(A_{1513}/A_{1720})_{MIP}/(A_{1513}/A_{1720})_{NIP}] \qquad (12)$$

where A_{1513}/A_{1720} MIP and A_{1513}/A_{1720} NIP are proportional to the amount of template bound to an imprinted and non-imprinted polymer, respectively. This normalization method removes binding due to non-specific interactions. Table 4 shows the binding of BPA to MIP and NIP in $CHCl_3$, ACN and water together with the fraction of H-bonded pyridine (f_b) after subtraction of an average fraction bonded towater vapor of 0.15 (calculated as in Section 2.6).

Table 4. Effect of Solvents on BPA rebinding to imprinted and non-imprinted polymers and BPF and caffeine rebinding in water.

Solvent	T	[T] mM	A_{1513}/A_{1720} MIP	A_{1513}/A_{1720} NIP	I	f_b MIP	f_b NIP
ACN	BPA	1.8	3.1E-03±1E-04	7E-04±2E-04	4.3	7E-02±1E-02	-
$CHCl_3$	BPA	1.8	1.7E-03±4E-04	1.4E-03±7E-04	1.2	4E-02±1E-02	-
		2.7	2.8E-03±5E-04	2.5E-03±5E-04	1.1	9E-02±2E-02	-
		4.5	4.7E-03±5E-04	2.3E-03±8E-04	1.9	1.0E-01±2E-02	-
Water	BPA	0.43	1.39E-02±2.9E-03	2.2E-03±6E-04	6.4	6E-02±2E-02	-
		1.8	2.94E-02±6.4E-03	2.60E-02±5.3E-03	1.1	1.7E-01±1E-02	1.4E-01±5E-02
		2.6	6.19E-02±3.2E-03	6.67E-02±2.5E-03	0.9	2.8E-01±2E-02	2.8E-01±2E-02
	BPF	1.8	3.25E-02±3.3E-03	1.78E-02±5.1E-03	1.8	1.8E-01±1E-02	1.1E-01±2E-02
	CAF	1.8	3.4E-03±5E-04	-	-	-	-

The first conclusion drawn from these data was that water enhanced the total binding capacity with respect to organic solvents, regardless the template concentration in the rebinding solution. Furthermore, the imprinting effect was maintained in ACN and water; albeit in the latter solvent only for small template concentrations. The lower binding capacity together with increased specific binding in ACN in contrast with aqueous solvents was previously reported for other BPA-4-Vpy-EGDMA MIPs [33, 34].

The low binding capacity in ACN could be reasonably explained. From the one hand, the template is readily soluble in ACN owing to the solvent capability of forming H-bonds with the BPA OH groups, thereby reducing the effect of H-bonding to 4-Vpy. Besides, the prepolymerization studies proved the formation of a weak 1:1 BPA:4- Vpy H-bonded complex. On the contrary, the template binding largely decreased in $CHCl_3$ and almost no imprinting effect was observed. The pre-polymerization studies demonstrated the formation of a strong 1:2 BPA:4-Vpy H-bonded complex; besides the solubility of BPA is limited in this solvent. As a result, it was expected that the template would have been preferentially adsorbed on MIP; yet, this was not the case.
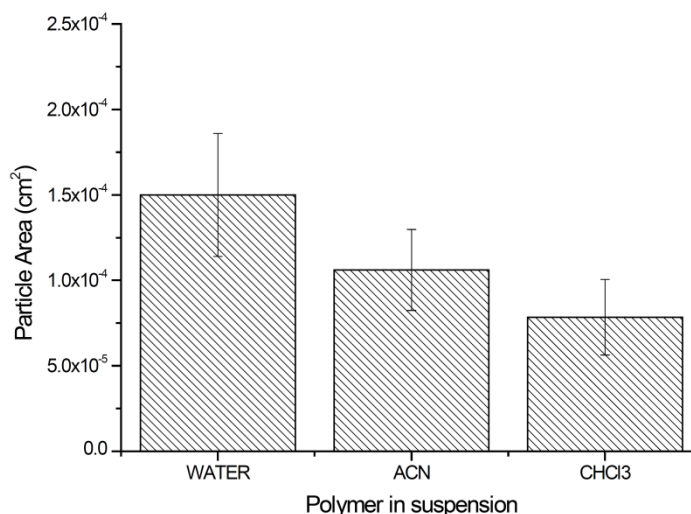
Figure 10. Conformational changes of MIP 3 polymer particles between water and organic solvents. Bars indicate particle size distribution.

The binding studies suggested that the polymer may undergo reversible conformational modifications affected by changes in solvent [29, 70, 73]. A series of particle size analysis experiments to determine the effect of solvent polarity on the polymer structure was performed. The method described in Section 2.7 was used to capture images of the particles in suspension and to calculate their size (Fig. 10). It was found that change from water to organic solvents resulted in polymer shrinking, conditions which are unfavorable for binding (site closing effect), the effect being more evident for $CHCl_3$. The factors that alter surface potential and conformation of polymer chains will change the size and shape of template-complementary binding pockets thus disrupting binding.
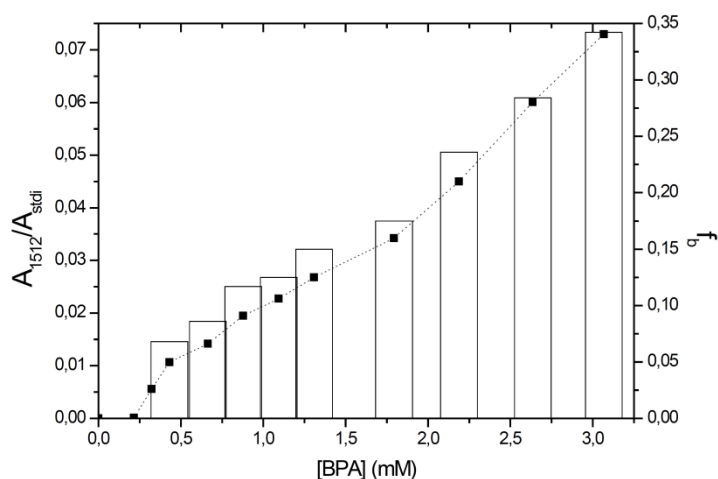
Figure 11. Sorption isotherm for BPA in water on imprinted polymers (solid squares, left-Y axis) and fraction of H-bonded pyridine (f_b) (bars, right-Y axis).

From another point of view, the loss of imprinting effect upon increasing the BPA content in the loading water solution was evident on examining the MIP (Fig.11 left axis) and NIP (not shown) binding isotherms. Whereas at concentrations up to 0.5 mM the binding to MIP seemed to follow a saturation function (specific binding), at higher analyte concentrations this was overlaid by another, non-specific adsorption; the slope in this part of the MIP curve was the same as for the sorption to the reference polymer. The results put forward that imprinting was not the major factor in the adsorption process in water at mid-high BPA concentrations. The driving force in this range could be the partitioning of the analyte between the aqueous phase and the polymer matrix [22] or in other words, the hydrophobic effect or hydrophobic repulsion resulting in "squeezing out" the low polar template molecules into the polymer matrix [70].

Moreover, the H-bonded pyridine fraction in rebound MIPs (Fig. 11 right axis) followed a parallel increase suggesting that once the specific sites had been saturated, the main interaction mechanism was still H-bonding but at unspecific randomly located pyridines. In any event, upon further increasing the BPA loading concentration additional template-polymer interactions became evident from the ATR spectra. At high BPA loading concentrations (1.30, 1.80 and 2.60 mM), the broadening of the carbonyl EGDMA band at 1720 cm^{-1} was detected ($w_{1/2}$ = 28, 29 and 30 cm^{-1}, respectively) in contrast with extracted polymers ($w_{1/2}$ = 27.5 ± 0.5 cm^{-1}), proving unspecific H-bonding to the abundant crosslinker carbonyl groups. Finally, at the highest concentrations assayed an increase of absorption around 3400 cm^{-1} was perceived, indicating the formation of BPA aggregates in the mesoand macro-pores.

In short, the BPA molecules compete with the solvent for specific and non-specific adsorption sites in the polymer matrix. At low BPA loading concentration, the template would be preferentially adsorbed in the accessible imprinted cavities (specific binding). Once saturated the imprint sites in the middle-high concentration range, the hydrophobic effect is the driving force explaining sorption, resulting in the solution rejection of the low polar template molecules into the polymer matrix. Within the polymer matrix, the template would H-bind the randomly located pyridines and on further increasing the BPA loading concentration, the template molecules would subsequently H-bind the crosslinker and/or self aggregate within the pores (non-specific binding).

3.2.4.2. Selectivity

Polymer selectivity in aqueous solutions is desirable because of the potential applications of these polymers in assays involving biological substances or in the development of sensors that can be use to assess water quality [74]. To measure the selective recognition of BPA, the binding of competitive compounds was performed. Where possible, the specific selectivity factor (S) was estimated by the ratio of ATR-imprinting factors:

$$S = I_{BPA}/I_X \qquad (13)$$

Being I_x the imprinting factor for X compound. The characteristic and intense peaks at 1513, 1652 and 1683 cm^{-1} corresponding to BPF, caffeine and paracetamol, respectively, were chosen for the ATR selectivity evaluation because they did not overlap with any polymer band. The rebinding results are displayed in Table 4 solely for BPF and caffeine as paracetamol was barely detected. The specific selectivity factor could only be calculated for BPF and its value was 0.61.

The general conclusions that can be extracted are in accordance with the selectivity studies previously performed with HPLC on identical MIPs for the same compounds [45]. The imprinting efficiency and selectivity recognition of BPF was greater than that of BPA suggesting that besides the same number of functional groups in the analyte molecule and a slightly higher apparent binding constant for the BPF:4-Vpy 1:2 complex in HCCl$_3$ (Table

2; the values in CCl_4 were not strictly comparable due to the different ACN content added to solve solubility problems), the molecular volume of the analyte was an additional factor governing the recognition mechanism. The two methyl groups of BPA have been replaced by two hydrogen atoms in BPF. Therefore, the smaller size of the BPF molecule facilitated the access to the BPA-imprinted cavities while the similar shape made it suitable to fit in.

On the other hand, paracetamol and caffeine showed lower affinities than bisphenol compounds. The poor results for paracetamol recognition were a surprise as its molecule includes two potential donor (N-H and O-H) groups which can theoretically be involved in H-bonding with the monomer pyridyl group. In fact, the ability of the basic 4-Vpy to interact with the weakly acidic phenol residue has been employed by former researchers in the synthesis of paracetamol selective polymers [75]. Regarding caffeine, H-bonding is not possible as both the analyte and monomer lack H-bonding donor groups. Besides, as has been stated in the preceding section sorption from solution is essentially an exchange process and hence, molecules absorb not only because they are attracted by solids but also because the solution may reject them [76]. Thus, the rebinding results were correlated with the pre-polymerization studies and physical properties of the analytes.
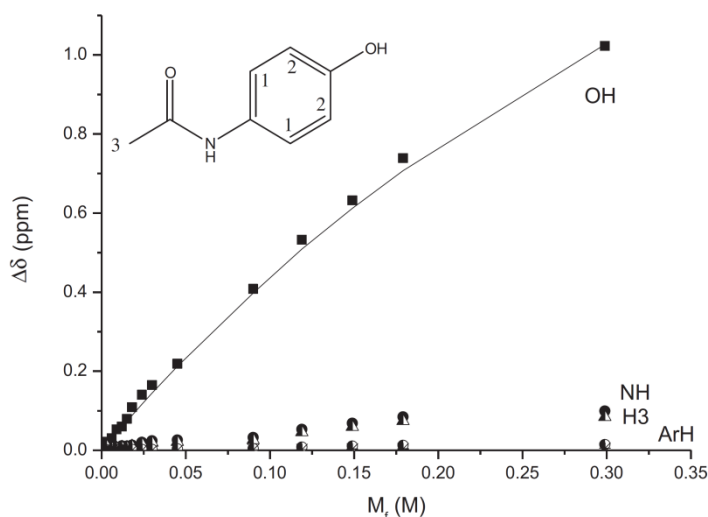
Figure 12. ^{1}H NMR titration of paracetamol with d_5-pyridine in CD_3CN ([Paracetamol] = 3 x 10^{-3} M). The symbols correspond to experimental data points; the solid curve is the best fit based on Eqs (4) and (5) for OH shifts: K_{11}= 1.76±0.28 M^{-1}; δ_{11}= 3.01±0.29 ppm. Regression is based on 16 data points and the goodness of the fit is 0.99.

Attempts to study the interactions between paracetamol and 4-Vpy in HCCl$_3$ by FTIR failed due to poor solubility. The complex stoichiometry was then explored in ACN by UV-Vis spectroscopy and 1:1 complex stoichiometry was found (results not shown). The formation of H-bonding complex was confirmed by ^{1}H NMR titration of paracetamol with d_5-pyridine in CD$_3$CN. The resonance from the OH proton was affected the most upon the sequential addition of d_5-pyridine (Fig. 12). The observed downfield is indicative of decreased shielding which was interpreted as arising from the formation of H-bonding between d_5-pyridine and the paracetamol OH group. The changes in chemical shifts were accompanied by peak broadening also indicative of hydrogen bonding. The other plausible point of interaction is the amide group but the amide proton was scarcely

influenced as it was not directly involved in complexation. Moreover, the aromatic protons surrounding the OH group were almost unaffected suggesting weak interaction. The magnitude of the binding constant is similar to those previously determined for BPA:d_5-pyridine 1:1 hydrogen bonded complex and in CD_3CN and D_2O:d_6-acetone (50:50).

In connection with caffeine, the two strong bands in the region of the carbonyl stretching fundamentals dominate the FTIR spectrum in $CHCl_3$: the peak at 1706 cm^{-1} due to the stretching of the isolated carbonyl, $\upsilon_{C=O}$, and the band at 1658 cm^{-1} allotted to the stretching of the conjugated carbonyl, $\upsilon_{C=O}$, coupled with C=C ring stretching vibrations. Less intense peaks at 1605 and 1555 cm^{-1} fall in the stretching vibration region of C=N and C=C bonds of the purine ring [77]. Upon titration with 4-Vpy, the intensity of the band at 1658 cm^{-1} underwent an initial increase and then became concentration-independent. The spectra suggested the presence of underlying components by the appearance of a high-wavenumber shoulder (Fig. 13). The difference spectra (Caffeine:4-Vpy mixture minus pure caffeine contribution normalized to the 1706 cm^{-1} peak) revealed a new band at 1673 cm^{-1}. Surprisingly, the caffeine peak at 1605 cm^{-1} was quenched at caffeine:4-Vpy molar ratios≥ 1.5 and a negative peak was detected in the corresponding difference spectra (Fig. 13 inset).
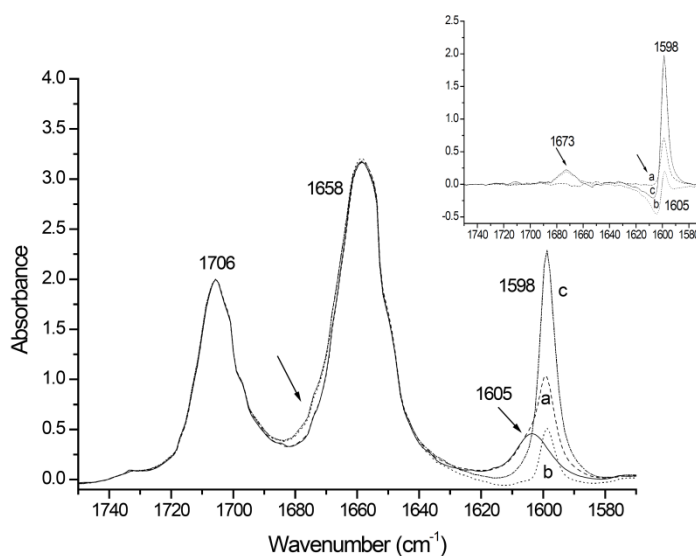
Figure 13. FTIR titration study of caffeine with 4-Vpy in CHCl$_3$ in the spectral region between 1750 and 1570 cm^{-1}: caffeine (4.0 x 10^{-3} M) (solid line); caffeine: 4-Vpy mixtures of (a) 1:1; (b) 1:1.5 and (c) 1:5 molar relationships (discontinuous lines); Inset: difference spectra.

To account for these spectral changes it must be born in mind that the FTIR region between 1800 and 1500 cm^{-1} is sensitive to purine pairing and stacking effects, causing band shifting and quenching [78]. From another point of view, apart from auto aggregation in aqueous solutions [79] caffeine and other methyl- xanthines form stacking pep complexes with aromatic molecules [80] and heterocyclic aromatic amines [81]. In a word, the observed spectral variations may arise from pep complex formation as the aromatic nature of both molecules offers the opportunity for such interaction.

The complex stoichiometry was explored using a Job's plot and UV-Vis spectroscopy. Both plots of (Absorbance at 244 nm x $X_{4\text{-}Vpy}$) against $X_{Caffeine}$ and (Absorbance at 271 nm x $X_{Caffeine}$) against $X_{4\text{-}Vpy}$ gave a maxima of 0.5, confirming 1:1 complex (results not shown). ^1H NMR titration in CDCl$_3$ corroborated the hypothesis of a pep stacking complex. A similar upfield shift was observed for all caffeine protons on addition of d$_5$-pyridine to a solution of caffeine, confirming a face to face stacking conformation [9, 82] (Fig. 14). The low values of the apparent binding constant, calculated using Eq. (4) and (5) for all the template protons, indicated very weak association.

In short, the different nature and magnitude of the interactions between caffeine:4-Vpy compared with those between BPA and 4- Vpy could partly explain the rebinding results in water however, this was not the case for paracetamol. Apart from the described attractive forces, other characteristics of the analyte that influence the sorption process are its molecular size, pK$_a$ if it is an electrolyte, and solubility [75]. Not relevant here the pK$_a$ and being paracetamol and caffeine slightly smaller than BPA, the present discussion is focused on solubility.
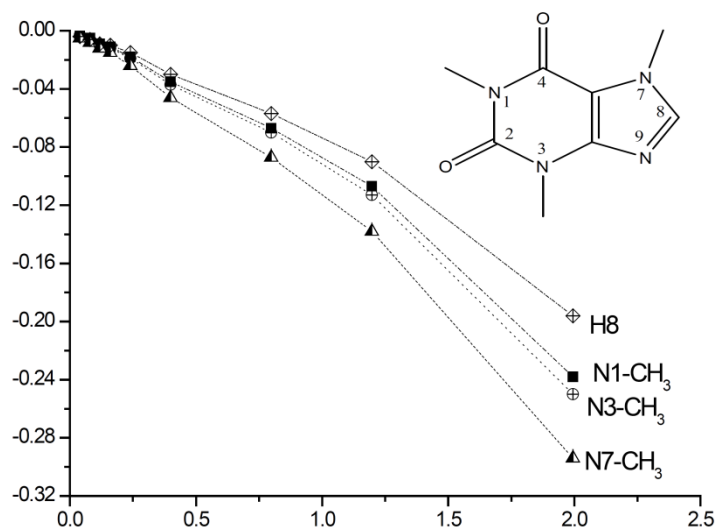
Figure 14. ^{1}H NMR titration of caffeine with d_5-pyridine in $CDCl_3$ ([Caffeine] = 2 x 10^{-2} M). The curves are calculated for: H8 (K_{11} = 1.10 x 10^{-2} M^{-1}; δ_{11}= 8.335 ppm); N1-CH$_3$ (K_{11} = 6.44 x 10^{-2} M^{-1}; δ_{11} = 1.715 ppm); N3-CH$_3$ (K_{11} = 8.20 x 10^{-2} M^{-1}; δ_{11} = 1.528 ppm); N7-CH$_3$ (K_{11} = 8.7 x 10^{-2} M^{-1}; δ_{11} = 1.600 ppm). Regression is based on 10 data points and the goodness of the fit is 0.97.

Water solubilities at room temperature are 3 x 10^2 mg L^{-1}, 1.49 x 10^4 mg L^{-1} and 1.60 x 10^4 mg L^{-1} for BPA [83], paracetamol [84] and caffeine [85], respectively. Water soluble templates are less retained on MIPs whereas templates of moderate to low solubility are more retained due to the hydrophobic effect. Besides, paracetamol capability to form strong H-bonding with the hydroxyl groups of water molecules [86] might account for the differences between paracetamol and caffeine rebinding results.

4. CONCLUSIONS

This work demonstrated the potential of complementary spectroscopic techniques for the optimization of pre-polymerization conditions in MIP synthesis. It is possible to combine FTIR, ^{1}H NMR and UV-Vis analysis to gain a better understanding of the template-monomer interactions in the pre-polymerization solution and predict MIP performance. In particular they complement each other in identifying the stoichiometry of the complex and calculation of binding constants by titration. In addition, FTIR and ^{1}H NMR allow a detailed simultaneous study of functional groups involved in prepolymerisation interactions. FTIR is an excellent means for detecting and studying H-bonds. On the other hand, valuable structural information, such as the topology of pep stacking complexes has been obtained from NMR chemical shift measurements.

From another point of view, the MIP ATR characterization provides direct physical evidence that non-covalent monomer-template interactions survive the polymerization process, thus supporting the purported basis for the molecular imprinting technique [10]. It has made possible to explore, the transition from liquid-phase self-assembled complexes to immobilized binding pockets within the polymer matrix, giving a new insight into the underlying mechanisms of MIP binding site formation and the subtle interactions among the MIP absorbent, template and solvent in subsequent rebinding.

185

From the present body of work, it can be concluded that:

• The primarily mechanism of recognition between BPA and 4- Vpy was H-bonding between BPA hydroxyl groups and the N atom of the pyridine molecule, both in the pre-polymerization solution and in the imprinted polymer. No spectroscopic evidence of π-π stacking had been proved in aqueous environment.

• The stoichiometry of the complex and strength of template-monomer interaction was dependent upon solvent polarity and/or its H-bonded capacity.

• The cross-linking agent, EGDMA did not perturb template functional monomer complexes significantly.

• Even though increasing the amount of template in the prepolymerization solution changed the distribution of monomers in the MIPs, the polymer composition and degree of crosslinking were unaffected.

• The MIP ATR analysis proved that non-covalent monomer template interactions survived the polymerization process. For low BPA:4VP molar ratios in the pre-polymerization mixture, the fraction of H-bonded pyridines in the corresponding polymer matrix supported the presence of two functional monomers in the binding sites. The number of functional groups in the polymer binding site was not determined directly by the solution phase pre-polymerization complex; rather it was determined during polymerization.

• Template-template interactions, although weaker than monomer-template interactions, were present during the polymerization process. As

the content of BPA raised, the self- H-bond in BPA and, in a minor extent, the hydroxyl-carbonyl association between BPA and EGDMA were competitive processes which favored template aggregation and unspecific interactions at the expense of the imprinting efficiency.

- Binding experiments were conducted under equilibrium conditions to evaluate the influence of solvent polarity on sorption capacity and specificity. Besides template-monomer and template-solvent interactions, polymer conformational modifications accounted for the poor results in organic solvents. On the contrary, the polymer was capable of binding BPA within an aqueous environment and based on spectroscopic evidence the rebinding mechanism in water has been fully clarified.

- Last but not the least, pre-polymerization studies alone did not account for the selectivity results with phenol analogs and other water common pollutants in water. They suggested that besides the number of functional groups in the analyte molecule and the nature and magnitude of the analyte:monomer interactions, shape complementarity and solubility were additional factors governing the recognition mechanism.

References

[1] A. Molinelli, J. O'Mahony, K. Nolan, M.R. Smyth, M. Jakusch, B. Mizaikoff, Anal. Chem. 77 (2005) 5196

[2] J. O'Mahony, K. Nolan, M.R. Smyth, B. Mizaikoff, Anal. Chim. Acta 534 (2005) 31-39

[3] H.S. Andersson, I.A. Nicholls, Bioorg. Chem. 25 (1997) 203

[4] W.M. Mullett, M.F. Dirie, E.P.C. Lai, H. Guo, X. He, Anal. Chim. Acta 414 (2000) 123

[5] G. Wang, Q. Cao, Z. Ding, Y. Wang, M. Yang, Helv. Chim. Acta 90 (2007) 1179

[6] G. Wang, Q. Cao, Z. Zhu, Z. Yang, M. Yang, Z. Ding, Polym. Sci. 113 (2009) 3049

[7] B. Sellergren, M. Lepistö, K. Mosbach, J. Am. Chem. Soc. 110 (1988) 5853

[8] I. Idziak, A. Benrebouh, F. Deschamps, Anal. Chim. Acta 435 (2001) 137

[9] J. O'Mahony, A. Molinelli, K. Nolan, M.R. Smyth, B. Mizaikoff, Biosens. Bioelectron. 20 (2005) 1884

[10] J. Svenson, J.G. Karlsson, I.A. Nicholls, J. Chromatogr. A 1024 (2004) 39

[11] T.H. Nguyen, R.J. Ansell, J. Mol. Recognit. 24 (2011) 1

[12] C. Alexander, H.S. Andersson, L.I. Andersson, R.J. Ansell, N. Kirsch, I.A. Nicholls, J. O'Mahony, M.J. Whitcombe, J. Mol. Recognit 19 (2006) 106

[13] D.J. Duffy, K. Das, S.L. Hsu, J. Penelle, V.M. Rotello, H.D. Stidham, J. Am. Chem. Soc. 124 (2002) 8290

[14] T.P. O'Brian, N. Grinberg, G. Bicker, J. Wyvratt, N.H. Snow, Enantiomer 7 (2002) 139

[15] J.Y. Wang, F. Liu, Z. Xu, K. Li, Chem. Eng. Sci. 65 (2010) 3322

[16] A. Katz, M.E. Davis, Macromolecules 32 (1999) 4113

[17] Y.-Q. Lv, Z. Lin, W. Feng, T. Tan, Chromatographia 66 (2007) 339

[18] Q. Osmani, H. Hughes, K. Flavin, J. Hedin-Dahlstrom, C.J. Allender, J. Frisby, P. Mc Loughlin, Anal. Bioanal. Chem. 391 (2008) 1229

[19] K.J. Shea, D.Y. Sasaki, J. Am. Chem. Soc. 113 (1991) 4109

[20] A.-F. Che, L.-S. Wan, J. Ling, Z.-M. Liu, Z.-K. Xu, J. Phys. Chem. B 113 (2009) 7053

[21] W. Dong, M. Yan, M. Zhang, Z. Liu, Y. Li, Anal. Chim. Acta 542 (2005) 186

[22] M. Jakusch, M. Janotta, B. Mizaikoff, Anal. Chem. 71 (1999) 4786

[23] E. Oral, N.A. Peppas, Polymer 45 (2004) 6163

[24] R. Volcu., K. Faid, A.A. Farah, F. Bensebaa, R. Barjovanu, C. Py, Y. Tao, Langmuir 23 (2007) 5452

[25] M. Bompart, L.A. Gheber, Y. De Wilde, K. Haupt, Biosens. Bioelectron. 25 (2009) 568

[26] K. Kantarovich, A.S. Belmont, K. Haupt, I. Bar, L.A. Gheber, Appl. Phys. Lett. 94 (2009) 194103-1

[27] D. Mc Stay, A.H. Al-Obaidi, R. Hoskins, P.J. Quinn, Journal of Optics A: Pure Appl. Opt. 7 (2005) S340

[28] P.V. Joshi, R.N. Karmalkar, M.G. Kulkarni, R.A. Mashelkar, Ind. Eng. Chem. Research 38 (1999) 4417

[29] N.W. Turner, E.V. Piletska, K. Karim, M. Whitcombe, M. Malecha, N. Magan, C. Baggiani, S.A. Piletsky, Biosens. Bioelectron. 20 (2004) 1060

[30] T. Ikegami, W.-S. Lee, H. Nariai, T. Takeuchi, J. Chromatogr. B 804 (2004) 197

[31] T. Ikegami, T. Mukawa, H. Nariai, T. Takeuchi, Anal. Chim. Acta 504 (2004) 131

[32] A.F. Navarro-Villoslada, B. San Vicente, M.C. Moreno-Bondi, Anal. Chim. Acta 504 (2004) 149

[33] B. San Vicente, F. Navarro-Villoslada, M.C. Moreno-Bondi, Anal. Bioanal. Chem. 380 (2004) 115

[34] Ch. Nantasenamat, Ch. Isarankura-Na-Ayudhya, L. Bülow, L. Ye, V. Prachayasittikul, EXCLI J. 5 (2006) 103

[35] Y. Ji, J. Yin, Z. Xu, Ch. Zhao, H. Huang, H. Zhang, Ch. Wang, Anal. Bioanal. Chem. 395 (2009) 1125

[36] T. Kubo, K. Hosoy, Y. Watabe, T. Ikegami, N. Tanaka, T. Sano, K. Kaya, J. Chromatogr. A 987 (2003) 389

[37] H. Sanbe, K. Hosoya, J. Haginaka, Anal. Sci. 19 (2003) 715

[38] Y. Watabe, K. Hosoya, N. Tanaka, T. Kubo, T. Kondo, M. Morita, J. Chromatogr. A 1073 (2005) 363

[39] M. Kawaguchi, Y. Hayatsu, H. Nakata, Y. Ishii, R. Ito, K. Saito, H. Nakazawa, Anal. Chim. Acta 539 (2005) 83

[40] X. Jiang, W. Tian, Ch. Zhao, H. Zhang, M. Liu, Talanta 72 (2007) 119

[41] N. Tsuru, M. Kikuchi, H. Kawaguchi, S. Shiratori, Thin Solid Films 499 (2006) 380

[42] Ch. Zhao, B. Yu, B. Qian, Q. Wei, K. Yang, A. Zhang, J. Membrane Sci. 310 (2008) 38

[43] W. Zhao, N. Sheng, R. Zhu, F. Wei, Z. Cai, M. Zhai, S. Du, Q. Hu, J. Hazard. Mater. 179 (2010) 223

[44] R. Zhu, W.H. Zhao, M.J. Zhai, F.D. Wei, Z. Cai, N. Sheng, Q. Hu, Anal. Chim. Acta 658 (2010) 209

[45] M.C. Cela-Pérez, M.M. Castro-López, A. Lasagabáster-Latorre, J.M. López-Vilariño, M.V. González-Rodríguez, L.F. Barral-Losada, Anal. Chim. Acta 706 (2011) 275

[46] I.A. Nicholls, K. Adbo, H.S. Andersson, P.O. Andersson, J. Ankarloo, J. Hedin-Dahlström, P. Jokela, J.G. Karlsson, L. Olofsson, J. Rosengren, S. Shoravi, J. Svenson, S. Wikman, Anal. Chim. Acta 435 (2001) 9

[47] Ch. Y. Huang, Methods Enzymol. 87 (1982) 509

[48] J.M. Bosque-Sendra, E. Almansa-López, A.M. García-Campaña, Anal. Sci. 19 (2003) 1431

[49] H.A. Benesi, J.H. Hildebrand, Journal of the Am. Chem. Soc. 71 (1949) 2703

[50] S. Mizyed, H. Tarabsheh, D. Marji, JJC 2 (2007) 145

[51] K.A. Connors, Binding Constants: The Measurement of Molecular Complex Stability, first ed., Wiley, New York, 1987

[52] K. Eliadou, K. Yannakopoulou, A. Rontoyianni, I. Mavridis, J. Org. Chem. 64 (1999) 6217

[53] J.Y. Lee, P.C. Painter, M.M. Coleman, Macromolecules 21 (1988) 346

[54] J.Y. Lee, P.C. Painter, M.M. Coleman, Macromolecules 21 (1988) 954

[55] L.C. Cesteros, J.R. Isasi, I. Katime, Macromolecules 26 (1993) 7256

[56] B. Fei, Ch. Chen, S. Peng, X. Zhao, X. Wang, L. Dong, Poym. Int. 53 (2004) 2092

[57] M.M. Coleman, X. Yang, P.C. Painter, J.F. Graf, Macromolecules 25 (1992) 4414

[58] E.J. Moskala, D.F. Varnell, M.M. Coleman, Polymer 26 (1985) 228

[59] N. Hameed, Q. Guo, Polymer 49 (2008) 922

[60] F.S.F. Jacinto, L.J.A. Siqueira, W.A. Alves, FT-Raman, J Raman Spectrosc 40 (2009) 1585

[61] V. Villar, L. Irusta, M.J. Fernández-Berridi, J.J. Iruin, M. Iriarte, L. Gargallo, D. Radic, Thermochim. Acta 402 (2003) 209

[62] J.J. Sangster, J Phys Chem Ref Data 18 (1989) 1111

[63] A.E. M Janssen, A. Van der Padt, H.M. Van Sonsbeek, K. Van't Riet, Biotechnol. Bioeng. 41 (1993) 95

[64] S. Wei, M. Jakusch, B. Mizaikoff, Anal. Bioanal. Chem. 389 (2007) 423

[65] F.-D. Zhu, K.-H. Choo, H.-S. Chang, B. Lee, Chemosphere 87 (2012) 857

[66] B. Zu, Y. Zhang, X. Guo, H. Zhang, J. Polym. Sci. A1 48 (2010) 532

[67] H. Kim, D.A. Spivak, J. Am. Chem. Soc. 125 (2003) 11269

[68] D.A. Spivak, Adv. Drug Deliver. Rev. 57 (2005) 1779

[69] L.C. Mendes, A.D. Tedesco, M.S. Miranda, Polym. Test. 24 (2005) 418

[70] B. Sellergren, Trend. Anal. Chem. 18 (1999) 164

[71] N. Heymans, S. Van Rossum, J. Mater. Sci. 37 (2002) 4273

[72] W. Cai, R.B. Gupta, Sep. Purif. Technol. 35 (2004) 215

[73] B. Sellergren, K.J. Shea, J. Chromatogr. A 635 (1993) 31

[74] F.A. Villamena, A.A. de la Cruz, J. Appl. Polym. Sci. 82 (2001) 195

[75] J.P. Rosengren-Holmberg, J.G. Karlsson, J. Svenson, H.S. Andersson, I.A. Nicholls, Org. Biomol. Chem. 7 (2009) 3148

[76] C. Moreno-Castilla, Carbon 42 (2004) 83

[77] S. Gunesakeran, G. Sankari, S. Ponnusamy, Spectrochim. Acta A 61 (2005) 117

[78] M. Lindqvist, A.J. Gräslun, J. Mol. Biol. 314 (2001) 423

[79] M. Falk, M. Gil, N. Iza, Can. J. Chem. 68 (1990) 1293

[80] M.W. Hanna, A. Sandoval, Biochim. Biophys. Acta 155 (1968) 433

[81] A. Woziwodzka, A. Gwizdek-Wisniewska, J. Piosik, Bioorg. Chem. 39 (2011) 10

[82] H. Jäckel, H. Stamm, J. Phys. Chem. 94 (1990) 3495

[83] A. Shareef, M.J. Angove, J.D. Wells, B.B. Johnson, J. Chem. Eng. Data 51 (2006) 879

[84] R.A. Granberg, A.C. Rasmuson, J. Chem. Eng. Data 44 (1999) 1391

[85] The Merck Index, thirteenth ed., (2001) nº 1636

[86] B.Y. Shekunov, D.J.W. Grant, J. Phys. Chem. B 101 (1997) 3973

SELECTIVE REMOVAL OF ATP DEGRADATION PRODUCTS FROM FOOD MATRICES I: DESIGN AND CHARACTERIZATION OF A DUMMY MOLECULARLY IMPRINTED SPECIFIC SORBENT FOR HYPOXANTHINE

Aurora Lasagabáster-Latorre[1,2], M.C. Cela-Pérez[1], Sara Fernández-Fernández[1], J. M. López-Vilariño[1], M.V. González-Rodríguez[1]

[1] Grupo de Polímeros, Centro de Investigaciones Tecnológicas (CIT), Departamento de Física, Escuela Universitaria Politécnica, Universidad de A Coruña (UDC), Campus de Ferrol, 15471 Ferrol, Spain, Tel.: +34 981 337 400 3051/3485; fax: +34 981 337 416, email: victoria.gonzalez.rodriguez@udc.es

[2] Dpto Química Orgánica I, Facultad de Óptica y Optometría, Universidad Complutense de Madrid, Arcos de Jalón no. 118, Madrid 28037, Spain

ABSTRACT

Specific molecularly imprinted polymers (MIPs) for hypoxanthine (HYP) recognition in aqueous organic media have been developed based upon UV, FTIR and ^{1}H-NMR prepolymerization studies in conjunction with batch rebinding UPLC analyses. The MIPs, which used the template mimics caffeine (CAF) and theophylline (TPH), are prepared in $CHCl_3$ by one step precipitation polymerization from acrylamide (AM), 2-hydroxiethyl-methacrylate (HEMA) and methacrylic acid (MAA) as functional monomers, whereas ethylene glycol dimethacrylate (EGDMA), divinylbenzene (DVB) and trimethylolpropane triacrylate (TMPTA) as cross-linkers. The magnitude of the pre-polymerisation binding constants between TPH and AM, MAA and HEMA is consistent with the complex stoichiometry (1:2 and 1: 1) and number of interaction points (3-, 2-, 1- hydrogen bonded motif). The strong (1:2) complex between TPH and AM (K_{11} =3.36 x $10^4 M^{-1}$ and K_{12} =1.33 x 10^2 M^{-1}) makes the corresponding MIP the most suitable for HYP recognition. The best performance of the TPH:AM:EGDMA (1:4:20) MIP is reflected in the high IF and high weighted average affinity based on the Freundlich isotherm. Further polymer characterization by ATR-FTIR, elemental analysis, surface area analysis (BET), swelling and SEM yield vital information regarding the degree of polymerization, real monomer: crosslinker ratio, morphology, pore size distribution plus conformational changes on exposure to different solvents.

Keywords: *Hypoxanthine, Molecular imprinting, Dummy–template, Spectroscopy, Morphology*.

1. INTRODUCTION

Hypoxanthine (HYP) is an essential metabolite to degrade adenine nucleotide, which is an indicator for the quality control of meat or fish products in food industries. Therefore, it is significant to develop a quick and effective analytical method for the determination of HYP. Various methods have been proposed for the evaluation of HYP concentration, such as chromatography, capillary electrophoresis and electrochemistry [1, 2]. Owing to the complexity of sample matrices and low levels of the analyte, sample pre-treatment and enrichment process become the crucial steps in these analytical procedures. So far, the most widely used sample pre-treatment methods are liquid-liquid extraction, solid-phase extraction (SPE), liquid-phase microextraction, cloud point extraction, ionic liquids extraction and stir bars microextraction, but most of these procedures suffer from several disadvantages such as large amounts of organic solvent, tedious procedure or low enrichment factor [3].

In order to solve these drawbacks molecularly imprinted polymers (MIPs) have been successfully applied as selective phases in solid phase extraction of analytes present in low concentrations or in complex matrices and have lead to enrichments and clean-up of the analytes to levels not achievable with alternative methods. Accordingly, molecularly imprinted solid phase extraction (MISPE) has been widely used in bioanalysis, food, pharmaceutical and environmental analysis in recent years [4-8], MIPs are synthetic polymeric materials with specific and selective recognition sites

complementary in shape, size, and functional groups to the template molecule (T), involving an interaction mechanism based on molecular recognition. MIPs can be synthesized either by covalent or by non-covalent procedures. The latter are based on the formation of relatively weak non-covalent interactions between the T and functional monomers (M) before polymerization.

Normally, the target molecules are used as templates to synthesize MIPs, but when the original T is very expensive or otherwise difficult-to-achieve or purified, involves safety consideration in the manipulation, or when polymerization conditions (thermal or UV irradiation) could result in unwanted compound degradation, a structural analogue or dummy template (DT) can be employed for the synthesis. The dummy approach is also selected to avoid the risk of residual T leaking from the polymer and causing erroneous results, particularly in MISPE applied to trace determination of compounds. At last, the strategy of DT can also be an option when the too low solubility of the target analyte does not allow its use for the synthesis of the MIP. Owing to cross-selectivity, the so-called "dummy molecularly imprinted polymer" (DMIP) should give rise to imprints that have the ability to bind the target analyte [5, 9, 10]. However, DMIPs are often inferior in terms of selectivity for the target analyte, losing recognition and extraction capacities for the compound from the matrices [11, 12]. Hence, to achieve both proper affinity and sufficient recovery, the selection of the DT is of great significance. As a pre-condition, the dummy molecule must resemble the target analyte in terms

of shape, size and functionalities [5] and should not interfere with its analytical determination.

From another point of view, most studies concern synthesis and new applications of MIPs with less emphasis on understanding the mechanisms and interactions occurring between T and M. Nonetheless, a thorough comprehension of the recognition mechanisms and physical parameters of corresponding polymers are very important to improve extraction. Accordingly, prepolymerization studies on self-assembling systems can be useful for the selection of suitable M and solvents for specific T molecules [13]. UV-Vis, FTIR and ^{1}H NMR spectroscopies are frequently applied to characterise the nature of prepolymerization interactions and the extent of complex formation between M and T in solution [7, 14-20]. On the other hand, the porous structure of imprinted materials can be intricate and affects their performance. Brunauer–Emmett–Teller analysis (BET) and scanning electron microscope (SEM) are used to elucidate the morphological characteristics which may provide valuable information for the synthesis and application of the MIPs [13, 21, 22].

The ultimate goal of our research work is to achieve a MIP for solid extraction and preconcentration of HYP from meat and fish samples which can be used as a simple and rapid method to evaluate freshness. The study has been divided in two articles: part I, the current paper, involving MIP design and characterization and part II describing the application [23]. So far, to the best of our knowledge, there is only one work dealing with HYP

based MIP in which the target analyte itself is used as T to prepare a MIP membrane to be applied as electrochemical sensor characterized by its detection speediness [24]. Notwithstanding, the MIP sensor does not tackle the "bleeding" issue which causes serious interferences when applied to quantitative analysis in real samples nor has it been tested in fish samples and its performance in biological matrices is unknown. Besides, our method, which is particularly remarkable for the instrumental simplicity and low cost, allows the selective extraction and purification of inosine in addition to HYP, both ATP derivatives present in fish samples [23].

As a preliminary step, the current study deals with the synthesis and characterization of several non-covalent MIPs, prepared by the precipitation polymerization technique and capable of recognising HYP in aqueous-organic solutions. Caffeine (CAF) and theophylline (TPH) have been selected as DT in order to avoid inherent bleeding and because of solubility problems of closely related compounds such as xanthine or uric acid in commonly used organic solvents. Nonetheless, the two analyte mimics share with HYP a highly delocalized fused ring system containing both a pyrimidine ring and an imidazole ring. The three M, methacrylic acid (MAA), 2-hydroxiethyl-methacrylate (HEMA) and acrylamide (AM) have been chosen because of their ability to form H-bonds and owing to their compatibility with aqueous systems, whereas three C of different functionalities, flexibilities and polarities have been probed namely ethylene glycol dimethacrylate (EGDMA), divinylbenzene (DVB) and trimethylolpropane triacrylate (TMPTA).

The first part of this paper describes the combination of UV, FTIR and ^{1}H-NMR spectroscopies to analyse the DT: M interactions in organic solvents. Based on this strategy the porogen, $CHCl_3$, is selected. To further explain the molecular recognition behavior, the synthesized MIPs are thoroughly characterized by ATR-FTIR spectroscopy, elemental analysis, Brunauer-Teller method (BET), swelling experiments and scanning electron microscope (SEM). Prior to rebinding analysis and in order to accurately design batch rebinding experiments, a kinetic assay has been conducted. Finally, the specific binding capability of the MIPs for HYP is evaluated by batch rebinding assays in ACN:water using UPLC in order to determine imprinting factors and adsorption isotherms.

2. EXPERIMENTAL

1.1. REAGENTS

Theophylline (TPH), trifluoroacetic acid (TFA), 2-hydroxiethyl-methacrylate (HEMA), methacrylic acid (MAA), ethylene glycol dimethacrylate (EGDMA), trimethylolpropane triacrylate (TMPTA) and d_1-chloroform (99.96%) ($CDCl_3$) have been purchased from Sigma Aldrich (Steinheim, Germany). Also from Sigma Aldrich, the divinylbenzene (DVB, technical grade 80%) has a monomer content of 80 wt% DVB and 20 wt% ethylvinylbenze (EVB). The meta- to para- isomer ratio for all monomers is 70 to 30.

Acrylamide (AM), Caffeine (CAF) and 2, 2-azobis (2-methylpropionitrile) (AIBN) have been obtained from Fluka (Buchs, Switzerland). Methanol

(MeOH), acetonitrile (ACN), chloroform (CH_3Cl), dichloromethane (CH_2Cl_2) and d_4-acetic acid (99.5%) (AA) are from Merck (Darmstadt, Germany). Acetic acid (HAc) has been supplied from Scharlab (Barcelona, Spain) and hypoxanthine (HYP) was obtained from Acros Organics (Geel, Belgium). Water used in the experiments has been purified using a Milli Q Ultrapure water-purification system (Millipore, Bedfore, MA, USA).

1.2. INSTRUMENTS

1.2.1. UV-Vis Spectroscopy

UV-Vis absorption spectra have been recorded on a Cary 100 Conc double –beam UV–Vis Spectrophotometer (Varian, USA) at 0.2 cm^{-1} resolution between 200 and 400 nm.

1.2.2. FTIR spectroscopy

The IR data have been recorded on a Bruker Vector 22 spectrometer. The transmission/absorption measurements of the pre-polymerization mixtures have been performed in a thin-film liquid cell at room temperature with a 1 mm Teflon spacer and CaF_2 windows (Spepac) in the spectral range of 4000-900 cm^{-1}. Each spectrum is obtained through the averaging of 64 repetitive scans at a resolution of 4 cm^{-1}.

The FTIR analysis of the pre-polymerization mixture in porogen and solid samples have been performed in the attenuated reflection mode (ATR) by using the already described spectrometer equipped with a thermostated

MK II Golden Gate^{TM} Diamond 45º ATR accessory. The non-polymerized sample solution, the analyte and monomers solved in porogen are flushed into the stainless steel micro reaction flow cell anvil (10568) clamped on the ATR crystal. For the polymerized samples, the disks are compressed onto the ATR crystal with the Sapphire Anvil (10531). Owing to the hygroscopic character of the copolymers, the study has been carried out after heating at 55 ºC during 15 minutes to avoid interferences due to water vapor sorption. Both the spectra of liquid and solid samples are the results of 100 coadded interferograms at 4 cm^{-1} resolution between 400 and 4000 cm^{-1}. Peak height measurements and integral absorbance have been performed with the spectral analysis software (Opus 5.5). All results are obtained with a baseline correction and the average values, corresponding to at least triplicate analysis together with the standard deviations, have been calculated.

1.2.3. ^{1}H-NMR Spectroscopy

^{1}H-NMR measurements have been performed on an AVANCE 500 (N/I 59369) spectrometer (Bruker, Germany) operating at 500 mHz at room temperature. Spectra have been calibrated with respect to the solvent peak (CDCl$_3$).

1.2.4. UPLC-PDA

UPLC analyses have been performed using an Acquity system from Waters (Milford, MA, USA) with a gradient pump and automatic injector.

Chromatographic experiments are carried out in a stainless steel column Acquity UPLCTM BEH C_{18} (2.1 x 50 mm, 1.7 μm) (Waters) kept at 30 ºC. Detection is carried out using a photodiode array detector (PDA) set in the range of 200-400 nm. Output signals are monitored and integrated using a personal computer operated under the Empower 2 software (Waters). A two solvent gradient elution has been performed, with flow rate of 0.5 mL min^{-1}, injection volume of 3 μL and detection wavelength 250 nm. Mobile phase is composed by 0.1% TFA in deionized water (pH 2.2, v/v) (A) and MeOH (B). Composition starts at 99% of A and is held during 0.08 min, followed by a linear increase to 70% A in 0.70 min, being held for an additional 0.90 min, then is brought back to the initial conditions in 1 min and held 2 further min.

1.2.5. Elemental Analysis

The C, H, N analysis of MIPs has been conducted using Thermo Finnigan Flash EA 1112 elemental analyzer. The average of three replicates is given.

1.2.6. BET analysis

The nitrogen adsorption–desorption isotherms at 77 K have been measured using an ASAP2020 instrument from Micromeritics (Norcross, GA). Prior to the measurements, samples have been degassed at 50 ºC under high vacuum (10^{-3} Torr) for 10 h. Porosity and surface area have been established on the basis of the nitrogen uptake and application of the Brunauer-Emmet-Teller (BET) theory.

1.2.7. SEM

Scanning electron micrographs have been obtained with the scanning electron microscope JEOL JSM-6400 at an accelerating voltage of 20 kV. The samples were coated with a thin gold film before observation.

2.3. PREPOLYMERIZATION STUDIES

2.3.1. UV-Vis Spectroscopy

The stoichiometry of the complexes has been determined by the method of continuous variation (Job plot) [25] based on the difference in absorbance of the DT (CAF and TPH band at 275 ± 1 nm) in the presence and absence of M in solvents of increasing polarity. To construct the Job plots, 1.00×10^{-4} M stock solutions of DT and MAA have been prepared in $CHCl_3$, CH_2Cl_2 and ACN then a set of 5.0 mL solutions are obtained by mixing different portions of DT and M. The mole fraction of DT (X_{DT}) is varied from 0 to 1 whereas the total concentration of DT and M is kept constant. The same concentrations were employed for the systems TPH:HEMA and TPH:AM in $CHCl_3$.

2.3.2. FTIR spectroscopy

The nature of the interactions between DT and M has been studied in $CHCl_3$ by FTIR. To support UV-Vis results, the stoichiometry of TPH complexes with MAA and AM has been calculated by both the Job plot method and the molar ratio plot (Yoe and Jone´s method) [26]; the apparent binding

constant for the TPH:MAA system has also been estimated by FTIR spectroscopy [27]. The experimental protocol is thoroughly described in the Supplementary Material manuscript (section 1.1.1).

2.3.3. ^{1}H NMR Spectroscopy

In order to calculate the association constants ^{1}H NMR titration studies have been conducted by maintaining a constant concentration of DT (4.0 x 10^{-2} M CAF in CDCl$_3$ and 1.5 x 10^{-3} M TPH in CHCl$_3$/ CDCl$_3$, 90/10, v/v) at increasing amounts of M (from 1 up to 50 or 100 equiv) with a constant sample volume of 750 µL. The monomers assayed are AM, HEMA and d$_4$-acetic acid (AA). For the purpose of spectral clarity MAA has been replaced with AA. The shifts have been used to calculate apparent association constants for the observed interactions applying a non-linear regression method using the software package Mathcad 11 based on equations described by Connors [28] and Eliadou et al. [29] for 1:1 (Eq. 1 and 2) and 1:2 stoichiometries (Eq. 3, 4 and 5), respectively (Footnotes[a, b] of Table 1). Each regression is based on 11-16 data points. The goodness of the fit R^2 is 0.98 or better in all cases.

Table 1. Parameter values obtained by fitting titration ^{1}H NMR curves for DT:M complex formation in CDCl$_3$ (CAF, 4 x 10^{-2} M) and CHCl$_3$/CDCl$_3$ (10/90 v/v) (TPH, 1.5 x 10^{-3} M).

Template	Monomer	Proton	K_{11} (M^{-1})	$\Delta\delta^0_{11}$ (ppm)	K_{12} (M^{-1})	$\Delta\delta^0_{12}$ (ppm)
CAF	AA-d$_4$ [a]	8-H	4.47±1.02	2.43E-01± 1.11E-02	-	-
TPH	AA-d$_4$ [a]	NH	-	2.99E-01	-	-
		8-H	1.39E02±3.6E01	2.70E-02± 2.0E-03	-	-
		N3-CH$_3$	8.99E01±5.2	5.70E-03± 1E-04	-	-
TPH	HEMA[a]	NH	1.30E01±2.6	5.70E-01± 6.9E-02	-	-
		8-H	1.26E01±2.2	7.21E-02± 1.4E-02	-	-
		N1-CH$_3$	1.15E-01±2.9	7.75E-02± 8.2E-03	-	-
TPH	AM [b]	NH	3.36E04±1.11E03	4.98± 3.52E-02	1.33E02± 5.77E01	8.60E-03± 3.85E-02
		N1-CH$_3$	1.71E04±9.57E03	9.40E-02± 3.96E-03	7.66E01± 9.46	8.00E-03± 2.92E-03

[a]Eq for 1:1 stoichiometry [28]: $\Delta\delta_{obs} = \frac{\Delta\delta^0_{11} \cdot K_{11}[L]}{1+K_{11}[L]}$ (1) and $[L] = [L]_t - [T]_t \cdot \left(\frac{\Delta\delta_{obs}}{\Delta\delta^0_{11}}\right)$ (2)

[b]Eq for 1:2 stoichiometry [29]: $\Delta\delta_{obs} = \frac{K_{11}\Delta\delta^0_{11} + 2K_{11}K_{12}[L]\Delta\delta^0_{12}}{1/[T] + K_{11} + 2K_{11}K_{12}[L]}$ (3) $[T] = \frac{[L]_t - [L]}{K_{11}[L] + 2K_{11}K_{12}[L]^2}$ (4) $[L] = \frac{[L]_t + 2K_{11}K_{12}[T]_t[L]_t^2}{1 + K_{11}[T]_t + 4K_{11}K_{12}[T]_t[A]_t}$ (5)

2.4. MIP preparation

MIPs have been prepared at a molar ratio of 1:4:20 of T: M: C to ensure a high level of cross-linking (Table 2). In all cases, the DT and M are dissolved in CHCl$_3$. Due to the lower solubility of TPH in CHCl$_3$, a higher porogen volume has been used for its MIP synthesis (60 mL) compared with that of the CAF-MIPs (40 mL). Then, the C and the initiator (AIBN, 0.50 mmol) have been added. The solutions have been purged with N$_2$ for 5 min in order to remove oxygen. Afterwards, glasswares with solutions have been immersed in a thermostatic water bath at 60º C and left during 24 h for the polymerization to proceed.

Table 2. Composition of the produced polymers and methods of preparation.

Polymer	Dummy Template (DT)	Functional Monomer (M)	Cross-linker (C)	Ratio T:M:C	Porogen (mL)	Initiation method 60 ºC, 24 h
MIP 1	CAFFEINE (0.19419 g)		EGDMA (3.990 g)			AIBN (0.08211 g)
NIP 1	-	MAA (0.3444 g)			CHCl$_3$ (40)	
MIP 2	CAFFEINE (0.19419 g)		DVB (3.2904 g)			AIBN (0.08211 g)
NIP 2	-					
MIP 3	THEOPHYLLINE (0.18016 g)		EGDMA (3.990 g)			AIBN (0.08211 g)
NIP 3	-	MAA (0.3444 g)		1:4:20		
MIP 4	THEOPHYLLINE (0.18016 g)		DVB (3.2904 g)			AIBN (0.08211 g)
NIP 4	-				CHCl$_3$ (60)	
MIP 5	THEOPHYLLINE (0.18016 g)	HEMA (0.5366 g)	TMPTA (5.940 g)			AIBN (0.08211 g)
NIP 5	-					
MIP 6	THEOPHYLLINE (0.18016 g)	AM (0.2843 g)	EGDMA (3.990 g)			AIBN (0.08211 g)
NIP 6	-					

After polymerization, MIPs have been dried at 40ºC. Precipitates with relatively uniform particle size have been obtained, which avoided crushing, grinding and sieving steps. In order to remove the DT, the remaining unreacted M and soluble oligomers, the collected polymers have been successively extracted with a mixture of MeOH/HAc (4:1, v/v) in Soxhlet extractor (5 h) and MeOH (5 h). Then, the MIPs have been dried at 40°C. The complete removal of template from the polymer has been traced

by the UPLC method and ATR spectroscopy. Control non-imprinted polymers (NIPs) have been similarly prepared, except that the DT is not present in the polymerization media.

2.5. POLYMER CHARACTERIZATION

2.5.1. ATR-polymer characterization

The percentage of unreacted carbon-carbon double bonds or degree of crosslinking (%DC) for EGDMA copolymers has been determined from the ratio of absorbance areas of the band allotted to the stretching vibration of C=C unreacted groups at 1634 cm^{-1} ($\upsilon_{C=C}$) against an internal standard (stdi) before and after polymerization (Eq 6 in Footnote[a] of Table 3) [30]. For MIPs and NIPs 1 and 3, the band at 1450 cm^{-1} (asymmetric δ_{CH3}, δ_{CH2}) has been selected as stdi. As for MIP and NIP 6, the band at 1723 cm^{-1} ($\upsilon_{C=O}$) has been used instead of the 1450 cm^{-1} band, which overlaps with the amide III band of AM.

In connection with TMPTA, before crosslinking it shows absorption bands at 810 cm^{-1}, alloted to the C=C twisting vibration of acrylate groups, and at 1635 and 1620 cm^{-1}, assigned to the stretching vibration of the same groups. Due to the overlapping of the latter, the curing reaction of MIP 5 and NIP 5 has been analysed by integrating the band at 810 cm^{-1}. The band at 1450 cm^{-1} has been adopted as stdi and Eq. 6 applied [31]. The area calculations are based on the 2nd derivative spectra to overcome band overlapping.

Moreover, the vinyl content (X_{VB}) and the %DC of polyDVB copolymers have been calculated by Eq. 7 and 8 (Footnoteb of Table 3) based on the modification of the technique of Bartholin proposed by Hubbard et al. [32].

Table 3. Elemental and ATR analysis of the produced polymers.

Polymer	Experimental value (%)			Theoretical value (%)			%DC
	C	O	N	C	O	N	
MIP 1	58.20	34.32	0.20	60.20	32.70	-	94±1[a]
NIP 1	57.25	34.97	0.62	60.20	32.70	-	88±1[a]
MIP 2	85.80	6.18	0.23	88.00	4.34	-	60±3[b]
NIP 2	86.06	5.87	0.22	88.00	4.34	-	60±2[b]
MIP 3	58.10	34.82	0.09	60.20	32.70	-	86±4[a]
NIP 3	57.94	34.94	0.08	60.20	32.70	-	87±3[a]
MIP 4	83.06	8.37	0.54	88.00	4.34	-	54±3[b]
NIP 4	84.9	7.28	0.17	88.00	4.34	-	49±4[b]
MIP 5	56.96	36.26	0.10	60.36	32.76	-	96±1[a]
NIP 5	57.08	34.81	0.09	60.36	32.76	-	97±1[a]
MIP 6	57.02	36.04	1.35	59.93	31.63	1.32	89±5[a]
NIP 6	56.59	36.26	1.42	59.93	31.63	1.32	90±2[a]

The peak heights multiplied by their various extinction coefficients give A, B, C, and D, for the vinyl peaks at 1630 cm^{-1} (A) and 990 cm^{-1} (B), and the para- (1510 cm^{-1}, C) and meta-di- substituted (795 cm^{-1}, D) peaks

[a]$\%DC = 100 - \frac{[(Abs(C=C)/Abs(stdi))_{polymerized}]}{[(Abs(C=C)/(Abs(stdi))_{monomer}]} x100$ (6) [30, 31]

[b]$X_{VB} = \frac{(A+B)}{2\,(C+D)} \times 100\%$ (7) and $\%DC = \% DVB - X_{VB}$ (8) being %DVB= 80% [32]

From another point of view, the status of carboxylic acid in MIPs and NIPs 2 and 4 has been studied by analyzing the 1733 cm^{-1} and 1698 cm^{-1} bands, assigned to the stretching carbonyl vibrational modes ($\upsilon_{C=O}$) of the free and cyclic acid dimers, respectively. A least-square curve fitting method has been applied to the $\upsilon_{C=O}$ bands. The band at 1733 cm^{-1} can be fitted to the Gaussian function whereas the band at 1698 cm^{-1} has been better adjusted

to a mixed Lorentz-Gaussion function. The fraction of H-bonded carbonyl group (F_b) has been calculated by Eq. 9:

$$F_b = \frac{A_b/a}{A_b/a + A_f} \qquad (9)$$

A_f and A_b denote peak areas corresponding to the free and the H-bonded carbonyl groups, respectively, and a is the ratio of the molar absorption coefficients. A value of 1.5 has been taken for the "a" ratio, according to previous infrared studies in similar systems [33].

2.5.2. Solubility parameters

The solubility parameter of random copolymers (δ_P) has been estimated from equation 10:

$$\delta_P = \phi_1 \delta_1 + \phi_2 \delta_2 \qquad (10)$$

Where ϕ_1 and ϕ_2 denote volume fractions of the M and C, δ_1 and δ_2 represent the solubility parameters of pure poly(M) and poly(C), respectively [34]. The current M:C ratios determined by elemental analysis for polymers 2, 4 and 6 have been used, whereas for the rest of the polymers the feed compositions have been selected for the calculations. The solubility parameter values for C, M and porogen have been taken from the literature: $CHCl_3$ (19.0 $MPa^{0.5}$), polyEGDMA (19.23 $MPa^{0.5}$) [35], polyDVB (17–18 $MPa^{0.5}$) [36], polyMAA (26.8 $MPa^{0.5}$) [37], polyHEMA (29.66 $MPa^{0.5}$) [35] and polyAM (36.00 $MPa^{0.5}$) [38]. The solubility parameter of poly(TMPTA), 24.29 $MPa^{0.5}$, has been evaluated theoretically

from the group contribution to Energy of Vaporization E_i and Molar Volume [39].

2.5.3. Polymer density and swelling

Analysis of polymer swelling has been conducted in the porogen (CH_3Cl) and rebinding solvent (ACN: water 4:1 v:v). Dry polymer ($\cong$ 0.20-0.30 mL) is placed in a 1 mL graduated test tube and weighed to calculate the apparent dry density of the polymer. Excess solvent is then added to the tube and the polymer sonicated in order to remove air bubbles. The tube is closed and left to stand for 24 h at room temperature. Excess solvent is then removed and final volumes recorded. The swelling ratio is given as volume of the swollen polymer to volume of dry polymer [21]. The average values of triplicate independent results have been obtained.

2.6. KINETICS TESTS

Kinetics of the MIPs have been examined at 153.7 mg L^{-1} HYP in ACN:water (4:1, v:v) solution onto 200 mg of the sorbent. ACN: water (4:1, v:v) has been chosen as rebinding solvent due to its ability to dissolve the target molecule and its expected compatibility with food matrices and aqueous environments. The mixture has been shaken in an ultrasonic bath for different time periods (2-180 min) at room temperature, then the polymer is removed by filtration (0.2 µm) and the resulting solution analyzed by UPLC-PDA at 250 nm. The amount of HYP

(q, μg g^{-1} or μmol g^{-1}) retained by the MIP has been calculated by subtracting the concentration of free HYP (C_f, μM) from C_0.

2.7. BATCH REBINDING

Affinity of the MIPs for HYP was investigated through batch binding experiments. An aliquot of 4 mL of eight different solutions of HYP in ACN:water (4:1, v:v), spanning the concentration range 5.124-1025 mg L^{-1} (C_0), has been added to 200 mg of the MIPs in vials. The resulting suspension has been shaken in an ultrasonic bath for 5 min at room temperature, then the polymer is removed by filtration and the resulting solution analyzed by UPLC-PDA at 250 nm. The amount of HYP bound to the polymers is determined as explained in section 2.6. The selected concentration range guarantee the suitability of MIPs for final application as adsorbents in a MSPD procedure, because the levels of HYP commonly found in fish samples in subsequent days after the capture are below 250 μg g^{-1} [40]. The same procedure is employed to characterize the NIPs.

The specificity of the polymers for HYP was estimated by the imprinting factor: IF= (K_{pMIP}/ K_{pNIP}) (11) where K_p= q/C_f [41]. IF values have been calculated for each concentration plus the IF average value corresponding to the whole range. Besides, linearized forms of Langmuir and bi-Langmuir and Freundlich adsorption isotherm models have been applied to fit the equilibrium data [42, 43].

3. RESULTS

3.1.   PREPOLYMERIZATION STUDIES

3.1.1. Complex structure elucidation

Job plots based on UV-Vis spectroscopy suggested 1:1 stoichiometry for all the systems and solvents studied, as the maxima of the curves coincide with X_{MAA}= 0.5 point (not shown). The low stoichiometries calculated for TPH:MAA and TPH:AM complexes are surprising as previous computational approach studies predicted an optimal ratio of 1:4 for both systems [44]. Several factors explain these inconsistencies. From the one hand, the experimental results emphasize the importance of the porogen absent in most computational calculations. Besides, when $C_0 << K_d$ a symmetrical Job plot will always be obtained regardless of the true binding stoichiometry [45]. Owing to the fact that increasing C_o lead to signal saturation in the UV-Vis spectra, we turned to FTIR spectroscopy to accurately determine the binding stoichiometry of the TPH:MAA and TPH:AM complexes in $CHCl_3$. Being $CHCl_3$ a fairly good solvent for both DT and due to its weak polarity it will not disturb the formation of hydrogen bonding (H-bonding) between the M and the DT, it was the solvent chosen as porogen.

The interactions between DT and M are detected by FTIR spectroscopy as a result of band shifting, band broadening and spectral substraction. A detailed description of the FTIR study is presented as Supplementary Material (section 1.1). As expected, H-bonding is the dominant driving force. The studies prove 1:1 stoichiometry for CAF:MAA, TPH:MAA,

215

TPH:HEMA systems whereas the formation of 1:2 complex is confirmed for TPH:AM (Fig S3.I and S3.II). Furthermore, ^{1}H-NMR spectroscopy corroborates that the primary DT: M interaction mechanism is based on H-bonding for all the systems studied (Supplementary Material: section 1.2). H-bonding leads to changes in the chemical shifts of ^{1}H resonances, which in conjunction with FTIR, have helped to identify the specific sites engaged in complexation. The proposed DT:M complex structures are depicted in Fig 1.

Concerning the TPH:AM complex, the observed modifications of FTIR and ^{1}H-NMR bands of both TPH and AM donor (NH) and acceptor (N_9 and C=O) groups suggest that the first AM molecule forms a two-point H-bonding motif; although the exact position of the second AM molecule remains unclear. Hence, two possible structures are proposed for the TPH:AM 1:2 complex with the second AM molecule bound either to the N_9 site or to the C_2=O group of TPH (Fig. 1d and 1e). Ab initio calculations of hydrated TPH crystal structures [46] suggest that the TPH:AM 1:2 complex depicted in Fig. 1d may be more stable than the structure in Fig. 1e. Alternatively, equilibrium between both structures cannot be discarded.

3.1.2. Binding Constants

The ^{1}H- NMR shifts have been used to calculate apparent association constants (Table 1). Results demonstrate that TPH interacts most strongly with AM and most weakly with HEMA. The strong TPH:AM (1:2) complex has a $K_{11} \cong 3.4 \times 10^4$-$1.7 \times 10^4$ M^{-1} and $K_{12} \cong 1.33 \times 10^2$-$77 \times 10^1$ M^{-1}

whereas the K_{11} binding constants for TPH:AA-d_4 (1:1) and TPH:HEMA (1:1) complexes are in the order of 1.39 x 10^2-9.0 x 10^1 M^{-1} and 1.2 x 10^1 M^{-1}, respectively. Hence, the molecular interaction strength between TPH and M has the order AM >> AA-d_4> HEMA, which is consistent with the complex stoichiometry (1:2 and 1:1) and number of interaction points (3-, 2-, 1-hydrogen bonded motif) (Fig. 1). These results differ from the computational approach of Dong et al. who found stronger interactions between TPH and MAA than with AM [44]. As stated in section 3.1.1, this discrepancy may be explained by the fact that the experimental results emphasize the importance of the porogen, absent in most computational calculations.

Likewise, the molecular interactions between the AA-d_4 and the DT have the order TPH> CAF, reflecting the greater stability of the 2-two point cyclic H-bonded TPH:MAA 1:1 complex which binding constant is nearly 30-20 superior compared to the simpler 1-point CAF:MAA complex. Within experimental error, the apparent binding constant for the TPH: AA-d_4 complex is of the same order of magnitude as the ones estimated by FTIR, $K_{11} = 133 \pm 46$ M^{-1} (Suplementary Material: sections 1.1.1 and 1.1.3), and by Wang et al. using a similar FTIR method and the same solvent [47]; on the contrary, the K_{11} obtained for the CAF: AA-d_4 system is 20 times smaller than the one estimated by Wang et al.
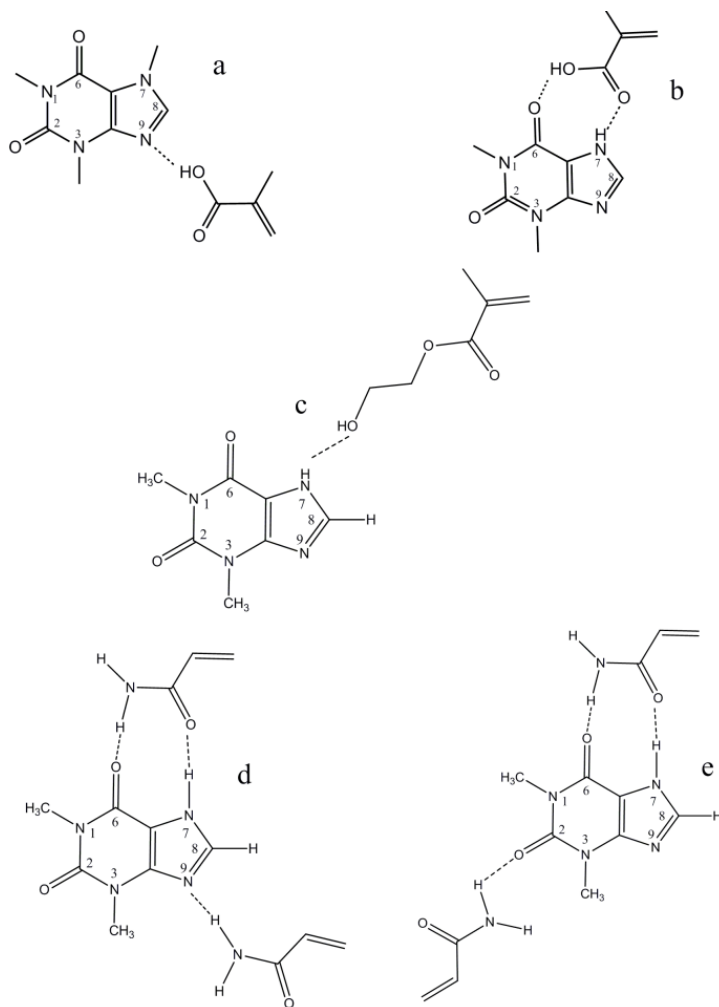
Figure 1. Proposed DT: M complex structures: CAF:MAA 1:1 (a); TPH:MAA 1:1 (b); TPH:HEMA 1:1 (c) and possible structures for TPH:AM 1:2 (d and e).

In summary, according to the prepolymerization studies, MIPs prepared with AM and TPH should, in principle, show stronger binding for xanthine derivatives than those synthesized with MAA or HEMA as M and/or CAF as DT. Besides, it may be emphasized at this point that the election of TMPTA instead of EGDMA for the TPH-HEMA formulation has been based on the

weak TPH: HEMA interactions in $CHCl_3$. Predicting poor results for HEMA-EDGMA based MIPs, TMPTA was selected as tri or tetrafunctional crosslinkers lead to more well-defined recognition sites and thus, higher selectivities and load capacities [48].

3.2. CHARACTERIZATION OF THE POLYMERS

3.2.1. ATR spectra of MIPs

ATR-FTIR analyses of the MIPs before and after the extraction process confirmed DT removal and polymer structural stability. After thoroughly washing, the CAF and TPH bands at 1665 cm^{-1} ($\upsilon_{C=O}$ at C_6) and at 1555 cm^{-1} ($\upsilon_{C=N, C=C}$ of the purine ring) disappeared and the extracted spectra were similar to those of NIPs. The M and C diagnostic signals have been identified for all the polymers (Supplementary Material, section *2*). The curing behavior of M and C has been monitored because the C=C vibration participates in the cross-linking reaction (Table 3). The percentage of unreacted C=C (%DC) for EGDMA and TMPTA copolymers are $\geq$ 86%, high enough for stabilizing the shape of the imprinted cavities. Besides, MIPs have roughly the same degree of pendant double bonds than the corresponding NIPs. By contrast, the polyDVB polymers have a lower degree of monomer conversion, although the estimated values are similar to the ones obtained by Hubbard et al. for commercial polyDVB-80 resins [32]. Nonetheless, the %DC of MIP 2 and NIP 2 (60%) are higher than the values estimated for MIP 4 (54%) and NIP 4 (49%)

In addition, the status of carboxylic acid in MIPs and NIPs 2 and 4 has been studied (section *2.5.1*). For comparison, the fractions of "H-bonded" carboxyl groups (F_b) in the prepolymerization mixture of the reference polymers have also been calculated: 0.96 ± 0.01 and 0.81 ± 0.05, for NIP 2 and NIP 4, respectively. The lower porogen volume employed for the synthesis of NIP 2 explains the greater fraction of carboxylic acid dimer in relation to NIP 4. Besides, F_b values are significantly reduced in the polymers with respect to the pre-polymerization mixture: 0.62 ± 0.03, 0.64 ± 0.03, 0.61 ± 0.05, 0.64 ± 0.02 for MIP 2, NIP 2, MIP 4 and NIP 4, respectively. No differences are detected between MIPs and NIPs, within experimental error. Thus, the presence of the DT does not affect the status of the carboxylic acid moieties in the polymers. These findings are in accordance with the observation of Yoshimatsu et al for the same kind of copolymers [49]. The effect of porogen volume is not observed in the polymers either. This study cannot be applied to poly(MAA-EGDMA) copolymers because the $\nu_{C=O}$ band of MAA overlaps with the strong $\nu_{C=O}$ band of EGDMA.

3.2.2. Elemental analysis

The carbon, oxygen and nitrogen content of the copolymers obtained by elemental analysis are shown in Table 3. This information can be used to calculate the comonomer composition of the polymer; such calculations are particularly straightforward when only one of the comonomers bears a heteroatom e.g. oxygen or nitrogen. The oxygen content has been used to

estimate the actual ratio of MAA:DVB in MIPs and NIPs 2 and 4, whereas the nitrogen content has been employed to estimate the ratio of AM: EGDMA in MIP and NIP 6. The nitrogen content found in MIPs and NIPs 1 to 5, due to AIBN initiator, has not been included in the calculations.

Being the experimental percent oxygen for MAA-co-DVB polymers 1.5 and twice-fold the theoretical values for MIP 2 and 4, respectively, the final carboxyl content in the copolymer is superior to what would be predicted from the feed composition. The actual MAA: DVB molar ratios are 4: 13; 4: 14: 4: 9 and 4:11 for MIP 2, NIP 2, MIP 4 and NIP 4, respectively, much lower than the theoretical value 4:20. The low efficiency of DVB incorporation corroborates the results of Yoshimatsu et al [49] for the same kind of copolymers. For AM-co-EGDMA polymers the experimental molar ratios are 4:18.5 and 4:17.5 for MIP 6 and NIP 6, respectively, slightly lower than the theoretical value 4:20. Similar M: C ratios or nearer to the feed compositions can be expected for copolymers 1, 3 and 5.

3.2.3. Surface area and porosity

BET analysis is a powerful tool to investigate the effect of the nature of M and C on the pore structure of the MIP. Textural parameters are collected in Table 4. The polymers show a wide distribution of surface areas (S_{BET}) and pore volumes (V_p). MAA-co-DVB polymers (2 and 4) have larger surface areas and larger pore volumes than MAA-co-EGDMA polymers (1 and 3). On the other hand, HEMA-co-TMPTA (MIP and NIP 5) and AM-co-EGDMA (MIP and NIP 6) polymers are non- porous. S_{BET} is higher than

external surface area (S_t) in polymers 1-5 due to the contribution of microporosity to the BET area.

Opposite to polymers 2 and 4, there are differences in morphology between MIPs and NIPs 1 and 3 which confirm imprinting. MIP 1 and 3 have higher BET areas and external surfaces than corresponding NIPs, even though the raises in cumulative pore volume and average pore diameter are more important. Moreover, S_{BET} of MIP 1 after soxhlet extraction shows a larger augment compared with that of the MIP without extraction. S_{BET} of NIP 1 has a smaller relative increase.

Table 4. Textural parameters from BET analysis and solubility parameters of produced MIPs and NIPs.

Polymer	S_{BET} ($m^2 g^{-1}$)	S_t ($m^2 g^{-1}$)	V_{micro} x10^{3}cm^{3}g^{-1}	V_P ($cm^3 g^{-1}$)	Average[c]pore diameter (nm)	δ_p (MPa)$^{1/2}$	$(\delta_s-\delta_p)^2$
MIP1[a]	207±3	195.4	4.7	0.56	10.80	-	-
NIP1[a]	272±4	232.4	17.5	0.60	8.77	-	-
MIP1[b]	326±4	231.7	40.0	0.60	7.34	-	-
NIP1[b]	314±4	225.1	37.4	0.43	5.44	19.83	0.69
MIP 2[b]	862±7	816.7	15.0	1.27	5.90	-	-
NIP 2[b]	859±7	799.7	21.1	1.19	5.53	19.28	0.08
MIP3[b]	270±3	197.5	30.3	0.54	8.02	-	-
NIP3[b]	266±3	169.2	40.3	0.33	4.95	19.83	0.69
MIP 4[b]	723±5	702.9	0.99	0.62	3.43	-	-
NIP 4[b]	729±5	714.5	0.55	1.00	5.49	19.57	0.32
MIP 5[b]	0.133	0.0621	0.037	0.00034	10.19	-	-
NIP 5[b]	0.122	0.0999	0.011	0.00032	10.46	24.73	32.9
MIP 6[b]	0.025	-	0.31	-	-	-	-
NIP 6[b]	0.013	-	0.35	-	-	20.36	1.8

[a]The polymers without soxhlet extraction.

[b]The polymers with soxhlet extraction as described in section 2.4.

[c]BJH adsorption average pore diameter (4 x pore volume/surface area) of pores between 0.1 and 400 nm.
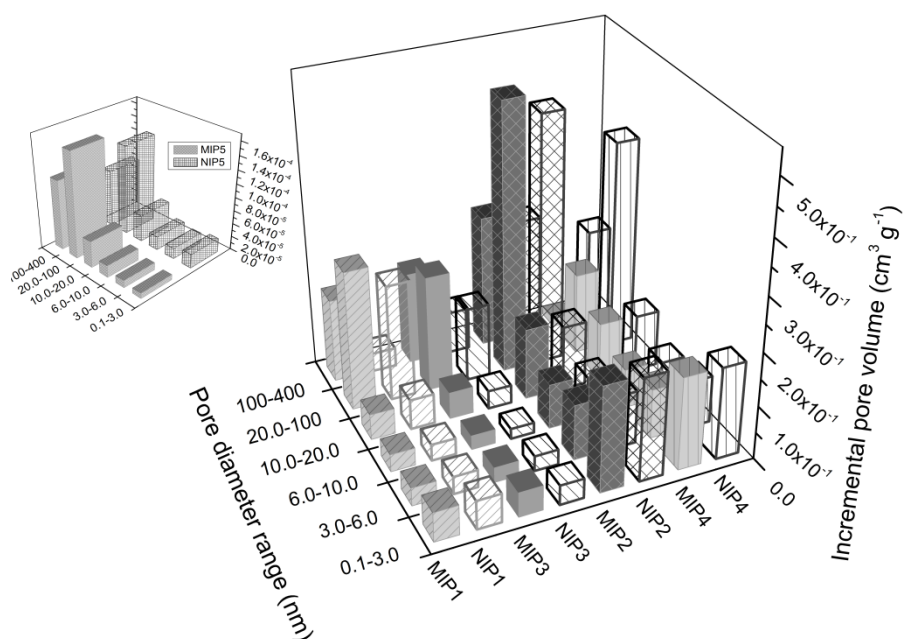
Figure 2. Histogram of pore size distributions for MIPs and NIPs 1-4. Inset: Pore size distributions of MIP and NIP 5.

Similar conclusions are drawn from the pore volume distribution plots illustrated in Fig. 2. The pores of MIPs 1 and 3 predominantly cluster in the range of 20-100 nm and 100-400 nm. In particular, approximately 50% of the pores are in the range 20-100 nm; the DT: M interactions change the pore size distribution of MIPs providing new porosity towards the macropore region (100-400 nm). By contrast, the pore size distribution of MAA-co-DVB polymers appears wider with higher values of both micro and mesopores. A similar pore size distribution is observed for MIP 2, NIP 2 and NIP 4 whereas MIP 4 has lower pore volume and lower pore size distribution, specifically in the ranges 20-100 and 100-400 nm. The latter

data may be explained by the lower MAA: DVB ratio found for MIP 4 compared to MIP 2, and NIPs 2 and 4 (section *3.2.2*).

At last, the polymer morphology has been correlated with the difference in solubility parameters between the porogen solvent (δ_s) and the copolymer (δ_p). This difference or its square $(\delta_s-\delta_p)^2$ are used to represent the solvating power of a diluent in a network formation system. According to Hildebrand theory, the solubility of a polymer in a solvent is favored when $(\delta_s-\delta_p)^2$ is minimized [50]. The estimated solubility parameters of the copolymers (section *2.5.2*, Eq. 10) and $(\delta_s-\delta_p)^2$ values are compiled in Table 4. It is concluded that it is difficult to create porosity when $(\delta_s-\delta_p)^2)$ is $\cong$ 2 or > 2 MPa$^{0.5}$. For copolymers 5 and 6, the disparity between both solubility parameters, causes premature phase separation of the polymer from the monomer phase and poor solvation of the polymer; consequently, products with insignificant porosity. By contrast, the similarity between the solubility parameters of CHCl$_3$ and DVB:MAA copolymers allows better solvation of the polymer, leading to well-developed pore structure and high specific surface areas (723-862 m^2 g^{-1}); MAA-co-EGDMA copolymers have intermediates values (266-326 m^2 g^{-1}).

3.2.4. Swelling study

The swelling study has been carried out to investigate the effect of chemical composition and solvents on MIP conformation. Fig. 3 depicts the apparent dry densities (3.I) and swelling ratio in the porogen and rebinding

solvent for all the polymers prepared (3.II). Some general observations can be made.

Independently of the solvent assayed, the swelling ratio increases in the following order: MAA-co-DVB < MAA-co-EGDMA < HEMA-co-TMPTA < AM-co-EGDMA. Often a large portion of unreacted double bonds remains in the polymer leading to high swelling, low pore volume and low surface area [21]. In the current study the number of residual double bonds in all (meth)acrylate polymers spans from 86 to 97% and is much higher than corresponding values in DVB-copolymers (49-60%). As a result, the different swellings are not ascribed to variable levels of residual bonds but to the textural properties discussed in section *3.2.3*. The polymers with higher surface areas and pore volumes have smaller apparent dry densities and lower swelling ratios (Fig.3). In addition, the greater rigidity of the DVB crosskinker may also contribute to the low swelling ratio of polymers 2 and 4.

Furthermore, MIPs 2, 4 and 5 swelled to the same degree compared to their related NIPs in both solvents within experimental error. In the case of MIP and NIP 2 this is in agreement with the similar pore volume and pore volume distribution plots. For MIPs 1 and 3 the increase in pore volume and the different pore size distribution accounts for the slightly higher swelling ratio with respect to their corresponding NIPs. On the contrary, a lower swelling ratio is observed for MIP 6 in contrast with NIP 6. This result may be ascribed to the difference in AM: EGDMA molar ratios, 4:18.5 and

4:17.5 for MIP 6 and NIP 6, respectively. Higher swelling may be expected with lower crosslink ratios as the greater flexibility causes greater expansion of the polymer network [21, 51].
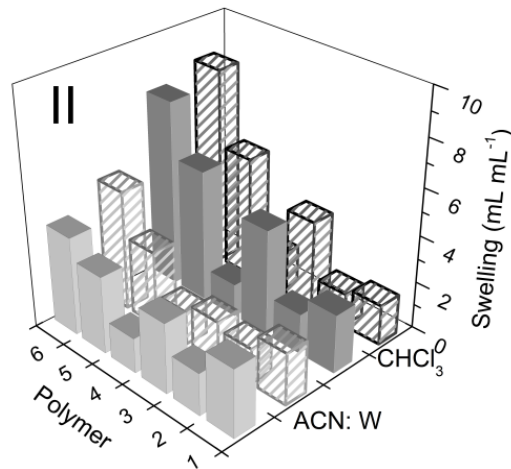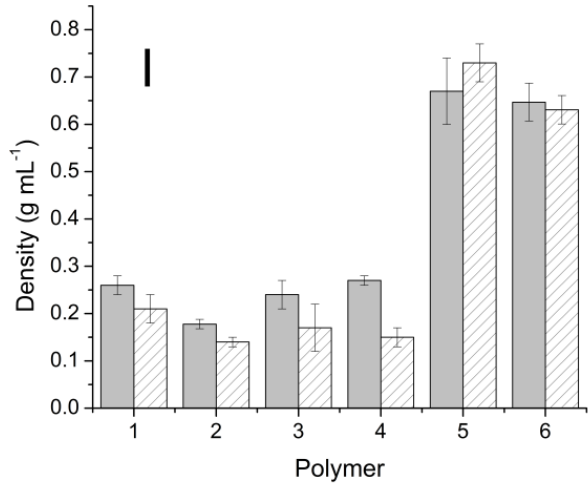
Figure 3. (I) Apparent dry densities and (II) swelling ratio in rebinding (ACN: water) and porogen ($CHCl_3$) solvents of produced MIPs (filled) and NIPs (pattern).

Ideally, matching the porogen with rebinding solvent improves molecular recognition in MIPs, most likely due to swelling effect that gives the desired functional group proximity [41]. Nonetheless, this is not always possible due to T solubility problems or inability to polymerize. Thus, an important issue is to compare the effect of the rebinding solvent and the porogen on the swelling properties. The swelling ratios for polymers 1, 2 and 4 are comparable in ACN: water and $CHCl_3$ which implies a similar morphology in the swollen state, theoretically preserving the binding site fidelity. By contrast, MIP 3, 5 and 6 swell in ACN: water to a lesser extent than in $CHCl_3$.

3.2.5. Scanning electron microscopy (SEM)

Scanning electron micrographs reveal the differences in morphology in the dry state between the polymers. In coherence with the BET results, polymers 1- 4 show a rough surface with visible pores. Besides, the SEM analysis clearly shows macropores and flow-through pores embedded in the network skeleton of MIP 1 absent in NIP 1, supporting imprinting (Fig 4.I and 4.II). By contrast, the differences observed in surface area and pore volume between EGDMA and DVB polymers are not appreciated by SEM. More to the point, polymers 5 and 6 show a smooth featureless image with no observable pores. The fractures observed most likely arise from stress created during shrinking. The morphology of the corresponding blank polymers is similar to the MIPs (Fig. 4.III and 4.IV).
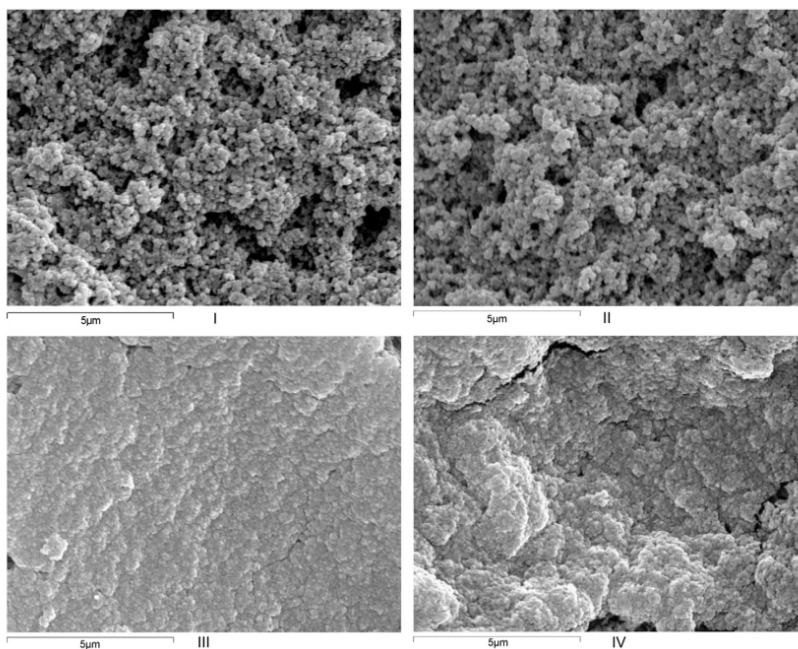
Figure 4. SEM micrographs of MIP 1 (I), NIP 1 (II), MIP6 (III) and NIP 6 (IV) with 10000x magnification.

3.3. KINETIC CONSIDERATIONS

A preliminary kinetic assay has been conducted. Kinetic of adsorption describes the rate of adsorbate uptake on MIPs and controls the equilibrium time; it is limited by the affinity to the adsorbent and the pore-size distribution of the polymers [52]. The adsorption equilibrium is reached within a short ultrasonic bath shaking period of 2 min for MIPs 1-4 and 5 min for MIPs 5 and 6 while the percentages of HYP bound to the polymers are 29, 25, 38, 18, 38 and 54 for MIP 1-6, respectively. As described in sections *3.2.3*, *3.2.4* and *3.2.5*, because of the gel like non-porous morphology, MIPs 5 and 6 experiment larger swelling and shrinking

228

with changes in the solution than copolymers 1-4, thus, increasing the adsorption equilibrium time. At any rate, these results indicate that the MIPs hold fast uptake kinetics and can thus be used as sorbent of SPE or MSPD for rapid determination of HYP from complex materials.

3.4. BINDING ISOTHERMS

Affinity of the various MIPs and NIPs for HYP (chemical formula in Fig. 5(II)) has been investigated through batch binding experiments in ACN: water (4:1, v:v). Their recognition ability was first examined through the *IF*. Successful imprinting occurred in the case of MIP 6 ($IF_{average}$ = 4.81), followed by MIP 1 ($IF_{average}$ = 1.41), MIP 5 ($IF_{average}$ = 1.29) and MIP 3 ($IF_{average}$ = 1.11). Above and beyond, the *IFs* of MIP 6 and MIP 5 are > 2.7 and > 1 for the entire range of values, respectively, whereas for MIP 1 and MIP 3 the IF is < 1 for some concentrations. DVB copolymers (MIP 2 and 4) seem to be non-specific, although the *IF* values for MIP 2 are still above 1 for intermediate loading solute concentrations (153.5 y 266.4 mg L^{-1}).

The binding isotherms are coherent with the *IF* values. Owing to the better behavior exhibited by MIP 6, its binding isotherm is displayed in Fig 5 (I) in comparison with NIP 6. The binding amount rises gradually upon increasing HYP concentration in the initial solution, up to 13000 and below 5000 µg g^{-1} for the maximum concentration assayed for MIP and NIP, respectively. These differences are ascribed to the molecular-imprinting effect.
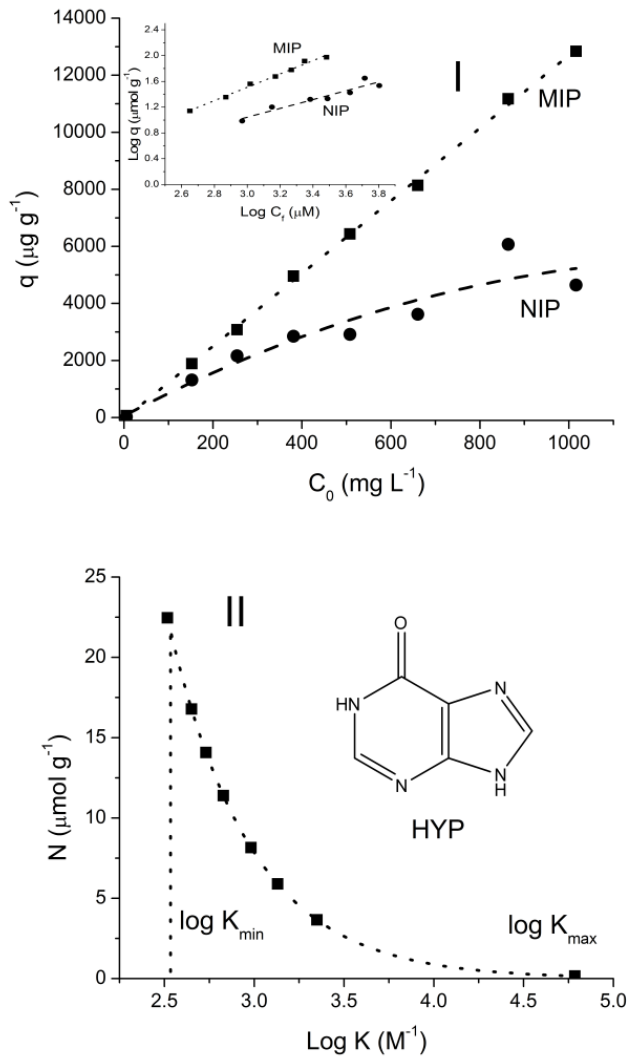
Figure 5. (I) Batch rebinding adsorption isotherm for HYP in ACN: water (4: 1 v/v) on MIP and NIP 6. Inset: fitting to the log-log Freundlich isotherm. (II) Affinity Distribution (AD) for HYP on MIP 6 and HYP chemical formula.

Owing to the fact that solubility problems of HYP in the rebinding solvent preclude the achievement of curve saturation linearized forms of Langmuir, bi-Langmuir and Freundlich (FI) models, which are suitable to characterize

the subsaturation region of the binding isotherm, have been applied to fit the equilibrium data [42]. The data do not fit the Langmuir and bi-Langmuir models, which have been discarded (not shown). By contrast, except for MIPs 2 and 4 ($R^2 \cong 0.62$), the FI appears to be a reasonable model as evidenced by the relatively good fit to linear regression analysis ($R^2 > 0.9$). As an example, the fitting of experimental points of MIP and NIP 6 to the log-log Freundlich isotherm is shown in Fig. 5(I) Inset.

The results of the mathematical treatment reveal some interesting facts (Table 5). Firstly, the high values of the *heterogeneity indices (m)* indicate that the polymers are approaching homogeneity. These data are surprising because they have been imprinted non-covalently which usually results in heterogeneity; nonetheless, some authors have previously obtained similar results [51]. These high *heterogeneity indices* may be related with the limitations of the FI model [51, 53]; on the other hand, the values may indeed reflect homogeneous polymers which are desirable for MIPSE applications. Heterogeneity usually limits the capacity and selectivity of MIPs and makes the binding properties of MIPs highly concentration dependent [42, 54].

From another point of view, MIP 6 is characterized by the highest weighted average affinity ($K= 1.89 \times 10^3$ M^{-1}) followed by MIP 5 ($K= 1.17 \times 10^3$ M^{-1}). A noteworthy point is that MIPs 1-4, which use MAA as M and differ in the C, DT and porogen volume, have similar weighted average affinity values ($K = 3.96 \times 10^2$-3.29×10^2 M^{-1}) but lower than MIP 6 and 5. Moreover, MIP

6 has nearly triple *weighted average affinity* with respect to NIP 6, again followed by MIP 5 with a K_{MIP}/K_{NIP} ratio of $\cong 1.26$. On the contrary, MIPs 1-4 have *lower weighted average affinity* than their corresponding NIPs.

Table 5. Isotherm parameters obtained for HYP on the synthesized MIPs and NIPs estimated by fitting the experimental data to the Freundlich isotherm model.

Polymer	*m*	*K* (M^{-1})	*N* (µmol g^{-1})	K_{MIP}/K_{NIP}	$N_{MIP}/_{NIP}$
MIP 1	1.032	3.92E02	3.157	0.77	0.06
NIP 1	1.412	5.12E02	54.57		
MIP 2	0.737	3.74E02	10.56	0.54	0.29
NIP 2	1.321	6.93E02	37.08		
MIP 3	1.147	3.96E02	17.90	0.50	1.07
NIP 3	1.142	7.89E02	16.73		
MIP 4	0.801	3.29E02	7.600	0.58	0.09
NIP 4	1.430	5.70E02	83.13		
MIP 5	1.122	1.17E02	22.52	1.26	0.34
NIP 5	1.292	9.32E02	67.26		
MIP 6	0.946	1.89E02	10.22	2.96	0.74
NIP 6	1.122	6.38E02	13.73		

Concerning the *number of binding sites (N)*, the value for MIP 6 throughout the entire affinity range ($N_=$ 10.22 µmol g^{-1} or 1.39 mg g^{-1}) lies within the range typically found for non-covalent MIPs (0.1-3.5 mg g^{-1}) [55, 56]. Furthermore, within the measured concentration window, the *number of binding sites* for MIPs 3 and 6 are of the same order of magnitude than their control polymers whereas MIPs 1, 2, 4, and 5 have considerable lower capacities (*N*) compared to the corresponding NIPs. Finally, as can be inferred from the affinity distribution of binding sites (*AD*) (Fig.5 (II)), MIP 6 has numerous low affinity binding sites and few high affinity binding sites and this is consistent with its high heterogeneity index value, *m,* and

hence, with the image of a rather homogenous MIP which may be well-suited for MIPSE application. Regrettably, the AD of NIP 6 could not be compared due to the heterogeneity index value.

In conclusion, MIP 6 showed the highest affinity for HYP as predicted by the prepolymerization studies between TPH and AM. Besides, despite the weak TPH: HEMA 1:1 prepolymerization complex, the flexible, highly hydrophilic trifunctional crosslinker leads to MIP 5 with reasonably high *weighted average affinity;* at any rate, the increase in oxygen groups of TMPTA may explain the high unspecific adsorption reflected in the higher number of NIP and MIP binding sites (N_F) and low *IF*.

On the contrary, the poor affinity of MAA based MIPs is unexpected from the DT: M apparent binding constants in $CHCl_3$. Several reasons account for this result. In the first place, recognition is modulated by H-bonding which is diminished by the high fraction of the strong carboxyl groups dimers ($F_b \cong 0.62$) (section *3.2.1*). Secondly, H-bonding is correlated to the intrinsic acidity and basicity of acceptor and donor groups in the M. In anionic polymeric networks, ionization takes place as the pH of the external medium rises above the pKa of the ionizable moiety. The pKa of MAA is 4.7 whereas the rebinding ACN: water (4:1, v:v) solutions have pH values between 5.5-5.6. At this pH> pKa MAA is partially in its ionized carboxylated form [57]. The decrease in the number of hydroxyl groups reduces the possibility of H-bonding between the DT and M; as a result, both retention and specificity are decreased. Even more, MIPs based on

DVB-co-MAA perform worse than EGDMA-co-MAA polymers. This fact has partly been ascribed to the low MAA: DVB ratio and the low monomer conversion proved by ATR and elemental analysis.

4. CONCLUSIONS

In this work the technique of molecular imprinting using a DT to avoid "bleeding" has been successfully used for the preparation of polymers capable of rebinding HYP in aqueous organic conditions. MIP 6 obtained from TPH:AM:EGDMA (1:4:20) by one step precipitation polymerization in CHCl$_3$ proved highly specific and superior to other DT:M:C combinations synthesized in similar conditions. The strong (1:2) H-bonded complex formed between TPH and AM makes the corresponding MIP the most suitable for HYP recognition in ACN:water. By contrast, monomer dimerization and partial ionisation of MAA somewhat explains the poor rebinding of MAA copolymers in comparison with neutral monomers.

In addition, the performance of MIPs is not only dictated by the interaction of DT with the M pre-and post-polymerisation on a molecular level, but also by the physical make up of the polymer on a macro level. High M:C content and high degree of M conversion have proved crucial for stabilizing affinity sites. Examination of the textural properties by BET and SEM shows substantial differences in morphology as function of the M: C combination employed. It is confirmed that a porous polymer is not a requirement in order to achieve an efficient matrix in molecular imprinting although

adequate swelling must take place in short time. Above and beyond, a reasonably high *IF* is achieved for HYP with MIP 6, despite the fact that it is a non-porous matrix which swelling ratio in the rebinding solvent is nearly half the value obtained in porogen and, thus, does not give the required functional group proximity. This may be partly due to abundant low affinity binding sites shown by the AD, which may not require an exact recreation of the shape and distance parameters as high affinity sites do and confirms that shape selectivity is not the prevailing mechanism for molecular recognition. Conversely, pre-organization of functional groups dominates the performance of MIPs elicited toward T with three or more functional groups capable hydrogen bonding interaction [58].

As a final point, MIP 6 has been chosen as adsorbent for the enrichment and separation of HYP and other ATP degradation products such as INO from natural fish matrices [23].

Appendix A. Supplementary data: *Supplementary data associated with this article can be found in the online version.*

References

[1] M. A. Carsol, G. Volpe, M. Mascini, Talanta 44 (1997) 2151

[2] Y. Zhang, S. Deng, J. Lei, Q. Xu, H. Ju, Talanta 85 (2011) 2154

[3] H. Yan, H. Wang, J. Qiao, G. Yang, J. Chromatogr. A 1218 (2011) 2182

[4] B. Sellergren, Trends Anal. Chem. 18 (3) (1999) 164

[5] V. Pichón, F. Chapuis-Hugon, Anal. Chem. Acta 622 (2008) 48

[6] B. Tse Sum Bui, K., Anal Bioanal Chem 398 (2010) 2481

[7] C. M. Lok and R. Son, Food Res. J. 16 (2009) 127

[8] R. Garcia, M. J. Cabrita, A. M. Costa Freitas, Am. J. Anal. Chem. 2 (2011) 16

[9] J. Wang, R. Guo, J. Chen, Q. Zhang, X. Liang, Anal. Chem. Acta 540 (2005) 307

[10] Y. Wang, Y. Cao, Ch. Fang, Q. Gong, Ana. Chim. Acta 673 (2010) 145

[11] X. Feás, J.A. Seijas, M.P. Vázquez-Tato, P. Regal, A. Cepeda, C. Fente, Ana. Chim. Acta 631 (2009) 237

[12] M. Kawaguchi, Y. Hayatsu, H. Nakata, Y. Ishii, R. Ito, K. Saito, H. Nakazawa, Anal. Chim. Acta 539 (2005) 83

[13] X. Shi, A. Wu, G. Qu, R. Li, D. Zhang, Biomaterials 28 (2007) 3741

[14] H.S. Andersson, I.A. Nicholls, Bioorg. Chem. 25 (1997) 203

[15] I. A. Nicholls, K. Adbo, H. S. Andersson,, P. O. Andersson, J. Ankarloo, J. Hedin-Dahlström, P. Jokela, J. G. Karlsson, L. Olofsson, J. Rosengren, S. Shoravi, J. Svenson and S. Wikman, Anal. Chim. Acta 435 (2001) 9

[16] H. Kim, D.A. Spivak, J. Am. Chem. Soc. 125 (37) (2003) 11269

[17] J. O'Mahony, A. Molinelli, K. Nolan, M.R. Smyth, B. Mizaikoff, Biosens. Bioelectron. 20 (2005) 1884

[18] Olivier Y. F. Henry, David C. Cullen, Sergey A. Piletsky, Anal Bioanal. Chem. 382 (4) (2005) 947

[19] Q. Osmani, H. Hughes, K. Flavin, J. Hedin-Dahlstrom, C. J. Allender, J. Frisby, P. McLoughlin, Anal Bioanal Chem. 391 (4) (2008) 1229

 [20] A. Lasagabáster-Latorre, M.C. Cela-Pérez, S. Fernández-Fernández, J.M. López-Vilariño, M.V. González-Rodríguez, M.J. Abad; L.F. Barral-Losada, Mater. Chem. Phys. 141 (2013) 461

[21] B. Sellergren, K. J. Shea, J. Chromatogr. 635 (1993) 31

[22] J. L. Urraca, M. C. Carbajo, M. J. Torralvo, J. González-Vázquez, G. Orellana, M. Moreno-Bondi, Biosens. Bioelectron. 24 (2008) 155

[23] M.C. Cela-Pérez, L. Barbosa-Pereira, X. Vecino, M. Pérez-Ameneiro, Aurora Lasagabaster Latorre, J.M. López-Vilariño, M.V. González Rodríguez, A.B. Moldes, J.M. Cruz, Talanta 135(2015) 58

[24] Z. Wang, Y. Chen, H. Zhang, X. Li, J. Kang, Chem. Res. Appl. 21 (2009) 1370

[25] P. Job, Formation and stability of inorganic complexes in solution, Ann. Chim. 9 (1928) 113

[26] J.H. Yoe, and A. L. Jones, Ind. Eng. Chem. Anal. Ed. 16 (1944) 111

[27] D. J. Duffy, K. Das, S. L. Hsu, J. Penelle, V. M. Rotello, H.D. Stidham, J. Am. Chem. Soc. 124(8) (2002) 8290

[28] K. A. Connors, Binding Constants: The Measurement of Molecular Complex Stability, first ed., Wiley, New York, 1987, Chap. 5, 194

[29] K. Eliadou, K. Yannakopoulou, A. Rontoyianni, I. Mavridis, J. Org. Chem. 64 (1999) 6217

[30] L.C. Mendes, A.D. Tedesco, M.S. Miranda, Polym. Test. 24 (2005) 418-422

[31] H. Joo, Y. Park, H. Do, H. Kim, S. Song, K. Choi, J. Adhes. Sci. Technol. 21 (7) (2007) 575

[32] K. L. Hubbard, J. A. Finch, G. D. Darling, React. Funct. Polym. 36 (1998) 17

[33] S. W. Kuo, S. Chan, F. Chang, F., Polymer 43 (2002) 3653

[34] A. F. M. Barton, Handbook of Solubility Parameters and Other Cohesive Parameters, CRC Press, Boca Ratón, FL, 1983.2nd ed. 1991

[35] M. Guvendiren, J. A. Burdick S. Yang, Soft Matter. 6 (2010) 5795-5801

[36] J. Wang, P. A. G. Cormack, D. C. Sherrington, E. Khoshdel, Pure Appl. Chem. 79 (9) (2007) 1505

[37] B.-C. Ho, W.-K., Chin, Y.-D. Lee,(1991), J. Appl. Polym. Sci., 42 (1991) 99

[38] K. Nakazato, K. Suzuki, Macromolecules 23 (1990) 1800

[39] R. F. Fedors, Polym. Eng. Sci. 1 (2) (1974) 147

[40] J.M. Barat, L. Gil, E. García-Breijo, M.C. Aristoy, F. Toldrá, R. Martínez-Máñez, J. Soto, Food Chem. 108 (2008) 681

[41] D.A. Spivak, Adv. Drug Deliv. Rev. 57 (2005) 1779

[42] R. J. Umpleby II, S. C. Baxter, A. M.C, G. T. Rushton, Y. Chen, K. D. Shimizu, J. Chromatogr. B 804 (2004) 141

[43] A. M. Rampey, R. J. Umpleby, II, G. T. Rushton, J. C. Iseman, R. N. Shah and K. D. Shimizu, Anal. Chem. 76(4) (2004) 1123

[44] W. Dong, M. Yan, M. Zhang, Z. Liu, Y. Li, Anal. Chim. Acta 542 (2005) 186

[45] Ch. Y. Huang, Methods Enzymol. 87 (1982) 509

[46] M.M. Nolasco, A. M. Amado, P. J. Ribeiro-Claro, Chem Phys Chem. 7(10) (2006) 2150

[47] J. Y. Wang, F. Liu, Z.L. Xu, K. Li, Chem. Eng. Sci. 65 (2010) 3322-3330

[48] M. Kempe, Anal. Chem. 68 (1996) 1948

[49] K. Yoshimatsu, K. Reimhult, A. Krozer, K. Mosbach, K., Sode, L. Ye, Anal. Chim. Acta 584 (2007) 112–121

[50] O. Okay, Prog. Polym. Sci. 25 (2000) 711

[51] N. Holland, J. Frisby, E. Owens, H. Hughes, P. Duggan, P. McLoughlin, Polymer 51 (2010) 1578

[52] W. H. Cheung, Y. S. Szeto, G. McKay, Bioresource Technol. 98(15) (2007) 2897

[53] G. T. Rushton, Ch. L. Karns, K. D. Shimizu, Anal. Chim. Acta 528 (2005) 107

[54] Sh. Wei, B. Mizaikoff, Biosens. Bioelectron. 23 (2007) 201

[55] S.V. Duy, I. Lefebvre-Tournier, V. Pichon, F. Hugon-Chapuis, J. Puy, C. Périgaud, J Chromatogr B 877 (2009) 1101

[56] N.S. Bibi, L. Galvisa, M. Grasselli, M. Fernández-Lahore, Process Biochem. 47 (2012) 1327

[57] C. Michailof, P. Manesiotis, C. Panayiotou, J. Chromatogr. A 1182 (2008) 25

[58] R. Simon, M. E. Collins, D. A. Spivak, Anal. Chim. Acta 591 (2007)

SYNTHESIS AND CHARACTERIZATION OF BISPHENOL-A IMPRINTED POLYMER AS A SELECTIVE RECOGNITION RECEPTOR

M. C. Cela-Pérez[1], M. M. Castro-López[1]

A. Lasagabáster-Latorre[2], J. M. López-Vilariño[1],

M. V. Gónzalez-Rodríguez[3], L. F. Barral-Losada[4]

[1] Laboratorio de Química, Centro de Investigacións Tecnolóxicas, Universidade da Coru˜na, Campus de Esteiro s/n, Ferrol 15403, Spain, email: iquimica@udc.es

[2] Dpto Química Orgánica I, Escuela de Óptica, Universidad Complutense de Madrid, Arcos de Jalón, n◦ 118, Madrid 28037, Spain, email: aurora@ucm.es

[3] Dpto. Química Analítica, E.U. Politécnica, Universidade da Coru˜na, Avda. 19 de Febrero s/n, Ferrol 15405, Spain, Tel. +34 981 337 400 3485/3051; fax: +34 981 337 416, email: victoria.gonzalez.rodriguez@udc.es

[4] Laboratorio de Plásticos, Centro de Investigacións Tecnolóxicas, Universidade da Coru˜na, Campus de Esteiro s/n, Ferrol 15403, Spain, email: iquimica@udc.es

ABSTRACT

Molecularly Imprinted Polymers (MIPs) are currently used to provide selectivity in chemical sensors. In this context, a non covalent bisphenol-A (BPA)-imprinted polymer using 4-vinylpyridine (4-Vpy) as the functional monomer, ethylene glycol dimethacrylate (EGDMA) as crosslinker and a low volatile solvent, triethylene glycol dimethyl ether (TRIGLYME), in combination with a non reactive linear polymer, poly (vinyl acetate) (PVAc), as porogen, was synthesized with a simple polymerization procedure. Batch rebinding experiments were carried out to evaluate the binding and selectivity properties of the BPA-MIP. The experimental adsorption isotherms were fitted and a heterogeneous distribution of the binding sites was found. The selectivity of MIP demonstrated higher affinity for target BPA and BPA-analogues over other common water pollutants. The adsorption kinetics followed the pseudo-second-order kinetic model so that the specific adsorption in the imprinted cavities by two strong hydrogen bonds could be described as a chemisorption process. The diffusion mechanism was determined by the intra-particle diffusion and Boyd models, both of them revealing that the adsorption was mainly governed by intra-particle diffusion. MIP was shown to be promising for regeneration without significant loss in adsorption capacity.

Keywords: *Molecularly imprinted polymer; Bisphenol-A; Affinity distribution; Kinetics; Adsorption.*

1. INTRODUCTION

Molecularly Imprinted Polymers (MIPs) are used as recognition element in sensors [1-3]. The common principle of chemical sensors is the immediate transduction of a chemical parameter (usually the concentration of an analyte of interest) into an easily processable, such as an electrical or optical signal. MIPs interact with the analyte to be detected, giving rise to a characteristic change in one of their physical properties (mass, refractive index, light absorbance…). Accordingly, the transducer part of the sensor transforms this physical property into the final readout [4].

In chemical sensing, the transducer provides sensitivity and MIPs provide selectivity [5]. Molecular imprinting involves the formation of cavities that completely match the template both in shape and functionality. Such imprinting is achieved when a cross-linker enwraps a pre-arranged complex, formed between the functional monomers and the template. After removal of the template from the polymers, the remaining cavity is specific for the template. The synthesis technique is simple and cheap; in addition, the polymers obtained exhibit high selectivity, excellent mechanical strength and durability to heat, acid and base conditions [5-9].

MIPs characterization is carried out by batch rebinding studies. Binding parameters can be estimated from the binding isotherms by the application of several mathematical models (the discrete Langmuir and the continuous Freundlich models are the most commonly applied) [10-13]. Kinetic studies

describe the rate of adsorbates uptake on MIPs, leading to the determination of the equilibrium time. The Lagergren first-order, pseudo-second-order kinetic models and Elovich equation are frequently applied to study the kinetics of the adsorption process [14]; whereas the intra-particle diffusion model is further tested to determine the diffusion mechanism of the adsorption systems [14-18].

Bisphenol A, [2,2-bis (4-hydroxyphenyl) propane], is an important intermediate in the industrial manufacture of several plastics (epoxy, phenolic, polysulfone and polyetherimide resins, polycarbonates, polyesters, polyacrylates and flame retardant materials) [19, 20]. Yet, many evidences have shown that BPA has toxic properties, inducing estrogenic endocrine disruption and promoting tumor progression. A recent study has concluded that even at an extremely low concentration (0.23 pg mL^{-1}) BPA can initiate the derangement of corpuscular functions, hence altering the estrogenic hormone secretion. For that reason, the detection of trace amounts of BPA is very important in maintaining an awareness of pollutants in our immediate environments [21].

Various analytical methods have been employed for the determination of BPA. Most of these methods are based on GC-MS and LC-MS. However, these techniques are expensive, require pretreatment and are unsuitable for "on-site" measurements. Thus, the development of portable sensors which would allow a quick and effective "on-site" analysis is requested [3].

245

In the literature there are several MIPs for the determination of BPA in water; however, their nature are not suitable to work attached, for example, to a QCM sensor [22-24]. In this sense, the literature citations are very limited [25]. In our research, a BPA imprinted polymer intended for future sensor applications has been developed and widely characterized. At first, the bi-Langmuir, Freundlich and Dubinin-Radushkevich isotherms have been used to determine the MIP binding properties. The selectivity of the obtained MIP was elucidated by performing adsorption experiments over other common competitive compounds. In addition, several kinetic models were applied to examine the controlling mechanism of the adsorption process. The Lagergren first-order and pseudo-second-order models were applied to study the kinetics of the adsorption process; whereas the intra-particle diffusion model was further tested to confirm the diffusion mechanism of the adsorption system. Finally, SEM was employed to capture the detailed morphology of BPA-MIP. At last, the regeneration of MIP was evaluated.

2. EXPERIMENTAL

2.1. REAGENTS

Bisphenol A (BPA), poly (vinyl acetate) (PVAc) (Mw=100 g/mol), 4-vinylpyridine (4-Vpy), triethylene glycol dimethyl ether (TRIGLYME) and acetaminophen (paracetamol) were purchased from Sigma Aldrich (Steinheim, Germany). Bisphenol F (BPF), caffeine, 2, 2-azobis (2-

methylpropionitrile) (AIBN) and ethylene glycol dimethacrylate (EGDMA) were obtained from Fluka (Buchs, Switzerland). Methanol (MeOH) was from Merck (Darmstadt, Germany). Acetic acid (HAc) was supplied from Scharlab (Barcelona, Spain). All water used in the experiments was purified using a Milli Q Ultrapure water-purification system (Millipore, Bedford, MA, USA).

2.2. INSTRUMENTATION

A method for the detection of BPA in the batch assays of the MIP was developed using ultrahigh performance liquid chromatography with PDA detector (UHPLC-PDA). UHPLC analyses were performed using an Acquity system from Waters (Milford, MA, USA) with a gradient pump and automatic injector. The chromatographic conditions and the linear solvent gradient are shown in Table 1. The signal acquired from the detector was recorded by a personal computer running Empower 2 software (Waters). The same method was employed to detect the compounds tested in selectivity batch assays.

Table 1. Chromatographic conditions and gradient elution of the developed method by UPLC-PDA.

Time	Flow	H$_2$O (%)	MeOH (%)	Curve
Initial	0.5	80	20	Initial
1	0.5	80	20	6
1.50	0.5	60	40	6
2.50	0.5	0	100	6
4	0.5	0	100	6
4.50	0.5	80	20	3
5	0.5	80	20	6
Column	Acquity UPLC^{TM} BEH C$_{18}$,(2.1 x 50 mm, 1.7 µm)			
Column oven temperature	30 ºC			
T sample	4 ºC			
Injection volume	10 µL			

2.3. SYNTHESIS OF BPA-MIP

Based on literature results, a low volatile solvent (with a low vapour pressure, P$_{vap}$) in combination with a non reactive linear polymer are used to create a matrix that helps the particles adhere and form a cohesive layer (film). Furthermore, the addition of a non-reactive linear polymer promotes porous morphology and thus enhances the MIPs binding capacity [26-28]. A mixture of TRIGLYME (P$_{vap}$ = 0.2 Torr at 25ºC [28]), as low volatile solvent, and PVAc (7.5%, wt% relative to pure solvent), as non reactive linear polymer, was used.

The template (T) (BPA) was mixed with the functional monomer (M) (4-Vpy), the cross-linker (C) (EGDMA) and the porogen at a ratio of 1:6:6 (T:M:C). AIBN was applied as initiator of the radical polymerization solution. A custom-made silicone device was used to contain the

prepolymerization solution and it was placed in a suitable airtight container to keep nitrogen atmosphere after purging with nitrogen gas for 5 min to completely evacuate the air, thus avoiding the polymerization inhibition. Finally, the polymerization was carried out at 60 ºC for 24 hours. Thin polymer disks were obtained. Non-imprinted control polymers (NIPs) were prepared by the above procedure excluding BPA.

2.4. EVALUATION OF THE BPA-MIP BY BATCH REBINDING METHOD

Several BPA-MIPs were synthesized and then washed with the elution solvent mixture (MeOH:HAc (4:1)) to remove the template from the cavities. Polymers were washed until BPA could no longer be detected at 270 nm in the elution. Twelve different solutions of BPA in pure water, spanning the concentration range 22.41-4482 µmol L^{-1}, were prepared. MIPs were sonicated during 15 min in 2 mL of each batch solution in a 5 mL vessel at room temperature. Then, the solutions were removed in order to determine the free template by UHPLC-PDA. The bound template concentration was calculated by difference from BPA total amount. Between rebinding tests, the polymers were washed twice with the elution solvent to ensure the extraction of bound BPA. For comparison, several NIPs were synthesized and subjected to the assays described above.

2.4.1. Characterization of BPA-MIP using adsorption models

Batch rebinding studies represent a key method to characterize and compare MIPs formulations. Therefore, heterogeneous distribution of binding sites and affinity of the polymer for a particular template can be evaluated by binding isotherm experiments using different binding models.

2.4.1.1.Langmuir and bi-Langmuir models

The discrete Langmuir and bi-Langmuir models are particularly easy to implement via Scatchard plots and generate the corresponding binding parameters: binding affinity (K) and number of binding sites (N). In the Scatchard analysis, the experimental binding isotherm is plotted in q/C versus q format (where q is the concentration of the analyte bound to a polymer in µmol g^{-1} and C is the concentration of free analyte remaining in the solution in µmol L^{-1}). In homogeneous systems that contain only one type of binding site, the Satchard plot falls on a straight line with a slope equal to the negative of the binding affinity (-K) and an x-intercept equal to the number of binding sites (N):

$$q/C = KN - Kq \qquad (1)$$

In contrast, the Scatchard plots for most MIPs are curved. This curvature has been cited as evidence for binding site heterogeneity. Heterogeneity can still be accommodated using the Scatchard analysis by modelling the curved isotherm as two separate straight lines (bi-Langmuir model). This limiting slopes method yields two separate sets of binding parameters (K_1,

N_1 and K_2, N_2) for two classes of sites. The steeper line measures the high-affinity sites and the gentle slope line measures the low-affinity sites [10].

To predict the favourability of the adsorption system, the Langmuir equation may also be expressed in terms of a dimensionless separation factor R_L defined as follows:

$$R_L = 1/(1 + KC_0) \qquad (2)$$

where C_0 is the initial BPA concentration (µmol L^{-1}) and K is the Langmuir adsorption equilibrium constant (L μmol^{-1}). The parameter $R_L > 1$, $R_L = 1$, $0 < R_L < 1$, $R_L = 0$, indicates the isotherm shape according to unfavourable, linear, favourable and irreversible, respectively [29, 30].

2.4.1.2. Freundlich model

The Langmuir and bi-Langmuir models are based on the assumption that MIPs are relatively homogeneous. The continuous Freundlich model of affinity distribution (FIAD model) can better accommodate the heterogeneous nature of MIPs and generate an affinity spectrum. This model assumes a power function relationship between q and C and it is more easily applied by plotting the experimental binding isotherm in log q versus log C format (Eq. 3). There are two fitting parameters a and m that both yield a measure of physical binding parameters. The second fitting parameter is known as the heterogeneity index. For homogeneous

materials, m would be equal to 1 and values approaching to zero increase the heterogeneous character of the polymer.

$$logq = mlogC + loga \qquad (3)$$

Recently, an analytically derived expression for the affinity distribution (AD) for a Freundlich isotherm (FI) has been developed [10]:

$$N(K) = 2.303am(1 - m^2)e^{-2.303mlogK} \qquad (4)$$

This AD expression allows the calculation of the AD within the limits (K_{min} and K_{max}) set by the concentration ranges of the experimental binding isotherm:

$$K_{max} = 1/C_{min} \quad and \quad K_{min} = 1/C_{max} \qquad (5)$$

Plotting Eq. (4) in log format (log N versus log K), the exponentially decaying distribution becomes a straight line, which greatly facilitates the visual comparison of the AD of different polymers. ADs with similar heterogeneity are easily identified as parallel lines because the slope is equal to m.

The binding parameters N_{K1-K2} and $\overline{K}_{K1-K2}$ (number of sites and weighted average affinity, respectively) can be measured for any set of the entire distribution for K_1 to K_2 values that are within the boundaries K_{min} and K_{max} as defined by Eq. (5). Nevertheless, to correctly compare the

binding parameters N_{K1-K2} and $\overline{K}_{K1-K2}$, they must have been calculated over the same range of binding sites (K_1 and K_2):

$$N_{K1-K2} = a(1 - m^2)(K_1^{-m} - K_2^{-m}) \qquad (6)$$

$$\overline{K}_{K1-K2} = \frac{m}{m-1} \frac{K_1^{1-m} - K_2^{1-m}}{K_1^{-m} - K_2^{-m}} \qquad (7)$$

2.4.1.2.1. Recognition selectivity of BPA-MIP by batch rebinding method

Batch rebinding assays were also carried out selectivity tests to compare the affinity of the polymer for different compounds. Bisphenol F was used as a structural related compound while paracetamol (phenolic compound) and caffeine (not phenolic compound) were selected between several pollutants usually found in natural waters as BPA. Their chemical structures are shown in Fig. 1.
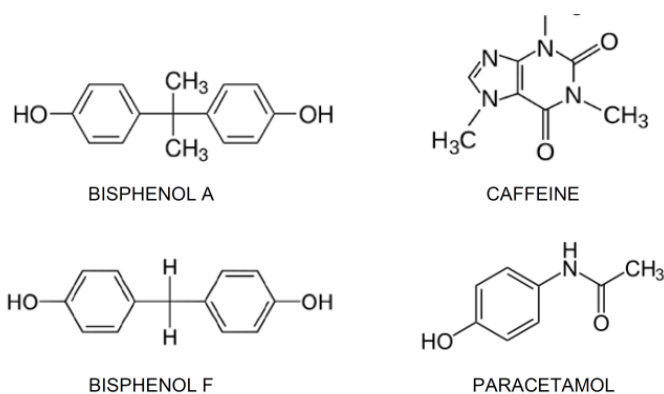
Fig. 1. Molecular structures of BPA, BPF, caffeine and paracetamol.

Twelve different solutions of BPF, caffeine and paracetamol in pure water, spanning the same concentration range as BPA batch studies, were prepared. MIPs were sonicated for 15 min in 2 mL of each batch solution in a 5 mL vessel at room temperature. Then, the solutions were removed in order to determine the free compound by UHPLC-PDA. The amount of analyte bound to the polymer was calculated from the initial and final concentrations in the supernatant. Between selectivity tests, the polymers were washed twice with the elution solvent to ensure the extraction of the binding compound.

The representation of Freundlich isotherms in log-format for BPA, BPF, caffeine and paracetamol, allows the study of the MIP selectivity upon comparison the binding capabilities: a higher position in the graph means a higher binding capacity, (N_{K1-K2}) [13].

2.4.1.3.Dubinin-Radushkevich model

Likewise, the Dubinin-Radushkevich isotherm model [17, 29-30] helps to study the interaction between adsorbate and sorbent, is generally used to distinguish between physical and chemical adsorption, it is described by Eq. (8):

$$lnq = lnq_m - K_{DR}\varepsilon^2 \qquad (8)$$

where q_m is the maximum adsorption capacity of MIP in µmol g^{-1}, K$_{DR}$ (kJ^2 mol^{-2}) is the Dubinin-Radushkevich constant and ε is the Polanyi potential, given in Eq. (9):

$$\varepsilon = RTln(1 + 1/C) \qquad (9)$$

K$_{DR}$ is related with the free energy (E, kJ mol^{-1}) of adsorption per molecule of adsorbate when it is transferred to the surface of the solid from infinity (in the solution). The adsorption behaviour could predict physical adsorption in the range of 1-8 kJ mol^{-1} and chemical adsorption at over 8 kJ mol^{-1} [31]. It can be calculated by Eq. (10):

$$E = (2K_{DR})^{-1/2} \qquad (10)$$

2.5. MEASUREMENT OF KINETIC ADSORPTION CURVE

The procedure of the kinetic adsorption tests was similar to the aforementioned batch studies except that two incubation procedures were used (US bath and contact incubation) and different incubation times were preset. The assays were performed with a 761.97 µmol L^{-1} BPA aqueous solution. Subsequetly, the time to reach the adsorption equilibrium could be derived from the two adsorption profiles.

Two kinetic models have been applied to the experimental data: the Lagergren pseudo-first-order model and the pseudo-second-order model. The pseudo-first-order rate of Lagergren is generally described by the following equation:

$$\partial q_t / \partial_t = k_1 (q_e - q_t) \qquad (11)$$

where k_1 is the pseudo-first-order rate constant. After integration, by applying the conditions, $q_t=0$ at $t=0$ and $q_t=q_t$ at $t=t$, Eq. (11) becomes

$$\log(q_e - q_t) = log q_e - \frac{k_1}{2.303} t \qquad (12)$$

Where q_e is the amount of BPA adsorbed at equilibrium in mg g^{-1}. The k_1 value was calculated from the plots of log (q_e-q_t) versus t for different concentrations of BPA [14].

The pseudo-second-order kinetic model is expressed as follows:

$$t/q = 1/k_2 q_e + t/q_e \qquad (13)$$

Where k_2 is the second-order rate constant (g mg^{-1} min^{-1}). In view of the linear relationship between t/q versus t, the values of k_2 and q_e were calculated from the intercept and slope of the corresponding plot [14].

Recently, Wu et al. (2005) pointed out that the pseudo-second-order model was suitable for the adsorption of low molecular weight adsorbates on small adsorbent particles. Based on this model, the initial adsorption rate and the half adsorption time were defined according to the following equations [32, 16]:

$$u = k_2 q_e^2 \qquad (14)$$

$$t_{1/2} = 1/k_2 q_e \qquad (15)$$

As the second order rate index, k_2q_e, is the inverse of the half-life of the adsorption process, this index was suitable to describe the adsorption kinetics.

2.6. STUDY OF THE ADSORPTION MECHANISM

As the above kinetic models were not able to identify the diffusion mechanism, the intra-particle diffusion model based on the theory proposed by Weber and Morris [15] was tested. It is an empirically functional relationship, common to most adsorption processes, where uptake varies almost proportionally with $t^{0,5}$ rather than with the contact time t:

$$q_t = k_i t^{0.5} + C_i \qquad (16)$$

Where k_i (mg g^{-1} min^{-1}) is the rate parameter of stage i, and it is obtained from the slope of the straight line of q_t versus $t^{0.5}$. C_i, the intercept of stage i, gives an idea of the thickness of the boundary layer, accordingly, the larger the intercept, the greater the boundary layer effect [17].

If the intra-particle diffusion occurs, then q_t versus $t^{0.5}$ will be linear. Furthermore, if the plot passes trough the origin, then the rate-limiting process is only due to the intra-particle diffusion. Otherwise, some other mechanism along with intra-particle diffusion is involved. If data exhibit multi-linear plots, then two or more steps influence the sorption process

[14, 16-17]. In order to determine the lowest step involved in the adsorption process, the Boyd model can be applied (Eq. 17):

$$B_t = -0.4977 - \ln{(1 - F)} \qquad (17)$$

F which represents the fraction of solute adsorbed at any time, t (min), is calculated using Eq. (18).

$$F = q_t / q_e \qquad (18)$$

The calculated B_t values were plotted against time t. If the plot of B_t versus t is a straight line passing through the origin, the rate limiting step is the intra-particle diffusion; otherwise, the adsorption process is mainly governed by the film diffusion [17, 18].

2.7. MORPHOLOGY CHARACTERIZATION BY SEM

The surface morphology of the film was characterized by scanning electron microscopy (SEM) JEOL JSM-6400. This microscopy has an accelerating voltage from 0.2 to 30 kV and provides a theoretical resolution of 3.5 nm to 8 mm working distance with a magnification range of 20X to 300000X.

The images were taken from the BPA-free-MIP; accordingly, these samples are polymers with cavities formed during the imprinting. All samples were sputter-coated with gold before SEM analysis to make them conductive. For comparison, NIPs samples were prepared in the same way.

2.8. REUSABILITY OF THE BPA-MIP

A sorption-desorption cycle was repeated 12 times by using the same imprinted material in order to show the reusability of the MIP. A suitable concentration of BPA-water solution was selected within the batch range.

From the data obtained, a control chart was generated to determine their probability distribution. The graph consists in a centreline (average or mean value) and two control limits above (Upper control limit, UCL = +3σ) and below (Low control limit, LCL = -3σ). If the process operates within this variability it is said to be 'in control'; on the contrary, if a point falls above the UCL or below the LCL this is an evidence that the process can be 'out of control' [33].

3. RESULTS AND DISCUSSION

3.1. ANALYSIS OF BINDING PROPERTIES BY LANGMUIR AND bi-LANGMUIR MODELS

Fig.2.a shows the Scatchard plot of the batch rebinding assay in the range 22.41-4482 µmol L^{-1} of BPA-water solutions. The curvature observed for BPA-MIP proves the heterogeneity of the binding sites, typical of non-covalent MIPs, due to the formation of prepolymerization complexes with different template: monomer stoichiometry, as well as the structural diversity and flexibility in the binding cavity and the conformational diversity of the prepolymerization complex [33, 34]. The obtained Scatchard regression equation of the high-affinity sites within the range 22.41-1210 µmol L^{-1} was:

$$q/C = -11.90q + 320.2$$

The binding affinity $K_{BPA-MIP1}$, 11.90 mL µmol^{-1} (1.19 x 10^4 M^{-1}), was about 1000 times as much as the $K_{BPA-MIP2}$ value of the low affinity sites (1.08 x 10^1 M^{-1}), suggesting that the affinity of these binding sites is very resilient. The maximum number of ligand-exchange interaction sites, $N_{BPA-MIP1}$, 26.9 µmol g^{-1}, was higher than the value reported by Ikegami et al. (2004) for a BPA-imprinted polymer synthesized by bulk polymerization and covalent imprinting techniques, 10.7 µmol g^{-1} [22], as well as the result achieved by Zhu et al. (2010) for BPA-imprinted silica nanoparticles synthesized by a sol-gel process, 16.4 µmol g^{-1} [23].
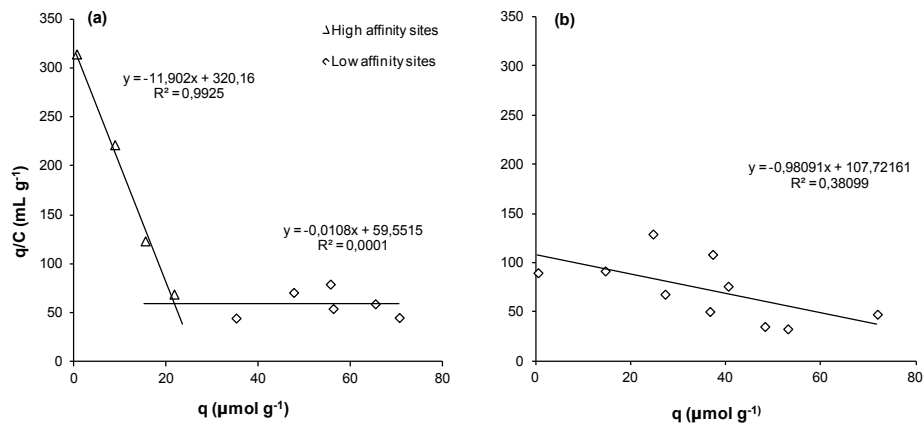
Fig. 2. Scatchard plot for BPA in: (a) BPA-MIP and (b) NIP within the range of 22.41-4482 µmol L^{-1}.

Conversely, the Scatchard analysis for BPA-NIP (Fig.2.b) had not the same curvature of the BPA-MIP. The data fitted a straight line, typical of a homogeneous system containing a single type of binding sites. The value

of the NIP binding affinity ($K_{BPA-NIP}$ = 9.81 x 10^2 M^{-1}), roughly 12 times lower than $K_{BPA-MIP}$, indicated a poor affinity between the template and the NIP binding sites.

From another point of view, the calculated R_L values versus the initial concentration of BPA for high affinity sites ($N_{BPA-MIP1}$) are illustrated in Fig. 3.a. The R_L values were between 0 and 1, supporting that the adsorption of BPA on the high affinity sites of BPA-MIP was favourable at the conditions studied. Fig. 3.b plots the low affinity sites ($N_{BPA-MIP2}$). All the R_L values were close to 1, suggesting a linear adsorption of BPA on low affinity sites of BPA-MIP.

3.2. ANALYSIS OF BINDING PROPERTIES BY FIAD METHOD

3.2.1. Examination of the Imprinting Effect

The experimental binding isotherm was further analyzed using the FIAD method which first objective was to examine differences between imprinted and non-imprinted polymer.

The corresponding log format ADs of both polymers showed an exponential decay. The highest AD, related to the polymer with the highest capacity, should be the AD of the MIP. Nonetheless in this study, both ADs were very similar. This qualitative assessment was confirmed by the calculation of the respective capacities: for a similar subset of sites (K_1 = K_{min} = 6.40 x 10^2 M^{-1} to K_2 = K_{max} = 6.25 x 10^5 M^{-1}), N_{K1-K2} values were 45.2 μmol g^{-1} and

37.4 µmol g^{-1} for the MIP and NIP, respectively. A possible explanation for this result is the solvent employed for the equilibrium binding experiments. As has been discussed in the literature, in aqueous media selective hydrogen-bonding interactions (BPA-pyridyl-groups) decrease in favour of hydrophobic interactions (BPA-polymer backbone) [24]. Notwithstanding, the obtained adsorption capacity from Freundlich equation, 45.2 µmol g^{-1}, was superior to those found for most BPA-MIPs reported in the literature [24] and was even greater than the adsorption capacity of BPA onto the great majority of mineral sorbents [36, 37] or several kinds of activated carbons [38]. As a final point, the MIP and NIP weighted average affinities were 1.07×10^4 M^{-1} and 4.96×10^2 M^{-1}, respectively, for the same subset of sites (the MIP being about 100 times more specific than the NIP).
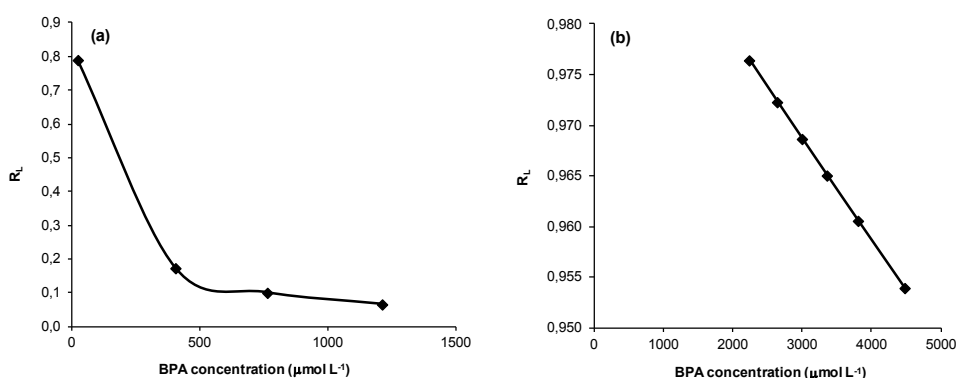
Fig. 3. Effect of BPA initial concentration on the separation factor R$_L$ at room temperature: (a) for batch concentrations of high affinity sites, (b) for batch concentrations of low affinity sites.

Therefore, the mean adsorption energy between the sorbate and the adsorbate calculated from Dubinin-Radushkevich model for MIP $\left(\overline{E}_{MIP} \right)$ was

158.1 kJ mol^{-1} (about 4 times higher than NIP adsorption energy (40.82 kJ mol^{-1}). If the MIP high affinity sites are only considered, these MIP interactions are almost 6 times higher (E_{MIP} = 223.6 kJ mol^{-1}) than NIP forces. The values of MIP hydrogen bond forces shows intensity closed to the chemical bonds.

3.2.2. Recognition selectivity of BPA-MIP by FIAD method

To measure the selective recognition of BPA, the binding of competitive compounds were performed. Fig. 4 exhibits the Freundlich isotherms represented in log format for visual comparison of the binding capabilities of BPA, BPF, caffeine and paracetamol. The fitting coefficients of BPA-MIP for the four compounds are summarized in Table 2 and Table 3. The former accounts for the range K_{min}-K_{max} while the latter represents the range of high affinity sites (K_1 =3.19 x 10^3 M^{-1} to K_2 = 6.25 x 10^5 M^{-1}, from bi-Langmuir model).

Table 2. Freundlich fitting parameters calculated for the range K_{min}–K_{max}.

BPA-MIP	Heterogeneity parameter(m)	K_{max} (M^{-1})	K_{min} (M^{-1})	N_{K1-K2} (μmol g^{-1})	$\overline{K}_{K1-K2}$ (M^{-1})
BPA	0.6893	6.25E05	6.41E02	45.2	1.07E04
BPF	0.6608	1.09E06	2.45E03	69.8	3.35E04
CAFFEINE	0.5271	6.72E04	2.65E02	7.66	3.97E03
PARACETAMOL	0.8066	5.76E04	4.95E02	7.21	3.19

As is evident from Fig. 4, the BPA affinity distribution (BPA-AD) and BPF affinity distribution (BPF-AD) are higher than the affinity distributions of the rest of the compounds essayed. Being both phenolic-related

compounds, their affinity can be attributed to the formation of hydrogen bonds with the pyridyl group of the 4-Vpy (functional monomer in the polymeric synthesis), apart from hydrophobic interactions with the polymer backbone [24]. Two hydrogen bonds can be formed between the BPA and BPF hydroxyl groups and two pyridyl groups in the 4-Vpy-co-EGDMA polymer, leading to binding sites of high specificity.

Table 3. Freundlich fitting parameters calculated for the range K_1-K_2.

BPA-MIP	Heterogeneity parameter(m)	K_{max} (M^{-1})	K_{min} (M^{-1})	N_{K1-K2} ($\mu mol\ g^{-1}$)	$\overline{K}_{K1-K2}$ (M^{-1})
BPA	0.7359	6.25E05	3.19E03	5.49	2.75E04
BPF	0.7810	1.09E06	7.19E03	12.7	5.23E04
CAFFEINE	0.8362	6.72E04	1.99E03	2.03	8.37E03
PARACETAMOL	0.9215	5.76E04	1.20E03	1.99	5.14E03

A noteworthy point is that N_{K1-K2} for BPF is greater than N_{K1-K2} for BPA in the two ranges considered and the same occurs with the weighted average affinity. The two methyl groups of BPA have been replaced by two hydrogen groups in BPF. Therefore, the shape and size of the BPF molecule make it suitable to fit the BPA-imprinted cavities. (Fig.1). Comparing the results of the heterogeneity index m, the imprinted polymer shows the same behaviour for the two phenolic compounds. It is also worth mentioning that the m values of BPA and BPF for the range K_1-K_2 are higher than for the range K_{min}-K_{max}, because the former represent high affinity sites (Table 3).
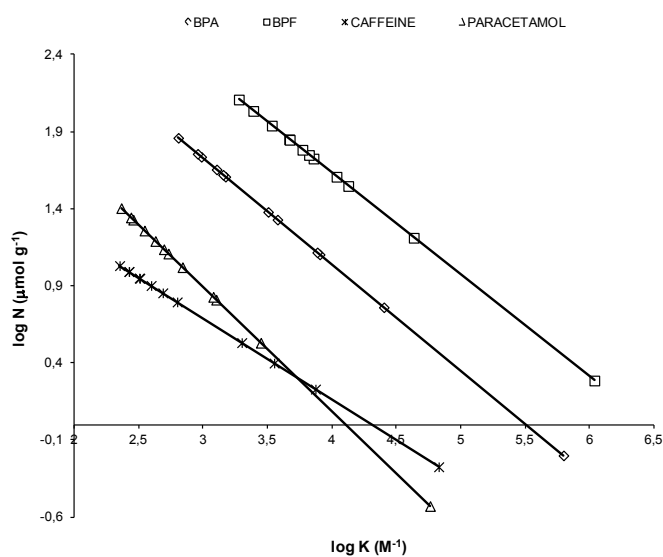
Fig. 4. Freundlich adsorption isotherm of BPA, BPF, caffeine and paracetamol on BPA-MIP.

On the other hand, as it is evident from Fig. 4, caffeine and paracetamol show lower affinities than bisphenol compounds. On the basis of its chemical structure (Fig. 1), paracetamol can form only one hydrogen bond with 4-Vpy, both with pyridines inside the imprinted cavities (specific binding) and pyridines outside the cavities and uniformly distributed in the polymer (unspecific binding). Moreover, the formation of another type of unspecific hydrogen bond with the carbonyl group of EGDMA (the N-H of the amide group acting as an hydrogen donor) is also possible. Regarding the caffeine molecule, hydrogen bonding is not even possible with a polymer lacking H-bonding donors. Besides, both analytes can generate hydrophobic interactions with the polymer backbone. Accordingly, the number of sites (N_{K1-K2}) and the weighted average affinity $(\overline{K}_{K1-K2})$

values for caffeine and paracetamol are one-fold lower than the corresponding parameters obtained for BPF and BPA.

Moreover, the heterogeneity parameter (m) for paracetamol is close to 1 in the two ranges considered, suggesting that the polymer is homogeneous with respect to this analyte. Consequently, despite the existence of different types of binding sites, all of them show the same affinity towards paracetamol (unspecific interactions). Similarly, the polymer behaves homogeneously in contact with an aqueous solution of caffeine (m = 0.8362) in the range K_1-K_2. In view of the possible physical interactions between caffeine and the polymer functional groups, the heterogeneous behaviour found when the whole set of values were considered (m = 0.5271) was more difficult to explain.

3.3. INTERPRETATION OF KINETIC RESULTS

In order to examine the adsorption mechanism such as mass transfer and involved reaction, kinetic assays have been conducted. First of all, we confirmed that the adsorption equilibrium was reached in 15 min and 48h for US bath incubation (Fig.5a) and contact incubation (Fig.5b), respectively. More to the point, the kinetic data obtained were analyzed using the pseudo-first-order and pseudo-second-order equations described in the experimental section. The adsorption rate constants and linear regression values were summarized in Table 4.
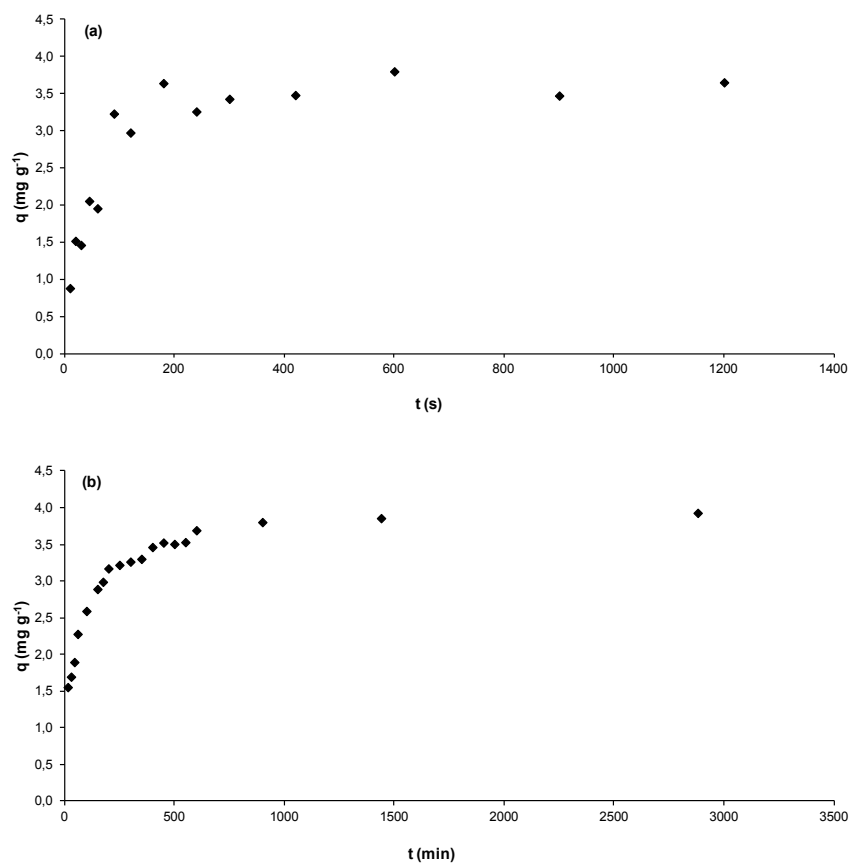
Fig. 5. Kinetic adsorption curve of BPA on BPA-MIP at room temperature and initial concentration of BPA 761.97 µmol L^{-1} for US bath incubation (a) and for contact incubation (b).

The applicability of these models to describe the adsorption process was further validated by the relative error, RE (%), which is defined as:

$$RE(\%) = 100\left(\left|q_{e,exp} - q_{e,cal}\right|\right) \qquad (19)$$

where $q_{e,exp}$ and $q_{e,cal}$ (mg g^{-1}) are the experimental and calculated adsorption uptake at equilibrium and at any time, t (min), respectively

267

[39]. The RE (%) obtained for US bath incubation and pseudo-first-order kinetic model, 36.4%, was high compared to the RE (%) value of 1.80% calculated using the pseudo-second-order kinetic model. Likewise, the RE (%) values for contact incubation were 58.3% and 1.70%, respectively.

Table 4. Pseudo-first-order, pseudo-second order constants and correlation coefficients for the adsorption of BPA on BPA-MIP at room temperature.

Incubation	Experimental	Pseudo first-order model		Calculated	Pseudo second-order model				Calculated
	q_e (mg g^{-1})	k_1 (min^{-1})	r^2	q_e (mg g^{-1})	k_2 (g mg^{-1} min^{-1})	r^2	U (mg g^{-1} min^{-1})	$t^{1/2}$ (h)	q_e (mg g^{-1})^3
US bath	3.802	0.3355	0.9275	2.417	0.5136	0.9971	7.427	0.5120	3.734
Contact	3.930	2.568E-03	0.9203	1.636	4.711E-03	0.9996	0.07279	54.00	3.998

The correlation coefficients for the linear plots of t/q_t against time from the pseudo-second order rate law are 0.9971 and 0.9996 for US and contact incubation (Table 4). This suggests that this sorption system is not a first order reaction and that the pseudo-second order model, based on the assumption that the rate-limiting step may be chemical sorption or chemisorption [40, 30], provides the best correlation of the data. BPA molecules are strongly held onto the binding sites of MIP by two hydrogen bonds between the sorbent and two pyridines of the adsorbate. Owing to the strength and specificity of the hydrogen bonds involved, the adsorption process is best described as chemisorption than as physisorption, supporting the conclusion extracted from the application of the Dubinin-Radushkevich isotherm model.

3.4. STUDY OF THE ADSORPTION MECHANISM

Fig.6. displays the plots of intra-particle diffusion model corresponding to the adsorption of BPA on BPA-MIP at an initial concentration of 762.0 µmol L^{-1} by means of two ways of incubation at room temperature, US bath and contact incubation. The former is divided into two stages (Fig. 6a). The initial sharp rise portion represents the intra-particle diffusion process while the plateau stage is attributed to the final equilibrium process. The US bath increases the adsorption kinetic of BPA on BPA-MIP because it reduces the external mass transfer resistance. The fact that the plot passes through the origin (Fig.6a) confirms the absence of an external layer diffusion process [16]. The intra-particle diffusion was the rate limiting mechanism in the adsorption process [17].
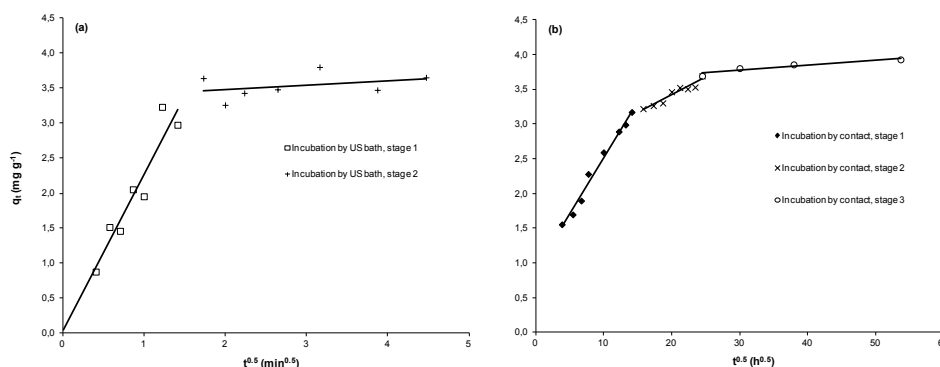
Fig.6. Plot of intra-particle diffusion model for adsorption of BPA on BPA-MIP at room temperature: (a) US incubation and (b) contact incubation.

Regarding the contact incubation tests, the plot can be divided into three stages: a first sharp rise step is followed by a less-sharp rise stage and a final plateau. The initial step represents the mass transfer of the BPA

molecules across the external boundary layer (this stage was completed within the first 200 min) while the second stage corresponds to the intra-particle diffusion process. As a final point, the plateau phase, spanning from 600 to 2880 min, is ascribed to the last equilibrium process. The depicted stages revealed that the adsorption rate was initially fast but slowed down as time increased. Furthermore, the fact that the lines of the second and third stages did not pass through the origin, suggested that the intra-particle diffusion may not be the only rate limiting mechanism in the adsorption process.

More to the point, the k_i, C_i values and the correlation coefficients obtained for the described plots, displayed in Table 5, supported the assumptions considered in the preceding paragraph. At any rate, at this point of the discussion the rate-limiting step remained unclear. In order to predict the slowest step involved in the adsorption process, the kinetic data were further analyzed using the Boyd model. The plot of B_t against t (min) was a straight line passing through the origin, proving that the rate-controlling step is the intra-particle diffusion.

Table 5. Intra-particle diffusion model constants and correlation coefficients for adsorption of BPA on BPA-MIP at room temperature.

Incubation	k_1 (mg g^{-1} min$^{0.5}$)	k_2 (mg g^{-1} min$^{0.5}$)	k_3 (mg g^{-1} min$^{0.5}$)	C_1	C_2	C_3	$(r_1)^2$	$(r_2)^2$	$(r_3)^2$
US bath	2.239	0.06514	–	0.02875	3.349	–	0.8988	0.1381	–
Contact	0.1621	0.05113	0.007385	0.8980	2.395	3.552	0.9847	0.9218	0.8821

3.5. MORPHOLOGY CHARACTERIZATION BY SEM

270

Concerning the polymers morphology, the scanning electron micrographs reveal spherical shapes and a narrow average size distribution of the resulting particles. Moreover, the particles appear to be aggregates of several microspheres (Fig 7a and 7b). The BPA-MIP particles have diameters ranging from 3 to 5 μm (Fig 7a), whereas the NIP particles (Fig. 7b) have a slightly larger size≈(5.5 μm). Anyhow, up to this date, the effect of the template feeding on the final particle size has not yet been sufficiently studied [41].

3.6. REUSABILITY OF THE BPA-MIP

The regeneration of sorbent, a key factor in improving values in MIPs sensor applications, was investigated in twelve sequential times of adsorption-desorption. To account for the natural variability of the process, a control chart was constructed under the assumption that the data came from a normal distribution, with the mean equal to 0.3218 mg and a standard deviation (σ) of 1.39×10^{-2} (Fig 8). In view of these results, the MIP was shown to be promising for regeneration without significant loss in adsorption capacity.
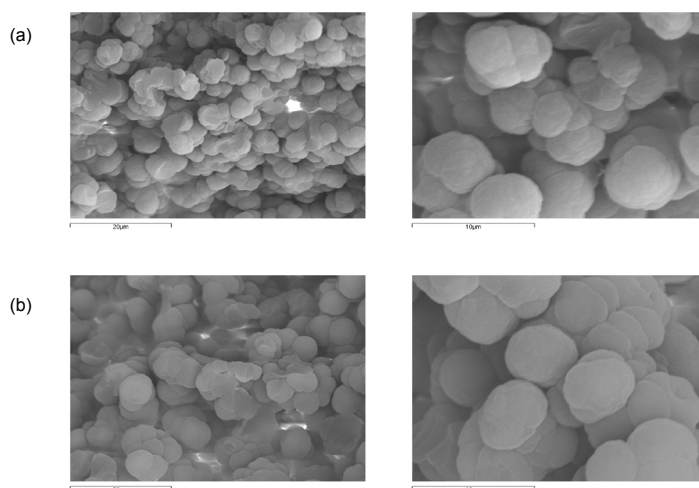
Fig.7. SEM images of the MIP (a) and the NIP (b) particle size with 2000X and 5000X magnification.
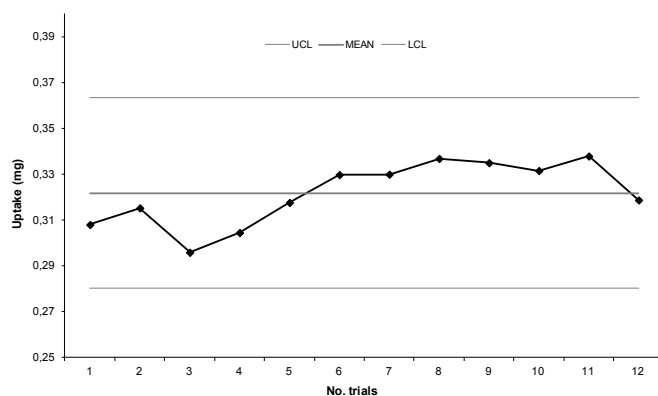
Fig. 8. Individual control chart for BPA adsorption uptake on BPA-MIP in contact with a 762.0 µmol L^{-1} BPA aqueous solution in a US bath over 15 min at room temperature.

4. CONCLUSIONS

In the present investigation a non covalent BPA-imprinted polymer using 4-vinylpyiridine as the functional monomer, EGDMA as crosslinker and a low volatile solvent, tryglyme, in combination with a non reactive linear

272

polymer, PVAc, as porogen, intended for future sensor applications, was successfully synthesized with a simple polymerization procedure. The results of characterization, binding properties, kinetics, adsorption mechanisms and regeneration were summarized below:

(1) Initially, equilibrium data were described by Langmuir, bi-Langmuir models. The first two models proved the heterogeneity of the binding sites, typical of non-covalent MIPs, most likely due to the formation of a prepolymer complex with 1:2 BPA:4-Vpy stoichiometry via intermolecular hydrogen bonding. In contrast with NIP, the binding affinity of the MIP high affinity sites was about 1000 times higher than the related values of the low affinity sites; this result was supported by the separation factor (R_L).

(2) On applying the Freundlich model to the same equilibrium data, the similar specificity found between MIP and NIP is attributable to the use of aqueous solutions of BPA in the equilibrium binding experiments. On the contrary, the selectivity studies suggested that the selectivity recognition of BPA and BPA-analogues for MIP was greater than that of other common compounds in environmental waters.

(3) Regarding kinetic assays, the US bath increases the adsorption kinetics of BPA on BPA-MIP with respect to contact incubation, because it reduces the external mass transfer resistance. The adsorption kinetics followed the pseudo-second-order kinetic model so that the specific adsorption in the imprinted cavities by two strong hydrogen bonds could be described as a chemisorption process.

(4) The diffusion mechanism was determined by the intra-particle diffusion and Boyd models, both of them revealing that the adsorption was mainly governed by intra-particle diffusion in which the insertion and binding to the imprinted cavities could be the rate limiting step of the global adsorption process.

(5) As a final point, MIP was applied in twelve regeneration cycles without significant loss in adsorption.

References

[1] B.S. Ebarvia, C.A. Binag, Anal. Bioanal. Chem. 378 (2004) 1331

[2] K. Haupt, Anal. Chem. 75 (17) (2003) 376A

[3] M. Romero-Guerra, I. Chianella, E.V. Piletska, K. Karim, A.P.F. Turner, S.A. Piletsky, Analyst 134 (2009) 1565

[4] M. Jakusch, M. Janotta, B. Mizaikoff, Anal. Chem. 71 (1999) 4786

[5] M. Ávila, M. Zougagh, A. Escarpa, Á. Ríos, Trends Anal. Chem. 27 (2008) No. 1

[6] M.S. Dopico-García, M.C. Cela-Pérez, J.M. López-Vilariño, M.V. Gónzalez-Rodríguez, L.F. Barral-Losada. J. Appl. Polym. Sci. 119 (2011) 2866

[7] E. Turiel, A. Martín-Esteban, Anal. Chim. Acta 668 (2010) 87

[8] A. Beltran, F. Borrull, P.A.G. Cormack, R.M. Marce, Trends Anal. Chem. 29 (2010) No. 11

[9] K. Karim, F. Breton, R. Rouillon, E.V. Piletska, A. Guerreiro, I. Chianella, A.S. Piletsky, Adv. Drug Deliv. Rev. 57 (2005) 1795

[10] R.J. Umpleby II, S.C. Baxter, A.M. Rampey, G.T. Rushton, Y. Chen, K.D. Shimizu, J. Chromatogr. B 804 (2004) 141

[11] R.J. Umpleby II, S.C. Baxter, M. Bode, J.K. Berch Jr, R.N. Shah, K.D. Shimizu, Anal. Chim. Acta 435 (2001) 35

[12] G. Pan, B. Zu, X. Guo, Y. Zhang, C. Li, H. Zhang, Polymer 50 (2009) 2819

[13] A.M. Rampey, R.J. Umpleby, G.T. Rushton, J.C. Iseman, R.N. Shah, K.D. Shimizu, Anal. Chem. 76 (2004) 1123

[14] B. Subramanyam, D. Ashutosh, Desalination 249 (2009) 914

[15] W.J. Weber, J.C. Morris, Journal of the Sanitary Engineering Division ASCE 89 (1963) 31

[16] Q.S. Liu, T. Zheng, P. Wang, J.P. Jiang, N. Li, Chem. Eng. J. 157(2010) 348

[17] I.A.W. Tan, A.L. Ahmad, B.H. Hameed, J. Hazard. Mater. 164 (2009) 473

[18] W. Liu, J. Zhang, C. Zhang, Y. Wang, Y. Li, Chem. Eng. J. 162 (2010) 677

[19] J. Maia, J.M. Cruz, R. Sendón, J. Bustos, J.J. Sanchez, P. Paseiro, Food Res. Int. 42 (2009) 1410

[20] F. Navarro-Villoslada, B. San Vicente, M.C. Moreno-Bondi, Analytica Chimica Acta, 504 (2004)149

[21] W. Zhao, N. Sheng, R. Zhu, F. Wei, Z. Cai, M. Zhai, S. Du, Q. Hu, J. Hazard. Mater. 179 (2010) 223

[22] T. Igekami, T. Mukawa, H. Nariai, T. Takeuchi, Anal. Chim. Acta 504 (2004) 131

[23] R. Zhu, W. Zhao, M. Zhai, F. Wei, Z. Cai, N. Sheng, Q. Hu, Anal. Chim. Acta 658 (2010) 209

[24] B. San Vicente, F. Navarro-Villoslada, M.C. Moreno-Bondi, Anal. Bioanal. Chem. 380 (2004) 115

[25] N. Tsuru, M. Kikuchi, H. Kawaguchi, S.Shiratori, Thin Solid Films 499 (2006) 380

[26] R.H. Schmidt, A. S. Belmont, K. Haupt, Anal. Chim. Acta 542 (2005) 118

[27] R.H. Schmidt, K. Mosbach, K. Haupt, Adv. Mater. 2004, 16, No. 8

[28] R.H. Schmidt, K. Haupt, Chem. Mater. 2005; 17: 1007

[29] T.Y. Guo, Y.Q. Xia, G.J. Hao, M.D. Song, B.H. Zhang, Biomaterials 25 (2004) 5905

[30] J. Pan, X. Zou, X. Wang, W. Guan, Y. Yan, J. Han, Chem. Eng. J. 162 (2010) 910

[31] C. Y. Chen, C. H. Wang, A. H. Chen, Talanta.84 (2011) 1038

[32] Z.J. Wu, H. Joo, K. Lee, Chem. Eng. J. 112 (2005) 227

[33] M.C. Ortiz, L.A. Sarabia, M.S. Sánchez, Anal. Chim. Acta 674 (2010) 123

[34] A. Gómez-Caballero, N. Unceta, M.A. Goicolea, R.J. Barrio, Sensor Actuat. B 130 (2008) 713

[35] Y. Tunc, N. Hasirci, A. Yesilada, K. Ulubayram, Polymer, 47 (2006) 6931

[36] W.T. Tsai, C.W. Lai, T.Y. Su, J. Hazard. Mater. 75 (2006) 134

[37] C. Namasivayam, S. Sumithra, Clean Technol. Environ. Policy 9 (2007) 215

[38] T. Asada, K. Oikawa, K. Kawata, S. Ishihara, T. Iyobe, A. Yamada, J. Health Sci. 50 (2004) 588

[39] L. Jian-Liang, W. Ming-Yan, Y. Xiao-Li, D. Zhan-Bo, Y. Jian-Hui, B. Devajit, S. Qing-Lei, L. Yue-Rong, J. Food Eng. 2010, 97: 555

[40] Y.S. Ho, G. McKay, Process Biochem. 34 (1999) 451

[41] K. Yoshimatsu, K. Reimhult, A. Krozer, K. Mosbach, K. Sode, L. Ye, Anal. Chim. Acta 584 (2007) 11

IMPACT OF FUNCTIONAL CROSS-LINKER ON RECOGNITION PROPERTIES OF A BISPHENOL-A IMPRINTED POLYMER FILM FOR COATING A QUARTZ CRYSTAL MICROBALANCE

M.C. Cela-Pérez[1], J.M.López-Vilariño[1],
M.V. González-Rodríguez[1]

[1] Grupo de Polímeros, Centro de Investigacións Tecnolóxicas, Universidade da Coruña, Campus de Esteiro s/n, Ferrol 15403, Spain, email: iquimica@udc.es

ABSTRACT

Robust systems could be generated based on Quartz Crystal Microbalance (QCM) combined with Molecularly Imprinted Polymers (MIPs) for on-site, in-time chemical sensing. A review of the literature demonstrates that, despite the large amount of available data to date on MIPs formulation, the main applications continue to be in the separation field, whereas the development of sensors and QCM sensors, in particular, is significantly slower. Bisphenol-A (BPA) imprinted polymers for future sensor applications were synthesized by non covalent precipitation polymerization. In order to optimize the binding properties, three different cross-linkers were used in the formulations: ethylene glycol dimethacrylate (EDMA), trimethylolpropane trimethacrylate and (TRIM) and divinylbenzene (DVB). Batch rebinding tests in aqueous media were carried out to evaluate the binding parameters fitting the adsorption isotherms by Langmuir, bi-Langmuir, Freundlich and Dubinin-Radushkevich models. Significant differences in the heterogeneity and capacity of the polymers were observed. TRIM crosslinked BPA imprinted polymer showed the best results.

1. INTRODUCTION

MIPs are used as recognition element in sensors [1-3]. Therefore, the transducer provides sensitivity and MIPs provide selectivity [4]. Molecular imprinting involves the formation of cavities that completely match the template both in shape and functionality. Such imprinting is achieved when a cross-linker enwraps a pre-arranged complex, formed between the functional monomers and the template. After removal of the template from the polymers, the remaining cavity is specific for the template. The synthesis technique is simple and cheap; in addition, the polymers obtained exhibit high selectivity, excellent mechanical strength and durability to heat, acid and base conditions [4-8].

The key to obtain good binding MIPs is the optimization of synthetic parameters [5]. For instance, the cross-linkers, which are involved in formation of a rigid polymer matrix, should be simultaneously flexible enough to make possible the mass transfer inside the pores [8]. Furthermore, the crosslinker is selected with the requirements that it should exhibit minimal interaction with the template in order to minimize non-specific binding [9]. However, high cross-linker ratios are generally used (80% in excess) [10].

On the other hand, BPA is an important intermediate in the industrial manufacture of several plastics. BPA has toxic properties, inducing estrogenic endocrine disruption and promoting tumor progression even at

an extremely low concentration. Consequently, the detection of trace amounts of BPA is very important in maintaining an awareness of pollutants in our immediate environments [11]. Most of analytical methods employed for the determination of BPA are based on GC-MS and LC-MS. However, these techniques are expensive, require pretreatment and are unsuitable for on-site measurements. Thus, the development of portable sensors which would allow a quick and effective on-site analysis is requested [3].

In this study, non-covalent approach was employed to prepare several BPA-MIPs for coating a QCM sensor. This target molecule was used as template. The cross-linkers EDMA, TRIM and DVB with different lengths and flexibilities were introduced to investigate the influence of the polymer chain mobility on the site integrity. Therefore, the above MIPs formulated by using three different crosslinker monomers were compared. Batch analysis was carried out and equilibrium data were fitted using the Langmuir, bi-Langmuir, Freundlich and Dubinin-Radushkevich isotherm models.

2. EXPERIMENTAL PROCEDURE

2.1. INSTRUMENTATION

A method to determine BPA in subsequent characterization experiments was developed using Ultra performance liquid chromatography with PDA detector (UPLC-PDA). UPLC analyses were performed using an Acquity system from Waters (Milford, MA, USA) with a gradient pump and automatic injector. The injection loop volume was 10µL and the mobile

phase for analysis was methanol:water with a volume ratio of 80:20. The flow rate of the mobile phase was 0.5 mL min^{-1}. The oven temperature was set at 30 ºC and 270 nm was selected as wavelength. An Acquity UPLC^{TM} BEH C$_{18}$ (2.1 x 50 mm, 1.7 μm) was used for above chromatographic experiments. The signal acquired from the detector was recorded by a personal computer running Empower 2 software (Waters).

2.2. SYNTHESIS OF IMPRINTED POLYMERS

MIPs were formulated using a 1:6:6 molar ratio between template (T), functional monomer (M) and crosslinker (C) respectively, into a porogenic mixture that contained 7.5 % of poly (vinyl acetate) (PVAc) dissolved in Triethylen glycol dimethyl ether (Triglyme) (w/w). After incorporate the initiator 2,2-azobis(2-methylpropionitrile) (AIBN), the polymerization mixture was mixed and purged with nitrogen for 5 min. Polymerization was initiated and carried out at 60 ºC for 24 h.

To remove the template, polymer was washed several times with MeOH:HAc (4:1, v/v). The polymer particles were dried and then stored at room temperature.

Blank polymers were prepared by the above procedure excluding the templates.

2.3. BATCH ANALYSIS

Twelve different solutions of BPA in water spanning the concentration range 5.000-1000 mg L^{-1} were prepared. MIPs and NIPs were sonicated 15 min into 2 mL of batch solutions in a 5 mL vessel at room temperature. Then, the solutions were removed in order to determine the free template by UPLC-PDA. The bound template concentration is calculated by difference from total.

Between rebinding tests, the polymers were washed twice with the elution solvent to ensure the extraction of rebinding BPA.

2.4. CHARACTERIZATION OF IMPRINTED POLYMERS BY ADSORPTION ISOTHERM MODELS

Binding isotherms, used to characterize and compare MIPs formulations, could be obtained from batch rebinding studies. The calculation of binding parameters from an isotherm requires the application of a specific binding model [12]

The discrete Langmuir isotherm model [13] assumes uniform adsorption on the surface. This model is particularly easy to implement via Scatchard plots and generate the corresponding binding parameters: binding affinity (K) and number of binding sites (N). In the Scatchard analysis, the experimental binding isotherm is plotted in q/C versus q format (where q is the concentration of the analyte bound to a polymer in µmol g^{-1} and C is the

concentration of free analyte remaining in the solution in µmol L^{-1}). In homogeneous systems that contain only one type of binding site, the Satchard plot falls on a straight line with a slope equal to the negative of the binding affinity (-K) and an x-intercept equal to the number of binding sites (N):

$$q/C = KN - Kq \qquad (1)$$

In contrast, the Scatchard plots for most MIPs are curved. This curvature has been cited as evidence for binding site heterogeneity. Heterogeneity can still be accommodated using the Scatchard analysis by modelling the curved isotherm as two separate straight lines (bi-Langmuir model). This limiting slopes method yields two separate sets of binding parameters (K_1, N_1 and K_2, N_2) for two classes of sites. The steeper line measures the high-affinity sites and the fatter line measures the low-affinity sites [12]. The continuous Freundlich isotherm-affinity distribution model (FIAD) [14] can better accommodate the heterogeneous nature of MIPs and generate an affinity spectrum. This model assumes a power function relationship between q and C and it is most easily applied by plotting the experimental binding isotherm in log q versus log C format, Eq. (2). There are two fitting parameters a and m that both yield a measure of physical binding parameters. The second fitting parameter is known as the heterogeneity index. For homogeneous materials, m would be equal to 1 and values approaching to zero increase the heterogeneous character of the polymer.

$$log q = m log C + log a \qquad (2)$$

Recently, an analytically derived expression for the AD for a Freundlich isotherm has developed:

$$N(K) = 2.303am(1 - m^2)e^{-2.303mlogK} \qquad (3)$$

This AD expression allows the calculation of the AD within the limits (K_{min} and K_{max}) set by the concentration ranges of the experimental binding isotherm:

$$K_{max} = 1/C_{min} \quad \text{and} \quad K_{min} = 1/C_{max} \qquad (4)$$

Plot the log format of Eq (4) (log N versus log K) the exponentially decaying distribution becomes a straight line, which greatly facilitates the visual comparison of the AD of different polymers. ADs with similar heterogeneity are easily identified as parallel lines because the slope in the format is equal to m.

The binding parameters N_{K1-K2} and K_{K1-K2} (number of sites and weighted average affinity, respectively) can be measured for any set of the entire distribution for K_1 to K_2 values that are within the boundaries K_{min} and K_{max} as defined by Eq. (4):

$$N_{K1-K2} = a(1 - m^2)(K_1^{-m} - K_2^{-m}) \qquad (5)$$

$$\overline{K}_{K1-K2} = \frac{m}{m-1} \frac{K_1^{1-m} - K_2^{1-m}}{K_1^{-m} - K_2^{-m}} \qquad (6)$$

287

Likewise, the Dubinin-Radushkevich isotherm model [15] helps to study the interaction between adsorbate and sorbent, is generally used to distinguish between physical and chemical adsorption, it is described by Eq. (7):

$$lnq = lnq_m - K_{DR}\varepsilon^2 \qquad (7)$$

where q_m is the maximum adsorption capacity of MIP in µmol g^{-1}, K_{DR} (kJ^2 mol^{-2}) is the Dubinin-Radushkevich constant and ε is the Polanyi potential, given in Eq (8):

$$\varepsilon = RTln(1 + 1/C) \qquad (8)$$

K_{DR} is related with the free energy (E, kJ mol^{-1}) of adsorption per molecule of adsorbate when it is transferred to the surface of the solid from infinity (in the solution). The adsorption behaviour could predict physical adsorption in the range of 1-8 kJ mol^{-1} and chemical adsorption at over 8 kJ mol^{-1} [16]. It can be calculated by Eq. (9):

$$E = (2K_{DR})^{-1/2} \qquad (9)$$

3. RESULTS AND DISCUSION

3.1. INFLUENCE OF CROSS-LINKER ON MOLECULAR RECOGNITION

Fig.1 shows the Scatchard plot (SP) of equilibrium data. The curvature obtained for EDMA-MIP and TRIM-MIP (Fig.1 (a) and (b)) is an evidence of

two separate sets of binding sites that are modelled by two separate straight lines (bi-Langmuir), the steeper line measures the high-affinity sites and the fatter line measures the low-affinity sites. SP of DVB-MIP showed ambiguous results. A more accurate measure of this heterogeneity could be obtained by the continuous Freundlich model which can better accommodate the heterogeneity than the discrete models.

Table 1 shows the fitting coefficients for bi-Langmuir, Freundlich and Dubinin-Radushkevich equations for adsorption of BPA on the imprinted polymers prepared in parallel with EDMA, TRIM and DVB cross-linkers. From Freundlich model, BPA TRIM cross-linked MIP exhibited better recognition properties than EDMA cross-linked polymer attributed to the fact that TRIM is more polar and less rigid than EDMA, results in a more flexible network which eases the template removal. The polymerization of NIP cross-linked with DVB was not completely achieved, may be due to DVB rigidity.

Fig.2 shows the affinity distribution based on the Freundlich model for EDMA and TRIM MIPs against respective NIPs plotted in log-format. An exponentially decaying distribution of binding sites with respect to the association constant is obtained. The most visible difference between the respective ADs should be the higher capacity of MIP within the measured concentration window. This could be seen in the higher positioning of the MIPs affinity distributions. However, for EDMA polymers, the ADs were very similar; there was only difference between MIP and NIP capacity al low concentrations of batch analysis. Changing the cross-linker EDMA by TRIM,

the difference between respective capabilities increased, being higher at low concentrations also. These assessments are consistent with the calculated values of the respective capacities shown in Table 1.
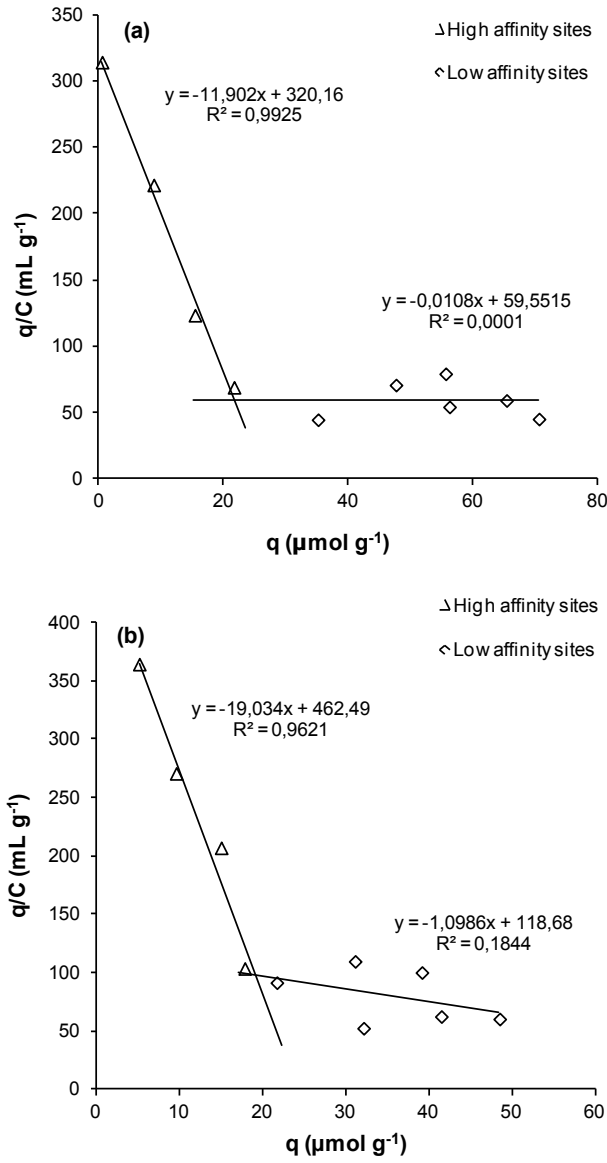
Fig.1. Scatchard plots of BPA-EDMA-MIP (a) and BPA-TRIM-MIP (b).
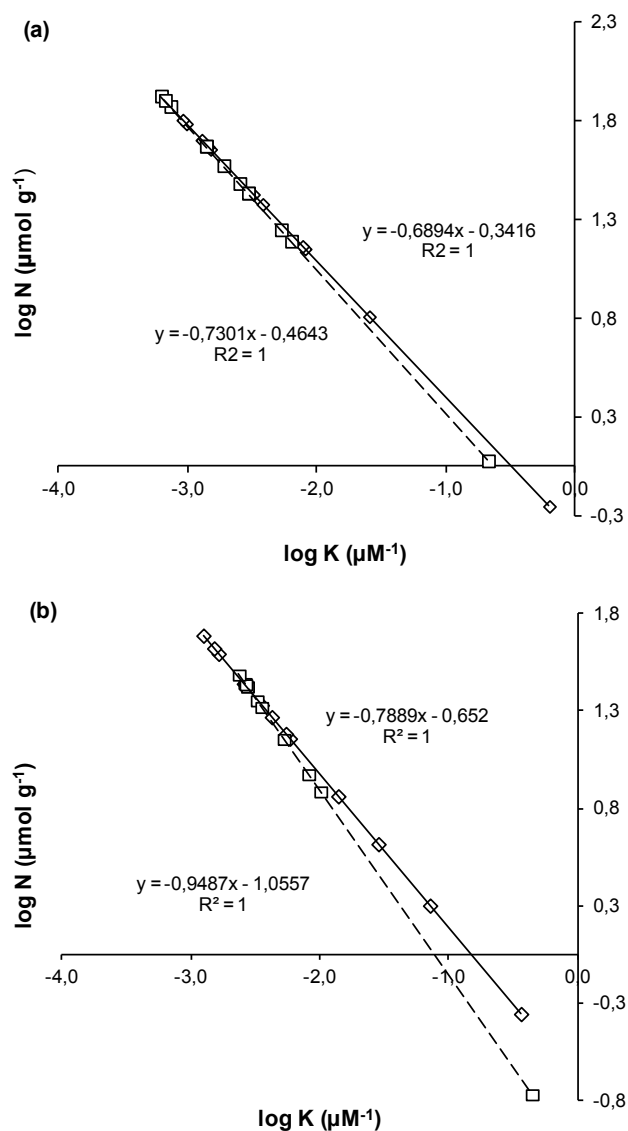
Fig.2. Freundlich adsorption isotherms of BPA-EDMA-MIP (-) and respective NIP (- -) (a) and ADs for BPA-TRIM-MIP and TRIM-NIP (b)

Table 1. Binding parameters of BPA-MIP cross-linked with EGDMA, TRIM and DVB

C	Polymer	K_{biL} (M^{-1})	N_{biL} (µmol g^{-1})	m	K_F (M^{-1})	N_F (µmol g^{-1})	E_{D-R} (KJ mol^{-1})
EDMA	MIP	1,19E04	26,90	0,6893	1,07E04	45,20	158,1
	NIP	9,81E02	109,8	0,7300	4,96E02	37,42	15,08
TRIM	MIP	1,90E04	24,30	0,7887	1,09E04	23,70	353,5
	NIP	1,37E03	42,71	0,9485	4,91E01	2,24	8,840
DVB	MIP	9,23E03	85,41	0,5780	1,27E04	102,33	235,7
	NIP	-	-	-	-	-	-

As noted in Freundlich binding parameters of Table 1, EDMA and TRIM MIPs resulted more heterogeneous than respective NIPs (6% and 20% respectively). The number of binding sites of TRIM-MIP was 11 times greater than TRIM-NIP and, accordingly with previous paragraph, a minimum difference between the capacity of EDMA-MIP and EDMA-NIP was observed. The average affinity of binding sites was 222 times higher for TRIM-MIP compared to TRIM-NIP and this ratio was about 20 for EDMA cross-linked polymers.

Dubinin-Radushkevich model suggested a strong interaction between BPA and both BPA-MIPs ($E_{D-R} > 8$ kJ mol^{-1}), the strength of the hydrogen bond between -OH groups in the sorbent and the pyridines of the adsorbate is comparable to a chemical bond. This interaction is stronger in BPA-TRIM-MIP than in BPA-EDMA-MIP. E_{D-R} values of NIPs indicated a chemical nature of the adsorption process in EDMA-NIP and physisorption process for TRIM-NIP.

4. CONCLUSIONS

The effect of synthetic procedure parameters (types of cross-linkers) on the binding properties of BPA non-covalent imprinted polymers was investigated. Langmuir and Freundlich models revealed the highest imprinted effect for BPA-TRIM-MIP. Freundlich model proved the heterogeneity of the binding sites. The E_{D-R} values calculated from the Dubinin-Radushkevich model indicated that adsorption proceeded via chemisorption in every case; however, the strength of hydrogen bonding involved is greater in BPA-TRIM-MIP.

From the explained in previous paragraph, BPA-TRIM-MIP appears to be optimal to employ it as coating of a QCM sensor in the concentration and determination of BPA in aqueous environments.

References

[1] B.S. Ebarvia and C.A. Binag, Anal. Bioanal. Chem. 378 (2004) 1331-1337

[2] K. Haupt, Anal. Chem. 75 (2003) 376A

[3]] M. Romero-Guerra, I. Chianella, E.V. Piletska, K. Karim, A.P.F. Turner and S.A. Pîletsky, Analyst 134 (2009) 1565

[4] M. Ávila, M. Zouzagh, A. Escarpa and Á. Ríos, Trends Anal. Chem. 27 (2008) No. 1

[5] M.S. Dopico-García, M.C. Cela-Pérez, J.M. López-Vilariño, M.V. Gónzalez-Rodríguez, and L.F. Barral-Losada, J. Appl. Polym. Sci. 119 (2011) 2866

[6] E. Turiel and A. Martín-Esteban, Anal. Chim. Acta 668 (2010) 87

[7] A. Beltran, F. Borrull, P.A.G. Cormack and R.M. Marce, Trends Anal. Chem., 29 (2010) No. 11

[8] P. A. G Cormack and A. Zurutuza-Elorza, J. Chromatogr. B 804 (2004) 173

[9] M Sibrian-Vazquez, D. A. Spivak, J. Appl. Polym. Sci. A: Polym. Chem. 42 (2004) 3668

[10] M. Kempe, Anal. Chem. 68 (1996) 1948

[11] W. Zhao, N. Sheng, R. Zhu, F. Wei, Z. Cai, M. Zhai, S. Du and Q. Hu, J. Hazard. Mater. 179 (2010) 223

[12] R. J. II Umpleby, S. C. Baxter, A. M. Rampey, G. T. Rushton, Y. Chen and K. D. Shimizu, J. Chromatogr. B, 804 (2004) 141

[13] A. Gómez-Caballero, N. Unceta, M.A. Goicolea and R. J. Barrio, Sensor Actuat. B-Chem. 130 (2008) 713

[14] A. M. Rampey, R. J. II Umpleby, G. T Rushon, J. C. Iseman, R. N. Shah and K. D. Shimizu, Anal. Chem. 76 (2004) 1123

[15] T. Y. Guo, Y. Q. Xia, G. J. Hao, M. D. Song and B. H. Zhang, Biomaterials 25 (2004) 5905

[17] C. Y Chen, C. H. Wang and A. H. Chen, Talanta 84 (2011) 1038

CAPÍTULO 2: APLICACIÓN DE MIPS EN EL TRATAMIENTO DE MUESTRA PREVIO AL ANÁLISIS

'An approach to imprint Irganox 1076: Potential application to the specific migration test in olive oil'

'Selective removal of ATP degradation products from food matrices II: Rapid screening of hypoxanthine and inosine by molecularly imprinted matrix solid-phase dispersion for evaluation of fish freshness'

'Water-compatible imprinted pills for sensitive determination of cannabinoids in urine and oral fluid by MISPE-LC-MS/MS'

3.2. CAPÍTULO 2: APLICACIÓN DE MIPS EN EL TRATAMIENTO DE MUESTRA PREVIO AL ANÁLISIS

Artículo 6: 'An approach to imprint Irganox 1076: Potential application to the specific migration test in olive oil'[***]

Artículo 7: 'Selective removal of ATP degradation products from food matrices II: Rapid screening of hypoxanthine and inosine by molecularly imprinted matrix solid-phase dispersion for evaluation of fish freshness'.

Artículo 8: 'Water-compatible imprinted pills for sensitive determination of cannabinoids in urine and oral fluid by MISPE-LC-MS/MS'[****].

[***] Trabajo desarrollado durante la realización del Máster que permite acceder a los estudios de Doctorado (2011)

[****] Trabajo enviado a revista científica incluida en JCR, pendiente de publicación

AN APPROACH TO IMPRINT IRGANOX 1076: POTENTIAL APPLICATION TO THE SPECIFIC MIGRATION TEST IN OLIVE OIL

M.S. Dopico-García[1], M.C. Cela-Pérez[1], J.M. López-Vilariño[1], M.V. González-Rodríguez[2], L.F. Barral-Losada[3]

[1] Grupo de Polímeros, Centro de Investigacións Tecnolóxicas, Universidade da Coruña, Campus de Esteiro s/n, Ferrol 15403, Spain

[2] Dpto. de Química Analítica, E.U. Politécnica, Universidade da Coruña, Avda. 19 de Febrero s/n, Ferrol 15405, Spain, email: victoria.gonzalez.rodriguez@udc.es

[3] Laboratorio de Plásticos, Centro de Investigacións Tecnolóxicas, Universidade da Coruña, Campus de Esteiro s/n, Ferrol 15403, Spain

ABSTRACT

Irganox 1076 is a hindered phenolic antioxidant commonly added to polyolefins, whose migration from the plastic packaging into the food is regulated by European legislation.

The work herein reports on an initial approach to obtain a molecularly imprinted polymer (MIP) for Irganox 1076, a previously non imprinted target. In a subsequent step, the application of the molecularly imprinted solid phase extraction (MISPE) to the fatty simulant olive oil is tested in order to get its determination free of interferences using high performance liquid chromatography with PDA detector.

The influence of five variables, namely porogen, functional monomer, crosslinker, initiator and initiation method was investigated through the synthesis of miniMIPs. The best results were obtained using methacrylic acid and ethylene glycol dimethacrylate in tetrahydrofuran under UV radiation with 2,2´-azobis-(2-methylpropionitrile). The application of MISPE to olive oil showed the potential of the imprinted polymer to clean up complex matrices.

303

1. INTRODUCTION

In recent years, molecularly imprinted polymers (MIPs) have shown its ability for the solid phase extraction and cleanup of such complex matrices as biological [1], environmental samples [2, 3] or food [4-7], for what highly selective extraction techniques are necessary.

MIPs are synthetic polymers with recognition sites able to specifically rebind a target molecule (template). In general, they are obtained by mixing the template with the complimentary functional monomers and crosslinkers in a suitable solvent. After the polymerization, the template can be extracted from the synthesized polymer [8, 9].

Irganox 1076 (Table 1) is a hindered phenolic antioxidant commonly added to polyolefins to improve their stability against the effects of thermo-oxidative and photo-oxidative degradation. Their migration from the packaging into the food is regulated by European legislation [10] that establishes a specific migration limit (SML) of 6 mg kg^{-1}. In principle the migration test should be carried out in the own food but to simplify the analysis, aqueous or fatty food simulants can be used [11]. Until the moment there is not any official analytical methodology to determine the migration of this compound in the allowed simulants.

Table 1. Structures of template, monomers and crosslinkers.

Compound	[SciFinder]	CAS	Mw [SciFinder]
Irganox 1076		2082-79-3	530.86
Monomers			
Methacrylic acid		79-41-4	86.09
4-vinylpyridine		100-43-6	105.14
Acrylamide		79-06-1	71.08
Crosslinkers			
EDMA		97-90-5	198.22
TRIM		3290-92-4	338.40
DVB80		1321-74-0	Incompletely defined substance

In aqueous food simulants two analytical methodologies have been developed in our laboratory using liquid-liquid extraction [12], or solid

phase extraction [13] and High Performance Liquid Chromatography with UV detector (HPLC-UV), that achieve detection limits quite lower than SML. Dispersive liquid-liquid microextraction followed by HPLC-UV has been also recently proposed for its determination in water at µL levels [14]. However, its determination in olive oil, the fatty simulant established by the legislation, has shown to be rather more difficult because of the high complexity of this matrix. O´Brien et al. [15] reported the analysis of Irganox 1076 in olive oil using HPLC and a fluorescence detector after the dilution of the sample with acetone, methodology that has been later applied by other authors [16]. Different tests performed in our laboratory at SML levels using the more common UV detector instead of fluorescence detector were not successful due to the interferences caused by the olive oil. In these assays either dilution of the sample with an organic solvent or a preconcentration step by liquid-liquid extraction or solid phase extraction before the chromatographic analysis were tested [17].

So, the work herein explores the possibility of obtaining an imprinted polymer of Irganox 1076 than can be later used for sample cleanup and/or preconcentration with MISPE. As far as we know Irganox 1076 has not been a target for imprinting, so that no bibliographic data were available. Considering that Irganox 1076 is a phenolic compound with a carboxylate group, the non covalent imprinting protocol proposed by Sellergren and Andersson [18] was followed.

Many parameters fixed in the polymerization can influence the performance and recognition capacity of MIP for a target template, such as the functional monomer, crosslinker, the porogenic solvent, the initiation method (i.e. thermal or UV initiation), polymerization time or degasification time. In order to screen a higher number of variables minimizing the experimental work required, the synthesis of miniMIPs proposed by Sellergren [18] and Takeuchi [19] was selected, that consists in the preparation of a quite large number of polymers in small scale.

This work deals with the initial development of a MIP for Irganox 1076 screening polymerization conditions in small-scale followed by the large scale preparation of the selected MIPs. The application of the imprinted material is subsequently tested in olive oil in order to determine Irganox 1076 free of interferences using HPLC-UV.

2. EXPERIMENTAL

2.1. CHEMICALS AND APPARATUS

Methanol and tetrahydrofuran (THF) of HPLC gradient grade were supplied by Merck (Darmstadt, Germany). Dichloromethane of ultragradient HPLC grade was supplied by J.T. Baker (Deventer, The Netherlands). Water was purified on a Milli-Q Ultrapure system (Millipore, Bedford, MA, USA). Filters 0.2 µm, 13 mm PTFE, were from Waters (Milford, MA, USA).

Irganox 1076 was obtained from Ciba (Basel, Switzerland). Acrylamide (> 99%), methacrylic acid (MAA, > 98%), 2,2´-azobis-(2-methylpropionitrile) (AIBN, CAS 78-67-1, >98%) and ethylene glycol dimethacrylate (EDMA, >97%) were from Fluka, Sigma-Aldrich (Steinheim, Germany); 2, 2-dimethoxy-2-phenylacetophenone (CAS 24650-42-8, 99%), divinylbenzene (DVB80, 80% mixture of isomers), trimethylolpropane trimethacrylate (TRIM) and 4-vinylpyridine (> 95%) were from Aldrich (St. Louis, USA). Structures and CAS numbers of monomers and crosslinkers are shown in Table I.

Two different systems with UV lamp were used in the photo-polymerizations: a high-pressure mercury vapour lamp (Phillips, HPK 350 W) and a second system built in the own laboratory. This last one consisted in a reactor equipped with two UV lamps (15 W each, 350 nm), placed in parallel on both sides of the reactor to irradiate the samples in a more homogeneous way, and a fan added to prevent the increasing of the temperature (T<30ºC).

A Milestone microwave laboratory system ETHOS TC (Sorisde, Italy) equipped with 10-vessel position carousel was employed; the instrument is controlled for temperature.

Visiprep™-DL Solid Phase Extraction Vacuum Manifolds, equipped with integral flow control valves and disposable Teflon® flow control valve liners were from SUPELCO (Bellefonte, PA, USA). The SPE tubes were 6 mL pre-

fritted polypropylene tubes and the frits were 6 mL polyethylene frits (20 µm porosity).

2.2. miniMIPS

Synthesis of miniMIPs: Screening for selection of the polymerization conditions.

The experimental procedure was carried out according to the one described by Sellergren and Andersson [18] to prepare miniMIPs. A stock solution was prepared for the scaled down version of the polymerization (Table 2). It was obtained by mixing template, crosslinker, initiator and solvent. The same volume of solvent (7 mL) was used throughout, previously purged with N_2 for at least 5 min.

From each stock solution 118 µL was dispensed into a 1.5 mL glass vial and mixed with 50 µmol of the functional monomer, so that the resulting polymerization mixture of the scaled down version had the following molar composition: 1:4:20 (template: functional monomer: crosslinker) for EDMA and DVB80, and 1:4:13 for TRIM. The vials (n = 4 for each assay) were sealed with a rubber septum and purged with nitrogen while being cooled in an ice water bath. Polymerization was induced by heat in a water bath (60ºC) or by UV irradiation (350 nm, < 30ºC).

As a control, non-imprinted polymers (NIP) were prepared for each assay (n = 4) and treated in exactly the same way except that the template was omitted from the polymerization stage.

Table 2. Preparation of miniMIPs.

polymer	MIP mother solution*			monomer	polimerization conditions
	crosslinker	initiator	porogen		
MIP-1	EDMA	AIBN	CH$_2$Cl$_2$	MAA 50 µmol (4 µL)	T= 60ºC (bath water) 24 h
MIP-2	25 mmol	0.35 mmol	7 mL	4-vinylpyridine 50 µmol (5 µL)	
MIP-3				MAA 50 µmol (4 µL)	T= 60ºC (bath water) 24 h
MIP-4	EDMA 25 mmol	AIBN 0.35 mmol	THF 7 mL	4-vinylpyridine 50 umol (5 µL)	
MIP-5				Acrylamide** 50 µmol (15 µL)	
MIP-6	EDMA 25 mmol	AIBN .35 mmol	THF 7 mL	MAA 50 µmol (4 µL)	UV (350 nm) (grande W, 24 h)
MIP-7				4-vinylpyridine 50 µmol (5 µL)	
MIP-8	EDMA 25 mmol	AIBN 0.35 mmol	THF 7 mL	MAA, 50 µmol	UV (350 nm) (2x15 w, 9 h)
MIP-9	EDMA 25 mmol	Phenone 0.35 mmol	THF 7 mL	MAA, 50 µmol	UV (350 nm) (2x15 w, 9 h)
MIP-10	EDMA, 25 mmol	AIBN 0.35 mmol	THF 7 mL	MAA, 50 µmol	UV (350 nm) (2x15 w, 19 h)
MIP-11	EDMA, 25 mmol	Phenone 0.51 mmol	THF, 7 mL	MAA, 50 µmol	UV (350 nm) (2x15 w, 19 h)
MIP-12	DVB80 25 mmol	AIBN 0.35 mmol	THF 7 mL	MAA, 50 µmol	UV (350 nm) (2x15 w, 30 h)
MIP-13	TRIM 16.25 mmol	AIBN 0.35 mmol	THF 7 mL	MAA, 50 µmol	UV (350 nm) (2x15 w, 24 h)

*1.25 mmol of Irganox 1076 was added as template to all the mother solutions. 118 µL of the mother solution were mixed with the monomer in a 1.5 mL glass vial.

**Acrylamide was dissolved in the minimum possible volume of THF and was not soluble in CH$_2$Cl$_2$.

2.3. EXTRACTION AND REBINDING EXPERIMENTS

A volume of 1 mL of the porogen was pipetted into each of the vials containing the blank test and imprinted polymers. The vials were then sonicated for 1 h without heating and the concentration of the released template was quantified in each extract by HPLC-UV. The supernatant was filtered (0.2 μm), diluted and injected.

The polymers were submitted to several washing steps using ultrasonic agitation until that no bleeding that could potentially interfere in the next rebinding assay was observed. Solvents as methanol or the mixture tetrahydrofuran: acetic acid 9:1, with higher polarity than the porogen were used. The concentration of the released template was quantified in most washing fractions by HPLC–UV.

A rebinding experiment was then performed by addition of 1mL of a solution of the template (1/10 of the concentration of the template in the polymerization mixture) followed by sonication of the vials for 1 h. The polymers were allowed to stand for 24 h and the concentration of free (unbound) template was determined by HPLC-UV. The rebinding percentage was calculated in the blank and in the imprinted polymers by subtracting the concentration of the template in the supernatant from the initial concentration.

2.4. MISPE WITH MIP SYNTHESIZED BY BULK POLYMERIZATION

2.4.1. Bulk polymerization

The experimental procedure was carried out according to Sellergren and Andersson [18] considering the polymerization mixture obtained by miniMIPs. To 3.8 mL (20 mmol) EDMA, 0.34 mL (4 mmol) MAA, and 1 mmol Irganox 1076 (or no template for NIP synthesis) in 5.6 ml THF 40 mg (0.24 mmol) AIBN was added as initiator. The mixture was transferred to thick-walled glass jars. These were sparged with nitrogen for 5 min. Porogen was also previously sparged with nitrogen. The polymerization was photochemically initiated; the jars were symmetrically placed at approximately 10-cm distance from a UV light source. After 22 h, the jars were crushed and the polymers ground in a ball mill with repeated sieving under water to a grain size fraction of 25-40 µm. Fines were removed by repeated sedimentation from acetone.

MIP and NIP were washed by using microwave energy to remove the template and other unreacted compounds. Sample weight: approximately 0.5 g, extraction solvent: 50 mL of THF:acetic acid (9:1), heating time: 2 min, extraction time: 15 min, temperature: 40 ºC. The liquid phase was filtered (through ashless filters and 0.2 µm filter) and analyzed by HPLC–UV.

2.4.2. MISPE column

A 250-400 mg amount of the MIP or NIP respectively, was packed into SPE glass syringe barrels. Prior to the use, the columns were conditioned with 3 mL of THF:hexan (3:1; v/v). 2 mL of sample were loaded onto the column. The olive oil sample consisted of 0.75 g of olive oil fortified with Irganox

1076 to 30 mg L^{-1} and diluted until 2 mL with THF: hexan 3:1. The retained Irganox 1076 was eluted using 3 mL of THF: acetic acid (9:1). The obtained extract was evaporated until a final volume of 2 mL under N$_2$ stream and analysed by HPLC-UV.

2.5. MISPE WITH MIP SYNTHESIZED BY PRECIPITATION POLYMERIZATION

2.5.1. Precipitation polymerization

The mixtures were prepared and treated in the same way than those for bulk polymerization except that a larger volume of solvent, 40 mL of THF, was employed. After 24 hours of polymerization under UV, a gel was obtained from every mixture. It was dried at 40ºC around 2 hours obtaining a fine powder.

2.5.2. MISPE column

A similar protocol as that described above was followed, at vacuum. Previously to the assay MIP and NIP were washed in the own column instead of using microwave energy. Amount of MIP or NIP in each column (n = 2): 200 mg; washing: repeatedly with THF: acetic acid (9:1) until no Irganox 1076 was detected; conditioning: 6 mL of THF; sample:0.75 g of olive oil fortified with Irganox 1076 to 15 mg L^{-1} and diluted until 2 mL with THF; elution:6 mL of THF:acetic acid (9:1). The obtained extracts were

evaporated until a final volume of 2 mL under vacuum and analysed by HPLC-UV.

2.6. HPLC ANALYSIS

HPLC-UV analyses were performed in a Waters Alliance 2695 system equipped with a quaternary pump, autosampler with the volume injection set to 20 µL, and a Waters 996 photodiode array detector. Chromatographic separation was performed on a reversed-phase SunFire C_{18} analytical column (3.0 x 150 mm, 3.5 µm particle diameter) from Waters, hold at 30ºC. The gradient mobile phase consisted of methanol and water and it was programmed as follows: from 70% of methanol to 100% in 2 minutes, with a hold of 20 minutes. Flow rate was 0.5 mL min^{-1}. The signal acquired from the detector was recorded by a personal computer operating under the Empore Pro software v. 5.0 (Waters).

Irganox 1076 was identified by comparison of its retention time with the corresponding peak in the standard solution and its UV spectrum (Fig. 1). It was quantified at 276 nm using a calibration plot of an external standard.
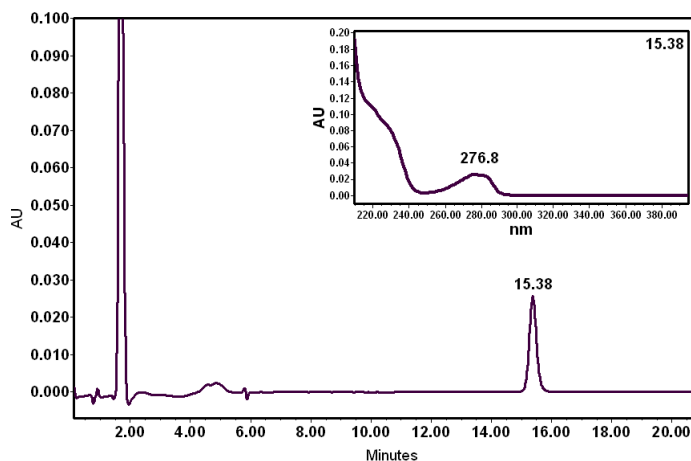
Figure 1. HPLC-UV chromatogram and absorption spectrum of Irganox 1076 (50 mg L^{-1}).

2.7. SPECTROSCOPIC ANALYSIS

Spectrophotometric analysis was performed on Cary 100 Conc UV-Vis Spectrophotometer (Varian, USA).

The changes in absorption spectra of Irganox 1076 were recorded by adding MAA into a constant concentration of Irganox 1076 solution (50 mg L^{-1}) in THF. Corresponding MAA solutions omitting Irganox 1076 were used as blank.

3. RESULTS AND DISCUSSION

3.1. INITIAL TESTS: SOLUBILITY AND STABILITY

Some initial tests have been performed using the standard protocol [18] to test whether this compound was suited for imprinting or not. Irganox 1076

solubility and stability were checked: the analyte showed to be soluble in dicloromethane and tetrahydrofuran at the high concentrations levels necessary for imprinting. The stability of the solution of Irganox 1076 (approximately 10000 mg L^{-1}) was also confirmed in these solvents under the polymerization conditions, at 60ºC (water bath), or UV irradiation (temperature lower than 30 ºC) during 24 hours. At comparing with the corresponding standard solutions kept at 4 ºC, recoveries between 86 and 110% were obtained.

3.2. SYNTHESIS OF miniMIPs

The influence of five variables on the performance of the MIP was tested, namely porogen, initiation method, monomer, initiator and crosslinker. The experimental conditions to prepare the polymers are shown in Table II. Degasification with N_2 showed to be an important parameter to control through the experimental study, due to the simultaneous presence of the phenolic compound and oxygen that could inhibit the polymerization [20].

The polymers that showed complete or approximately complete release using the corresponding porogen as solvent were discarded, whereas those that showed to retain the template were subjected to the wash and rebinding steps. Considering that the lack of grinding can make the process slower [19], rebinding time was 22-24 hours to allow to get the desorption equilibrium.

A first screening to select the porogen, functional monomer and initiation method was carried out according to Fig. 2.

3.2.1. Porogen

Analyte binding properties of molecularly imprinted sorbents are influenced by the type of solvent, or porogen, used in the polymer synthesis and the solvent used in the particular application of the MIP [21]. As porogen, it is a general procedure to choose an aprotic solvent, as apolar as possible without compromising the solubility of the template [8]. So, THF and dichloromethane were initially selected considering their low polarity and the good solubility shown by Irganox 1076 in these solvents, as reported above.

All the polymers synthesized in dichloromethane with either MAA (MIP 1) or 4-vinylpyridine (MIP 2) were discarded due to the almost complete release of the template observed (Fig. 2). The best results obtained with THF were ascribed to its lower polarity.

3.2.2. Initiation method

According to the references, temperature can have a double effect on the imprinted polymer: low temperature is an advantage to stabilize the monomer-template assemblies but a higher temperature polymerization is favourable for the complete polymerization reaction and therefore to improve the number and quality of MIP recognition sites [22]. The

comparison between these methods, photo or thermal polymerization, has showed different results: while He et al. [22] did not find important differences, other authors [21, 23, 24] recommended the use of photoionization at low temperature to improve the properties of the obtained polymers.
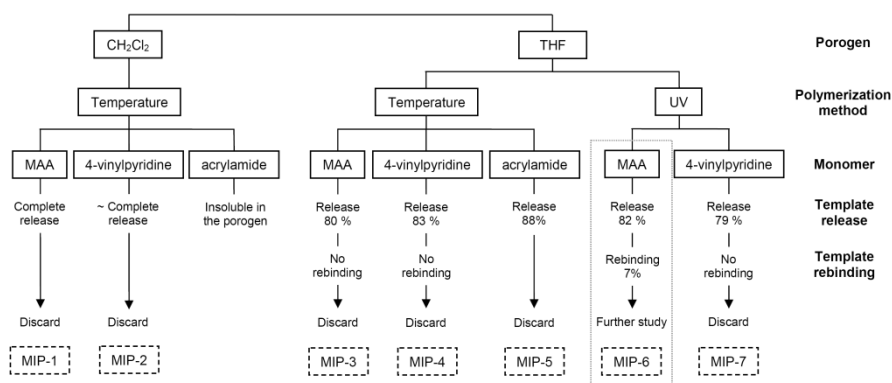
Figure 2. Selection of the monomer, porogen and polymerization method. Experimental conditions according to Table 1.

In the first assays thermal polymerization at 60 ºC or photo initiation at room temperature was employed, both during 24 hours. Results were analyzed considering MIP 3 and MIP 4 for thermal polymerization and MIP 6 and MIP 7 (Fig. 2) for photo initiation: similar release (around 80 %) was obtained. Considering also the references reported above, photo initiation was selected as polymerization method. In order to prevent the increasing of the room temperature around the vials, a reactor with 2 smaller UV lamps and a fan was built in the own laboratory. It was employed for the next assays allowing a temperature lower than 30 ºC.

3.2.3. Functional monomer

Functional monomer is considered to be the most important variable to select for imprinting [9]. Once Irganox 1076 could potentially present either acidic or basic behaviour due to its structure with one phenolic group and one carboxylate (Table 1), three monomers were compared: MAA, 4-vinylpyridine and acrylamide (Table 1). They are classified as acidic, basic and uncharged, respectively [18]. All these monomers have been previously reported for imprinting of phenolic compounds: acrylamide for catechin [25] or quercetin [26, 27]; 4-vinylpyridine for phenol [28] and quercetin [4]; MAA for quercetin [29] or flavonol [30].

Acrylamide was discharged (MIP 5) due to its worse compatibility with the porogens used and it did not show any advantage for the imprinting of the template compared to the other monomers. The polymers synthesized with MAA (MIP 3, 6) or 4-vinylpyridin (MIP 4, 7) in THF were subjected to the rebinding step (Fig. 2). The best rebinding results (7.5%) were achieved using MAA as monomer, THF as porogen and UV radiation as polymerization method (MIP 6). Irganox 1076 was loaded in THF:hexan (3:1), with the addition of hexan to decrease the polarity of the solvent [30].

Therefore, methacrylic acid was chosen as monomer. The acidic MAA showed to be more suitable to bind to Irganox 1076 than the other tested monomers, the basic 4-vinylpyridine or the uncharged acrylamide.
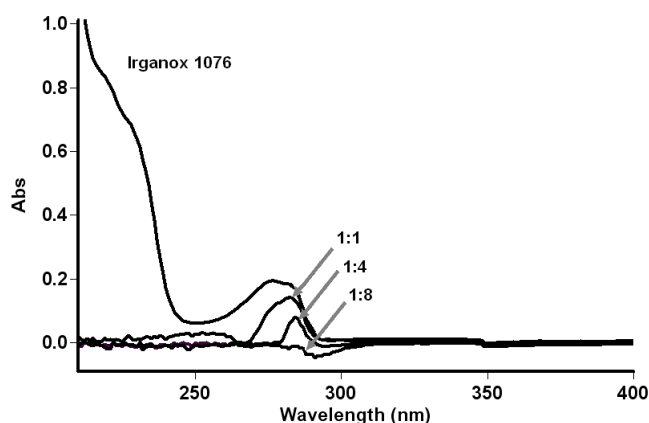
Figure 3. UV absorption spectra of Irganox 1076 in the presence of various concentrations of MAA. [Irganox 1076] = 50 mg L^{-1}, molar ratio Irganox 1076:MAA 1:1, 1:4, 1:8. Corresponding MAA solution without Irganox 1076 as blanks.

Interaction between MAA and Irganox 1076 in THF was confirmed carrying out a spectroscopic analysis to study the interaction between the monomer and the template, as proposed by He et al. [22]. The UV spectral changes upon the addition of MAA to Irganox 1076 solution with ratios template: functional monomer of 1:1, 1:4 and 1:8 are shown in Fig. 3. The UV absorption band characteristic of Irganox 1076 is obviously decreasing with increasing the concentration of MAA. This result allows us to think that a stable functional monomer:template interaction is formed in the prepolymerization solution, and the ratio 1:4 was kept for the next assays.

A schematic illustration of the possible interaction between monomer and template is shown in Fig. 4.
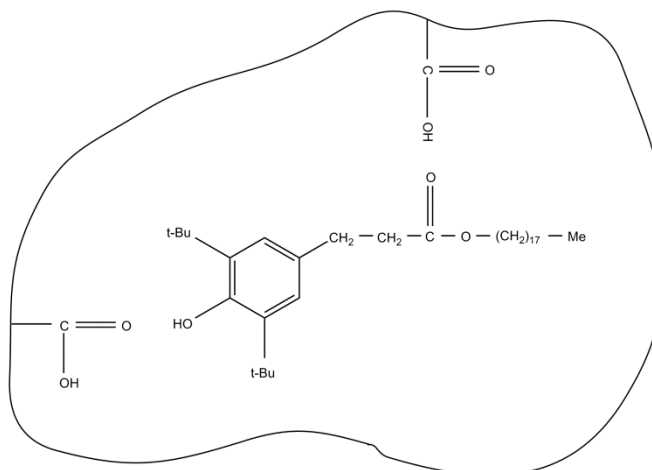
Figure 4. Schematic illustration of the possible interaction between Irganox 1076 and methacrylic acid.

3.2.4. Selection of the initiator

The influence of the type of initiator in the polymer performance has been shown by Mijangos et al [24], that compared the use of azo and phenone derivatives recommending the synthesis of the MIP for a long period of time using low concentration of initiator and low temperature.

In the study herein, a set of polymers were imprinted using also two types of initiators (Table 2): AIBN (azo), commonly used for thermal and photo initiation [18, 24] or 2,2 dimethoxy-2-phenylacetophenone (phenone), a photoionitiator [24, 31].

A first set of experiments was carried out using the same molar amount of both initiators with a polymerization time of 9 hours (MIP 8, MIP 9). The

progress of the polymerization seemed to be quicker with AIBN than with the phenone, although 9 hours showed to be an insufficient time for both.
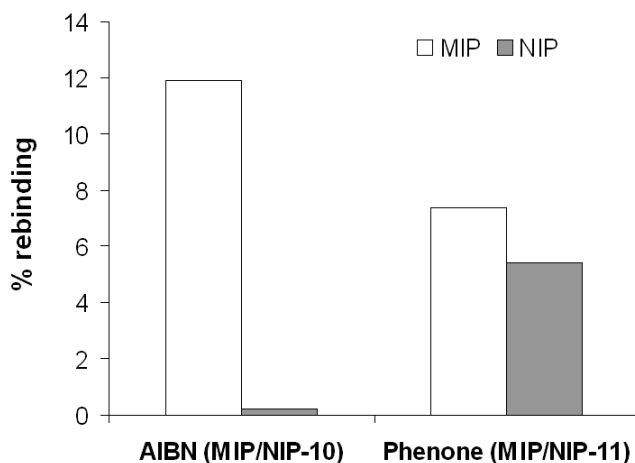
Figure 5. Selection of the initiator. Experimental conditions according to Table I.

In the next assay, the phenone proportion was increased until 1% respect to the total mass (g) of the mixture and the polymerization time until 19 hours, which showed to be suitable for completeness polymerization (MIP 10, MIP-11). The best rebinding results were obtained using AIBN (Fig. 5) whereas that for phenone lower selectivity was achieved, with similar result for MIP and NIP, that may be due to the higher percentage of initiator used [24].

3.2.5. Selection of the crosslinker

The crosslinker "freezes" the template–monomer complex upon polymerization and provides the polymeric backbone leading to the

polymer mechanical stability [9]. The effect of three crosslinkers selected considering their different structures (Table 1) was compared: ethylene glycol dimethacrylate, EDMA; trimethylolpropane trimethacrylate, TRIM; and divinylbenzene, DVB 80 (MIP 10, MIP 12, MIP 13).

Both methacrylates EDMA and TRIM have 2 and 3 similar functional groups, respectively, being EDMA more rigid and TRIM more flexible. EDMA has been commonly used for imprinting [18] while TRIM has been suggested in the last years to imprint large molecules because of the possibly improved mass transfer in low cross-linking density polymers [32]. On the other hand DVB80 lacks oxygen groups and can only establish π-π interaction with the template and it is known to enhance the rigidity of the polymer chains [33].

Depending on the crosslinker used, different template:monomer:crosslinker ratios were used (Table 2): for EDMA and DVB80, the most common 1:4:20, as suggested in the Sellergren and Andersson protocol [18]. For TRIM, the ratio was decreased until 1:4:13 considering previous studies [32]. Polymers synthesized with DVB80 or TRIM needed a longer polymerization time than EDMA.

The best results for each assay were obtained loading the sample in THF for TRIM or in THF:hexane 3:1 for EDMA and DVB80. EDMA allowed obtaining both the highest recovery values for MIP and the highest specificity compared to the NIP (Fig. 6).
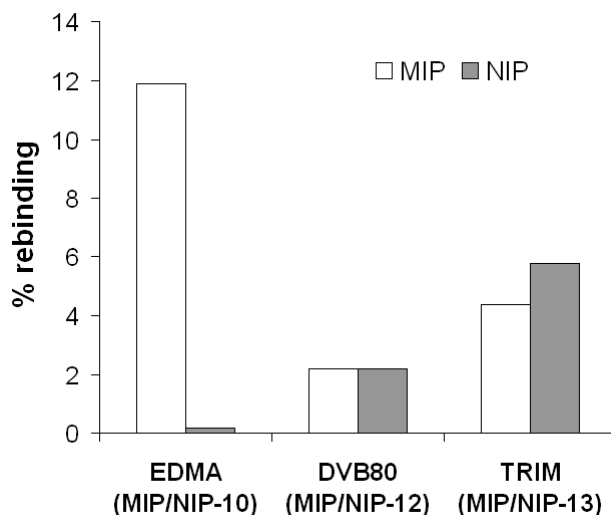
Figure 6. Selection of the crosslinker. Experimental conditions according to Table 1.

3.3. APPLICATION OF THE MISPE FOR CLEAN-UP OF OLIVE OIL SPIKED WITH IRGANOX 1076

The possible application of the imprinted polymer as a cleanup method of a complex matrix was tested using olive oil fortified with Irganox 1076 as sample. Two types of MIPs prepared by bulk and precipitation polymerization were tested, packing 400 or 200 mg of polymer in each column respectively.

In the rebinding assay the percentage of Irganox 1076 retained from the sample of olive oil raised from 17 % to 42 % for the MIP prepared using bulk polymerization and precipitation polymerization respectively. For this last MIP prepared using precipitation polymerization, 92 % of the retained Irganox 1076 could be eluted allowing the cleaning up of the matrix.

4. CONCLUSION

This work has presented an initial approach to prepare a MIP of Irganox 1076, a previously non imprinted target. The influence of 5 variables namely monomer, crosslinker, porogen, polymerization, and initiator was explored achieving the most promising results with MAA, EDMA, and AIBN in THF under UV radiation. The application of MISPE to determine Irganox 1076 in olive oil showed the potential of the imprinted polymer as clean up method of complex matrices.

References

[1] N. Masquè; R.M. Marcè, F. Borrull, TrAC Trends Anal. Chem. 20 (2001) 477

[2] M.T. Muldoon, L.H. Stanker, Anal. Chem. 69 (1997) 803

[3] He, C.; Long, Y.; Pan, J.; Li, K.; Liu, F. J. Biochem Biophys Methods 2007, 70, 133.

[4] A. Molinelli; R. Weiss, B. Mizaikoff, J Agric Food Chem 50 (2002) 1804

[5] F. Puoci; C. Garreffa, F. Iemma, R. Muzzalupo, U.G. Spizzirri, N. Picci, Food Chem. 93 (2005) 349

[6] C. Schirmer, H. Meisel, J. Chromatogr. A 1132 (2006) 325

[7] C. Baggiani, L. Anfossi, C. Giovannoli, Anal. Chim. Acta 591 (2007) 29

[8] L.I. Andersson, J. Chromatogr. B (2000) 739 163

[9] N.M. Bergmann, N.A. Peppas, Prog. Polym. Sci. 33 (2008) 271

[10] Commission Directive 2002/72/EEC. Off. J. Eur. Communities 2002, L 220, 18; Corrigendum OJ L39 13/2/2003, p 1.

[11] Council Directive 85/572/EEC. Off. J. Eur. Communities 1985, L 372, 14.

[12] M.S. Dopico-García, J.M. López-Vilariño, M.V. González-Rodríguez, J. Chromatogr. A, 1018 (2003) 53

[13] M.S. Dopico-García, J.M. López-Vilariño, M.V. González-Rodríguez, Talanta 66 (2005) 1103

[14] M.A. Farajzadeh, M. Bahram, J.A. Jönsson, Anal. Chim. Acta 591 (2007) 69

[15] A.P. O´Brien, I. Cooper, P.A. Tice, Food Addit. Contam. 14 (1997) 705

[16] I.E Helmroth; M. Dekker, Hankemeier, T. Food Addit. Contam. 19 (2002) 176

[17] M.S. Dopico-Garcia, Ph.D. Thesis. University of Coruña; 2005

[18] B. Sellergren, L.I. Andersson, Methods 22 (2000) 92.

[19] T. Takeuchi, D. Fukuma, J. Matsui, Anal. Chem. 71 (2000) 285

[20] R.G. Caldwell, J.L. Ihrig, J. Am. Chem. Soc. 84 (1962) 2878

[21] D.J. O´Shannessey, B. Ekberg, L.I. Andersson, K. Mosbach, J. Chromatogr. 470 (1989) 391.

[22] J. He, Q. Zhu, Q. Deng, Spectrochim. Acta Part A 67 (2007) 1297

[23] F. Lanza, A.J. Hall, B. Sellergren, A. Bereczki, G. Horvai, S. Bayoudh, P.A.G. Cormack, D.C. Sherrington, Anal. Chim. Acta 435 (2001) 91

[24] I. Mijangos, F. Navarro-Villoslada, A. Guerreiro, E. Piletska, I. Chianella, K. Karim, A. Turner, S. Piletsky, Biosens. Bioelectron. 22 (2006) 381

[25] E. Blahová, J. Lehotay, I.S. Skacáni, J. Liq. Chromatogr. Relat. Technol. 27 (2005) 2715

[26] J. Xie, L. Chen, C. Li, X. Xu, J. Chromatogr. B 788 (2003) 233

[27] J. Xie, L. Zhu, H. Luo, L. Zhou, C. Li, X. Xu, J. Chromatogr. A 934 (2001) 1

[28] Y-Q. Lv, Z. Lin, W. Feng, T. Tan, Chromatographia 66 (2007) 339

[29] Y. Xia, T. Guo, M. Song, B. Zhang, B. Zhang, React Funct Polym 66 (2006) 1734

[30] J.L. Suárez-Rodríguez, M.E. Díaz-García, Ana.l Chim. Acta 405 (2000) 67

[31] W.Z. Xia, W.D. Cook, Polymer 44 (2003) 79

[32] C. Yu, K. Mosbach, J. Chromatogr. A 888 (2000) 63

[33] C. Michailof, P. Manesiotis, C. Panayiotou, J. Chromatogr. A 1182 (2008) 25

[34] A. Ellwanger, C. Berggren, S. Bayoudh, C. Crecenzi, L. Karlsson, P.K. Owens, K. Ensing, P. Cormack, D. Sherrington, B. Sellergren, Analyst 126(6) (2001) 784.

SELECTIVE REMOVAL OF ATP DEGRADATION PRODUCTS FROM FOOD MATRICES II: RAPID SCREENING OF HYPOXANTHINE AND INOSINE BY MOLECULARLY IMPRINTED MATRIX SOLID-PHASE DISPERSION FOR EVALUATION OF FISH FRESHNESS

M.C. Cela-Pérez[1], L. Barbosa-Pereira[2],
X. Vecino[2], M. Pérez-Ameneiro[2],
Aurora Lasagabaster Latorre[1,3], J.M. López-Vilariño[1],
M.V. González Rodríguez[1], A.B. Moldes[2], J.M. Cruz[2]

[1] Grupo de Polímeros, Centro de Investigaciones Tecnológicas (CIT), Departamento de Física, Escuela Universitaria Politécnica, Universidad de A Coruña (UDC), Campus de Ferrol, 15471 Ferrol, Spain, Tel: +34 981 337 400 3051/3485, Fax: +34 981 337 416, email: victoria.gonzalez.rodriguez@udc.es

[2] Departamento de Ingeniería Química, Escuela de Ingeniería Industrial (EEI), Universidad de de Vigo, Campus As Lagoas, Marcosende 36310, Vigo-Pontevedra-Spain

[3] Dpto Química Orgánica I, Facultad de Óptica y Optometría, Universidad Complutense de Madrid, Arcos de Jalón nº 118, Madrid 28037, Spain

ABSTRACT

A water compatible molecularly imprinted polymer (MIP), synthesized using theophylline (TPH) as dummy-template and acrylamide (AM) as functional monomer, has been employed as supporting material in matrix solid-phase dispersion combined with ultra performance liquid chromatography-photodiode array detection (MSPD-UPLC-PDA) for selective determination of adenosine triphosphate (ATP) derivatives in fish samples. ATP degradation products are used as freshness index for assessment of fish quality. The solid sample was directly blended with MIP in MSPD procedure resulting in sample disruption and subsequent adsorption of the compounds on the MIP. By using *n*-hexane and ammonium hydroxide aqueous solution at pH 9 as the washing and elution solvent, respectively, satisfactory recoveries and clean chromatograms have been obtained. Good linearity for hypoxanthine (HYP) and inosine (INO) has been observed with correlation coefficients (R^2) of 0.9987 and 0.9986, respectively. The recoveries of the two ATP derivatives at three different spiked levels ranged from 106.5% to 113.4% for HYP and from 103.1% to 111.2% for INO, with average relative standard deviations lower than 4.2% in both cases. This new method, which is rapid, simple and sensitive, can be used as an alternative tool to conventional tedious methods.

Keywords: *molecularly imprinted polymer, matrix solid-phase dispersion, freshness, fish samples, hypoxanthine, inosine.*

1. INTRODUCTION

A large number of post-mortem reactions are initiated in fish (glycolysis, proteolysis and lipolysis) immediately after the animal is slaughtered, affecting its quality and freshness conditions. One of the most important changes consists of the formation of nucleotide and nucleoside metabolites resulting from ATP degradation [1]. ATP degradation to ADP (adenosine diphosphate) and AMP (adenosine monophosphate) takes place rapidly, with the subsequent accumulation of IMP (inosine 5′-monophosphate) [2]. The IMP is hydrolysed by autolytic enzymes ′(5′-nucleotidase) to inosine (INO), which, in turn, is degraded to hypoxanthine (HYP) by autolytic and/or microbial action (nucleoside phosphorylase) [3-4]. Next, HYP will be oxidized to xanthine (XAN) and then to uric acid (UA) through a much slower reaction, due to xanthine oxidase (XO) in case of spoilage by microorganisms [5-7].

The pathway of ATP catabolism as a degradative sequence has been widely studied in different fish species [7-12] besides beef [13-14], chicken [15-16] or pork meat [2-3, 17-19] and some of the above mentioned nucleotide metabolites have been proposed as freshness indexes in quality assessment [18-19]. Several analytical methods such as electrophoresis [20-21], radioimmunoassay [22], nuclear magnetic resonance spectroscopy (NMR) [23] or amperometric and voltamperometric methods [24] have been reported for quantitative determination of these compounds. Besides, in recent years, the use of biosensors has been

introduced as an alternative [15]. In particular, a significant number of biosensors have been designed based on the enzymatic reaction catalysed by the XO [25-26]. However these XO based biosensors have some common drawbacks such as poor stability, non-reusability, slow electron transfer and complexity of immobilization. Conversely, versatility, short analytical time and high resolution have made high performance liquid chromatography (HPLC) the most widely used technique for the analysis of nucleotides and nucleosides in biological samples [7, 27-28].

Prior to HPLC determination, a sample preparation process is needed which is really the critical step of the whole analytical process. It should remove potential interferences, pre-concentrate analytes and sometimes, convert them into a suitable form for determination or separation. More to the point, it must provide a robust and reproducible method, independent of variations in the matrix sample. Nowadays, it is also very important to reduce the initial sample size, improve the selectivity of the extraction process, minimize the use of organic solvents and facilitate the automation of the procedure [29]. Solid-phase extraction (SPE) is probably the most widely used technique of sample preparation today, but sample matrix interferences co-elute with the analytes of interest due to the lack of selectivity of common sorbents used; hence, subsequent clean-up steps are required. The use of molecularly imprinted polymers (MIPs) as selective sorbent materials in SPE (MISPE) avoids this problem. MIPs allow analyte pre-concentration and elimination of sample interferences [29-30] in a single step, since they are synthetic materials with artificially

generated recognition sites able to rebind a target molecule specifically, even in preference to other closely-related compounds [31-32].

As a general rule for tissue samples, an exhaustive treatment is always required before SPE. The tissue is usually homogenized and centrifuged and only the extract is passed through the MISPE cartridge. However, cell disruption is often incomplete. By contrast, molecularly imprinted matrix solid-phase dispersion (MIP-MSPD) performs simultaneous disruption, extraction and clean-up of solid, semi-solid and highly viscous samples [33-36]. Furthermore, the complete sample disruption and dispersal onto MIP particles occurs, providing an enhanced surface area for subsequent extraction step. MIP-MSPD is less time consuming and manual-intensive as well as more eco-compatible than MISPE. Experimentally, the sample is placed in a glass mortar and blended with the sorbent until complete disruption and dispersion of the sample on the solid support is attained. Then, the mixture is directly packed into an empty cartridge and analytes are eluted after a proper washing step to remove interfering compounds.

This work represents the first attempt to use MIPs as MSPD sorbent to develop a new MIP-MSPD-UPLC-PDA method for the selective extraction and determination of ATP related compounds in fish samples. Besides, it is well known that IMP contributes to the pleasant flavor of fresh fish and its degradation to INO and then to HYP is responsible for the progressive loss of the desirable flavor and the development of the stinking fishy smell [37-38]. In addition, it is accepted that HYP is accumulated owing to INO rapid

degradation to HYP and its subsequent slow transformation into XAN and UA by xanthine oxidase [17-18]. Thus, HYP has been chosen to determine the freshness of fish.

2. EXPERIMENTAL

2.1. MATERIAL

Theophylline (TPH), INO, XAN, UA and trifluoroacetic acid (TFA) were obtained from Sigma–Aldrich (Steinheim, Germany). Acrylamide (AM), ethylene glycol dimethacrylate (EGDMA), 2,2-azobisisobutyronitrile (AIBN) and ammonium hydroxide solution (25% in water) were supplied from Fluka (Buchs, Switzerland). Ethanol (EtOH), Methanol (MeOH) and hexane were obtained from Merck (Darmstadt, Germany), chloroform ($CHCl_3$) was from Scharlab (Barcelona, Spain) and acetic acid glacial (AcOH) from Panreac (Barcelona, Spain). HYP was purchased from ACROS organics (Geel, Belgium). Water used in the experiments was purified using a Milli Q Ultrapure water-purification system (Millipore, Bedford, MA, USA).

2.2. UPLC-PDA ANALYSIS

UPLC analyses were performed using an Acquity system from Waters (Milford, MA, USA) with gradient pump and automatic injector. Chromatographic experiments were carried out using a stainless steel column Acquity UPLC^{TM} BEH C_{18}, 2.1 x 50 mm, 1.7 μm (apt to work in a 1-12 pH range, at temperatures between 20 and 90ºC, and capable of

operating at pressures up to 15000 psi). Detection was carried out using a photodiode array detector (PDA) set in the range of 200 - 400 nm. Output signals were monitored and integrated using a personal computer operated under the Empower 2 software (Waters). Wavelength of 250 nm for HYP analysis was selected as output PDA signals. A two solvent gradient elution was performed, with flow rate of 0.5 mL min^{-1} and injection volume of 3 µL. The mobile phase consisted of aqueous TFA (A) (0.1% TFA in deionized water, pH 2.2, v/v) and MeOH (B) gradient [39]. The gradient elution profile starts at 99% of A, was linearly increased to 70% of A in 0.70 min and then brought back to the initial conditions at 1 min.

2.3. PREPARATION OF THE MOLECULARLY IMPRINTED POLYMER

The MIP having HYP recognition sites was prepared according to a previous work performed by our research group by non-covalent precipitation polymerization. The MIP has already been fully characterized [40]. TPH as dummy-template molecule (1 mmol) was dissolved in 60 mL of chloroform and subsequently, 4 mmol of AM as functional monomer was mixed until homogenization. Next, 20 mmol of EGDMA as cross-linker monomer was added to the mixture, followed by 0.5 mmol of the initiator of the polymerization, AIBN.

The pre-polymerization mixture was degassed in a sonicating bath and purged with nitrogen for 5 min. Polymerization took place in a water bath

at 60ºC for 24 h. The final polymer was dried at 40ºC. TPH was removed by Soxhlet extraction with MeOH for 48 h. The complete removal of TPH from the MIP was assessed via UPLC-PDA method. A non-imprinted polymer (NIP) was similarly prepared excluding TPH from the pre-polymerization media.

2.4. BINDING EVALUATION OF TPH-AM-EDMA-MIP

Batch binding assays were carried out for evaluation of the MIPs molecular recognition behavior. Taking into account the fact that these MIPs will be used to extract HYP from fish samples, the solvent for batch rebinding assays was selected according to community legislation [41], which establishes water: EtOH (9:1) as simulant for fresh, cooled, processed salted or smoked fish.

Pre-weighed amounts (0.2 g) of cleaned MIPs were placed into glasses for 5 min incubation in ultrasonic bath at room temperature with eight water:EtOH (9:1) solutions (4 mL) of HYP (from 5.25 to 1009 µg mL^{-1}). After incubation, supernatants were removed by filtration and analyzed by UPLC-PDA at 250 nm to determine HYP residual concentrations, C (µmol L^{-1}). HYP adsorbed concentrations, q (µmol g^{-1} or µg g^{-1}), were calculated by subtracting C from the initial concentrations of HYP. Batch binding experiments were done in a similar way with blank polymers.

The specificity of the polymer was then estimated by the imprinting factor (*IF*) $IF = K_{pMIP}/K_{pNIP}$, where K_{pMIP} is the partition coefficient of a compound

on the imprinted polymer and K_{pNIP} is the partition coefficient of the same compound on the non-imprinted polymer. The partition coefficient is defined as the ratio of the amount of HYP bound to the polymer (q, µmol g^{-1}) relative to the concentration of free HYP (C, µmol L^{-1}). This normalization method removes binding due to non-specific interactions [42-43].

To further investigate the imprinting effect and determine the binding properties (adsorption capacity, binding constants etc.) several binding models such as the discrete Langmuir and bi-Langmuir models and the continuous Freundlich isotherm model (FI), were applied to fit the equilibrium data. The model with the highest degree of correlation was finally chosen [43-44].

2.4.1. *Swelling*

To further explain rebinding behaviour MIP and NIP swelling was conducted in the binding solvent water:EtOH (9:1) for comparison with results in ACN: water 4:1 (v:v) and CHCl$_3$, performed in a previous work [40]. The experimental procedure is similar to that described by Sellergren and Shea [45]. Dry polymer ($\cong$ 0.20-0.30 mL) was placed in a 1 mL graduated test tube. Excess solvent was then added to the tube and the polymer sonicated in order to remove air bubbles. The tube was closed and left to stand for 24 h at room temperature. Excess solvent was then removed and final volumes recorded. The swelling ratio was given as volume of the swollen polymer to volume of dry polymer. The average values of triplicate independent results were obtained.

2.5. SELECTIVITY EVALUATION OF TPH-AM-EDMA-MIP

Additional batch binding assays were performed to test selectivity of the MIP towards other ATP degradation products such as INO, XAN and UA. Individual solutions of INO (from 5.000 to 1,000 µg mL^{-1}), XAN and UA (from 5.000 to 400.0 µg mL^{-1}) in water: EtOH (9:1) were employed for individual selectivity analysis and mixture solutions (from 5.000 to 400.0 µg mL^{-1}) were used in competitive assays for cross-selectivity evaluation. These concentration ranges have been selected according to solubility properties. The above mentioned binding isotherm models were also applied to determine the selectivity properties. The specific selectivity factor (*SF*) was calculated taking the ratio of imprinting factors, $SF = IF_1/IF_2$ where *IF$_1$* and *IF$_2$* are the imprinting factors for two different substrates [42- 44].

2.6. MSPD PROCEDURE

The schematic procedure of the MIP-MSPD-UPLC-PDA is shown in Fig. 1. An aliquot of 0.2 g of fish meat and 0.4 g of MIP sorbent (1:2) were placed in a small porcelain mortar and blended together until a homogeneous mixture was obtained. Then, the mixture was loaded into a SPE cartridge (6 mL pre-fritted, 20 µm porosity, polypropylene tubes) which was pre-packed with 0.05 g of cleaned MIP and the column was connected to a Visiprep^{TM}-DL Solid Phase Extraction Vacuum Manifolds, equipped with integral flow control valves and disposable Teflon® flow control valve liners

(SUPELCO, Bellefonte, PA, USA). The cartridge was rinsed with 2 mL of hexane, the eluent was evaporated to dryness under vacuum at room temperature and the residues were re-dissolved in 2 mL of Milli Q water for further UPLC-PDA analysis. Subsequently, the cartridge was eluted with 4 mL of ammonium hydroxide solution (5.55×10^{-6} M, pH 9) and the basic eluent was directly carried to UPLC-PDA for HYP determination.
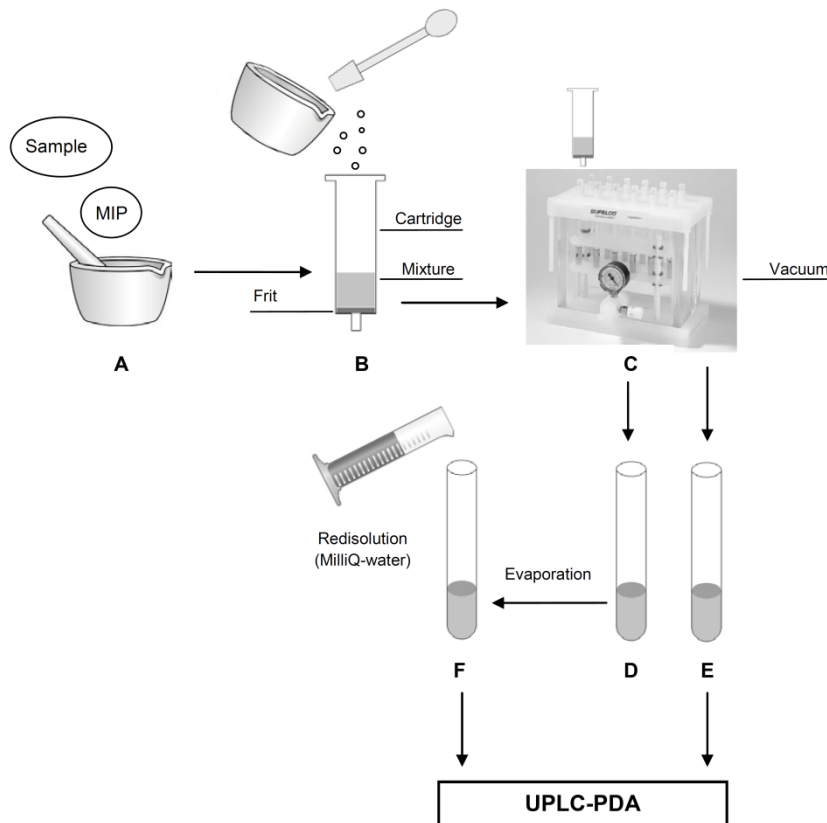
Fig. 1. Schematic procedure of MIP–MSPD: (A)sample-MIP sorbent blending, (B) transfer blend to cartridge, (C) washing and elution under vacuum, (D) washing eluate (hexane) to be evaporated, (E) redisolution of D in Milli-Q water and (F) basic extraction eluate containing the ATP derivatives

3. RESULTS AND DISCUSSION

3.1. RECOGNITION PROPERTIES OF THE TPH-AM-EDMA-MIP

Fig. 2(a) compares the adsorption isotherm of HYP on MIP and NIP. Batch concentrations and binding amounts have been plotted as the abscissa and ordinate, respectively. A different behavior is observed for MIP and NIP. While the amount of HYP bound to the MIP at equilibrium rinsed gradually with concentration, a saturation level was reached for NIP at the fourth concentration assayed. The MIP capacity for template concentration studied in this work (until 1000 µg mL^{-1}), was nearly 3,500 µg g^{-1}, which is in the range of other MIPs prepared by non-covalent imprinting [46-47], whereas the corresponding NIP value lied below 1,500 µg g^{-1}. These data suggest a molecular imprinting effect [48].

The *IF* values > 1 confirmed the conclusion explained in the preceding paragraph. The average *IF* ($\overline{IF}$) was 2.25, although some variability was observed throughout the concentration range; the maximum value of 6.82 was found for the first concentration tested (5.246 µg mL^{-1}).

The equilibrium data fitted well the FI model as evidenced by the relatively good fit to linear regression analysis (R^2≥ 0.9) (Table 1). Fig. 2(b) depicts the FI in logK-logN format. The most visible difference between MIP and NIP is the higher capacity of the former within the measured concentration window. This can be seen in the higher positioning of the MIP line. This qualitative assessment was confirmed by the parameters calculated from

the FI model which are summarized in Table 1. The MIP binding capacity value (N_{K1-K8}) was 368.3 µg g^{-1} or 2.706 µmol g^{-1} which was about 100-fold the corresponding N_{NIP} value (3.811 µg g^{-1} or 0.028 µmol g^{-1}). Furthermore, the average affinity of binding sites ($\bar{K}_{K1-K8}$) for the MIP (7.95 x 10^2 M^{-1}) was 2.5 times higher than the NIP value (3.16 x 10^2 M^{-1}).

The range of binding affinity was constrained within the limits of the analytical window (K_{min}-K_{max}) in Fig. 2 (c). The graph shows the relationship between the fraction of binding sites (N, µmol g^{-1}) and the affinity constants in log format (*logK*, M^{-1}). The control polymer had very few binding sites distributed throughout the entire affinity range compared with MIP, although the latter had numerous low affinity binding sites and a few high affinity binding sites.

In fact, reasonably good binding parameter values have been achieved for HYP on the MIP in aqueous solvent. Nonetheless, these values are lower than those obtained in ACN: water (4:1 v/v) [40], owing to the fact that the rebinding to MIPs is strongly dependent on the solvent. The solvent can affect rebinding in two ways. First of all, molecular recognition with the MIP in solvents of low to medium polarity is mainly driven by H-bonding [49]. When increasing the aqueous content in the rebinding solvent, polar templates such as HYP are less retained on MIPs due to the entropy driven hydrophobic effect.
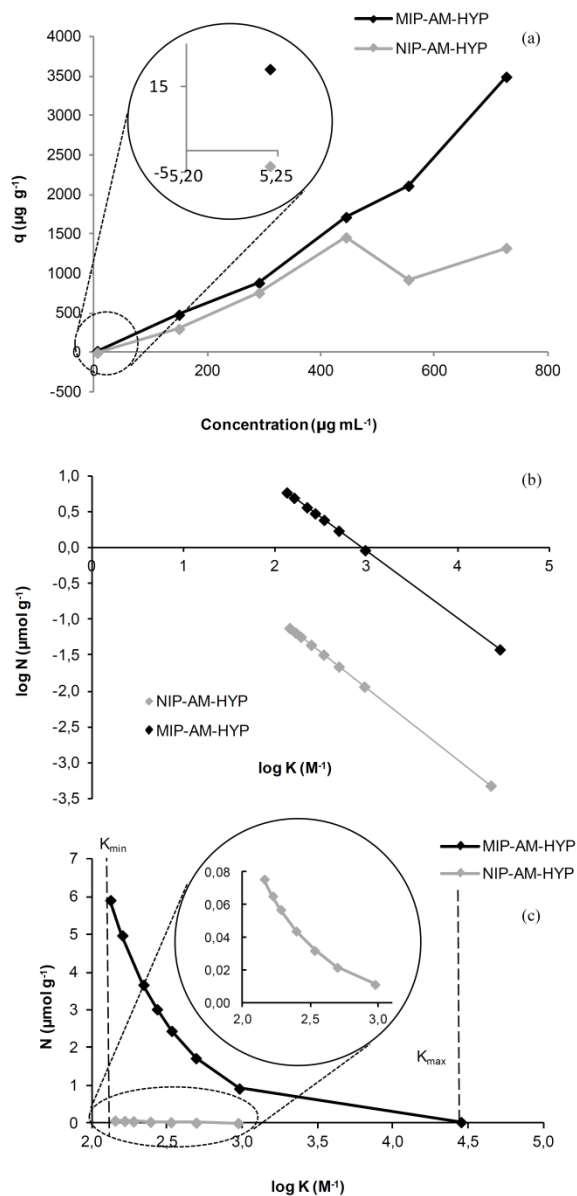
Fig. 2. (a) Adsorption isotherm of HYP on MIP and NIP in the range 5.246–726.3 mg mL-1, (b) fitting plots of MIP and NIP with the Freundlich isotherm model, and (c) binding affinity distribution for MIP and NIP within the analytical window derived from the fitting parameters of the Freundlich equation.

Table 1. Isotherm parameters for HYP on MIP and NIP estimated by fitting data to the Freundlich isotherm model.

Compound	Polymer	Relative coefficient (R^2)	m	N_{K1-K8} (μmol g^{-1})	$\bar{K}_{K1-K8}$ (M^{-1})
HYP	**MIP**	0.956	0.940	2.706	7.95E02
	NIP	0.854	0.999	0.028	3.16E02
Ratio MIP/NIP				**96.9**	**2.51**

Secondly, a solvent induced swelling/shrinking process can affect the shape of the cavity and the distance between functional groups and due to this, MIP can lose its specificity when exposed to the "wrong conditions" [50]. MIP and NIP swell in water: EtOH (9:1) but to a lesser extent than in ACN: water (4:1 v/v) and the porogen, CHCl$_3$ (MIP swelling ratios are: 2.2± 0.1, 4.2± 0.7 and 7.9± 0.1 and NIP swelling ratios are: 2.8± 0.1, 5.1± 0.1 and 8.4± 0.8 in water: EtOH (9:1), ACN: water (4:1 v/v) and CHCl$_3$, respectively) [40].

Anyway, the observed relatively good behavior of the MIP for HYP in aqueous media is mainly attributed to the following two reasons: 1) the addition of a certain amount of organic solvent (10% ethanol) into the pure aqueous solutions of the template and 2) the election of a highly polar functional monomer such as AM, instead of the more usual MAA, which increases the MIP´s surface hydrophilicity. AM is more soluble in water, 2,150 g·L^{-1} compared to 89 g·L^{-1} for acrylic acid, and forms stronger hydrogen-bonds in polar protic solvents than acrylic acid. Both strategies reduce the hydrophobically driven nonspecific bindings of the MIP, thus

leading to its water compatibility despite the lower swelling compared to porogen [51-53]

3.2. SELECTIVITY PROPERTIES

3.2.1. Individual selectivity properties

To measure the selective recognition of HYP, the separate binding of competitive compounds was performed in the first place. Fig. 3(a) exhibits the FI isotherms in log format for visual comparison of the binding capabilities of INO, XAN and UA. The log K-log N FI isotherm obtained for HYP was overlaid for comparison. Strikingly, the highest position in the graph was occupied by the bulky INO molecule, followed by HYP and XAN, which crossed each other, which are in turn over UA. Furthermore, the most important binding parameters determined by the FI model are compiled in Table 2. The data confirm the greater binding capacity (N_{K1-K8}) for INO (508.8 µg g^{-1} or 1.897 µmol g^{-1}) and HYP (368.3 µg g^{-1} or 2.706 µmol g^{-1}) (Table 1) in relation to XAN (119.9 µg g^{-1} or 0.788 µmol g^{-1}) and UA (89.26 µg g^{-1} or 0.531 µmol g^{-1}. According to the FI model, the average affinity of binding sites ($\bar{K}_{K1-K8}$) for INO was about 4-fold higher in the MIP (2.50 x 10^3 M^{-1}) than in the NIP (6.18 x 10^2 M^{-1}) and thrice the value calculated for HYP (7.95 x 10^2 M^{-1}).

Moreover, a high similar average *IF* has been achieved for INO, $\overline{IF}$ = 2.20, compared to and HYP ($\overline{IF}$ = 2.25); again the highest *IF$_{max}$* = 9.51 was obtained for the lowest INO concentration tested. Hence, it can be

345

concluded that the MIP are appropriate to determine INO in addition to HYP, within the range of concentrations studied.

Regarding XAN, the corresponding affinity constant value ($\bar{K}_{K1-K6}$ =2.47 x 10^3 M^{-1}) was higher than the value calculated for HYP, although the number of binding sites decreased 3-fold. Moreover, the average imprinting factor ($\overline{IF}$ = 1.85) is $\cong$ 1.5-fold lower than HYP. The highest *IF* values for XAN are also encountered at the lowest concentration assayed (IF_{max}= 6.13), although the *IF* was below 1 for higher amounts of XAN, indicating unspecific adsorption. These data reveal that the MIP could also be used to determine XAN in fish samples, provided that the amount of XAN in the sample is $\leq$ 5 µg mL^{-1}. On the contrary, the results obtained for UA show a MIP binding capacity and affinity constant quite lower than the NIP values. In coherence with this, the corresponding imprinting factors are the smallest and close to unity ($\overline{IF}$ = 1.10). Furthermore, no adsorption of UA was observed at the lowest concentration tested (400.0 µg mL^{-1}). Thus, the MIP is less suitable to determine the last ATP derivative in aqueous media.

From another point of view, the average selectivity factors ($\overline{SF}$) for HYP in relation to INO, XAN and UA were 0.969, 1.45 and 2.99 respectively. These $\overline{SF}$ values were calculated considering the $\overline{IF}$ of the three lowest concentration studied for HYP and INO to avoid false interpretations of relative selectivity (since the assays were carried out for HYP and INO from 5.000 to 1000 µg mL^{-1} and for XAN and UA from 5.000 to 400.0 µg mL^{-1}).

Furthermore, SF_{max} at the lowest concentration assayed ($\cong$ 5 µg mL^{-1}) were 0.717 (INO), 1.11 (XAN) and 6.40 (UA). These results corroborate the highest selectivity of the MIP for INO followed by HYP, XAN and UA in agreement with the conclusions extracted from Fig 3(a) and Tables 1 and 2.

Table 2. Individual selectivity parameters for INO, XAN and UA on MIP and NIP estimated by fitting data to the Freundlich isotherm model.

Compound	Polymer	Relative coefficient (R²)	m	N_{K1-K8} (µmol g^{-1})	$\bar{K}_{K1-K8}$ (M^{-1})
INO	**MIP**	0.996	0.875	1.897	2.50E+3
	NIP	0.904	0.834	1.576	6.18E+2
	Ratio MIP/NIP			**1.20**	**4.04**
XAN	**MIP**	0.978	0.736	0.788	2.47E+3
	NIP	0.805	0.884	0.545	1.63E+3
	Ratio MIP/NIP			**1.45**	**1.51**
UA	**MIP**	0.825	0.877	0.531	2.14E+3
	NIP	0.874	0.461	1.850	3.17E+3
	Ratio MIP/NIP			0.29	0.67

In summary, both swelling and selectivity studies suggest that shape selectivity is not the dominant mechanism for molecular recognition. First of all, among the different ATP derivatives assayed, the highest binding affinity is found for INO which has different shape and greater size than the dummy template, TPH; consequently, it would experience steric exclusion in the high affinity binding cavities. Secondly, as stated in section 3.1 the MIP is a non-porous matrix gel which swells in water but only a quarter the value reached in the porogen.
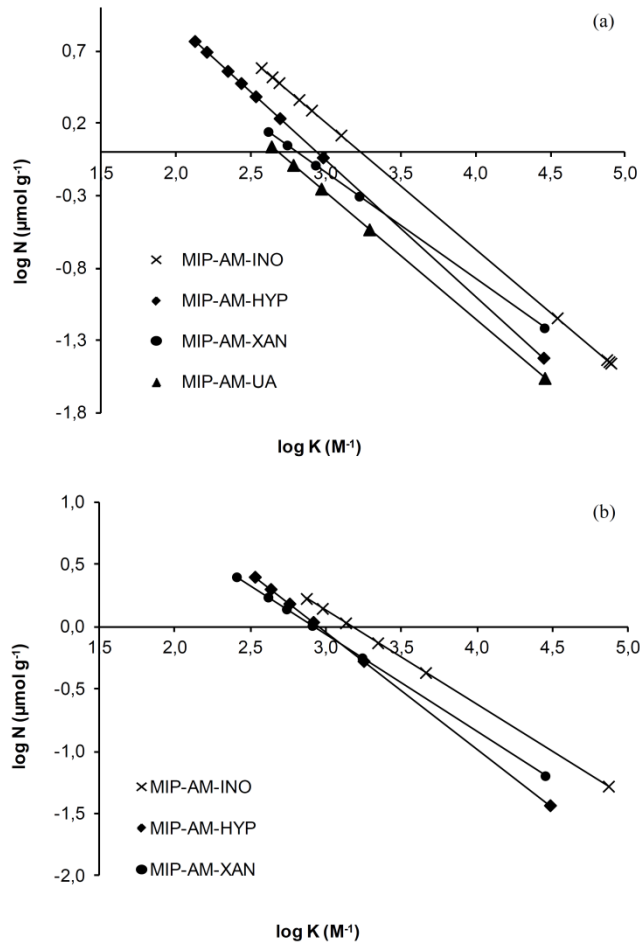
Fig. 3. (a) Individual selectivity log–log Freundlich isotherms of HYP, INO, XAN, UA on MIP and (b) cross-selectivity log–log Freundlich isotherms of HYP, INO and XAN on MIP.

Conversely, as discussed by Simon et al. [54] pre-organization of functional groups may dominate the performance of MIPs designed for analytes with three or more functional groups capable of hydrogen bonding interaction with the functional monomer. Thus, the MIP may not require an exact recreation of the shape and distance parameters for binding ATP

derivatives due to the presence of 2 to 4 H-donor groups and 3 H-acceptor groups per analyte molecule, besides abundance of low affinity binding sites within the MIP. On the other hand, the MIP- analyte interaction seems to diminish upon increasing the number of carbonyl (C=O) groups either in the pyrimidine ring or imidazole ring of the ATP derivatives, whereas the extra three OH groups of INO may promote adsorption despite the larger size of the molecule.

3.2.2. Cross-selectivity properties

The performance of the MIP was evaluated in the presence of a mixture of INO, HYP and XAN as ATP degradation compounds to estimate its applicability in real samples. UA was not included in cross-selectivity studies due to the poor adsorption observed in individual selectivity analysis. Fig. 3 (b) shows the FI in log K-log N format for cross-selectivity experiments. Apparently the plot is similar to the one described in Fig 3 (a) for individual selectivity assays: the INO line lies above the HYP and XAN lines which crossed each other. Nonetheless, the *IF* values differ from the individual selectivity assays. The average imprinting factor for HYP (2.06) was higher than for INO (1.32), while the IF_{max} was 5.88 and 2.37 for HYP and INO respectively. Accordingly, the average *SF* value for HYP related to INO was 1.56, although the SF_{max} increased up to 3.92 at the lowest concentration studied. Concerning XAN, the IF_{max} was 4.70 for the lowest concentration tested with a corresponding *SF* compared to HYP of 1.25, however, the *IF* was below 1 for higher amounts of XAN, indicating

unspecific adsorption. In short, according to cross-selectivity studies, the MIP can be used as sorbent in MSPD procedure to determine HYP and INO in fish samples, since the MIP had demonstrated its efficiency to discriminate and pre-concentrate these compounds among all the ATP derivatives.

3.3. OPTIMIZATION OF THE MIP-MSPD PROCEDURE

The influence of several parameters, such as the ratio of sample to MIP sorbent, the pH of the sorption process, the washing solvent or the elution solvent, on MIP-MSPD efficiency was investigated. A suitable sample/sorbent ratio in MSPD process could increase the interface area between the analytes and sorbent and allow complete sorption of the sample components to facilitate their transfer into sorbent. In the same way, the sequence and design of an elution profile should strive to retain the target analytes on the MIP with a high degree of specificity, while removing the sample matrix interferences as much as possible. Moreover, the MIP pre-packed in the bottom of the cartridge could act as MSPD sorbent for further removing interfering matrix components and isolate analytes to perform high recoveries [55].

3.3.1. Optimization of sample/sorbent ratio

Ratios of sample to sorbent typically range from 1:1 to 1:4, since higher or lower ratios often lead to lower recoveries because the packing material in the cartridge is more heterogeneous [56-62]. Therefore, ratios of

sample/sorbent ranging from 1:1 to 1:3 were evaluated. Recoveries (*R*) increased from 50 to 100% upon increasing the sample: sorbent ratio from 1:1 to 1:2 (ΔR $\sim$ 50%), then remained constant within experimental error. Accordingly, 1:2 was applied as optimum sample/sorbent ratio in the subsequent studies in order to obtain the best recoveries with the lowest polymer consumption.

3.3.2. *Optimization of sorption process*

pH is an important factor in the sorption process, because pH not only affects the properties of the sorbent surface, but also influences the target analyte speciation in solution and the extent of dissociation of functional groups on the actives sites of the sorbent [63].

HYP is a purine with pK_a values of pK_1= 1.79-1.90 for N_7, pK_2= 8.70-8.91 for the amine group close to carbonyl group and pK_3= 10.27-12.07 for the amine group at 9 position of the purine at 25ºC (the atoms in the purines are named from 1 to 9 following conventional nomenclature rules) [64]. Under strong acidic conditions (pH< 2), N_7 wins one H^+ and HYP^+ becomes the main form while at alkaline pH, HYP is present predominantly in the dissociated forms HYP^- and HYP^{2-}. The prevalence of HYP charged forms decreases the molecular recognition at the imprinting sites, reducing the sorption efficiency. Thus, the pH of the sorption step should be adjusted to neutral or slightly acidic conditions to promote extraction of neutral HYP. Moreover, these pH conditions are close to the isoelectric point (*IP*) of HYP ($\cong$ 5) [65]; at this pH value HYP does not have any electrical charge and

maximum sorption may be expected. On the other hand, only at the strongest acidic conditions (pH<1), acrylamide turns into AM^+ (the carbonyl oxygen is protonated) [66] within the MIP. Under these pH conditions, HYP and AM are positively charged and electrostatic repulsive interaction between HYP and MIP occurs, leading to a decrease in molecular recognition.

To prove the influence of pH on the sorption process, HYP solutions (182.5 µg mL^{-1}) in water: ethanol (9:1) were prepared at pH values spanning from 2 to 8 by addition of hydrochloric acid or sodium hydroxide solutions; then, sorption experiments were carried out following an experimental procedure similar to batch binding. According to the preceding paragraph, quantitative sorption was obtained at pH $\geq$ 5 (Fig. 4(a)). At slightly acidic and neutral conditions hydrogen bonding between the analyte and AM is maximized, whereas ionic interactions are not significant. Therefore, pH values ranging between 5 and 8 are considered the optimum pH conditions for the MSPD procedure to achieve the highest sorption capacity, conditions which are already found in fish meat.
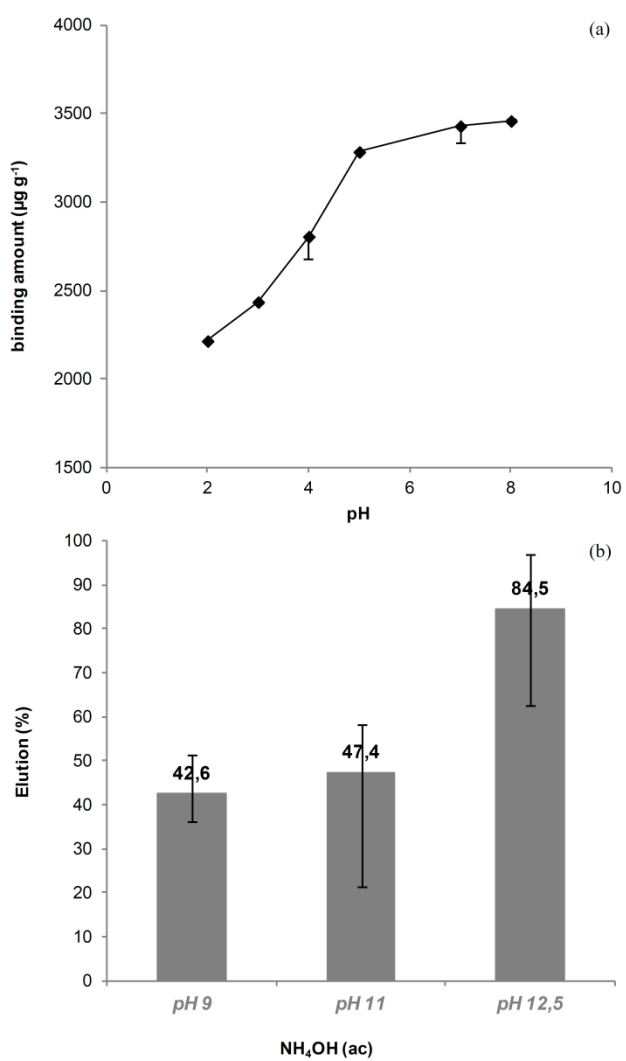
Fig. 4. (a) Sorption of HYP on MIP as function of pH (MIP dose: 0.2 g, solution volume: 4 mL, US contact time: 5 min, room temperature), (b) Influence of the elution solvents (4 mL) on the % HYP recovered

3.3.3. Optimization of the clean-up procedure

It is generally recommended to use a solvent in the washing step as similar as possible to the nature of the sample [59]. Nonetheless, the ATP derivatives are highly water-soluble compounds and the use of the aqueous mixture, proposed as sample stimulant, probably elutes a significant portion of HYP retained in the MIP at this stage. Consequently, different washing solvents were investigated in order to remove the non-polar fraction, containing fats and other less polar compounds present in fish samples, and promote total retention of the analyte within the MIP. The solvents assayed are in increasing order of polarity: *n*-hexane, dicloromethane, the mixture *n*-hexane: dichloromethane (1:1) and acetonitrile.

Despite the fact that pH 12.5 lead to optimal elution conditions, several practical drawbacks on the application of MIP-MSPD procedure to real samples makes pH 9 the best option for final application.

From another point of view, the volume of the elution solvent loaded on the cartridge affects the recovery of HYP: small volumes lead to incomplete elution whereas excessive volumes would require a longer dryness step. After several trials, 4 mL was found to be the optimum volume. In fact, this volume of elution solvent is frequently used in MSPD procedure.

3.4. VALIDATION OF THE MIP-MSPD-UPLC-PDA METHOD

To validate the procedure, two methods of quantitative evaluation of the analysis were compared by statistical treatment and direct comparison: external calibration and standard additions [67]. External calibration curves were plotted for HYP and INO with concentration ranging from 0.05 to 25 µg mL^{-1} and standard addition curves were plotted preparing duplicate base ´zero` samples and standard addition samples from 10.00 to 40.00 µg mL^{-1}. Statistical treatment applying the t-test for the slopes of the calibration curves has shown matrix effect for both compounds in fish samples. The use of the method of standard additions for the quantification of these compounds in the studied samples was thus preferred.

This MIP-MSPD-UPLC-PDA method was validated in terms of linearity, limits of detection (LOD), limits of quantification (LOQ) and precision under the selected optimum conditions. The linearity of the method was tested for HYP and INO, since selectivity experiments demonstrated that the MIP is suitable to determine both compounds. Calibration curves were constructed by performing the linear regression analysis using the chromatographic peak areas measured at three increasing spiked levels in a range of 10.00-40.00 µg mL^{-1}. This range was selected according to the ATP derivatives levels in hake samples [68-69]. The results showed good linearity for the analytes with correlation coefficients of 0.9987 for HYP and 0.9986 for INO. Detection and quantification limits were calculated according to a procedure described by Shabir [70] using the calibration

graphs, being LOD=yB+3×SB and LOQ=yB+10×SB. Representing yB (blank signal) = a (intercept of the calibration graph) and SB (standard deviation of the blank) = Sy/x. Relative standard deviations (RSDs) were evaluated by performing replicate analysis of the middle spiked level (20 µg mL^{-1}) (Table 3).

Table 3. Features of the MIP-MSPD-UPLC-PDA method (n = 5).

Analytes	Regression equation	R^2	LOD (µg mL^{-1})	LOQ (µg mL^{-1})	RSD (%)
HYP	*y* = 84.29 *x* + 6.59E02.	0.9987	1.702	5.672	0.8
INO	y = 47.83 x + 4.82E02	0.9986	1.785	5.950	0.7

Precision was calculated in terms of intra-day repeatability and inter-day reproducibility. The intra-day repeatability was performed by analyzing spiked fish samples five times in one day at three different fortified concentrations (10.00, 20.00 and 40.00 µg mL^{-1}) for HYP and INO. RSDs values lied between 0.84% and 7.50% for HYP and between 1.05% and 13.0% for INO. The inter-day reproducibility was performed similarly over three consecutive days and RSDs were in the range of 2.84-8.91% for HYP and 2.68-13.6 for INO.

3.5. ANALYSIS OF FISH SAMPLES

To evaluate the performance of the proposed MIP-MSPD-UPLC-PDA method, three commercial defrosted hake samples were pretreated under MIP-MSPD procedure. The results which are shown in Table 4 lie well above the quantification limit except for sample 1. Besides, INO values were

greater than those of HYP, according to the trend shown by most fish species studied in subsequent days after the capture [68-69].

Table 4. Contents of the nucleotides in hake samples (n = 3).

Hake sample	HYP µg mL^{-1}	INO µg mL^{-1}
1	D^a	D^a
2	12.55	13.34
3	7.821	10.08

^{a} Detectable but not quantifiable

Moreover, a recovery study was carried out to develop a more detailed analysis of the sample matrix effect by spiking three different levels of HYP and INO into the hake samples (10.00-40.00 µg mL^{-1}). High recoveries were obtained after MIP-MSPD pre-treatment. Recoveries ranged from 103.1% to 113.4% with an average RSD $\leq$ 4.2% in all cases (Table 5).

Table 5. Recoveries of the MIP-MSPD-UPLC-PDA method for spiked hake samples (n = 3).

Spiked level of the analytes	10.00 µg mL^{-1}		20.00 µg mL^{-1}		40.00 µg mL^{-1}	
	Recovery (%)	RSD (%)	Recovery (%)	RSD (%)	Recovery (%)	RSD (%)
HYP	113.4	4.0	110.9	2.2	106.5	1.5
INO	111.2	4.2	108.2	1.7	103.1	2.1

As a final point, endogenous interferences from the fish muscle were eluted out in the washing fraction so that clean chromatograms of both original and spiked samples were obtained at the end of the process, demonstrating the excellent purification ability and high affinity and selectivity of the MIP-MSPD protocol for HYP and INO; hence, it can be

potentially applied for the determination of these compounds in complicated bio-matrix samples (Fig. 5).
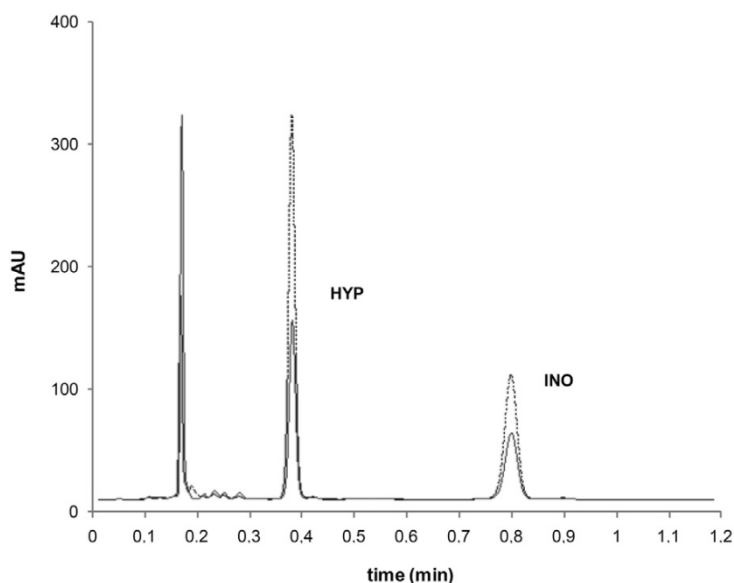
Fig. 5. Chromatograms of the hake samples (— hake sample — spiked hake sample) after the MIP-MSPD protocol

4. CONCLUSION

A novel, simple and reliable MIP-MSPD-UPLC-PDA method was developed for selective extraction and purification of HYP and INO ATP derivatives used as freshness index in fish samples. The method is based on the selective retention of HYP and INO (at pH near *IP* in neutral forms) in a polar sorbent (MIP), elimination of less polar interferences with *n*-hexane and selective elution of the analytes with NH$_4$OH aqueous solution at pH 9 (anionic forms). The method has been validated by analyzing three commercial defrosted hake samples at spiked levels of 10.00-40.00 µg mL$^-$

[1]. All recoveries were around 100% and RSD of repeatability and reproducibility were $\leq$ 4.2%.

The developed method combines the high affinity and selectivity of MIP technology with the simple, rapid and efficient sample pre-treatment of MSPD plus the highly effective separation of UPLC, to achieve a significant time reduction of the total analytical process. In addition to the analytical advantages, the method has other practical improvements over conventional methods of sample treatment, such as lower cost, lower consumption of organic solvents and simple instrumentation involved.

References

[1] L. Mora, A.S. Hernández-Cázares, M.C. Aristoy, F. Toldrá, Food Chem. 123 (2010) 1282

[2] N. Batlle, M.C. Aristoy, F. Toldrá, J. Food Sci. 65 (3) (2000) 413

[3] R. Tasai, R.G. Cassens, E.J. Briskey, M.L. Greaser, J. Food Sci. 37 (1972).612

[4] M.E. Surette, T.A. Gill, P.J. LeBlanc, J. Agr. Food Chem. 36 (1988) 19

[5] V. Venugopal, Biosens. Bioelectron. 17 (2002) 147

[6] A. Mulchandani, J.H.T. Luong, K.B. Male, Anal. Chim. Acta 221 (1989) 215

[7] M. T. Veciana-Nogues, M. Izquierdo-Pulido, M. C. Vidal-Carou, Food Chem. 59 (1997) 467

[8] L. Gil, J. M. Barat, E. Garcia-Breijo, J. Ibañez, R. Martínez-Máñez, J. Soto, E. Llobet, J. Brezmes, M.C. Aristoy, F. Toldrá, Sensor. Actuat. B 131 (2008) 362

[9] G. Volpe, M. Mascini, Talanta 43 (1996) 283

[10] D. Balladin, D. Narinesingh, V. Stoute, T. Ngo, Appl. Biochem. Biotech. 62 (1997) 317

[11] E. Watanabe, K. Ando, I. Karube, H. Matsuoka, S. Suzuki, J. Food Sci. 48 (1983) 496

[12] M.A. Carsol, G. Volpe, M. Mascini, Talanta 44 (1997) 2151

[13] Y. Yano, N. Miyaguchi, M. Watanabe, T. Nakamura, T. Youdou, J. Miyai, M. Numatab, Y. Asano, Food Res. Int. 28 (1995) 611

[14] Y. Yano, N. Kataho, M. Watanabe, T. Nakamura, Y. Asano, Food Chem. 52 (1995) 439

[15] A.T. Lawal, S.B. Adeloju, Talanta 100 (2012) 217

[16] R. Grau, A.J. Sánchez, J. Girón, E. Iborra, A. Fuentes, J.M. Barat, Food Res. Int. 44 (2011) 331

[17] A.S. Hernández-Cázares, M.C. Aristoy, F. Toldrá, Food Chem. 123 (2010) 949

[18] N. Batlle, M.C. Aristoy, F. Toldrá, J. Food Sci. 66 (2001) 68

[19] T.L. Scheffler, D.E. Gerrard, Meat Sci. 77 (2007) 7

[20] T. Richter, L.L. Shultz-Lockyear, R.D. Oleschuk, U. Bilitewski, D.J. Harrison, Sens. Actuators B 81 (2002) 369

[21] A.L. Nguyen, J.H.T. Luong, C. Masson, Anal. Chem. 62 (1990) 2490

[22] B. Roberts, B.A. Morris, M.N. Clifford, Food Chem. 42 (1991) 1

[23] G. Van den Thillart, A. Van Waarde, H.J. Muller, C. Erkelens, J. Lugtenburg, Comp. Biochem. Phys. 95B (1990) 789

[24] J. Pei, X.Y. Li, Anal. Chim. Acta 414 (2000) 205

[25] Y. Lui, N. Lo, W. Tao, S. Yao, Electroanal. 16 (2004) 1271

[26] H.S. Nakatani, L.V. Santos, C.P. Pelegrine, M. Gomes, M. Matsushita, N.E. Desouza, J.V. Visentainer, Am. J. Biochem. Biotechnol. 1 (2005) 85

[27] N. Cooper, R. Khosravan, C. Erdmann, J. Fiene, J.W. Lee, J. Chromatogr. B 837 (2006) 1

[28] M.L. Dornelles, K.L. Tatsuo, Food Chem. 77 (2002) 237

[29] A. Martín-Esteban, Trends Anal. Chem. 45 (2013) 169

[30] E. Caro, R.M. Marcé, F. Borrull, P.A.G. Cormack, D.C. Sherrington, Trends Anal. Chem. 25 (2006) 143

[31] N. Fontanals, R.M. Marcé, F. Borrull, J. Chromatogr. A 1152 (2007) 14

[32] F.G. Tamayo, E. Turiel, A. Martin-Esteban, J. Chromatogr. A 1152 (2007) 32

[33] S.A. Barker, J. Biochem. Biophys. Methods 70 (2007) 151

[34] E.M. Kristenson, L. Ramos, U.A.Th. Brinkman, Trends Anal. Chem. 25 (2006) 96

[35] S.A. Barker, J. Chromatogr. A 880 (2000) 63–68.

[36] S.A. Barker, J. Chromatogr. A 885 (2000) 115

[37] N.R. Jones, J. Murray, J. Sci. Food Agric. 13 (1962) 475

[38] M. Tikk, K. Tikk, M.A. Torngren, L. Meinert, M.D. Aaslyng, A.H. Karlsson, J. Agr. Food Chem. 54 (2006) 7769

[39] D. Farthing, D. Sica, T. Gehr, B. Wilson, I. Fakhry, T. Larus, C. Farthing, H.T. Karnes, J. Chromatogr. B 854 (2007) 158

[40] A. Lasagabaster-Latorre, M.C. Cela-Pérez, S. Fernández-Fernández, , J.M. López-Vilariño, M.V. González Rodríguez, React. Funct. Polym. 91-92 (2015) 51

[41] Commission Regulation (EU) Nº 10/2011 of 14 January 2011 on plastic materials and articles intended to come into contact with food Text with EEA relevance, Off. J. Eur. Communities 2011, L 12, 1.

[42] D.A. Spivak, Adv. Drug Deliv. Rev. 57 (2005) 1779

[43] M. Castro López, M.C. Cela Pérez, M.S. Dopico García, J.M. López Vilariño, M.V. González Rodríguez, L.F. Barral Losada, Anal. Chim. Acta 721 (2012) 68

[44] M.C. Cela-Pérez, M.M. Castro-López, A. Lasagabáster-Latorre, J.M. López-Vilariño, M.V. González-Rodríguez, L.F. Barral-Losada, Anal. Chim. Acta 706 (2011) 275

[45] B. Sellergren, K. J. Shea, J. Chromatogr. 635 (1993) 31

[46] S.V. Duy, I. Lefebvre-Tournier, V. Pichon, F. Hugon-Chapuis, J. Puy, C. Périgaud, J Chromatogr B 877 (2009) 1101

[47] N.S. Bibi, L. Galvis, M. Grasselli, M. Fernández-Lahore, Process Biochem. 47 (2012) 1327

[48] Y. Hu, Y. Li, R. Liu, W. Tan, G. Li, Talanta 84 (2011) 462

[49] B. Sellergren, TRAC Trend. Anal. Chem. 18 (3) (1999) 164

[50] N.W. Turner, E.V. Piletska, K. Karim, M. Whitcombe, M. Malecha, N. Magan, C. Baggiani, S.A. Piletsky, Biosens. Bioelectron. 20 (2004) 1060

[51] H. Zhang, Polymer 55 (2014) 699

[52] Y. Zhang, Y. Li, Y. Hu, G. Li, Y. Chen, J. Chromatogr. A 1217 (2010) 7337

[53] N. Henry, R. Delepee, J.M. Seigneuret, L.A. Agrofoglio, Talanta 99 (2012) 816

[54] R. Simon, M. E. Collins, Anal. Chim. Acta 591 (2007) 7

[55] H. Yan, H. Wang, J. Qiao, G. Yang, J. Chromatogr. A 1218 (2011) 2182

[56] F. Qiao, H. Yan, J. Chromatogr. B 879 (2011) 3551

[57] F. Qiao, H. Sun, J. Pharmaceut. Biomed. 53 (2010) 795

[58] F. Quiao, J. Du, J. Chromatogr. B, 923-924 (2013) 136

[59] H. Sun, F. Qiao, G Liu, S. Liang, Anal. Chim. Acta 625 (2008) 154

[60] L. Enríquez-Gabeiras, A. Gallego, R.M. Garcinuño, P. Fernández-Hernando, J.S. Durand, Food Chem. 135 (2012) 193

[61] H. Yan, F. Wang, H. Wang, G. Yang, J. Chromatogr. A 1256 (2012) 1

[62] H. Yan, X. Cheng, N. Sun, T. Cai, R. Wu, K. Han, J. Chromatogr. B 908 (2012) 137

[63] C.M. Dai, J. Zhang, Y.L. Zhang, X.F. Zhou, Y.P. Duan, S.G. Liu, Chem. Eng. J. 211-212 (2012) 302

[64] J.J. Christensen, J.H. Rytting, R.M. Izzat, Biochemistry 9 (1970) 4907

[65] M. Soleimani, S. Ghaderi, M. G. Afshar, S. Soleimani, Microchem. J. 100 (2012) 1

[66] Marvin was used for drawing, displaying and characterization chemical structures, substructures and reactions, Marvin 14.12.8.0, 2014, ChemAxon (http://www.chemaxon.com)

[67] M. M. Castro-López , J. M. López-Vilariño, M. V. González-Rodríguez, L. F. Barral-Losada, Microchemical J. 99 (2011) 461

[68] J. M. Barat, L. Gil, E. García-Breijo, M. C. Aristoy, F. Toldrá, R. Martínez-Máñez, J. Soto, Food Chem. 108 (2008) 681

[69] P. T. Lakshmanan, P. D. Antony, K. Gopakumar, Food Control 7 (1996) 277

[70] G.A. Shabir, J. Chromatogr. A 987 (2003) 57

WATER-COMPATIBLE IMPRINTED PILLS FOR SENSITIVE DETERMINATION OF CANNABINOIDS IN URINE AND ORAL FLUID BY MISPE-LC-MS/MS

M.C. Cela-Pérez[1], Ferdia Bates[3], Cristian Jiménez-Morigosa[2], Elena Lendoiro[4], Ana de Castro[4], Angelines Cruz[4], Manuel López-Rivadulla[4], J.M. López-Vilariño[3], M.V. González-Rodríguez[3]

[1] Grupo de Polímeros, Centro de Investigaciones Tecnológicas, Universidad de A Coruña, Campus de Esteiro s/n, 15403 Ferrol, Spain, e-mail: iquimica@udc.es

[2] Servicio de Toxicología, Instituto de Ciencias Forenses, Universidad de Santiago de Compostela, San Francisco s/n, 15782 Santiago de Compostela, Spain, e-mail: elena.lendoiro@usc.es

ABSTRACT

A novel molecularly imprinted solid phase extraction (MISPE) methodology followed by liquid chromatography tandem mass spectrometry (LC-MS/MS) has been developed using cylindrical shaped molecularly imprinted pills for detection of Δ^9-tetrahydrocannabinol (THC), 11-nor-Δ^9-tetrahydrocannabinol carboxylic acid (THC-COOH), cannabinol (CBN) and cannabidiol (CBD) in urine and oral fluid (OF). The composition of the molecular imprinted polymer (MIP) was optimized based on the screening results of a non-imprinted polymers library (NIP-library) consisted of twelve NIPs synthesized from combination of four functional monomers and three cross-linkers in a suspension of poly vinyl acetate in triethylene glycol dimethyl ether as porogen. The binding ratio values of the NIP-library in aqueous and organic solvent were used to estimate the affinity of the NIPs to THC. Thus, acrylamide as functional monomer and ethylene glycol dimethacrylate as cross-linker were selected for prepare the MIP, using catechin as mimic template. The MISPE pill demonstrated an imprinting factor of 4,0 and selectivity factor values related to caffeine and acetaminophen of 1.39 and 1.48 respectively. MISPEs were incubated with 0.5 mL urine or OF sample for adsorption of analytes. For desorption, the MISPE was transferred to a vial with 2 mL of methanol:acetic acid (4:1) and sonicated for 15 min. The elution solvent was evaporated and reconstituted in methanol:formic acid (0.1%) 50:50 to inject in LC-MS/MS. The developed method was linear over the range from 1 to 500 ng mL^{-1} in

urine and from 0.75 to 500 ng mL^{-1} in OF for all four analytes. Intra- and inter-day imprecision were <15 %. Extraction recovery was 50-111 %, process efficiency 15.4-54.5% and matrix effect ranged from -78.0 to -6.1%. Finally, optimized and validated method was applied to 4 urine and 5 OF specimens. This is the first method for the determination of THC, THC-COOH, CBN and CBD in urine and OF using MISPE technology.

Highlights: *First report on MISPE-LC-MS/MS analysis of four cannabinoids in urine and oral fluid; Screening a NIP-library to optimize the synthesis of MIPs for cannabinoids; Recoveries ranging from 50.3 to 81.3% and 64.9 to 111% in urine and OF, respectively; Sensitive, simple and cost effective methodology for routine analysis in urine; Identification of recent cannabis consumption in both matrices.*

Keywords: *Water-compatible, MISPE, LC-MS/MS, cannabinoids, urine, oral fluid*

1. INTRODUCTION

According to the United Nations 2014 World Drug Report, cannabis remains the most widely used illicit substance in the world [1]. Urine is the primary matrix used for the detection of cannabis intake, since cannabinoids could be detected up to four days in light smokers and even after several months in chronic smokers [2]. The primary urinary compound for testing purposes is the mayor metabolite of THC, THC-COOH, excreted mainly as glucoronic-acid conjugate (THC-COOH-glucoronide). Positivity is set at concentrations above 15 ng mL^{-1}, eliminating the possibility of false positive due to passive inhalation [3] but providing no information about drug administration or exposure [4]. CBN and CBD are minority compounds of cannabis and rarely analized in urine, but they have been recently purposed as biomarkers of recent cannabis intake [5-7].

In the last years, oral fluid (OF) monitoring has been increased [8,9], because it is a better indicator of recent use than urine monitoring [10,11]. In addition, the use of OF for testing has the advantage of a non-invasive, simple and observed specimen collection, which reduces the opportunity for adulteration [9,11,12]. On the other hand, disadvantages of OF testing include small sample volume, especially after cannabis smoking and low concentrations requiring high sensitivity [8]. THC is the primary target in OF for detecting cannabis intake. However, probably false positive test result after passive exposure to cannabis, since THC was found in passive smokers at a concentration exceeding 4 ng mL^{-1}, while the metabolite THC-

369

COOH was never detected in this kind of population [8,13-16]. But THC-COOH was detected in chronic daily cannabis smokers OF up to 4 weeks of abstinence, thus, the detection of this cannabinoid in OF may not reflect recent use [17]. Also in OF, CBD and CBN are being proposed as markers of recent consumption [8,18,19]. Therefore, the simultaneous determination of THC, THC-COOH, CBD and CBN in OF allows the correct interpretation of cannabis intake by eliminating the possibility of passive inhalation and providing markers of recent cannabis smoking.

Traditionally, cannabinoids in urine was subjected to basic or enzymatic hydrolysis for cleavage of glucoronic acid fraction in order to increase the sensitivity of the analysis, normally, by chromatography tandem mass spectrometry (GC-MS/MS) [20,21] or LC-MS/MS [2,6,22,23]. Then, solid phase extraction (SPE) is usually selected as clean-up treatment. Moreover, when GC-MS/MS is employed, a derivatization process prior to injection is required to improve the quantification [20,24]. When the matrix is OF, highly sensitive analytical methods are required as THC-COOH it is present at low pg mL^{-1} concentrations. Only a few methods with the sensitivity required are available [17-19]. These methods were developed by GC-MS/MS [25], 2D-GC-MS [19,24,26] or LC-MS/MS [8,9,27-30], but in most of them tedious sample treatment are involved and derivatization of the extract to increase the sensitivity was required. Only two recent papers describe LC-MS/MS methodologies without derivatization step [8,9]. At time, this team published the first method to determine the THC and its primary metabolite in urine and OF using MISPE

coupled to LC-MS/MS [31] with previous hydrolysis of urine specimens but no derivatization of the extract for both matrices. The use of MIPs as SPE sorbent allowed a simple, rapid, effective and selective extraction compare to traditional SPE due to they are materials prepared in the presence of a target analyte (template) or closely related species (mimic) that serves as a mould for the formation of complementary binding-sites. In this report, the MIP was synthesized using catechin as mimic-template, getting a LOQ of 1 and 2.5 ng mL^{-1} for THC and THC-COOH in OF and urine, respectively. In order to improve the MISPE procedure and enhanced the sensitivity of the methodology, new formulations of MIP were investigated.

Traditional combinatorial screening approaches were employed successfully in the past to predict binding properties and optimize the composition of MIPs [32-35], nevertheless, these methods are tedious and too much time consuming to routine applications. Pre-polymerization studies by molecular modelling or spectroscopic techniques could help to optimize the polymer synthesis analyzing the interactions at molecular level in the pre-polymerization mixture [36-38], but these methods have experimental limitations since they not consider the influence of the cross-linker agent, the polymerization step or the interfering compounds in real samples. The use of a new MIP design methodology based on a screening library of NIPs, could overcome these limitations [39-43], since it is based on the premise 'if a NIP shows binding properties toward a target molecule, the corresponding MIP will show a significant imprinting effect', the presence of

the template molecule in the pre-polymerization mixture acts to improve binding properties that already exists in a NIP [41].

Here, a non-imprinted polymer (NIP) library was developed with monomers capable of forming high affinity complexes with the template and the cross-linkers of different degrees of functionality and rigidity. Their maximum 'water-compatibility' [40,44] should be also considered since urine and OF are aqueous media and traditionally, MIPs demonstrated a poor performance in aqueous environments against in hydrophobic organic solvents [45]. Thus, the binding capacity of the NIPs was analyzed in polar and apolar conditions to value non-specific and specific interactions respectively. The NIP with the highest affinity to THC based on the ratio of binding capacities in both media was selected and this monomer-cross-linker composition was used to prepare the MIP. The MISPE procedure was optimized regarding to the type of elution solvent. The novel MISPE-LC-MS/MS method for the determination of THC, THC-COOH, CBD and CBN in urine and OF specimens was fully validated. Finally, the method was applied to the analysis of 5 OF and 4 urine specimens.

2. EXPERIMENTAL

2.1. CHEMICALS AND REAGENTS

Reagents involved in polymer preparation, binding evaluation, optimization of the procedure and HPLC-PDA analysis: Triethylene glycol dimethyl ether (TRIGLYME), poly (vinylacetate) (PVAc, Mw = 100 g

mol^{-1}), 2-hydroxiethyl-methacrylate (HEMA), methacrylic acid (MAA), ethylene glycol dimethacrylate (EGDMA), trimethylolpropane trimethacrylate (TRIM), trimethylolpropane triacrylate (TMPTA), (+)-Catechin hydrate (CATE), acetaminophen (AAP), and N,N-dimethylformamide (DMF) were obtained from Sigma-Aldrich (Steinheim, Germany). Acrylamide (AM), 2,2-azobisisobutyronitrile (AIBN), caffeine (CAF) and ammonium hydroxide solution (25 % in water) were supplied from Fluka (Buchs, Switzerland). The functuional monomer 4-vinylpyridine (4-Vpy) was purchased from ACROS organics (Geel, Belgium). Ethanol (EtOH) and methanol (MeOH) were obtained from Merck (Darmstadt, Germany) and acetic acid glacial (AcOH) from Panreac (Barcelona, Spain), while formic acid (98-100%) reagent grade and acetonitrile (ACN) as mobile phase were from Riedel-de Haën (Seelze, Germany) and BDH Prolabo chemicals (Briare, France) respectively. Pure THC (Dronabinol) was obtained from LGC Standards (Barcelona, Spain). Water was purified using a Milli Q Ultrapure water-purification system (Millipore, Bedford, MA, USA).

Reagents involved in the validation of the MISPE-LC-MS/MS methodology*:* THC, THC-COOH, CBN and CBD at 1 mg mL^{-1} in methanol, and THC-d$_3$, THC-COOH-d$_3$, CBN-d$_3$ and CBD-d$_3$ at 0.1 mg mL^{-1} in methanol were purchased from Cerilliant™ (Round Rock, TX, USA). Methanol Chromasolv® LC-MS from Sigma Aldrich (St. Louis, USA), formic acid (98-100%) reagent grade and acetic acid (99.8%) reagent grade from Scharlau (Sentmenat, Spain), and acetonitrile LC-MS from Panreac (Castellar del Vallès, Spain). Water was purified with a Milli Q water system

(Millipore, Le-Mont-sur-Lausanne, Switzerland). Salivette® oral fluid collection devices were from Sarstedt (Nümbrecht, Germany).

2.2. INSTRUMENTATION

HPLC-PDA analysis for binding evaluation*:* HPLC-PDA analysis were performed using a Waters 2695 (Waters, Mildford, MA, USA) with gradient pump and automatic injector. Chromatographic experiments were carried out using a stainless steel column packed with SunFire ^{TM} C_{18} (150 mm × 3.0 mm, 3.5 μm) (Waters). Isocratic elution was performed with formic acid 0.1% (0.1% formic acid in deionized water): ACN (20: 80, v/v) as the mobile phase at a flow rate of 0.5 mL min^{-1} and injection volume of 20 μL. Column oven temperature was set at 30 ºC. Detection was carried out using a photodiode array detector (PDA, model 996 UV) set in the range of 200–400 nm. Output signals were monitored and integrated using a personal computer operated under the Empower 2 software (Waters). Wavelength of 235 nm for THC analysis was selected as output PDA signals.

LC-MS/MS analysis to validate the methodology and analyze real samples: The methodology employed was described in previous paper [31]*.*

2.3. DESIGN OF MIPS

The selection of the optimal formulation for imprinted polymer preparation is a crucial step in molecular imprinting technology, since the stability of the complex formed between functional monomer and template molecule in pre-polymerization mixture determines the efficiency of the imprinting process.

In the present study, the computational screening of a virtual library of functional monomers capable to form hydrogen bonding with the cannabinoids previously mentioned was compared with the screening of a library of synthesized NIP polymers in order to optimize the MIP composition and investigate the correlation between 'virtual' and 'real' results [38,40].

2.3.1. Molecular modelling

Autodock-related calculations were done on the Linux-based Ubuntu 15.04 (Vivid Vervet) 64bit OS (releases.ubuntu.com/15.04/), installed with default settings onto a Lenovo S540 ThinkPad laptop computer with an Intel Core i7-4500U CPU system of 4 x 1.80GHz processors @ 7.5GiB RAM. Openbabel [46] was installed via the Ubuntu Software Center, Autodock 4.2.6 and Autodock Tools [47] were each then downloaded from the Scripps institute (autodock.scripps.edu/downloads).

For Autodock experiments, all molecules were initially downloaded in neutral form from chemspider (chemspider.com) in .mol format. All structures were inspected in text editor and then in Pymol. Conversion to

.pdb format was done using the 'babel' command in the OS terminal following energy minimization via 'obminimize' for 20000 iterations via steepest descent using the Generalized Amber Force field (GAFF). All molecules were then assigned gasteiger charges, rotatable bonds were detected and torsional degrees of freedom (TORSDOF) were set (for ligands only) by Autodock Tools 1.5.6 [47,48] (ADT) and saved in .pdbqt format.

For primary affinity screening of monomers against template molecules, all templates were processed as receptor files while monomers were treated as ligand files. For screening using the Autodock 4 [47] (AD4) algorithm, modified parameter weights were introduced in a parameter file modified from the 'AD4.1_bound' weights available at the Scripps institute website (autodock.scripps.edu); the grid box was not modified from the default. Search parameters used were those of the Lamarkian Genetic Algorithm and modified only for the maximum number of evaluations to 250,000 (short). The binding energy values obtained were listed in Table 1.

Table 1. Binding energy values of CATE, THC, THC-COOH, CBN and CBD with the monomers contained in the virtual library

Monomer	Binding Energy (Kcal mol^{-1})				
	CATE	**THC**	**THC-COOH**	**CBN**	**CBD**
4-Vpy	-19.7	-13.0	-13.5	-21.3	-17.5
MAA	-30.1	-21.1	-21.1	-23.6	-23.9
HEMA	-32.5	-24.7	-24.6	-25.3	**-29.4**
AM	**-32.5**	**-26.0**	**-29.1**	**-27.2**	-25.4

2.3.2. Synthesis of the NIP library

To synthesize the NIP library, four functional monomers and three cross-linkers were co-polymerized using AIBN as initiator and TRIGLYME:PVAc (7.5%) as porogen under 60ºC during 24 hours. In this sense, 4-Vpy, MAA, HEMA and AM were selected as functional monomers due to their ability to interact with THC.

According to our previous studies [31,49], the solvent was mixed with the functional monomers, the cross-linkers (ratio M:C of 1:1) and the radical initiator AIBN (0.006 mmol) in a 2 mL vial. Then, 4 x 50 µL of the pre-polymerization solution were transferred to a custom-made silicone mould and was introduced into an airproof container and purged with N_2 for 5 min to completely evacuate the air and avoid the polymerization inhibition [49]. Finally, the sealed container was left to polymerize at 60ºC for 24 hours. The pills are cylindrical in shape and their dimensions (4.14 x 3.50 mm and 0.0216 g) guarantee the simplicity of the MISPE procedure, since grind, sieve and pack them in a cartridge is not necessary.

2.3.3. Binding analysis of NIP library

The polymer binding to the analyte in polar and nonpolar solvent helps to evaluate the relative contribution of specific (such as hydrogen bonds) and non-specific interactions (hydrophobic interactions) in molecular recognition.

The NIP library was tested for adsorption of 2.5 μg mL^{-1} of THC in two solvents, water:ethanol (6:4) and DMF. The pills were placed in vials and were mixed with 1 mL of the above solutions at room temperature for 72 h. After incubation, the supernatant was measured by HPLC-PDA. The binding recovery was calculated and used for the identification of best binding polymer by the ratio of binding recoveries in both solvents.

The screening of the synthesized NIPs was compared with the computational screening of monomers to evaluate the agreement of both approaches.

The selected composition will be used for molecular imprinting.

2.4.   SYNTHESIS OF THE MIPS

CATE-MIP was synthesized by mixing the mimic-template with the monomer and the cross-linker selected from composition screening studies at 1:6:6 (T:M:C) ratio, based on our previous works [31,49]. Experimentally, CATE (0.05 mmol) was dissolved in 170 μL of TRIGLYME: PVAc (7.5%) and mixed with the functional monomers (0.3 mmol) in a 2 mL vial. After sonication, the cross-linkers were added (0.3 mmol) and the reaction mixture was sonicated again until homogenization. Then, AIBN as free radical initiator (0,006 mmol) was incorporated and four 50 μL portions of the reaction mixture were transfer to the silicone mould described in previous section (2.3.2.) and were sealed after degasification with N$_2$ for 5 min. The polymers were cured at 60ºC for 24 h. The MIP pills

378

were washed with MeOH (containing 7% of aqueous ammonia solution (25%) until no CATE was detected in the extract and then washed with MeOH to remove the basic media.

2.5. KINETICS STUDIES

Binding experiments were performed with THC 2.5 µg mL^{-1} in water:EtOH (6:4) at room temperature and different times of static incubation. Two kinetic models have been applied to the experimental data: the Lagergren pseudo-first-order model and the pseudo-second order model. To identify the diffusion mechanism, the intra-particle diffusion model based on the theory proposed by Weber and Morris was applied to kinetic data [49-51].

2.6. EVALUATION OF THE IMPRINTING EFFECT

Binding analysis on MIPs was carried out in the same way as NIPs ones. Then, the binding properties of polymers could be evaluated by calculation of the distribution coefficient (k) from binding data: $k = C_p/C_s$, where C$_p$ (µmol g^{-1}) is the concentration of analyte on the polymer and C$_s$ (µmol mL^{-1}) is the concentration of free analyte in the solution. Finally, the imprinting effect is calculated by the imprinting factor: $IF = K_{pMIP}/K_{pNIP}$, where K_{pMIP} is the partition coefficient of THC on the imprinted polymer and K_{pNIP} is the partition coefficient of the same compound on the non-imprinted polymer. This normalization method removes binding due to non-specific interactions and serves to validate the connections between the binding properties of NIPs and MIPs [37,43,52,53].

2.7. CROSS-SELECTIVITY EVALUATION

Additional binding assays were performed to test selectivity of MIP towards several compounds commonly found in urine samples (CAF, AAP). Mixture aqueous solution was used in competitive assays for cross-selectivity evaluation. The specific selectivity factor (SF) was calculated taking the ratio of imprinting factors, $SF = I_1/I_2$, where I_1 and I_2 are the imprinting factors for two different substrates [53].

2.8. MISPE PROCEDURE

The adsorption of THC, THC-COOH, CBN and CBD into MIP occurs after add 0.5 mL of oral fluid or 0.5 mL of urine (and 25 µL of internal standard solution at 1 µg mL^{-1}) to a vial with a MISPE-pill at room temperature. After the incubation period required, the pill was transferred to a clean vial and the analytes desorption was performed with 2 mL of MeOH:HAc (4:1) (pH 2) sonicating for 15 min. This solvent was evaporated and reconstituted in 50 µL of methanol and 50 µL of formic acid 0.1 %. After centrifugation at 14,500 rpm (10 min), the supernatant was collected and injected into the LC-MS/MS (Fig. 1).
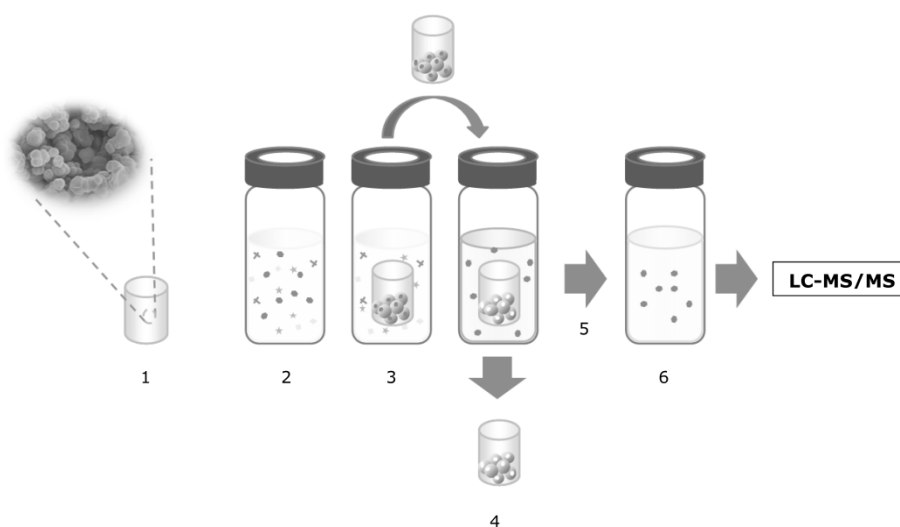
Fig.1. MISPE procedure: 1) MISPE-pill with imprinting sites available, 2) Sample, 3) Adsoption of analytes, 4) Desorption of the analyte, 5) Evaporation and redisolution of eluate, 6) Injection in LC-MS/MS

2.9. VALIDATION OF MISPE-LC-MS/MS METHODOLOGY

The method was validated in urine and oral fluid for selectivity, limit of detection (LOD) and quantification (LOQ), accuracy and imprecision (intra- and inter-day and total imprecision), extraction recovery, matrix effect, process efficiency and stability after 72 h in the autosampler.

Selectivity of the method was evaluated for endogenous and exogenous interferences. Interferences for endogenous matrix components were evaluated by analyzing urine (n=10) and oral fluid samples (n=10) after fortification with 25 μL of internal standard solution (1 μg mL^{-1}). Exogenous interferences were evaluated by the analysis of urine and OF samples fortified with potentially interfering common drugs of abuse and medicines

(a total of 39) at 500 µg mL^{-1}. Endogenous and exogenous interferences are considered insignificant if cannabinoids are in a concentration lower than the LOD [31].

Linearity was verified through 4 calibration curves analyzed on 4 different days. Acceptable linearity was achieved when correlation coefficient (R^2) was at least 0.99 and calibrators quantified within ±15% of target, except for LOQ within ±20%.

LOD was defined as the lowest concentration of analytes with acceptable chromatography (presence of all product ions with signal-to-noise ratios ≥3) and was evaluated by fortifying blank specimens at decreasing cannabinoids concentrations (1, 0.75, 0.5 and 0.25 ng mL^{-1}). LOQ was the lowest concentration that could be quantified with acceptable imprecision (≤20%) and accuracy (80-120%) of target concentration (signal-to-noise ratio≥10). LOQ was evaluated by the analysis of 5 replicates [54].

Imprecision and accuracy were determined at 3 concentrations (2.5, 25, and 75 ng mL^{-1}) with the analysis of 5 replicates on 4 different days (n=20). The imprecision intra- and inter-day and the total imprecision were calculated. Acceptable values were achieved when %CV was ≤15% [55]. Accuracy was expressed as the percentage of the nominal concentration (n=20) and was required to be within 85-115% of the target concentration.

Extraction recovery (%ER), matrix effect (%ME) and process efficiency (%PE) were determined at two concentration levels (2.5 and 75 ng mL^{-1}). Extraction recovery was calculated after comparing mean peak areas of blank specimens fortified prior to extraction (n=6) with those obtained in samples fortified after extraction (n=6). Matrix effect was determined through mean peak areas in blank specimens (n=10, from different sources) fortified after extraction with mean peak areas of the cannabinoids prepared in mobile phase (n=6). Process efficiency examines the overall effect of the extraction recovery and the matrix effect on quantification of target analytes and was determined by comparing mean peak areas of blank specimens fortified prior to extraction (n=6) with mean peak areas of samples prepared in mobile phase at the same concentration (n=6).

In order to prove the stability of the cannabinoids, samples fortified at 2.5, 25 and 75 ng mL^{-1} were re-injected after 72 h storage at 6 ºC on the autosampler (n=5). Stability was considered acceptable when these samples quantified within ±15% of freshly prepared samples (n=5).

2.10. URINE AND ORAL FLUID SAMPLE COLLECTION

Fresh OF (collected with the Salivette$^{®}$ device) and urine samples were donated by the staff personnel for the preparation of calibrators and quality controls (QC). Calibrators at 0.75, 1, 2.5, 5, 10, 50, 100 and 500 ng mL^{-1} were prepared by the addition of 25 or 50 μL of the appropriate working solutions (0.01, 0.1, 1 and 10 μg mL^{-1}, prepared in methanol). QC

samples at low (2.5 ng mL^{-1}), medium (25 ng mL^{-1}) and high (75 ng mL^{-1}) concentrations were generated using different working solutions (0.025, 0.25 and 0.75 µg mL^{-1}, prepared in methanol) than calibrators.

Moreover, authentic specimens obtained from forensic cases (5 OF and 4 urine samples) with a previous positive result for cannabinoids were re-analyzed using the present methodology. OF and urine samples were stored at -20ºC.

3. RESULTS AND DISCUSSION

3.1. COMPOSITION SCREENING

As presented in Table 2, the binding percentage varied significantly for the four functional monomers tested, both in polar an nonpolar conditions, which is indicative of different intensity interaction between THC and functional monomers. The binding ratio varied from 0.14 to 0.31. Polymers containing 4-Vpy was weakly binding to THC, followed by MAA and the hydrophilic monomers HEMA and AM in the last position, which interact strongly with the cannabinoid, probably due to these functional monomers increase the surface hydrophilicity of the polymer and reduce the nonspecific binding analyte-polymer in aqueous solutions [44].

On the other hand, polymers containing EGDMA as cross-linker resulted in the best binding ratios. According to previous papers, TRIM and TMPTA, as ternary cross-linkers, should provide higher rigidity to the MIPs, leads to

more well-defined recognition sites and therefore, higher affinities and capacities. Nevertheless, the low polarity and hydrophobic properties of these cross-linkers finally results in a poor water-compatible ability of TRIM and TMPTA NIPs while EGDMA-NIPs, because of its hydrophilic properties, were beneficial to the synthesis of water-compatible MIPs [44,56].

Back to computational screening of monomers, the scores of virtual screening was contained in Table 1. The top one monomer was AM, followed by HEMA and MAA, while 4-Vpy takes the last position with the lowest binding energy value to THC. The strength of the hydrogen bonding between THC and AM is -25.98 kcal mol^{-1} while for the interaction between 4-Vpy and THC this value is -12.95 kcal mol^{-1}. The hydrogen bond covers a wide and continues energy scale ranging from 0.48 kcal mol^{-1} to 39.91 kcal mol^{-1} depending on the atoms involved in the interaction, they could be weak as Van der Waals interactions or strong as weak covalent bonds, reaching 38.96 kcal mol^{-1} for [F-H---F]$^{-}$ [57]. Therefore, the hydrogen bond between THC and AM is comparable to the strongest H-bonds resulting of the most electronegative atoms.

For THC-COOH and CBN, monomers follow the same sequence than THC, with AM in the first position. The estimated energy value for the interaction between CBD and AM (-25.38 kcal mol^{-1}) was comparable to cannabinoid-AM interaction mentioned, but slightly lower than the achieved by CBD-HEMA (-29.39 kcal mol^{-1}). From Table 1, AM also was the optimal

monomer to interact with template molecule CATE, (-32.51 kcal mol^{-1}), which influencing the quality of binding sites of the future MIP.

Table 2. Binding percentage and binding ratio values of THC 2.5 µg mL^{-1} in DMF and water:EtOH (6:4) on NIP-library

| Monomer | Cross-linker | NIP | Binding recovery | | Binding Ratio (BR) | $\overline{BR}$ |
			DMF	water:EtOH		
4-Vpy	EGDMA	1	13.6	82.3	0.17	
	TRIM	2	13.6	94.8	0.14	0.16
	TMPTA	3	14.1	86.7	0.16	
MAA	EGDMA	4	14.3	64.4	0.22	
	TRIM	5	15.0	75.3	0.20	0.21
	TMPTA	6	15.2	76.0	0.20	
HEMA	EGDMA	7	17.6	66.0	0.27	
	TRIM	8	19.5	77.5	0.25	0.24
	TMPTA	9	16.9	81.3	0.21	
AM	EGDMA	10	17.3	55.2	**0.31**	
	TRIM	11	19.8	75.3	0.26	**0.28**
	TMPTA	12	19.9	77.1	0.26	

According to the above evaluation, a good correlation was found between the screening tests and modeling of monomer-THC interactions performed used computational approach.

Briefly, AM and EGDMA (NIP 10) were selected for molecular imprinting from screening of NIPs library.

3.2. EVALUATION OF THE IMPRINTING EFFECT

CATE-AM-EGDMA-MIP was prepared and binding analysis were carried out in both aqueous and organic conditions. The IF value was employed to evaluate the imprinting effect. In addition, two imprinted pills, MIP 2 and

MIP 9, were prepared to validate the connections between the binding properties of MIPs and NIPs; NIP 2 had the worst binding ratio value of the NIP-library and NIP 9 was chosen randomly.

The k and IF values of NIPs and MIPs in aqueous media are shown in Table 3.

Table 3. Binding percentage, distribution coefficient (k) and imprinting factor (IF) values of THC 2.5 µg mL^{-1} in water:EtOH (6:4) on MIPs (n=3, RSD<5.31%)

Monomer	Cross-linker	Polymer	Binding (%)		k_{NIP} (mL g^{-1})	k_{MIP} (mL g^{-1})	IF
			NIP	MIP			
4-Vpy	TRIM	2	94.8	91.6	578	521	0.90
HEMA	TMPTA	9	81.3	78.7	129	174	1.35
AM	EGDMA	10	55.2	75.4	47	190	**4.05**

The results proved that the composition of the NIP with the higher binding ratio led to a MIP with excellent binding properties (IF = 4.05), whereas the NIP formulation with the lower binding ratio results in a MIP with poor affinity to THC (IF < 1). Moreover, from Table 3, binding ratio and k value for NIP 2 in aqueous media were comparable to MIP 2, even higher. This fact indicates the presence of non-specific interactions analyte-polymer. The basic monomer 4-Vpy employed on formulation of NIP and MIP 2 has been widely and successfully applied for molecular imprinting, but very strong π-π interactions occur during the analyte binding in aqueous conditions that could lead to extremely high levels of non-specific binding analyte-polymer and often, imprinted and reference polymers show identical abilities to the analyte [58]. Moreover, this high fraction of non-

specific binding leads to poor selectivity properties and other compounds of matrix sample could interact with MIPs and significantly reduce their efficiency.

The k and IF values of NIPs and MIPs in DMF are shown in Table 4.

Table 4. Binding percentage, distribution coefficient (k) and imprinting factor (IF) values of THC 2.5 µg mL^{-1} in DMF on MIPs

Monomer	Cross-linker	Polymer	Binding (%)		k_{NIP} (mL g^{-1})	k_{MIP} (mL g^{-1})	IF
			NIP	**MIP**			
4-Vpy	TRIM	2	13.6	17.9	4.98	12.5	2.51
HEMA	TMPTA	9	16.9	18.2	6.31	12.5	1.98
AM	EGDMA	10	17.3	16.5	8.37	15.9	**8.37**

In organic conditions (Table 4), despite the low k values for NIP and MIP 2 obtained compared to aqueous conditions, the imprinting effect could be observed (IF = 2.51) since no π-π interactions occur. Again, the highest affinity is achieved with MIP 10 formulation (IF = 8.37).

3.3.   KINETIC EVALUATION

In order to examine the adsorption mechanism, such as mass transfer and involved reaction, kinetic assays described in the experimental section have been conducted.

Kinetic data obtained were analyzed using the pseudo-first-order and pseudo-second-order equations and the adsorption rate constants and linear regression values (R^2) were summarized in Table 5. The applicability

of these models to describe the adsorption process was validated by R^2 and the relative error, RE (%), which is defined as:

$$RE(\%) = 100\,(q_{e,cal} - q_{e,exp})/q_{e,exp}$$

where $q_{e,exp}$ and $q_{e,cal}$ (µg g^{-1}) are the experimental and calculated adsorption uptake at equilibrium and at any time, t (h), respectively. The RE (%) values obtained were similar in both cases (15.1 and 15.5%), nevertheless, the pseudo-second-order kinetic model provides the best correlation of the data (0.9920 against 0.9588). This model is based on the assumption that the rate-limiting step may be chemical sorption or chemisorptions [59,60], this means, despite hydrogen bonds are non-covalent interactions, due to the strength and specificity of the hydrogen bond involved, the process is best described as chemisorption than as physisorption, supporting the results explained in the 'Monomer screening' section.

Table 5. Pseudo-first-order and pseudo-second order constants and correlation coefficients values for the adsorption of THC 2.5 µg mL^{-1} in water:EtOH (6:4) on CATE-MIP

	K_1 (h^{-1})	0.0346
Pseudo-first order model	R^2	0.9588
	Calculated q_e (µg g^{-1})	206
	K_2 (g µg^{-1} h^{-1})	0.0003
	R^2	0.9920
Pseudo-second order model	U (µg g^{-1} h^{-1})	8.11
	$t^{1/2}$ (h)	22.1
	Calculated q_e (µg g^{-1})	207
Experimental q_e (µg g^{-1})		179

Generally, the adsorption rate is controlled by the external mass transfer or the intra-particle diffusion or both. In order to evaluate the relative importance of the two steps, time-course THC sorption data were processed using the intra-particle diffusion and the Boyd model. Fig. 2 (A) exhibits the plot of Weber–Morris intra-particle diffusion model. The graph could be divided into three stages: a first sharp rise step is followed by a less sharp rise stage and a final plateau. The initial step represents the mass transfer of the THC molecules across the external boundary layer while the second stage corresponds to the intra-particle diffusion process and the final step, the plateau phase, is ascribed to the last equilibrium process. The plotted stages revealed that the adsorption rate was slowed down as time increased; the k_i and C_i values and the correlation coefficients obtained, displayed in Table 6, supported this assumption. The existence of different regions indicated that both external diffusion and intra-particle diffusion are simultaneously occurring. To try to identify the rate limiting step, Boyd model was applied to kinetic data, resulting in a straight line which no pass through the origin (intercept equal to -0.6381), indicating that the adsorption of THC on CATE-MIP was mainly governed by external diffusion process (Fig.2 (B).

Table 6. Intra-particle diffusion model constants and correlation coefficients values for the adsorption of THC 2.5 µg mL^{-1} in water:EtOH (6:4) on CATE-MIP

Intra-particle diffusion model	k_1 (µg g^{-1} h^{0,5})	k_2 (µg g^{-1} h^{0,5})	k_3 (µg g^{-1} h^{0,5})	C_1	C_2	C_3	R_1^2	R_2^2	R_3^2
	21.2	11.3	0.807	-12.8	56.8	169	0.9914	0.9999	1.000
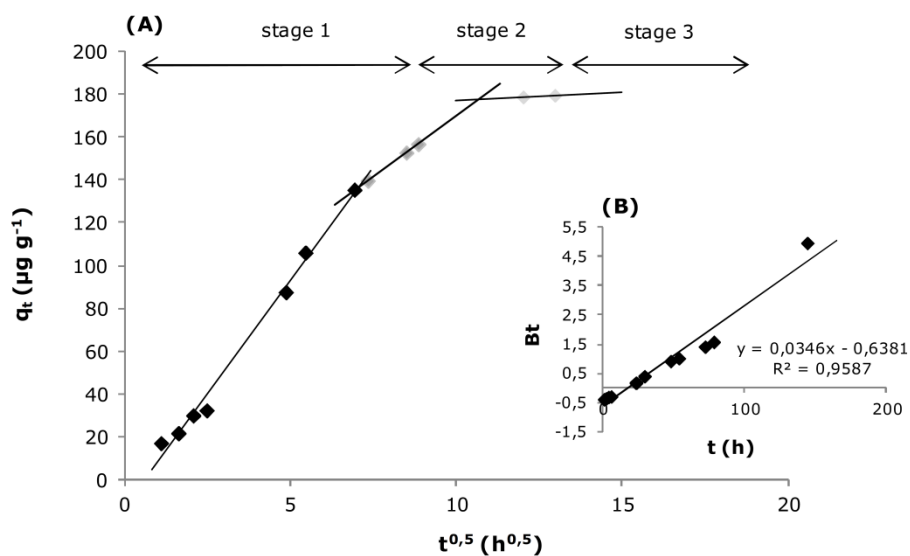
Fig.2. Plot of Weber-Morris intra-particle diffusion model (A) and Boyd model (B)

3.4. CROSS-SELECTIVITY EVALUATION

The selectivity of the MIP to THC was investigated against caffeine and acetaminophen, since these compounds are usually found in urine samples due to their high consumption in today society. Aqueous competitive binding assays were carried out. Table 7 shows the binding parameters and the SFs obtained.

The adsorption of the drugs tested as interferences was minimal. The retention percentages and k values of CAF and AAP were higher on NIP than on MIP, IF < 1, while for THC IF=1.26. SF values of THC against CAF and AAP were 1.39 and 1.48 respectively.

CATE-AM-EGDMA-MIP is selective to THC under the aqueous conditions evaluated.

Table 7. Binding parameters and selectivity factor (SF) values for de adsorption of CAF, AAP and THC 2.5 µg mL^{-1} in aqueous competitive binding assays on CATE-MIP

COMPOUND	Binding (%)		K$_{POLYMER}$ (mL g^{-1})		IF	SF
	NIP	MIP	NIP	MIP		
CAF	11.7	10.7	10.7	9.65	0.91	**1.39**
PAR	3.85	3.31	3.27	5.79	0.85	**1.48**
THC	39.9	45.6	54.0	68.2	1.26	—

3.5.   OPTIMIZATION OF MISPE PROCEDURE

The pH conditions under which adsorption and elution steps are performed influence the efficiency of MISPE procedure since pH not only affects the properties of the sorbent surface, the target analyte speciation in solution and the extent of dissociation of functional groups on the actives sites of the sorbent are also affected [61]. Therefore, pH value of sample influences the interaction between analyte and sorbent during MISPE procedure, especially when target analytes have neutral, acidic and basic properties as cannabinoids. The prevalence of THC charged forms decreases the molecular recognition at the imprinting sites, reducing the sorption efficiency. Thus, the pH of the sorption step should be adjusted below the pK$_a$ value of the cannabinoid and close to the isoelectric point (IP), where THC does not have any electrical charge and maximum sorption may be expected. The –OH group in THC has a pK$_a$ value of 9.34 and the IP is equal to 2.22 (Marvin 14.12.8.0, 2014, ChemAxon), therefore, acidic conditions should be optimal to develop the sorption process. Urine and oral fluid are slightly acidic samples, suitable pH

conditions to perform the MISPE procedure. On the other hand, only at the strongest acidic conditions (pH<1), acrylamide turns into AM^+ by protonation of the carbonyl group; at sample pH, neutral acrylamide remains on the binding sites of MIP.

To desorb the analytes, the elution solvent should have enough elution ability to remove the analytes and facilitate additional sample treatments. The protonation of THC to promote the disruption of the hydrogen bond interaction between THC and AM is required. Now, basic pHs seems to be needed. Three solvents covering the whole range of pHs were tested: MeOH:HAc (4:1) at pH 3, water at pH 6.5 and MeOH (containing 7% of aqueous ammonia solution (25%) at pH 10.5. The elution profile is shown in Fig. 3. Contrary to expectations, an effective elution was achieved at pH 3. This suggested that the interaction between THC and AM occurs between the hydrogen bond acceptor dihydropyran group of THC and the hydrogen bond donor amino group of AM, the -OH group of THC is not involved in the adsorption process, therefore, pH not influence the adsorption process. To desorb THC, at pH 3, AM experiments an acid catalyzed nucleophilic substitution process (methanolisis) to acrylic ester and the appropriate amine, resulting in the disruption of the hydrogen bonding. The mechanism proceeds via protonation of the carbonyl group of AM. At neutral and basic conditions the performance of the elution process was very poor. Probably because water is a weak nucleophile and the carbonyl group in AM is a poor electrophile and, at neutral pH, the possible

hydrolysis of AM is very slow. On the other hand, alkaline hydrolysis may be inhibited since NH_4OH (ac) is a weak nucleophile.
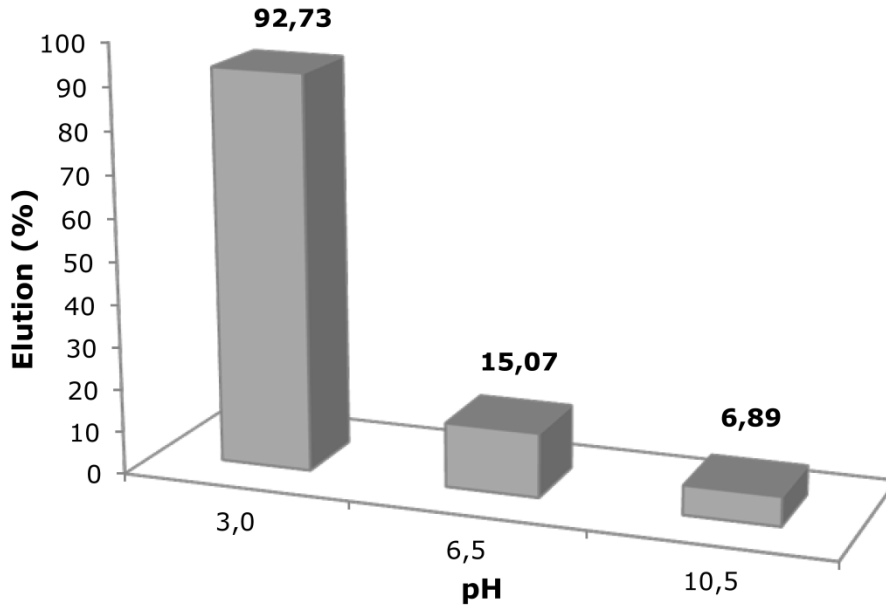
Fig.3. Elution profile at acidic, neutral and basic conditions (n=3, RSD<4.26%)

3.6. VALIDATION OF MISPE-LC-MS/MS METHOD

The method proved to be selective after the analysis of 10 different blank urine and oral fluid samples, since no interferences from endogenous or exogenous compounds were detected, indicating no interferences with the cannabinoids.

Linearity of analyte/internal standard peak area ratio versus theoretical concentration was verified by least square regression with 1/x weighting

factor. The curvature tested on a set of 4 calibration curves shown correlation coefficients (R^2) above 0.9950 with residuals within ±15% for all calibrators. Dynamic range in urine was 0.75-500 ng mL^{-1} while it was 1-500 ng mL^{-1} for OF samples. LOD were 0.75 and 0.5 ng mL^{-1} and LOQ 1 and 0.75 ng mL^{-1} for urine and OF, respectively. Linearity results are summarized in Table 8.

Table 8. LOD and LOQ, calibration ranges, and linearity results in urine and OF

	Analyte	LOD (ng mL^{-1})	LOQ (ng mL^{-1})	Range (ng mL^{-1})	Intercept±SD (n=4)	Slope±SD (n=4)	r^2±SD (n=4)
Urine	THC	0.75	1	1-500	0.756 ± 0.342	0.280 ± 0.194	0.9973 ± 0.0013
	THC-COOH	0.75	1	1-500	1.12 ± 0.669	0.253 ± 0.116	0.9950 ± 0.0015
	CBN	0.75	1	1-500	3.60 ± 6.61	1.684 ± 0.784	0.9975 ± 0.0017
	CBD	0.75	1	1-500	2.08 ± 1.36	2.79 ± 1.63	0.9984 ± 0.0014
Oral fluid	THC	0.5	0.75	0.75-500	0.735 ± 0.643	0.265 ± 0.144	0.9953 ± 0.0009
	THC-COOH	0.5	0.75	0.75-500	1.34 ± 0.638	0.274 ± 0.092	0.9976 ± 0.0012
	CBN	0.5	0.75	0.75-500	2.04 ± 3.48	1.89 ± 0.918	0.9973 ± 0.0021
	CBD	0.5	0.75	0.75-500	2.22 ± 3.13	2.86 ± 1.58	0.9984 ± 0.0009

Imprecision (intra-day, inter-day and total imprecision) and accuracy results were satisfactory in both matrices (Table 9). Intra-day, inter-day and total imprecision values were lower than 8.15%, 8.88% and 11.6% respectively in OF while these values in urine were lower than 9.35%, 9.10% and 10.0% for THC, CBN and CBD. For THC-COOH in urine, the %CV in any case at 25 and 75 ng mL^{-1}, was lower than 6.82%, but at 2.5 ng mL^{-1}, the total imprecision up to 19.8%. This concentration is close to the lowest level quantified, for which an imprecision lower than 20% is acceptable [62]. Accuracy was also satisfactory, ranging from 89.5 to 101% and 94.1-104% for urine and OF respectively.

Table 9. Intra-day, inter-day and total imprecision, and accuracy values at low (2.5 ng mL^{-1}), medium (25 ng mL^{-1}) and high (75 ng mL^{-1}) cannabinoids concentrations in urine and OF

	Analyte	Within-day imprecision (*n*=20, %CV)			Between-day imprecision (*n*=20, %CV)			Total imprecision (*n*=20, %CV)			Accuracy (*n*=20, %target)		
		Low	Med	High	Low	Med	High	Low	Med	High	Low	Med	High
Urine	THC	8.50	4.18	2.77	0.00	9.10	3.42	8.50	10.0	4.40	98.7	102	89.5
	THC-COOH	13.7	3.51	1.27	14.4	5.84	2.59	19.8	6.82	2.89	101	94.1	91.2
	CBN	9.35	5.73	4.72	0.00	0.00	3.17	9.35	5.73	5.69	100	103	91.0
	CBD	7.69	6.69	1.87	3.12	1.07	3.28	8.30	6.77	3.78	97.3	102	90.2
Oral fluid	THC	6.27	5.74	1.81	3.14	8.34	5.88	7.01	10.1	6.16	101	104	100
	THC-COOH	8.15	4.11	2.66	8.19	8.52	4.27	11.6	9.46	5.03	101	96.1	96.4
	CBN	7.62	5.36	3.65	2.73	6.68	8.88	8.09	8.56	9.60	98.2	94.1	96.4
	CBD	7.85	6.91	2.62	6.17	7.01	4.00	9.98	9.84	4.79	96.7	98.2	98.5

Extraction recovery, matrix effect and process efficiency was shown in Table 10. Extraction recoveries ranged from 50.3 to 81.3% in urine, with the lowest values for all the four compounds at 75 ng mL^{-1}. In OF, extraction recoveries varied from 64.9 to 111%, with similar %ER al low and high concentrations. In urine, THC, THC-COOH and CBN show ion suppression at low and high concentrations (19.5-35.4%), while no matrix effect was observed for CBD (14.8 and 6.14% at low and high concentration respectively). Higher matrix effect was showed for all cannabinoids in OF specimens, with ion suppression ranging from 53.0 to 78.0%. Process efficiency varied between 34.0 and 54.5% in urine matrix and from 15.4 to 45.5% in OF.

The cannabinoids were stable after 72 h in storage in the autosampler at 6 ºC, with a percentage of loss <11.0% in urine and <14.2% in OF.

Table 10. Extraction recovery (n=6), matrix effect (n=10), and process efficiency (n=6) values at low (2.5 ng mL^{-1}), and high (75 ng mL^{-1}) cannabinoids concentration levels in urine and OF

	Analyte	% ER		% ME		% PE	
		Low	High	Low	High	Low	High
Urine	THC	53.3	50.3	-19.5	-24.6	42.9	38.0
	THC-COOH	81.3	57.6	-35.4	-28.7	52.6	41.1
	CBN	51.2	50.3	-33.6	-30.4	34.0	35.0
	CBD	64.0	54.5	-14.8	-6.14	54.5	51.2
Oral fluid	THC	83.1	83.3	-53.1	-55.2	38.9	37.3
	THC-COOH	111	96.2	-59.1	-59.8	45.5	38.7
	CBN	69.5	72.7	-53.0	-55.5	32.7	32.4
	CBD	64.9	69.9	-74.1	-78.0	16.8	15.4

3.7.   FORENSIC APPLICATIONS

Four urine specimens obtained from chronic cannabis users were re-analyzed using the present methodology. All the specimens were positive for THC-COOH, however, no positive results were found for THC, CBN and CBD. THC-COOH concentrations ranged between 16.1 and 54.5 ng mL^{-1}.

Five oral fluid specimens with a previous positive result for THC were analyzed with MISPE procedure validated. THC, CBN and CBD were detected at level concentrations ranging from 146.8 to 1135.0 ng mL^{-1}, 4.0 to 87.6 ng mL^{-1} and 5.4 to 128.9 ng mL^{-1} respectively.

3.8.   DISCUSSION

The analysis of THC binding ratio in aqueous and organic media of a NIP-library and the computational screening of a virtual library of functional

monomers was employed to find a water-compatible MIP with selective recognition to cannabinoids. The formulation containing AM as hydrophilic functional monomer and EGDMA as hydrophilic cross-linker agent in the porogenic mixture TRIGLYME-PVAc (7.5%), resulted in the highest binding ratio (0.31). Subsequently, CATE-AM-EGDMA-MIP reached IF values of 4.0, or 36.6% expressed as percentage $(B_{MIP}-B_{NIP})/B_{NIP}$ (where B_{MIP} is the binding obtained using MIP and B_{NIP} is the recovery obtained on NIP), which was higher than IF reached M. Nestić et al. [21] (average IF of 16.3%) with a THC–OH-MAA-EGDMA-MIP polymerized in MeOH, in the only precedent found. The application of pseudo-second-order kinetic model to kinetic data, in addition to the binding energy of THC-AM complex estimated by molecular modelling experiments, demonstrated the strong nature of the interaction involved in the recognition process, which occurs trough the amino group in the MIP and the oxygen of the dihydropyran ring in THC, as suggested the optimization of the MISPE adsorption and elution steps.

The MISPE-LC-MS/MS methodology derived was fully validated for simultaneous determination of THC, THC-COOH, CBN and CBD in urine and OF specimens. According to the validation parameters, the developed method could be applied in routine analysis of urine samples. The LOD and LOQ achieved (0.75 and 1 ng mL^{-1} for all four compounds respectively) were better than those reached by the MISPE-LC-MS/MS methodology developed by M. Nestić et al. (2.5 and 3 ng mL^{-1} for THC and 1 and 2 ng mL^{-1} for THC-COOH) [21]. Moreover, here, no hydrolysis was required (the

recoveries achieved with or without hydrolysis were comparable) and no derivatization step was carried out prior to LC-MS/MS analysis; therefore the MISPE procedure was simpler, saving time and costs. Related to the previous work published by this team [31], the new method achieved better extraction recoveries values (50.3-81.3% against 15.9-34.5%) and lower concentrations of detection and quantification (0.75 and 1 ng mL^{-1} vs 1 and 2.5 ng mL^{-1}) with no hydrolysis of urine samples.

A review of the literature shows only a few papers which described LC-MS/MS methodologies to simultaneous determination of cannabinoids in urine, including CBN and CBD [2,5,7,63], but none of them results in better sensitivity than the present methodology. A recent published work [2] describes a μ-SPE (OMIX C$_{18}$ tips)-LC-MS/MS procedure with tandem hydrolysis process involved (enzymatic and basic) for the determination of the four cannabinoids mentioned and THC-OH, achieving LODs values from 2 to 4 ng mL^{-1} and LOQs between 6 and 10 ng mL^{-1}, too high compared to the sensitivity reached with the present methodology. Moreover, the sample preparation involved in μ-SPE procedure was tedious since after two hydrolysis steps, the μ-SPE employed needs two condition operations, five loading phases, three washing steps and five elution operations, while with MISPE pill, adsorption and desorption process occurred directly, only one step was involved in each case.

On the other hand, for OF specimens, few studies have developed sensitive enough methodologies to determine the metabolite THC-COOH at the pg

mL^{-1} level required [8,9,24-30]. The MISPE-LC-MS/MS method developed in this paper achieved a LOQ of 0.75 ng mL^{-1} for all four cannabinoids. The cutoff of 20 pg mL^{-1} suggested to ruling out passive cannabis exposure [17] was not achieved. Nevertheless, the THC cutoff recommended by The Substance Abuse and Mental Health Services Administration (SAMHSA) [64] and the Driving Under the Influence of Drugs, Alcohol and Medicines (DRUID) [65] European Union Project in oral fluid (2 and 1 ng mL^{-1}, respectively) was reached by the present methodology. CBN and CBD cutoff proposed of 1 ng mL^{-1} to identify recent cannabis consumption (≤6 h) also was attained [19,66].

Related to the first paper developed with MISPE pills [31], a significant improvement was reached since extraction recoveries percentages in OF increase from 26.3-53.6% to 64.9-111%.

4. CONCLUSIONS

The simple and cost effective methodology developed in addition to the sensitivity achieved (1 ng mL^{-1}) for simultaneous quantification of all four cannabinoids, results in a methodology which meets the needs of toxicological analysis in urine samples and could be applied in routine.

The application of the novel MISPE-LC-MS/MS method to OF matrices, was satisfactory for the four cannabinoids, with low sample volume required (0.5 mL) and simple MISPE procedure involved. The sensitivity achieved (0.75 ng mL^{-1}) was appropriate to THC, CBN and CBD quantification to

prove cannabis consumption (THC) and distinguish between recent cannabis smoke and residual excretion from chronic smoking (CBN and CBD). Nevertheless, the cutoff of low pg mL^{-1} concentrations required for the metabolite THC-COOH to rule out passive cannabis exposure was not achieved. In this sense, the introduction of a derivatization step prior to LC-MS/MS analysis could improve the THC-COOH quantification in OF.

Anyway, the simultaneous analysis of both types of specimens (urine and OF) from the same smoker with present methodology allows the complete interpretation of cannabis intake by eliminating the possibility of passive inhalation and providing markers of recent cannabis smoking.

This MISPE application improves the results shown in the previous paper published by this team [31] due to an optimization of the sorbent material, the MIP. Molecular modeling and the screening of a NIP-library containing different combinations of functional monomers and cross-linkers in porogenic solvent, allowed the selection of the appropriate composition to synthesize the optimal MIP for determination of THC in aqueous media. The average extraction recoveries achieved with the new MIP formulation (CATE-AM-EGDMA-MIP) increase a 48%; individually, 21.2 and 43.3% for THC and 45.3 and 60.2% for THC-COOH in urine and oral fluid respectively. This improvement of extraction recoveries validates the imprinted polymer design methodology employed.

On the other hand, this MISPE-LC-MS/MS method involves a slow adsorption process of cannabinoids on CATE-AM-EGDMA-MIP. Static

incubation time of 72 h at room temperature is required. Recently, US binding kinetic experiments carried out by this team demonstrated a slightly diminution of THC binding percentage on the MIP ($\cong$ 20%) after 4 h of ultrasonic incubation at room temperature. This finding suggests a real option to improve the method and the total time of the analysis.

References

[1] United Nations Office on Drugs and Crime (UNODC). World Drug Report 2014; United Nation Publications, Sales No. E.14.XI.7. 2014.

[2] C. Montesano, M. Sergi, S. Odoarni, M.C. Simeoni, D. Compagnone, R. Curini, A µ-SPE procedure for the determination of cannabinoids and their metabolites in urine by LC–MS/MS, J. Pharmaceut. Biomed. 91 (2014) 169-175.

[3] J. Rohrich, I. Schimmel, S. Zorntlein, J. Becker, S. Drobnik, T. Kauffmann, V. Kunz, R. Urban, Concentrations of Delta9-tetrahydrocannabinol and 11-Nor-9-carboxytetrahydrocannabinol in blood and urine after passive exposure to cannabis smoke in a coffee shop, J. Anal. Toxicol. 34 (2010) 196-203.

[4] M.A. Huestis, Pharmacokinetics and metabolism of the plant cannabinoids, Delta9-tetrahydrocannabinol, Cannabidiol and Cannabinol, Handbook Exp. Pharmacol. 168 (2005) 657-690.

[5] E. Jagerdeo, M.A. Montgomery, R.P. Karas, M. Sibum, A fast method for screening and/or quantitation of Tetrahydrocannabinol and metabolites in urine by automated SPE/LC/MS/MS, Anal. Bioanal. Chem. 398 (2010) 329–338.

[6] K.B. Scheidweiler, N.A. Desrosiers, M.A. Huestis, Simultaneous quantification of free and glucuronidated cannabinoids in human urine by Liquid Chromatography Tandem Mass Spectrometry, Clin. Chim. Acta, 413 (2012) 1839–1847.

[7] M. Moradi, Y. Yamini, T. Baheri, Analysis of abuse drugs in urine using Surfactant-Assisted Dispersive Liquid-Liquid Microextraction, J. Sep. Sci. 34 (2011) 1722–1729.

[8] M. Concheiro, D. Lee, E. Lendoiro, M.A. Huestis, Simultaneous quantification of Δ9-Tetrahydrocannabinol, 11-Nor-9-carboxy-tetrahydrocannabinol, Cannabidiol and Cannabinol in oral fluid by Microflow-Liquid Chromatography–High Resolution Mass Spectrometry, J. Chromatogr. A 1297 (2013) 123-130.

[9] M. Sergi, C. Montesano, S. Odiardi, L. Mainero-Rocca, G. Fabrizi, D. Compagnone, R. Curini, Micro extraction by packed sorbent coupled to Liquid Chromatography Tandem Mass Spectrometry for the rapid and sensitive determination of cannabinoids in oral fluids, J. Chromatogr. A 1301 (2013) 139-146.

[10] R.S. Niedbala, K.W. Kardos, D.F. Fritch, S. Kardos, T. Fries, J. Waga, J. Robb, E.J. Cone, Detection of marijuana use by oral fluid and urine analysis following single-dose administration of smoked and oral marijuana, J. Anal. Toxicol. 25 (2001) 289–303.

[11] E.J. Cone, L. Presley, M. Lehrer, W. Seiter, M. Smith, K.W. Kardos, D. Fritch, S. Salamone, R.S. Niedbala, Oral fluid testing for drugs of abuse: positive prevalence rates by intercept immunoassay screening and GC-MS-MS confirmation and suggested cutoff concentrations, J. Anal. Toxicol. 26 (2002) 541–546.

[12] W.M. Bosker, M.A. Huestis, Oral fluid testing for driving under the influence of drugs: history, recent progress and remaining challenges, Forensic Sci. Int. 150 (2005) 143-150.

[13] C. Moore, C. Coulter, D. Uges, J. Tuyay, S. van der Linde, A. van Leeuwen, M. Garnier, J. Orbita Jr., Cannabinoids in oral fluid following passive exposure to marijuana smoke, Forensic Sci. Int. 212 (2011) 227-230.

[14] K.H. Davis, I.A. McDaniel, I.W. Cadwel, P.L. Moody, In the Cannabinoids: Chemical, Pharmacologic and Therapeutic Aspects, Agurell S., Dewwy W.L., Willette R.E. Eds., Academic Press, Orlando, 1984, pp. 97-109.

[15] H. Sachs, U. Dressier, Detection of THC-COOH in hair by MSD-NCI after HPLC clean-up, Forensic Sci. Int. 107 (2000) 239-247.

[16] G. Milman, A.J. Barnes, D.M. Schwope, E.W. Schwilke, W.D. Darwin, R.S. Goodwin, D.L. Kelly, D.A. Gorelik, M.A. Huestis, Disposition of cannabinoids in oral fluid after controlled around-the-clock oral THC administration, Clin. Chem. 56 (2010) 1261-1269.

[17] D. Lee, G. Milman, A. Barnes, R.S. Goodwni, J. Hirvonen, Huestis M.A., Oral fluid cannabinoids in chronic, daily cannabis smokers during sustained, monitored abstinence, Clin. Chem. 57 (2011) 1127-1136.

[18] D. Lee, D.M. Schwope, G. Milman, A.J. Barnes, D.A. Gorelick, M.A. Huestis, Cannabinoid disposition in oral fluid after controlled smoked cannabis, Clin. Chem. 58 (2012) 748-756.

[19] G. Milman, D.M. Schwope, D.A. Gorelick, M.A. Huestis, Cannabinoids and metabolites in expectorated oral fluid following controlled smoked cannabis, Clin. Chim. Acta 413 (2012) 765-770.

[20] T.T. Abraham, R.H. Lowe, S.O. Pirnay, W.D. Darwin, M.A. Huestis, Simultaneous GC-EI-MS determination of Δ9-Tetrahydrocannabinol, 11-Hydroxy-Δ9-tetrahydrocannabinol, and 11-Nor-9-carboxy-Δ9-tetrahydrocannabinol in human urine following tandem enzyme-alkaline hydrolysis, Anal. Toxicol. 31 (2007) 477–485.

[21] M. Nestić, S. Babić, D. Mutavdžić Pavlović, D. Sutlović, Molecularly imprinted solid phase extraction for simultaneous determination of Δ9-

Tetrahydrocannabinol and its main metabolites by Gas chromatography–Mass Spectrometry in urine samples, Forensic Sci. Int. 231 (2013) 317-324.

[22] H. Teixeira, A. Verstraete, P. Proenca, F. Corte-Real, P. Monsanto, D.N. Vieira, Validated method for the Simultaneous Determination of Δ9-THC and Δ9-THC-COOH in oral fluid, urine and whole blood using solid-phase extraction and Liquid Chromatography–Mass Spectrometry with Electrospray Ionization, Forensic Sci. Int. 170 (2007) 148–155.

[23] M. Felli, S. Martello, M. Chiarotti, LC–MS–MS method for simultaneous determination of THC-COOH and THC-COOH-glucuronide in urine: application to workplace confirmation tests, Forensic Sci. Int. 204 (2011) 67–73.

[24] G. Milman, A.J. Barnes, R.H. Lowe, M.A. Huestis, J. Chromatogr. A. simultaneous quantification of cannabinoids and metabolites in oral fluid by Two-Dimensional Gas Chromatography, Mass Spectrometry 1217 (2010) 1513-1521.

[25] D. Day, D.J. Kuntz, M. Feldman, L. Presley, Detection of THCA in oral fluid by GC-MS-MS, J. Anal. Toxicol. 30 (2006) 645-650.

[26] C. Moore, W. Ross, C. Coulter, L. Adams, S. Rana, M. Vincent, J. Soares, Detection of the marijuana metabolite 11-Nor-Δ9-tetrahydrocannabinol-9-carboxylic acid in oral fluid specimens and its contribution to positive results in screening assays, J. Anal. Toxicol. 30 (2006) 413-418.

[27] C. Coulter, M. Garnier, C. Moore, Analysis of tetrahydrocannabinol and its metabolite, 11-Nor-Δ9-tetrahydrocannabinol-9-carboxylic acid, in oral fluid using Liquid Chromatography with Tandem Mass Spectrometry, J. Anal. Toxicol. 36 (2012) 413-417.

[28] X. He, M. Kozak, S. Nimkar, Ultra-sensitive measurements of 11-Nor-Δ9-tetrahydrocannabinol-9-carboxylic acid in oral fluid by Microflow Liquid Chromatography–Tandem Mass Spectrometry using a Benchtop Quadrupole/Orbitrap Mass Spectrometer, Anal. Chem. 84 (2012) 7643-7647.

[29] P.D. Lee, Y.J. Chang, K.L. Lin, Y.Z Chang, Simultaneous determination of Δ9-Tetrahydrocannabinol and 11-Nor-9-carboxy-Δ9-tetrahydrocannabinol in oral fluid using Isotope Dilution Liquid Chromatography Tandem Mass Spectrometry, Anal. Bioanal. Chem. 402 (2012) 851-859.

[30] M. Fabritius, C. Staub, P. Mangin, C. Giroud, Analysis of cannabinoids in oral fluid by Liquid Chromatography-Tandem Mass Spectrometry, Forensic Toxicol. 31 (2013) 151-163.

[31] E. Lendoiro, A. de Castro, H. Fernández-Vega, M.C. Cela-Pérez, J.M. López-Vilariño, M.V. González-Rodríguez, A. Cruz, M. López-Rivadulla, Molecularly imprinted polymer for selective determination of Δ9-Tetrahydrocannabinol and 11-Nor-Δ9-tetrahydrocannabinol carboxylic acid using LC-MS/MS in urine and oral fluid, Anal. Bioanal. Chem. 406 (2014) 3589-3597.

[32] T. Takeuchi, D. Fukuma, J. Matsui, Combinatorial molecular imprinting: an approach to synthetic polymer receptors, Anal. Chem. 71 (1999) 285-290.

[33] F. Lanza, B. Sellergren, Method for synthesis and screening of large groups of molecularly imprinted polymers, Anal. Chem. 71 (1999) 2092-2096.

[34] A.A. Qader, J. Urraca, S.B. Torsetnes, F. Tønnesen, L. Reubsaet, B. Sellergren, Peptide imprinted receptors for the determination of the small cell lung cancer associated biomarker progastrin releasing peptide, J. Chromatogr. A 1370 (2014) 56–62.

[35] M.S. Dopico-García, M.C. Cela-Pérez, J.M. López-Vilariño, M.V. González-Rodríguez, L.F. Barral-Losada, An approach to imprint Irganox 1076: potential application to the specific migration test in olive oil, J. Appl. Polym. Sci. 119 (2011) 2866–2874.

[36] A. Lasagabáster-Latorre, M.C. Cela-Pérez, S. Fernández-Fernández, J.M. López-Vilariño, M.V. González-Rodríguez, M.J. Abad, L.F. Barral-Losada, A study of competitive molecular interaction effects on imprinting of molecularly imprinted polymers, Mater. Chem. Phys. 141 (2013) 461-476.

[37] M.C. Cela-Pérez, A. Lasagabáster-Latorre, M.J. Abad-López, J.M. López-Vilariño, M.V. González-Rodríguez, A study of competitive molecular interaction effects on imprinting of molecularly imprinted polymers, Vib. Spectrosc. 65 (2013) 74–83.

[38] S.A. Piletsky, K. Karim, E.V. Piletska, C.J. Day, K.W. Freebairn, C.H. Legge, A.P.F. Turner, Recognition of ephedrine enantiomers by molecularly imprinted polymers designed using a computational approach, Analyst 126 (2001) 1826-1830.

[39] E.V. Piletska, A.R. Guerreiro, M. Romero-Guerra, I. Chianella, A.P.F. Turner, S.A. Piletsky, Design of molecular imprinted polymers compatible with aqueous environment, Anal Chim. Acta 607 (2008) 54-60.

[40] T. Muhammad, L. Ciu, W. Jide, E.V. Piletska, A.R. Guerreiro, S.A. Piletsky, Rational design and synthesis of water-compatible molecularly imprinted polymers for selective solid phase extraction of amiodarone, Anal. Chim. Acta 709 (2012) 98-104.

[41] C. Baggiani, C. Giovannoli, L. Anfossi, C. Passini, P. Baravalle, G. Giraudi, A connection between the binding properties of imprinted and non-imprinted

polymers: a change of perspective in molecular imprinting, J. Am. Chem. Soc. 134 (2012) 1513-1518.

[42] I. Bakas, N.B. Oujii, G. Istamboulié, S. Piletsky, E. Piletska, E. Ait-Addi, I. Ait-Ichou, T. Noquer, R. Rouillon, Molecularly imprinted polymer cartridges coupled to high performance Liquid Chromatography (HPLC-UV) for simple and rapid analysis of Fenthion in olive oil, Talanta 125 (2014) 313-318.

[43] L. Chen, W. Ji, W. Duan, X. Wang, Q. Gao, Y. Geng, L. Huang, Effectively designed molecularly imprinted polymers for selective extraction of Glabridin from Glycyrrhiza Glabra L. residues by screening the library of non-imprinted polymers, J. Chromatogr. B 965 (2014) 1-6.

[44] H. Zhang, Water-compatible molecularly imprinted polymers: promising synthetic substitutes for biological receptors, Polymer 55 (2014) 699-714.

[45] J.L. Urraca, M.C. Moreno-Bondi, A.J. Hall, B. Sellergren, Direct extraction of Penicillin G and derivatives from aqueous samples using a stoichiometrically imprinted polymer, Anal. Chem. 79 (2007) 695-701.

[46] N.M. O'Boyle, M. Banck, C.A. James, C. Morley, T. Vandermeersch, G.R. Hutchison, Open babel: an open chemical toolbox, J. Cheminformatics 3 (2011) 33.

[47] G.M. Morris, R. Huey, W. Lindstrom, M.F. Sanner, R.K. Belew, D.S. Goodsell, A.J. Olson, AutoDock4 and AutoDockTools4: automated docking with selective receptor flexibility, J. Comput. Chem. 30 (2009) 2785–2791.

[48] M.F. Sanner, Python: a programming language for software integration and development, J. Mol. Graph. Model. 17 (1999) 57–61.

[49] M.C. Cela-Pérez, M.M. Castro-López, A. Lasagabáster-Latorre, J.M. López-Vilariño, M.V. González-Rodríguez, L.F. Barral-Losada, Synthesis and

characterization of Bisphenol-A imprinted polymer as a selective recognition receptor, Anal Chim. Acta 706 (2011) 275-284.

[50] M.M. Castro-López, M.C. Cela-Pérez, M.S. Dopico-García, J.M. López-Vilariño, M.V. González-Rodríguez, L.F. Barral-Losada, Preparation, evaluation and characterization of Quercetin-molecularly imprinted polymer for preconcentration and clean-up of Catechins, Anal. Chim. Acta 721 (2012) 68–78.

[51] L. Zhang, J. Lv, T. Xu, L. Yang, X. Jiang, Q. Li, High efficiency removal and recovery of an endocrine disrupting compound-Bisphenol A from wastewaters, Sep. Purif. Technol. 116 (2013) 145–153.

[52] D.A. Spivak, Optimization, evaluation and characterization of molecularly imprinted polymers, Adv. Drug Deliv. Rev. 57 (2005) 1779–1794.

[53] M.C. Cela-Pérez, L. Barbosa-Pereira, X. Vecino, M. Pérez-Ameneiro, A. Lasagabáster-Latorre, J.M. López-Vilariño, M.V. González-Rodríguez, A.B. Moldes, J.M. Cruz, Selective removal of ATP degradation products from food matrices II: rapid screening of Hypoxanthine and Inosine by molecularly imprinted matrix solid-phase dispersion for evaluation of fish freshness, Talanta 135 (2015) 58–66.

[54] European Union Decision 2002/657/EC (17/8/2002), Off. J. Eur. Commun. 221 (2002) 8-36.

[55] J.S. Krouwer, R. Rabinowitz, How to improve estimates of imprecision, Clin. Chem. 30 (1984) 290-292.

[56] H. Sun, F. Qiao, G. Liu, S. Liang, Simultaneous isolation of six fluoroquinolones in serum samples by selective molecularly imprinted matrix solid-phase dispersion, Anal. Chim. Acta. 625 (2008) 154-159.

[57] L. Pauling, The nature of the chemical bond, Cornell University Press, Ithaca, NY, 1939.

[58] A.G. Mayes, M.J. Whitcombe, Synthetic strategies for the generation of molecularly imprinted organic polymers, Adv. Drug Deliver. Rev. 57 (2005) 1742–1778.

[59] J. Pan, X. Zou, X. Wang, W. Guan, Y. Yan, J. Han, Selective recognition of 2,4-dichlorophenol from aqueous solution by uniformly sized molecularly imprinted microspheres with β-cyclodextrin/attapulgite composites as support, Chem. Eng. J. 162 (2010) 910–918.

[60] Y.S. Ho, G. McKay, Pseudo-second order model for sorption processes, Process Biochem. 34 (1999) 451–465.

[61] C.M. Dai, J. Zhang, Y.L. Zhang, X.F. Zhou, Y.P. Duan, S.G. Liu, Selective removal of acidic pharmaceuticals from contaminated lake water using multi-templates molecularly imprinted polymer, Chem. Eng. J. 211–212 (2012) 302–309.

[62] M. Concheiro, A. de Castro, O. Quintela, M. López-Rivadulla, A. Cruz, Determination of MDMA, MDA, MDEA and MBDB in oral fluid using High Performance Liquid Chromatography with Native Fluorescence Detection, Forensic Sci. Int. 150 (2005) 221-226.

[63] S.B. Grauwiler, A. Scholer, J. Drewe, Development of a LC/MS/MS method for the analysis of Cannabinoids in human EDTA-plasma and urine after small doses of cannabis sativa extracts, J. Chromatogr. B 850 (2007) 515-522.

[64] http://www.samhsa.gov/ (Accessed July 2015)

[65] http://www.druid-project.eu/ (Accessed July 2015)

[66] S. Anizan, G. Milman, N. Desrosiers, A.J. Barnes, D.A. Gorelick, M.A. Huestis, Oral fluid cannabinoid concentrations following controlled smoked

cannabis in chronic frequent and occasional smokers, Anal Bioanal Chem. 405 (2013) 8451–8461.

DISCUSIÓN

4. DISCUSIÓN

En el artículo 1, la combinación de las técnicas FTIR y UV-Vis se empleó para estudiar las interacciones entre Atmer-129, aditivo plástico con propiedades antiestáticas, y los monómeros 4-Vpy y MAA en la mezcla de prepolimerización. La mezcla acetona:ACN (3:1) y DCM demostraron ser los disolventes más adecuados para llevar a cabo la impresión. Los espectros de FTIR demostraron la gran estabilidad del complejo formado entre el Atmer-129 y la 4-Vpy en DCM, a través del enlace de hidrógeno entre el grupo alcohol del antiestático (dador de hidrógeno) y la piridina del monómero (aceptor de hidrógeno), siendo más favorable la formación de este enlace de hidrógeno intermolecular que el intramolecular en el Atmer-129. Tras el análisis del sistema mediante espectroscopía UV-Vis se propone una estequiometria 1:2 para este complejo en acetona:ACN (3:1) y DCM, empleando para el cálculo el método de las variaciones continuas (Job plot). El estudio de las interacciones entre Atmer-129 y MAA reveló que no se producen enlaces de hidrógeno entre ambos en DCM al predominar la dimerización del MAA y se observó una estequiometria 1:1 para la unión entre Atmer-129 y MAA en acetona:ACN (3:1).

Los ensayos de unión postpolimerización seguidos de la determinación del antiestático libre por HPLC-PDA, indicaron un mayor reconocimiento molecular para el MIP Atmer-129:MAA:EGDMA (1:4:20) en acetona:ACN (3:1), IF = 2,46, así como una mejor selectividad frente a ácido oleico y

linoleico. El polímero impreso Atmer-129:4-Vpy:EGDMA (1:4:20) en acetona:ACN (3:1) obtuvo un valor de IF de 1,62.

La correlación entre los resultados obtenidos de los análisis en prepolimerización y postpolimerización no fue completa. El estudio mediante la combinación de las técnicas analíticas TGA, DSC, ATR-FTIR y SEM, de la estabilidad térmica, el grado de polimerización, la incorporación del agente entrecruzante a la mezcla molécula plantilla-monómero funcional y la morfología de los polímeros, entre otros factores, explican las discrepancias observadas.

En el artículo 2, el interés suscitado alrededor del contaminante emergente en aguas naturales bisfenol-A, un disruptor endocrino capaz de causar desequilibrios en el sistema hormonal incluso a muy bajas concentraciones, fue el punto de partida en la búsqueda de un polímero impreso con capacidad de reconocimiento molecular hacia este polifenol.

Se usó en el presente estudio la combinación de UV-Vis, FTIR y ^{1}H-RMN para el análisis del complejo formado entre BPA y 4-Vpy en la etapa de prepolimerización. Las tres técnicas se complementaron para realizar la estimación de la estequiometria del complejo y el cálculo de su constante de estabilidad aparente. La interacción responsable del reconocimiento molecular es un enlace de hidrógeno entre el fenol del BPA (dador de hidrógeno) y el átomo de nitrógeno del anillo de la piridina del monómero funcional (aceptor de hidrógeno), aunque la estequiometria y la fortaleza de la unión varían con la polaridad del disolvente en la mezcla de

prepolimerización, en función de su capacidad para formar enlaces de hidrógeno con los grupos –OH del BPA, situación que conlleva una disminución de este tipo de uniones entre el BPA y la 4-Vpy. En general, disolventes de muy baja polaridad como DCM, $CHCl_3$ y CCl_4, generaron complejos de estequiometria 1:2 muy estables, con constantes de enlace entre 2,15 y 4,95 x 10^3 M^{-1}, mientras que en otros de mayor polaridad como el ACN se observaron estequiometrias 1:1 y bajas constantes de estabilidad. Requerimientos sintéticos derivados de la hipotética aplicación final del MIP condicionaron la selección del porogen, eligiéndose una mezcla de TRIGLYME y PVAc de polaridad intermedia, en el que quedó demostrada la formación de enlace de hidrógeno entre el BPA y la 4-Vpy y la independencia de esta unión respecto a la adición del agente entrecruzante, EGDMA.

Los análisis ATR-FTIR en postpolimerización demostraron que el enlace de hidrógeno entre monómero funcional y molécula plantilla se mantiene después de la polimerización y que son 2 las piridinas implicadas por cada molécula de BPA. Además, esta técnica permitió observar que las propiedades de enlace derivadas de ensayos de unión están muy influenciadas por el tipo de disolvente involucrado, ya que cuando los ensayos se llevaron a cabo en disolventes orgánicos como ACN y $CHCl_3$, el IF fue menor que el calculado en medio acuoso. Ensayos de 'swelling' posteriores indicaron que en ambos medios orgánicos estudiados, sobre todo en cloroformo, el MIP sufre un cambio en la conformación de los sitios de enlace que provoca esa disminución del reconocimiento molecular. En

medio acuoso sin embargo, IF alcanzó valores de hasta 6,4, observándose sin embargo, que una vez saturados los sitios de alta afinidad, el BPA disponible comienza a unirse de forma no específica a los grupos carbonilo del agente entrecruzante y/o termina formando agregados consigo mismo.

En el artículo 3 se aborda la preparación de un MIP para el reconocimiento de hipoxantina en medios acuosos. La hipoxantina es un derivado metabólico de las purinas, considerada un indicador del grado de frescura en carnes y pescados. Cuanto mayor sea su concentración en el alimento, menor será la frescura y calidad del mismo.

De nuevo, las técnicas espectroscópicas ya comentadas se usaron para determinar las estequiometrias y constantes de enlace de los complejos derivados de la combinación de 2 'mimic' (cafeína y teofilina) y 3 monómeros funcionales (MAA, HEMA y AM). La composición TPH:AM resultó ser la más adecuada para preparar un MIP en $CHCl_3$ que reconozca y enlace hipoxantina, dada la estabilidad del complejo 1:2 formado entre TPH y AM en el porogen a través de enlaces de H (K_{11} = 3,36 x 10^4-1,71 x 10^4 M^{-1} y K_{12} = 1,33 x 10^2-7.66 x 10^1 M^{-1}).

El mayor rendimiento alcanzado por TPH-AM-EGDMA-MIP en los estudios de prepolimerización se confirmó a través de la evaluación de la totalidad de MIPs sintetizados. Los ensayos de unión se llevaron a cabo con disoluciones de HYP en ACN:agua (4:1) en el rango 5-1000 mg mL^{-1}, calculándose la fracción de analito enlazada al polímero como la diferencia entre la concentración inicial y la libre determinada por UPLC-PDA,

resultando valores de IF de 4,81 y valores de 1,89 x 10^3 M^{-1} y 10,22 µmol g^{-1} para la constante de afinidad media y la capacidad de enlace, ajustando los datos de equilibrio a la isoterma de Freundlich.

A continuación y para completar el estudio, se determinó el grado de polimerización, la morfología, la distribución de tamaño de poro y cambios conformacionales en la exposición a diferentes disolventes, para el conjunto de MIPs, mediante análisis ATR-FTIR, BET, 'swelling' y SEM respectivamente.

En la segunda parte de este capítulo se profundizó en la evaluación de diferentes MIPs sintetizados. Los artículos 4 y 5 continúan el estudio iniciado en el artículo 2, en el cual se preparó un MIP para la determinación de BPA en agua. En el primer trabajo, el MIP se sometió a ensayos de unión en agua, a 12 niveles de concentración entre 5 y 1000 mg L^{-1} y se calculó el BPA enlazado al polímero via UPLC-PDA. Los datos de equilibrio se ajustaron a los modelos de isotermas de Langmuir, bi-Langmuir y Freundlich, y se calcularon los valores de capacidad de enlace y constante de afinidad derivados. Al aplicar el modelo de Freundlich, éste calculó un valor del índice de heterogeneidad de 0,6893, alejado de la homogeneidad en cuanto a sitios de enlace que indica un valor próximo a la unidad, por lo que el modelo discreto de Langmuir, que supone la homogeneidad del polímero, se descartó en el estudio de las propiedades de enlace. El modelo de bi-Langmuir fue capaz de determinar la existencia de 2 tipos de sitios de unión, clasificados según su afinidad al analito en sitios de alta y

baja afinidad ('Scatchard plot'); para los primeros se obtuvo una afinidad de $1,19 \times 10^4$ M^{-1} y una capacidad de enlace de 26,9 µmol g^{-1}, con un valor de R^2 de 0,9925. Sin embargo, para poder medir cuantitativamente la distribución de los sitios de unión y la heterogeneidad del MIP, se necesitó aplicar un modelo continuo. Mediante la aproximación de Freundlich se determinó una afinidad media de $1,07 \times 10^4$ M^{-1} y una capacidad de enlace total de 45,2 µmol g^{-1}. Por otro lado, el ajuste de los datos al modelo de isotermas de Dubinin-Radushkevich indicó que la interacción por enlace de hidrógeno entre BPA y 4-Vpy en el MIP es comparable en fortaleza a un enlace químico, mediante la estimación de la energía de enlace asociada ($\bar{E}$ = 158 kJ mol^{-1}, E_{max} = 223 kJ mol^{-1}).

Continuando con el estudio del reconocimiento molecular, el MIP se sometió de nuevo a ensayos de unión, esta vez con disoluciones acuosas de sustancias que podrían actuar como interferentes, como el bisfenol-F (análogo estructural) o cafeína y paracetamol (contaminantes emergentes que aparecen con frecuencia junto con BPA en muestras de aguas naturales) también a 12 niveles de concentración (entre 5 y 1000 mg L^{-1}). La aplicación del modelo de Freundlich a los datos de equilibrio resultó en una mayor afinidad del MIP hacia BPF frente a BPA ($K = 3,35 \times 10^4$ M^{-1} y N = 69,8 µmol g^{-1}), justificable por la similitud estructural pero menor tamaño e impedimento estérico de la molécula de BPF. Sin embargo, tal y como era de esperar, CAF y PAR presentaron afinidades y capacidades de enlace mucho menores al BPA.

Para completar la evaluación del MIP, se elaboró el perfil de adsorción cinético a partir de ensayos de unión en medio acuoso a un único nivel de concentración y distintos tiempos de contacto estático y en ultrasonidos. Los datos se ajustaron al modelo cinético de pseudo segundo orden con valores de regresión lineal de 0,9996 y 0,9971 respectivamente, lo que confirmó la 'naturaleza química' de la unión BPA-4-Vpy, tal y como predijo el modelo de D-R. Para identificar el mecanismo a través del cual el BPA se adsorbe en el MIP, se empleó el modelo de difusión intrapartícula; éste determinó que la etapa que controla el proceso en el caso de la adsorción asistida por US es la difusión intrapartícula, mientras que para la adsorción estática se empleó el modelo de Boyd para confirmar que la etapa limitante es también la difusión del BPA a través de los poros de MIP.

El artículo 5 investiga la influencia del agente entrecruzante en el reconocimiento molecular del MIP. El estudio se desarrolló a partir de la formulación utilizada en la publicación anterior, preparando dos MIPs idénticos a éste pero entrecruzados con TRIM y DVB en lugar de con EGDMA.

Después de la realización de los ensayos de unión correspondientes y posterior aplicación de los modelos de isotermas, la comparación de las propiedades de enlace determinó una afinidad comparable de los 3 MIPs (valores de $\bar{K}$ muy similares), mientras que la capacidad de adsorción se redujo a la mitad al cambiar EGDMA por TRIM (de 45,2 a 23,7 µmol g^{-1}) pero aumentó más del doble cuando fue DVB el agente entrecruzante

usado (102 µmol g^{-1}). En cuanto a la fortaleza del enlace de hidrógeno, el modelo de Dubinin-Radushkevich calculó un valor de energía de enlace asociada de 353 kJ mol^{-1} para la formulación que contiene TRIM, seguida de la de DVB con valores de 235 kJ mol^{-1}; lo que indicó la 'naturaleza química' de la interacción BPA-MIP en cualquier caso, aunque el enlace más fuerte tiene lugar en el MIP de BPA-4-Vpy-TRIM.

En los 3 artículos que forman el capítulo 2 se demostró la aplicabilidad de los MIPs como material adsorbente en técnicas separativas. Además, en cada uno de ellos se desarrolló una metodología diferente para el diseño del polímero impreso.

En el artículo 6 se empleó la técnica MISPE convencional (en cartucho) para la determinación en aceite de oliva de Irganox 1076. Se trata de un antioxidante fenólico empleado con frecuencia en la aditivación de envases plásticos alimentarios y que presenta un nivel de migración limitado por la normativa europea que hace necesario el control de su cesión a alimentos, control que en el caso del simulante indicado para alimentos grasos (aceite de oliva) es de gran complejidad, por lo que en este trabajo se propuso el empleo de MIPs como alternativa frente a los adsorbentes tradicionalmente empleados en SPE.

Se prepararon una serie de miniMIPs en formato 'bulk' (partículas amorfas) con distintas formulaciones en las que se usó como molécula plantilla el propio analito y se variaron los restantes componentes de la mezcla de prepolimerización y las condiciones de síntesis. Los monómeros funcionales

ensayados fueron MAA, 4-Vpy y AM (de carácter ácido, básico y neutro respectivamente), combinados con los agentes entrecruzantes EGDMA, TRIM y DVB en proporciones T:M:C de 1:4:20 para las composiciones con EGDMA y DVB y 1:4:13 para las de TRIM. Como agentes porógenos se emplearon el DCM y el THF, siendo AIBN y DPMA los iniciadores de la polimerización bajo condiciones térmicas (60 ºC, 24 horas) y fotoquímicas (UV, T < 30 ºC, 9-19-24-30 horas).

El conjunto de miniMIPs así obtenidos se lavaron con 1 mL de porogen en ultrasonidos durante 1 hora y se cuantificó el Irganox 1076 contenido en el sobrenadante por HPLC-PDA. Esta medida se utilizó como un indicador de la impresión lograda en el polímero, de manera que los miniMIPs que liberaron porcentajes importantes de molécula plantilla en esta etapa fueron descartados para continuar el estudio. A continuación, y después de eliminar la molécula plantilla en sucesivas etapas de lavado, los miniMIPs se sometieron a un ensayo de enlace con una disolución de Irganox 1076 de concentración una décima parte de la concentración de síntesis. El porcentaje de Irganox enlazado se determinó por HPLC-PDA. Finalmente, el 'mejor' miniMIP se seleccionó en función del balance entre estas dos etapas descritas.

Con la composición elegida, se prepararon dos formatos de polímero impreso, por un lado, de nuevo un MIP tipo bulk y por otro, un MIP con mayor homogeneidad de sitios de enlace por polimerización por precipitación. El primero se molió y tamizó hasta un tamaño de partícula

de 25-40 µm y posteriormente se lavó en microondas con THF acidificado para eliminar la molécula plantilla. El segundo, como polimerizó en forma de gel, se dejó secar hasta conseguir que el particulado estuviese suelto y posteriormente la eliminación de Irganox se llevó a cabo directamente en el cartucho SPE con la misma mezcla ácida.

Se prepararon dos tipos de columnas MISPE. Para empaquetar el MIP obtenido como partículas amorfas se empleó una jeringa de vidrio para SPE en la que se introdujeron 400 mg de MIP, mientras que en el caso del particulado homogéneo, 200 mg se empaquetaron en un cartucho SPE de polipropileno. El protocolo MISPE fue similar en ambas columnas. Para el condicionamiento de la fase estacionaria homogénea se usaron 6 mL de THF, luego, se introdujo la muestra (0,75 g de aceite de oliva fortificados a 15 mg L^{-1} con Irganox 1076) diluida a 2mL en el mismo disolvente. La etapa de elución del antioxidante ocurrió con 6 mL de THF:HAc (9:1). En la columna de vidrio (cargada con MIP obtenido en formato bulk) el protocolo seguido empleó 3 mL de THF:hexano (3:1) en el acondicionamiento, disolvente en el que también se cargó la muestra (fortificada ahora con 30 mg L^{-1} de Irganox 1076). La elución se llevó a cabo, al igual que en la otra columna, con THF acidificado. El eluato en ambos casos se inyectó en HPLC-PDA para determinar los niveles de recuperación.

Finalmente, la mejor separación se obtuvo con las columnas MISPE preparadas con el polímero impreso obtenido via polimerización por

precipitación, consiguiendo este sistema un 45% de retención del Irganox cargado y elución posterior superior al 90%.

El artículo 7 constituye la segunda parte del artículo 3 del primer capítulo. En aquel estudio, los ensayos de prepolimerización y postpolimerización desarrollados concluyeron en la obtención de un MIP de TPH-AM-EGDMA adecuado para la determinación de hipoxantina en medios acuosos. Los ensayos de unión desarrollados entonces se llevaron a cabo en ACN:agua (4:1); la fracción orgánica se introdujo para evaluar correctamente la afinidad, las interacciones específicas HYP-monómero funcional, mientras que la fracción acuosa fue necesaria para garantizar la solubilidad de la HYP. En este último artículo, antes de usar el MIP como adsorbente en MSPD en la determinación de HYP y otros derivados de ATP en carne de pescado, fue necesaria una caracterización previa en agua:EtOH (9:1), simulante apropiado para carne de pescado según la legislación comunitaria, para predecir el comportamiento del MIP en la aplicación final. De esta forma, se obtuvieron valores de $\overline{IF}$ = 2,25, siendo IF_{max} = 6,82 para una concentración próxima a los 5 mg L^{-1}. La afinidad media en el rango 5-1000 mg L^{-1} fue de 7,95 x 10^2 M^{-1}, mientras que la capacidad N llegó a los 368,3 μg g^{-1}. En general, estos valores son menores que los obtenidos en ACN:agua (4:1); la principal causa del diferente comportamiento en ambos medios es el mayor efecto hidrofóbico presente cuando los ensayos de unión se llevan a cabo en el simulante, al aumentar la proporción de agua respecto a la mezcla ACN:agua (4:1), además de la ratio de 'swelling' menor en comparación con la mezcla que contiene ACN y

con el porogen (2.2 ± 0.1 para el simulante, 4.2 ± 0.7 para ACN:agua (4:1) y 7.9 ± 0.1 para CHCl$_3$) y que afecta a la conformación del sitio de enlace. De todas formas, a pesar de que en el simulante disminuyen los valores de los indicadores de reconocimiento molecular respecto a los otros disolventes, las propiedades de enlace son buenas y la impresión quedó demostrada, debido probablemente a que AM aumenta la superficie hidrofílica del polímero y es más soluble en agua, con lo que se reducen las interacciones hidrófobicas no específicas y se consigue la compatibilidad del MIP con medios acuosos. Estudios de selectividad cruzada frente a precursores y derivados de HYP en la ruta de degradación del ATP (inosina, xantina y ácido úrico) mostraron la existencia de reconocimiento molecular no sólo para HYP sino también para INO, con valores de $\overline{IF}$ = 1,32 e IF_{max} = 2,37. El factor de selectividad SF para HYP alcanzó valores medios de 1,56 y un valor máximo de 3,92 para concentraciones de INO e HYP próximas a los 5 mg L^{-1}.

Una vez probada la eficacia del MIP en la determinación de HYP e INO, el estudio continuó con la optimización del procedimiento MIP-MSPD. En primer lugar se investigó la ratio muestra/adsorbente adecuada, imprescindible para lograr la mayor adsorción posible de los analitos en el MIP, observándose que la ratio 1:2 consigue retenciones cercanas al 100%. A continuación, se investigó cómo afecta el pH al proceso de adsorción, al tratarse la HYP de un analito con comportamiento ácido-base. Conocidos los valores de pK$_a$ de HYP y sabiendo que cuando los analitos están cargados, la eficacia de la adsorción disminuye, las condiciones

ideales para una retención satisfactoria deben ser ligeramente ácidas o neutras. Además, el punto isoeléctrico de HYP es próximo a 5, lo que significa que para pHs cercanos a este valor, la carga eléctrica de la HYP es nula. Ensayos de unión desarrollados en el rango de pH 2-8 probaron esta hipótesis.

La técnica MSPD incluye una etapa de SPE en la que es necesaria una optimización del protocolo de elución para garantizar el éxito de la separación. Primero, el disolvente empleado en el lavado debe eliminar en lo posible compuestos interferentes poco polares contenidos en la carne de pescado, como las grasas, al tiempo que debe mantener la adsorción de los analitos (polares). Se probaron disolventes de distintas polaridades y varios volúmenes de los mismos, resultando 2 mL de hexano la opción idónea. Por último, en el proceso de elución debe utilizarse un disolvente que provoque la ruptura de las uniones HYP-MIP y su subsecuente eliminación. Un volumen de 4 mL de hidróxido amónico acuoso al 25%, de pH 12,5, resultó ser la mejor solución, eluyendo una media de un 85% de la HYP retenida en repetidos ensayos de adsorción. Posteriormente, en la aplicación de la metodología optimizada a muestras reales se observó que a este pH la elución es lenta y en ocasiones se forman burbujas, fenómenos que se repiten a pH 11, por lo que finalmente, la elución se lleva a cabo a pH 9 (valor de pH todavía por encima del pK_a de HYP) en ausencia de dificultades.

Al final del artículo 7, la metodología desarrollada se validó a tres niveles de concentración, seleccionados conforme a las cantidades de HYP e INO habitualmente encontradas en muestras de pescado que recoge la bibliografía consultada (rango 10-40 mg L^{-1}). Los resultados mostraron linealidad en ambos casos, con valores de regresión de 0,9987 y 0,9986 para HYP e INO. Los límites de detección y cuantificación calculados fueron 1,702 y 5,672 µg mL^{-1} para HYP y 1,785 y 5,950 µg mL^{-1} para INO respectivamente, con RSD inferiores en ambos casos al 0.8%. La precisión se calculó en términos de repetibilidad y reproducibilidad (5 medidas en el mismo día y en 3 días sucesivos), obteniéndose en cualquier caso valores aceptables de RSD (< 13,6%). Las recuperaciones obtenidas se movieron entre 103,1 y 113,4% con RSD ≤ 4.2 %.

En el artículo 8, se realizó una aproximación a otra analítica muy compleja, como es la determinación de cannabinoides en fluidos biológicos. Para ello se preparó una 'NIP library' conteniendo 4 monómeros con distintas características hidrofílicas y ácido-base (4-Vpy, MAA, HEMA y AM) y 3 agentes entrecruzantes de distintas funcionalidades y flexibilidades (EGDMA, TRIM y triacrilato de trimetilpropano TMPTA), con el fin de, tras oportunos ensayos de enlace en medio acuoso y orgánico, obtener la composición más apropiada con la que sintetizar un polímero impreso capaz de purificar y concentrar muestras de orina y saliva en el compuesto activo de la droga más ampliamente consumida, el tetrahidrocannabinol, así como en su metabolito principal, el carboxi-THC, y en compuestos minoritarios identificados con indicadores de consumo reciente, cannabinol

y cannabidiol. Al mismo tiempo, se comprobó la valía de esta metodología en el diseño de MIPs y su correlación con el diseño computacional.

En este caso, tanto la 'NIP library' como el polímero impreso se prepararon en forma de pequeñas pastillas, listas para ser usadas como adsorbentes en SPE sin necesidad de operaciones de molienda y tamizado. Se trata de una técnica de polimerización totalmente nueva, ya que es un formato que nunca se había preparado. Esta nueva configuración presenta una serie de ventajas como son la rapidez de la metodología MISPE derivada, así como el empleo de muy bajos volúmenes de muestra (inferiores a 300 μL), siendo ambas características de especial importancia en el tratamiento de matrices biológicas.

Los ensayos de unión del conjunto de NIPs tuvieron lugar por incubación estática de las pastillas con 1 mL de disolución de THC en agua:EtOH (6:4) y en DMF en el interior de un vial, a un sólo nivel de concentración (2,5 mg L^{-1}). La inyección en HPLC-PDA del sobrenadante transcurridas 72 horas permitió calcular el THC retenido por diferencia con la concentración disponible al inicio. La ratio de unión en ambos medios sirvió para evaluar la especificidad de cada NIP, ya que la retención en medio orgánico se debe exclusivamente a los enlaces de hidrógeno específicos entre THC y cada uno de los monómeros, mientras que en la retención en medio acuoso se suman las interacciones de tipo hidrofóbico, entre otras. AM-EGDMA-NIP obtuvo la ratio de enlace más favorable, 0,31, por lo que su formulación se usó para preparar el MIP más adecuado al fin descrito.

Como molécula plantilla se utilizó la catequina, similar en su estructura al THC y soluble a las concentraciones de síntesis requeridas en TRIGLYME, disolvente porógeno de constante dieléctrica y presión de vapor bajas, condiciones indispensables para la obtención de MIPs en formato pastilla.

La pastilla de MIP así preparada se sometió a ensayos de unión en medio acuoso y orgánico, de la misma forma que se hizo en la 'NIP-library', y se calcularon los valores de IF asociados. En ambos medios el reconocimiento molecular es eficaz, tomando valores de IF = 4,05 en agua:EtOH (6:4) y llegando a 8,37 en medio orgánico. Al tiempo que CATE-AM-EGDMA-MIP, dos pastillas impresas más fueron preparadas y ensayadas en las mismas condiciones, en un intento de validar la conexión entre las propiedades de enlace de NIPs y MIPs; las formulaciones elegidas fueron por un lado, la que menor ratio de unión presentó en el estudio con NIPs (4-Vpy-TRIM, 0,14) y otra de ratio intermedio (HEMA-TMPTA, 0,27). La validez de este procedimiento de diseño de MIPs quedó demostrada al comprobar que los valores de IF en estos dos casos son 0,90 y 1,35 respectivamente en medio acuoso y 2,51 y 1,98 en medio orgánico. De la misma manera, se comprobó también la correlación de esta metodología con la modelización molecular en cuanto a fortaleza de la interacción responsable del reconocimiento; AUTODOCK 4 calculó valores de la energía de enlace de -26,0 kcal mol^{-1} para AM-THC, superiores a los calculados para HEMA (-24,7 kcal mol^{-1}), MAA (-21,1 kcal mol^{-1}) y 4-Vpy (-13,0 kcal mol^{-1}).

Para completar la evaluación del reconocimiento molecular, se estudió la selectividad de MIP y NIP frente a cafeína y paracetamol, dos sustancias con presencia habitual en muestras de orina. Estudios de enlace competitivos de los tres compuestos (THC, CAF y PAR) en concentración 2,5 mg L^{-1} en medio acuoso, proporcionaron valores de SF de 1,39 y 1,48 para el THC frente a estas interferencias, datos indicativos de la valía del MIP para la aplicación final.

Por último, la optimización del procedimiento MISPE determinó que las condiciones de pH propias de las muestras de orina y saliva (pHs próximos a la neutralidad) son las adecuadas para efectuar la carga de la muestra, ya que la simulación molecular mostró que el enlace de hidrógeno se produce entre el -O- aceptor de hidrógeno del THC y el -N- dador de hidrógeno de la AM, y ambos grupos funcionales permanecen sin carga a esos valores de pH, condiciones óptimas para la formación del enlace de hidrógeno mencionado. Por otro lado, la elución tuvo que desarrollarse a pH ácido con MeOH:HAc, 4:1, para favorecer una metanólisis sobre AM que provocó la ruptura del enlace de hidrógeno formado y la liberación del THC adsorbido en el MIP.

La metodología MISPE-LC-MS/MS derivada fue validada para la determinación simultánea de THC, THC-COOH, CBN y CBD en orina y saliva. Los parámetros de validación obtenidos en orina demostraron la aplicabilidad del método en la rutina de laboratorio, alcanzando un valor de LOQ de 1 ng mL^{-1} para THC-COOH que supera apmliamente los 15 ng mL^{-1}

establecidos en esta matriz para la identificación de consumo de cannabis. Los valores de recuperación variaron entre 50,3 y 81,3%, con RSDs inferiores a 14,4% en cualquier caso. La validación en saliva alcanzó LOQ de 0,75 ng mL^{-1} para todos los cannabinoides analizados con valores de recuperación entre 64,9 y 111% (RSD < 8,88%). Una vez más, la nueva metodología desarrollada es capaz de identificar el consumo de cannabis, superándose los límites propuestos para el THC (2 y 1 ng mL^{-1}), del mismo modo puede identificarse el consumo reciente a través de CBN y CBD (1 ng mL^{-1}). Sin embargo, el método no sirve para diferenciar entre consumo de cannabis activo y pasivo, al no alcanzarse para THC-COOH la sensibilidad requerida (2 pg mL^{-1}).

Finalmente, la metodología validada se aplicó a la determinación simultánea de THC, THC-COOH, CBN y CBD en 4 muestras de orina y 5 de saliva de origen forense en las que previamente había sido confirmada la presencia de cannabinoides.

CONCLUSIONES

5. CONCLUSIONES

1. Se ha comprobado la efectividad de la tecnología de MIPs en la purificación y/o concentración en medios acuosos de contaminantes emergentes (BPA), indicadores de calidad alimentaria (HYP o INO) y drogas de abuso (THC), así como en medios de naturaleza orgánica de los aditivos de plásticos Atmer 129 e Irganox 1076.

2. Se ha desarrollado un nuevo método de polimerización no covalente que permite obtener MIPs en un formato totalmente novedoso (pastilla) y con grandes posibilidades en su aplicación como material adsorbente en SPE, ya que supera eficazmente dificultades prácticas derivadas del empleo de las configuraciones de polímeros impresos convencionales, como son el elevado volumen de muestra requerido y la tediosa purificación de matrices biológicas.

3. La metodología MISPE en cartucho convencional ha sido aplicada con éxito en la extracción de Irganox 1076 de aceite de oliva, mientras que la novedosa técnica MISPE en formato pastilla sirvió para desarrollar una eficaz y sencilla metodología para la determinación de THC, THC-COOH, CBN y CBD en fluidos biológicos. La combinación MIP-MSPD ha sido validada y probada en la determinación selectiva de HYP e INO en carne de pescado.

4. Distintas estrategias involucradas en el diseño de polímeros impresos, como el estudio de la interacción entre posibles moléculas plantilla y

monómeros funcionales en ensayos de prepolimerización mediante técnicas espectroscópicas, el estudio de la fortaleza de la interacción molécula plantilla-monómero funcional a través de la modelización molecular o los estudios de enlace postpolimerización en una 'NIP-library' formada con las distintas formulaciones posibles y viables, resultaron imprescindibles en la búsqueda de la composición óptima para obtener un MIP eficaz.

5.   La evaluación de las propiedades de enlace de los polímeros impresos (IF, SF, etc.) y el establecimiento del perfil cinético a través de ensayos de unión en el simulante de la matriz de la muestra a una concentración determinada, demostraron su utilidad en la predicción del comportamiento del MIP en la aplicación final a muestras reales.

6.   El ajuste de los datos de equilibrio derivados de ensayos de unión en MIPs en un rango de concentraciones a diversos modelos de isotermas (Langmuir, bi-Langmuir, Freundlich y/o Dubinin-Radushkevich) permitió calcular las constantes de afinidad y la capacidad de adsorción analito-MIP, mientras que la aplicación del modelo de difusión intrapartícula y/o el modelo de Boyd al conjunto de datos de la cinética de adsorción sirvió para identificar el mecanismo mediante el cual se produce dicha unión.

7. El estudio de los polímeros impresos por ATR-FTIR, SEM, BET o 'swelling', proporcionó información estructural del material polimérico y reveló cambios conformacionales de los sitios de enlace en las diferentes condiciones de contacto producidas en la aplicación de MIPs a muestras reales.

ANEXOS

ANEXOS

ANEXO 1: PORTADA PUBLICACIONES

ANEXO 2: CONTRIBUCIONES A CONGRESOS

ANEXOS

A study of competitive molecular interaction effects on imprinting of molecularly imprinted polymers

M.C. Cela-Pérez[a], A. Lasagabáster-Latorre[a,b], M.J. Abad-López[a], J.M. López-Vilariño[a], M.V. Gónzalez-Rodríguez[a,*]

[a] Grupo de Polímeros, Centro de Investigacións Tecnolóxicas, Universidade da Coruña, Campus de Esteiro s/n, Ferrol 15403, Spain
[b] Dpto Química Orgánica I, Escuela de Óptica, Universidad Complutense de Madrid, Arcos de Jalón n° 118, Madrid 28037, Spain

ARTICLE INFO

ABSTRACT

The work herein reports on an approach to obtain molecularly imprinted polymers (MIPs) for Atmer 129, an antistatic added to polyolefins and a previously non imprinted template with intra molecular H-bonding capability. The template–monomer interactions occurring in pre- and post-polymerization media were analyzed by FTIR and ATR-FTIR, respectively. After the prepolymerization study, the synthesis conditions were discussed and suitable porogens and potential template:monomer stoichiometries were suggested. The imprinting efficiency and selectivity of MIPs were evaluated in batch assays by HPLC or UPLC and compared with thermal behavior and morphological characteristics checked by Thermogravimetric Analysis (TGA), Differential Scanning Calorimetry (DSC) and Scanning Electron Microscopy (SEM). The best results were obtained for MIPs synthesized at 60 °C. A relation between imprinting effect and template shape recognition was suggested by selectivity studies. The major conclusion, which has been drawn from FTIR and DSC studies, is that independently of the H-bonding strength between Atmer 129 and monomer, the template started to crystallize out during the polymerization reaction, thus reducing the imprinting effect.

© 2012 Elsevier B.V. All rights reserved.

1. Introduction

MIPs have been a focus of research as a consequence of their molecular recognition properties and are now receiving considerable attention for applications that require binding and release of specific molecular species [1–3]. The relative ease with which these polymers may be prepared, the wide range of chemical compounds which could be imprinted and the apparent mechanical and chemical stability of these polymers have made them extremely attractive in numerous areas ranging from chromatography, assays, sensor technology, catalysis to controlled delivery systems [4–10].

MIP polymerizations follow a general procedure. In a solution of appropriate functional monomers, a template molecule (or the molecule to be recognized) is added, and the solution is mixed. This mixing allows for "self-assembly" of the template with the complementary monomers to form a pre-polymerization complex. The functional monomer contains specific chemical structures designed to interact with the template either by covalent chemistry, non covalent chemistry or both. The polymerization occurs by free radical initiation in the presence of a crosslinking monomer and an appropriate solvent. The template can then be extracted from the formed polymer usually via diffusion, and the structure formed is a porous matrix with specific recognition elements for the template molecule. Thus, MIP creates stereo-specific three-dimensional binding cavities based on the template molecule of interest [6,7,11–18].

Initially, any chemical compound could be made a corresponding MIP. However, the efficiency of the imprinting process is reported only for a limited number of compounds. Different factors play an important role, such as the forming of a stable complex during MIP preparation, the disruption of monomer–template complexes by the cross-linker or porogen and competitive molecular interactions if the template or the functional monomer form intra- or/and self-intermolecular interactions. The latter can affect the proportion of the template–monomer complex because the use

---

Contents lists available at SciVerse ScienceDirect

Materials Chemistry and Physics

journal homepage: www.elsevier.com/locate/matchemphys
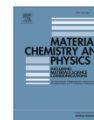
Insight into BPA–4-vinylpyridine interactions in molecularly imprinted polymers using complementary spectroscopy techniques
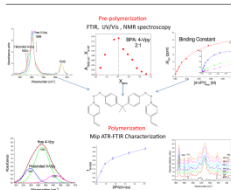
CrossMark

A. Lasagabáster-Latorre [a], M.C. Cela-Pérez [b], S. Fernández-Fernández [b], J.M. López-Vilariño [b], M.V. González-Rodríguez [b,*], M.J. Abad [b], L.F. Barral-Losada [b]

[a] Dpto Química Orgánica I, Escuela de Óptica, Universidad Complutense de Madrid, Arcos de Jalón nº 118, Madrid 28037, Spain
[b] Grupo de Polímeros, Centro de Investigacións Tecnolóxicas, Universidade da Coruña, Campus de Esteiro s/n, Ferrol 15403, Spain

HIGHLIGHTS

- MIP ATR analysis confirmed BPA:4Vpy H-bonded complexes survived polymerization.
- MIP ATR analysis confirmed two functional groups in MIP binding sites.
- Reversible conformational changes explained the poor results in nonpolar solvents.
- Detailed description of rebinding mechanism in water based on MIP-ATR spectroscopy.
- Selectivity depended on analyte:monomer interactions, shape, solubility.

GRAPHICAL ABSTRACT

ARTICLE INFO

ABSTRACT

The influence of solvent polarity on the nature and extent of non-covalent interactions responsible for BPA:4-Vinlypyridine complex formation has been investigated in the pre-polymerization mixture and correlated with polymer-ligand recognition. The combination of FTIR, ^{1}H NMR and UV–Vis spectroscopy has made possible the development of a more comprehensive understanding of pre-polymerization events at a molecular level, and how they govern the properties of subsequent polymerized MIPs. The MIP ATR characterization provides direct insight into the bonding within matrix-template system, confirming that monomer:template H-bonded complexes survived the polymerization process and the presence of two functional monomers in the binding sites. The polymer has shown an excellent affinity for BPA in aqueous solutions with poor recognition in organic solvents. Loss of affinity in organic solvents together with selectivity studies suggested that the binding mechanism depended critically on the conformation of the polymeric binding pockets, which when combined with H-bonding and weak electrostatic interactions allowed for selective recognition.

1. Introduction

Molecularly imprinted polymers (MIPs) synthesized via non-covalent self-assembly processes are biomimetic recognition

* Corresponding author. Tel.: +34 981 337 400x3051, +34 981 337 400x3485; fax: +34 981 337 416.
  E-mail address: victoria.gonzalez.rodriguez@udc.es (M.V. González-Rodríguez).

materials selectively binding a target analyte in analogy to biological receptor–substrate interactions. Since non-covalent MIPs rely on complex formation between the target analyte and functional monomers in porogenic solution prior to radical copolymerization, the achievable selectivity is governed by the nature and stability of these complexes. Prior studies correlating polymer recognition properties with characteristics of the pre-polymerization mixture system can be found in the literature and include

Contents lists available at ScienceDirect

Reactive & Functional Polymers

journal homepage: www.elsevier.com/locate/react

REACTIVE &
FUNCTIONAL
POLYMERS

CrossMark

Selective removal of ATP degradation products from food matrices I: Design and characterization of a dummy molecularly imprinted specific sorbent for hypoxanthine

Aurora Lasagabaster Latorre [a,b], Mª. Concepción Cela Pérez [a], Sara Fernández Fernández [a], J.M. López Vilariño [a], M.V. González Rodríguez [a,*]

[a] Grupo de Polímeros, Centro de Investigaciones Tecnológicas (CIT), Departamento de Física, Escuela Universitaria Politécnica, Universidad de A Coruña (UDC), Campus de Ferrol, 15471 Ferrol, Spain
[b] Dpto Química Orgánica I, Facultad de Óptica y Optometría, Universidad Complutense de Madrid, Arcos de Jalón no. 118, Madrid 28037, Spain

ABSTRACT

Specific molecularly imprinted polymers (MIPs) for hypoxanthine (HYP) recognition in aqueous organic media have been developed based upon UV, FTIR and ^{1}H NMR prepolymerization studies in conjunction with batch rebinding UPLC analyzes. The MIPs, which used the template mimics caffeine (CAF) and theophylline (TPH), are prepared in $CHCl_3$ by one step precipitation polymerization from acrylamide (AM), 2-hydroxyethyl-methacrylate (HEMA) and methacrylic acid (MAA) as functional monomers, whereas ethylene glycol dimethacrylate (EGDMA), divinylbenzene (DVB) and trimethylolpropane triacrylate (TMPTA) as cross-linkers. The magnitude of the pre-polymerization binding constants between TPH and AM, MAA and HEMA is consistent with the complex stoichiometry (1:2 and 1:1) and number of inter-action points (3-, 2-, 1-hydrogen bonded motif). The strong (1:2) complex between TPH and AM ($K_{11} = 3.36 \times 10^4\,M^{-1}$ and $K_{12} = 1.33 \times 10^2\,M^{-1}$) makes the corresponding MIP the most suitable for HYP recognition. The best performance of the TPH:AM:EGDMA (1:4:20) MIP is reflected in the high IF and high weighted average affinity based on the Freundlich isotherm. Further polymer characterization by ATR–FTIR, elemental analysis, surface area analysis (BET), swelling and SEM yield vital information regarding the degree of polymerization, real monomer:crosslinker ratio, morphology, pore size distribution plus conformational changes on exposure to different solvents.

© 2015 Elsevier B.V. All rights reserved.

1. Introduction

Hypoxanthine (HYP) is an essential metabolite to degrade adenine nucleotide, which is an indicator for the quality control of meat or fish products in food industries. Therefore, it is significant to develop a quick and effective analytical method for the determination of HYP. Various methods have been proposed for the evaluation of HYP concentration, such as chromatography, capillary electrophoresis and electrochemistry [1,2]. Owing to the complexity of sample matrices and low levels of the analyte, sample pretreatment and enrichment process become the crucial steps in these analytical procedures. So far, the most widely used sample pre-treatment methods are liquid–liquid extraction, solid-phase extraction (SPE), liquid-phase microextraction, cloud point extraction, ionic liquids extraction and stir bars microextraction, but most of these procedures suffer from several disadvantages such as large amounts of organic solvent, tedious procedure or low enrichment factor [3].

In order to solve these drawbacks molecularly imprinted polymers (MIPs) have been successfully applied as selective phases in solid phase extraction of analytes present in low concentrations or in complex matrices and have lead to enrichments and clean-up of the analytes to levels not achievable with alternative methods. Accordingly, molecularly imprinted solid phase extraction (MISPE) has been widely used in bioanalysis, food, pharmaceutical and environmental analysis in recent years [4–8], MIPs are synthetic polymeric materials with specific and selective recognition sites complementary in shape, size, and functional groups to the template molecule (T), involving an interaction mechanism based on molecular recognition. MIPs can be synthesized either by covalent or by non-covalent procedures. The latter are based on the formation of relatively weak non-covalent interactions between the T and functional monomers (M) before polymerization.

Synthesis and characterization of bisphenol-A imprinted polymer as a selective recognition receptor

M.C. Cela-Pérez [a], M.M. Castro-López [a], A. Lasagabáster-Latorre [b], J.M. López-Vilariño [a], M.V. González-Rodríguez [c,*], L.F. Barral-Losada [d]

[a] *Laboratorio de Química, Centro de Investigacións Tecnolóxicas, Universidade da Coruña, Campus de Esteiro s/n, Ferrol 15403, Spain*
[b] *Dpto Química Orgánica I, Escuela de Óptica, Universidad Complutense de Madrid, Arcos de Jalón nº 118, Madrid 28037, Spain*
[c] *Dpto. Química Analítica, E.U. Politécnica, Universidade da Coruña, Avda. 19 de Febrero s/n, Ferrol 15405, Spain*
[d] *Laboratorio de Plásticos, Centro de Investigacións Tecnolóxicas, Universidade da Coruña, Campus de Esteiro s/n, Ferrol 15403, Spain*

ABSTRACT

Molecularly imprinted polymers (MIPs) are currently used to provide selectivity in chemical sensors. In this context, a non-covalent bisphenol-A (BPA)-imprinted polymer using 4-vinylpyridine (4-Vpy) as the functional monomer, ethylene glycol dimethacrylate (EGDMA) as crosslinker and a low volatile solvent, triethylene glycol dimethyl ether (TRIGLYME), in combination with a non-reactive linear polymer, poly (vinyl acetate) (PVAc), as porogen, was synthesized with a simple polymerization procedure. Batch rebinding experiments were carried out to evaluate the binding and selectivity properties of the BPA-MIP. The experimental adsorption isotherms were fitted and a heterogeneous distribution of the binding sites was found. The selectivity of MIP demonstrated higher affinity for target BPA and BPA-analogues over other common water pollutants. The adsorption kinetics followed the pseudo-second-order kinetic model so that the specific adsorption in the imprinted cavities by two strong hydrogen bonds could be described as a chemisorption process. The diffusion mechanism was determined by the intra-particle diffusion and Boyd models, both of them revealing that the adsorption was mainly governed by intra-particle diffusion. MIP was shown to be promising for regeneration without significant loss in adsorption capacity.

1. Introduction

Molecularly imprinted polymers (MIPs) are used as recognition element in sensors [1–3]. The common principle of chemical sensors is the immediate transduction of a chemical parameter (usually the concentration of an analyte of interest) into an easily processable, such as an electrical or optical signal. MIPs interact with the analyte to be detected, giving rise to a characteristic change in one of their physical properties (mass, refractive index, light absorbance...). Accordingly, the transducer part of the sensor transforms this physical property into the final readout [4].

In chemical sensing, the transducer provides sensitivity and MIPs provide selectivity [5]. Molecular imprinting involves the formation of cavities that completely match the template both in shape and functionality. Such imprinting is achieved when a cross-linker enwraps a pre-arranged complex, formed between the functional monomers and the template. After removal of the template from the polymers, the remaining cavity is specific for the template. The synthesis technique is simple and cheap; in addition, the polymers obtained exhibit high selectivity, excellent mechanical strength and durability to heat, acid and base conditions [5–9].

MIPs characterization is carried out by batch rebinding studies. Binding parameters can be estimated from the binding isotherms by the application of several mathematical models (the discrete Langmuir and the continuous Freundlich models are the most commonly applied) [10–13]. Kinetic studies describe the rate of adsorbates uptake on MIPs, leading to the determination of the equilibrium time. The Lagergren first-order, pseudo-second-order kinetic models and Elovich equation are frequently applied to study the kinetics of the adsorption process [14]; whereas the intra-particle diffusion model is further tested to determine the diffusion mechanism of the adsorption systems [14–18].

Bisphenol A, [2,2-bis(4-hydroxyphenyl)propane], is an important intermediate in the industrial manufacture of several plastics (epoxy, phenolic, polysulfone and polyetherimide resins, polycarbonates, polyesters, polyacrylates and flame retardant materials) [19,20]. Yet, many evidences have shown that BPA has toxic

* Corresponding author. Tel.: +34 981337400(3485/3051); fax: +34 981337416.
E-mail addresses: iquimica@cdf.udc.es (M.C. Cela-Pérez), iquimica@cdf.udc.es (M.M. Castro-López), aurora@quim.ucm.es (A. Lasagabáster-Latorre), iquimica@cdf.udc.es (J.M. López-Vilariño), victoria.gonzalez.rodriguez@udc.es (M.V. González-Rodríguez), iquimica@cdf.udc.es (L.F. Barral-Losada).

Impact of functional cross-linker on recognition properties of a Bisphenol-A imprinted polymer film for coating a Quartz Crystal Microbalance

M.C. Cela-Pérez, J.M.López-Vilariño, M.V. González-Rodríguez

Grupo de Polímeros – Laboratorio de Química, Centro de Investigacións Tecnolóxicas, Universidade da Coruña, Campus de Esteiro s/n, Ferrol 15403, Spain

e-mail: iquimica@cdf.udc.es

Abstract—**Robust systems could be generated based on Quartz Crystal Microbalance (QCM) combined with Molecularly Imprinted Polymers (MIPs) for on-site, in-time chemical sensing. A review of the literature demonstrates that, despite the large amount of available data to date on MIPs formulation, the main applications continue to be in the separation field, whereas the development of sensors and QCM sensors, in particular, is significantly slower. Bisphenol-A (BPA) imprinted polymers for future sensor applications were synthesized by non covalent precipitation polymerization. In order to optimize the binding properties, three different cross-linkers were used in the formulations: ethylene glycol dimethacrylate (EDMA), trimethylolpropane trimethacrylate and (TRIM) and divinylbenzene (DVB). Batch rebinding tests in aqueous media were carried out to evaluate the binding parameters fitting the adsorption isotherms by Langmuir, bi-Langmuir, Freundlich and Dubinin-Radushkevich models. Significant differences in the heterogeneity and capacity of the polymers were observed. TRIM crosslinked BPA imprinted polymer showed the best results.**

I. INTRODUCTION

MIPs are used as recognition element in sensors [1-3]. Therefore, the transducer provides sensitivity and MIPs provide selectivity [4]. Molecular imprinting involves the formation of cavities that completely match the template both in shape and functionality. Such imprinting is achieved when a cross-linker enwraps a pre-arranged complex, formed between the functional monomers and the template. After removal of the template from the polymers, the remaining cavity is specific for the template. The synthesis technique is simple and cheap; in addition, the polymers obtained exhibit high selectivity, excellent mechanical strength and durability to heat, acid and base conditions [4-8].

The key to obtain good binding MIPs is the optimization of synthetic parameters [5]. For instance, the cross-linkers, which are involved in formation of a rigid polymer matrix, should be simultaneously flexible enough to make possible the mass transfer inside the pores [8]. Furthermore, the crosslinker is selected with the requirements that it should exhibit minimal interaction with the template in order to minimize non-specific binding [9]. However, high cross-linker ratios are generally used (80% in excess) [10].

On the other hand, BPA is an important intermediate in the industrial manufacture of several plastics. BPA has toxic properties, inducing estrogenic endocrine disruption and promoting tumor progression even at an extremely low concentration. Consequently, the detection of trace amounts of BPA is very important in maintaining an awareness of pollutants in our immediate environments [11]. Most of analytical methods employed for the determination of BPA are based on GC-MS and LC-MS. However, these techniques are expensive, require pretreatment and are unsuitable for on-site measurements. Thus, the development of portable sensors which would allow a quick and effective on-site analysis is requested [3].

In this study, non-covalent approach was employed to prepare several BPA-MIPs for coating a QCM sensor. This target molecule was used as template. The cross-linkers EDMA, TRIM and DVB with different lengths and flexibilities were introduced to investigate the influence of polymer chain mobility on the site integrity. Therefore, the above MIPs formulated by using three different crosslinker monomers were compared. Batch analysis was carried out and equilibrium data were fitted using the Langmuir, bi-Langmuir, Freundlich and Dubinin-Radushkevich isotherm models.

II. EXPERIMENTAL PROCEDURE

A. Instrumentation

A method to determine BPA in subsequent characterization experiments was developed using Ultra performance liquid chromatography with PDA detector (UPLC-PDA). UPLC analyses were performed using an Acquity system from Waters (Milford, MA, USA) with a gradient pump and automatic injector. The injection loop volume was 10μL and the mobile phase for analysis was methanol:water with a volume ratio of 80:20. The flow rate of

An Approach to Imprint Irganox 1076: Potential Application to the Specific Migration Test in Olive Oil

M. S. Dopico-García,[1] Concepción Cela-Pérez,[1] J. M. López-Vilariño,[1] M. V. González-Rodríguez,[2] L. F. Barral-Losada[3]

[1]*Laboratorio de Química, Centro de Investigacións Tecnolóxicas, Universidade da Coruña, Campus de Esteiro s/n, Ferrol 15403, Spain*
[2]*Dpto. de Química Analítica, E.U. Politécnica, Universidade da Coruña, Avda. 19 de Febrero s/n, –Ferrol 15405, Spain*
[3]*Laboratorio de Plásticos, Centro de Investigacións Tecnolóxicas, Universidade da Coruña, Campus de Esteiro s/n, –Ferrol 15403, Spain*

ABSTRACT: Irganox 1076 is a hindered phenolic antioxidant commonly added to polyolefins, whose migration from the plastic packaging into the food is regulated by European legislation. The work herein reports on an initial approach to obtain a molecularly imprinted polymer (MIP) for Irganox 1076, a previously nonimprinted target. In a subsequent step, the application of the molecularly imprinted solid-phase extraction (MISPE) to the fatty simulant olive oil is tested to get its determination free of interferences using high-performance liquid chromatography with PDA detector. The influence of five variables, namely porogen, functional monomer, crosslinker, initiator, and initiation method was investigated through the synthesis of miniMIPs. The best results were obtained using methacrylic acid and ethylene glycol dimethacrylate in tetrahydrofuran under UV radiation with 2,2′-azobis-(2-methylpropionitrile). The application of MISPE to olive oil showed the potential of the imprinted polymer to clean up complex matrices. © 2010 Wiley Periodicals, Inc. J Appl Polym Sci 119: 2866–2874, 2011

Key words: antioxidants; Irganox 1076; food packaging; high-performance liquid chromatography (HPLC); molecular imprinting

INTRODUCTION

In recent years, molecularly imprinted polymers (MIPs) have shown its ability for the solid-phase extraction and cleanup of such complex matrices as biological,[1] environmental samples[2,3] or food,[4–7] for what highly selective extraction techniques are necessary.

MIPs are synthetic polymers with recognition sites able to specifically rebind a target molecule (template). In general, they are obtained by mixing the template with the complimentary functional monomers and crosslinkers in a suitable solvent. After the polymerization, the template can be extracted from the synthesized polymer.[8,9]

Irganox 1076 (Table I) is a hindered phenolic antioxidant commonly added to polyolefins to improve their stability against the effects of thermo-oxidative and photo-oxidative degradation. Their migration from the packaging into the food is regulated by European legislation[10] that establishes a specific migration limit (SML) of 6 mg kg^{-1}. In principle the migration test should be carried out in the own food but to simplify the analysis, aqueous or fatty food simulants can be used.[11] Until the moment there is not any official analytical methodology to determine the migration of this compound in the allowed simulants.

In aqueous food simulants, two analytical methodologies have been developed in our laboratory using liquid–liquid extraction,[12] or solid-phase extraction[13] and high-performance liquid chromatography with UV detector (HPLC-UV), that achieve detection limits quite lower than SML. Dispersive liquid–liquid microextraction followed by HPLC-UV has been also recently proposed for its determination in water at microliter levels.[14] However, its determination in olive oil, the fatty simulant established by the legislation, has shown to be rather more difficult because of the high complexity of this matrix. O'Brien et al.[15] reported the analysis of Irganox 1076 in olive oil using HPLC and a fluorescence detector after the dilution of the sample with acetone, methodology that has been later applied by other authors.[16]

Selective removal of ATP degradation products from food matrices II: Rapid screening of hypoxanthine and inosine by molecularly imprinted matrix solid-phase dispersion for evaluation of fish freshness

M.C. Cela-Pérez [a], L. Barbosa-Pereira [b], X. Vecino [b], M. Pérez-Ameneiro [b],
Aurora Lasagabaster Latorre [a,c], J.M. López-Vilariño [a], M.V. González Rodríguez [a,*],
A.B. Moldes [b], J.M. Cruz [b]

[a] Grupo de Polímeros, Centro de Investigaciones Tecnológicas (CIT), Departamento de Física, Escuela Universitaria Politécnica, Universidad de A Coruña (UDC), Campus de Ferrol, 15471 Ferrol, Spain
[b] Departamento de Ingeniería Química, Escuela de Ingeniería Industrial (EEI), Universidad de de Vigo, Campus As Lagoas, Marcosende 36310, Vigo-Pontevedra, Spain
[c] Departamento de Química Orgánica I, Facultad de Óptica y Optometría, Universidad Complutense de Madrid, Arcos de Jalón no. 118, Madrid 28037, Spain

ARTICLE INFO

ABSTRACT

A water compatible molecularly imprinted polymer (MIP), synthesized using theophylline (TPH) as dummy-template and acrylamide (AM) as functional monomer, has been employed as supporting material in matrix solid-phase dispersion combined with ultra performance liquid chromatography–photodiode array detection (MSPD–UPLC–PDA) for selective determination of adenosine triphosphate (ATP) derivatives in fish samples. ATP degradation products are used as freshness index for assessment of fish quality. The solid sample was directly blended with MIP in MSPD procedure resulting in sample disruption and subsequent adsorption of the compounds on the MIP. By using n-hexane and ammonium hydroxide aqueous solution at pH 9 as the washing and elution solvent, respectively, satisfactory recoveries and clean chromatograms have been obtained. Good linearity for hypoxanthine (HYP) and inosine (INO) has been observed with correlation coefficients (R^2) of 0.9987 and 0.9986, respectively. The recoveries of the two ATP derivatives at three different spiked levels ranged from 106.5% to 113.4% for HYP and from 103.1% to 111.2% for INO, with average relative standard deviations lower than 4.2% in both cases. This new method, which is rapid, simple and sensitive, can be used as an alternative tool to conventional tedious methods.

© 2014 Elsevier B.V. All rights reserved.

1. Introduction

A large number of post-mortem reactions are initiated in fish (glycolysis, proteolysis and lipolysis) immediately after the animal is slaughtered, affecting its quality and freshness conditions. One of the most important changes consists of the formation of nucleotide and nucleoside metabolites resulting from ATP degradation [1]. ATP degradation to ADP (adenosine diphosphate) and AMP (adenosine monophosphate) takes place rapidly, with the subsequent accumulation of IMP (inosine 5′-monophosphate) [2].

The IMP is hydrolyzed by autolytic enzymes (5′-nucleotidase) to inosine (INO) which, in turn, is degraded to hypoxanthine (HYP) by autolytic and/or microbial action (nucleoside phosphorylase) [3,4]. Next, HYP will be oxidized to xanthine (XAN) and then to uric acid (UA) through a much slower reaction, due to xanthine oxidase (XO) in case of spoilage by microorganisms [5–7].

The pathway of ATP catabolism as a degradative sequence has been widely studied in different fish species [7–12] besides beef [13,14], chicken [15,16] or pork meat [2,3,17–19] and some of the above mentioned nucleotide metabolites have been proposed as freshness indexes in quality assessment [18,19]. Several analytical methods such as electrophoresis [20,21], radioimmunoassay [22], nuclear magnetic resonance spectroscopy (NMR) [23] or ampero-metric and voltammetric methods [24] have been reported for quantitative determination of these compounds. Besides, in recent

* Corresponding author.
Tel.: +34 981 337 400 (3051/3485); fax: +34 981 337 416.
E-mail address: victoria.gonzalez.rodriguez@udc.es (M.V. González Rodríguez).

Elsevier Editorial System™ ×

← → C ⌂ 🔒 ees.elsevier.com/chroma/default.asp

JOURNAL OF CHROMATOGRAPHY A

Contact us ✉ Help ?

Username: jmlvila@udc.es
Switch To: Author ▼ Go to: My EES Hub

Maintenance outage on 13 September 2015... more
Alert to Editors: CrossCheck maintenance on 19 September 2015... more
'My EES Hub' available for consolidated users ... more

home | main menu | submit paper | guide for authors | register | change details | log out

Submissions Being Processed for Author Jose Manuel Lopez Vilariño

Page: 1 of 1 (1 total submissions)

Display 10 ▼ results per page.

☐ Action ▲	Manuscript Number ▲▼	Title ▲▼	Initial Date Submitted ▲▼	Status Date ▲▼	Current Status ▲▼
View Submission Send E-mail	JCA-15-1554	Water-compatible imprinted pills for sensitive determination of cannabinoids in urine and oral fluid by MISPE-LC-MS/MS	24 Aug 2015	08 Sep 2015	Under Review

Page: 1 of 1 (1 total submissions)

Display 10 ▼ results per page.

<< Author Main Menu

Version: EES 2015.8

447

Parte del trabajo incluido en esta tesis doctoral ha sido presentado en diversos congresos nacionales e internacionales:

Desarrollo, evaluación y caracterización de polímeros impresos:

1. 'Development of Molecularly Imprinted Polymers with specific recognition for antistatic additive of plastics packaging'; Cela Pérez, M.C., Castro López, M.M., Dopico García, M.S., López-Vilariño, J.M., Noguerol Cal, R., González Rodríguez, M.V.; 34th Internacional Symposium on High-Performance Liquid Separations and Related Techniques, Dresden (Alemania) 28 Junio-2 de Julio de 2009.

2. 'Characterization of Molecularly Imprinted Polymers for Atmer-129'; Cela-Pérez M. C., Castro López M. M., Dopico García M. S, Noguerol Cal R., Lasagabáster Latorre A., López Vilariño J. M., González-Rodríguez M. V.; MACRO2010: 43rd IUPAC World Polymer Congress. Polymer Science in the Service of Society, Glasgow (Reino Unido) 11-16 de Julio de 2010.

3. 'Molecularly Imprinted QCM sensor system for Bisphenol-A recognition in water samples'; Cela-Pérez M. C., Castro López M. M., Noguerol Cal R., Dopico García M. S, López Vilariño J. M., González-Rodríguez M. V.; MIP2010: The future of Molecular Imprinting. The 6th International meeting on Molecular Imprinting. Nueva Orleáns (Louisiana, Estados Unidos) 11-16 de Julio de 2010.

4. 'Impact of cross-linkers on recognition properties of a Bisphenol-A imprinted polymer film for coating a Quartz Crystal

Microbalance'; M. C. Cela-Pérez, J. M. López-Vilariño, M. V. González-Rodríguez: IEE SENSORS 2011 CONFERENCE Limerick (Irlanda) 28-31 de Octubre de 2011.

5. 'Estudio de la Influencia del disolvente en las interacciones monómero-template en la mezcla de polimerización de polímeros de impresión molecular (MIPs)'; S. Fernández-Fernández, A. Lasagabáster-Latorre, M. C. Cela Pérez, M. M. Castro López, M. V. González; VI Congreso Nacional de jóvenes investigadores en polímeros JIP2012, Islantilla (Huelva, España) 22-26 de Abril 2012.

6. 'The role of cross-linker on molecular recognition'; M. C. Cela Pérez, J. M. López Vilariño, M. V. González Rodríguez; MIP 2012: 7th International Conference on Molecularly Imprinted Polymers Science and Technology, París (Francia) 27-30 de Agosto de 2012.

Desarrollo de metodologías de preparación de muestra empleando MIPs como material adsorbente:

7. 'MIPSE system optimization based on prepolymerization studies for selective extraction of inosine from biological samples'; M. C. Cela Pérez, S. Fernández Fernández, A. Lasagabáster Latorre, J. M. López Vilariño, M. V. González Rodríguez; MIP 2012: 7th International Conference on Molecularly Imprinted Polymers Science and Technology, París (Francia) 27-30 de Agosto de 2012.

8. 'Molecularly imprinted polymers for rapid fish freshness determination'; L. Barbosa-Pereira, X. Vecino, M. Pérez-Ameneiro, M. C. Cela-Pérez, V. González-Rodríguez, J. M. López-Vilariño, A. B. Moldes, J. M. Cruz; Polymar 2013, Barcelona (España) 3-7 de Noviembre de 2013.

Desarrollo de nuevos formatos de MIPs y metodologías analíticas derivadas:

9. 'Determinación selectiva de Tetrahidrocannabinol en fluido oral usando pastillas de impresión polimérica'; E. Lendoiro, H. Fernández-Vega, A. De Castro, M.C. Cela-Pérez, J.M. López-Vilariño, M.V. González-Rodriguez, A. Cruz, M. López-Rivadulla; XX Congreso Español de toxicología y IV Iberoamericano, Salamanca (España) 26-28 Junio de 2013.

10. 'Molecularly imprinted polymer (MIP) pills for the selective extraction of THC and its main metabolite THCCOOH in urine by LC-MSMS analysis'; E. Lendoiro, H. Fernández-Vega, A. De Castro, M.C. Cela-Pérez, J.M. López-Vilariño, M.V. González-Rodriguez, A. Cruz, M. López-Rivadulla; 51ST Annual Meeting of the International Association of Forensic Toxicologist, Funchal (Madeira, Portugal) 2-6 de Septiembre de 2013.

11. 'MIP-Pills, a new tool in MISPE applications'; J.M. López-Vilariño, M.C. Cela-Pérez, E. Lendoiro, A. De Castro, M. López-Rivadulla, M.V.

González-Rodríguez; MIPs 2014: The 8th International conference on Molecular Imprinting, Shanghái (China) 18-21 de Septiembre de 2014.

12. 'Desarrollo de una metodología de extracción en fase sólida con polímeros de impresión molecular para la purificación y concentración de cannabinoides en orina'; M.C. Cela, F. Bates, J.M. Vilariño, M.V. González; XXXV Bienal RSEQ, A Coruña (España) 19-23 Julio de 2015.